

DEVELOPMENT OF FIRE-PROTECTIVE WATER-BORNE  
INTUMESCENT COATING INCORPORATED WITH  
RUBBERWOOD ASH FOR STEEL

BEH JING HAN

DOCTOR OF PHILOSOPHY (SCIENCE)

LEE KONG CHIAN FACULTY OF ENGINEERING AND SCIENCE  
UNIVERSITI TUNKU ABDUL RAHMAN  
JAN 2022

**DEVELOPMENT OF FIRE-PROTECTIVE WATER-BORNE INTUMESCENT  
COATING INCORPORATED WITH RUBBERWOOD ASH FOR STEEL**

By

**BEH JING HAN**

A dissertation submitted to the Lee Kong Chian Faculty of Engineering and Science,  
Universiti Tunku Abdul Rahman,  
in partial fulfillment of the requirements for the degree of  
Doctor of Philosophy (Science)  
January 2022

## **ABSTRACT**

### **DEVELOPMENT OF FIRE-PROTECTIVE WATER-BORNE INTUMESCENT COATING INCORPORATED WITH RUBBERWOOD ASH FOR STEEL**

**Beh Jing Han**

This research was carried out to study the re-use of a type of agricultural by-product as natural substitute of mineral fillers in the fire-protective water-borne intumescent coating. This research aims to explore the potential use of natural agricultural waste in the intumescent coating, with effort to minimise the reliance on exotic industrial fillers and work towards conserving the environment in a more sustainable way along with SDG 17 goals. Rubberwood biomass ash (BioAsh), which was derived from the combustion of rubberwood biomass in a fuel factory, was obtained for reuse as a natural mineral filler substitute in water-based intumescent coatings. The specific surface area of the BioAsh was  $3.10 \text{ m}^2/\text{g}$ , with the particle's surface areas predominant composed of mesopores, which was justified using the Brunauer-Emmett-Teller Test (BET). BioAsh coatings (BAIC) formulated with 3.5 wt% BioAsh exerted the most homogenous and durable surface matrix in the Freeze-thaw cycle test (FCT). Fire-resistant test (FRT) and thermogravimetric analysis (TGA) demonstrated the incorporation of the BioAsh with the intumescent flame-retardant formulation, generated positive effects in equilibrium end temperature, thermal decomposition, and weight loss reductions. These effects are most prominent in the BAIC 3-5, which was comprised of 3.5 wt% BioAsh, and 50/40/6.5 wt% vinyl acetate (VA)/intumescent flame retardant additive (IFRA)/ pigment. The BAIC 3-5 showed the lowest equilibrium end temperature at  $112.5^\circ\text{C}$ , the lowest thermal degradation at

70.52 wt%, and the highest carbonaceous char formation at 13.0 mm. The Surface Electron Microscopy (SEM) and Energy Dispersive X-Ray Spectroscopy (EDX) results exhibited a dense, compact, and coherent char formation for the BAIC 3-5 sample. These results are supported by the evidence from Fourier-Transform Infrared Spectroscopy (FTIR), and X-Ray Diffractometer (XRD), which revealed the stretching of the O-H, P-O-C, and P=O molecular functional groups, and the presence of thermally stable phosphate compounds in the BAIC 3-5. These results revealed an appropriate amount of 3.5 wt% renewable BioAsh incorporated as natural mineral fillers substitute in the intumescent coating could lead to a better fire resistance and mechanical properties to protect steel structures from fire.

## **ACKNOWLEDGEMENTS**

Foremost, I would like to take this opportunity to express my appreciation to the main supervisor, Ts. Dr. Yew Ming Chian and co-supervisor, Ir. Dr. Bernard Saw Lip Huat for their guidance in this PhD research project. Their research suggestions and technical advice are valuable.

In addition, I would like to thank Universiti Tunku Abdul Rahman (UTAR) for giving me such opportunity and the scholarship to further my PhD study. UTAR is dedicated in providing supports in research funding, equipment, facilities, and materials. Without the support of UTAR this research project would not be made possible. This PhD research project was funded by Universiti Tunku Abdul Rahman Research Fund (UTARRF) project number: IPSR/RMC/UTARRF/2019-C2/B01.

Lastly, I would like to express my gratitude to my beloved family for their unconditional love, continuous moral supports throughout the 4 years my PhD academic journey.

## APPROVAL SHEET

This dissertation/thesis entitled “**DEVELOPMENT OF FIRE-PROTECTIVE WATER-BORNE INTUMESCENT COATING INCORPORATED WITH RUBBERWOOD ASH FOR STEEL**” was prepared by BEH JING HAN and submitted as partial fulfilment of the requirements for the Doctor of Philosophy (Science) at Universiti Tunku Abdul Rahman.

Approved by:



---

(Ts. Dr. Yew Ming Chian)

Date:...28.01.2022.....

Supervisor

Department of Mechanical and Material Engineering

Lee Kong Chian Faculty of Engineering and Science

Universiti Tunku Abdul Rahman

*bernard saw*

---

(Ir. Dr. Bernard Saw Lip Huat)

Date:...28.01.2022.....

Co-supervisor

Department of Mechanical and Material Engineering

Lee Kong Chian Faculty of Engineering and Science

Universiti Tunku Abdul Rahman

**LEE KONG CHIAN FACULTY OF ENGINEERING AND SCIENCE**  
**UNIVERSITI TUNKU ABDUL RAHMAN**

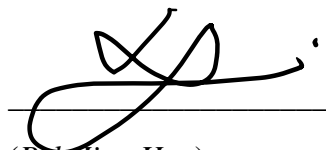
Date: \_\_28.01.2022\_\_

**SUBMISSION OF DISSERTATION**

It is hereby certified that **Beh Jing Han** (ID No: **18UED00971**) has completed this dissertation entitled “Development of Fire-Protective Water-Borne Intumescent Coating incorporated with Rubberwood Ash for Steel” under the supervision of Ts. Dr. Yew Ming Chain (Main Supervisor) from the Department of Mechanical and Material Engineering, Lee Kong Chain Faculty of Engineering and Science, and Ir. Dr. Bernard Saw Lip Huat (Co-Supervisor) from the Department of Mechanical and Material Engineering, Lee Kong Chain Faculty of Engineering and Science.

I understand that Universiti will upload softcopy of my dissertation in pdf format into UTAR Institutional Repository, which may be made accessible to UTAR community and public.

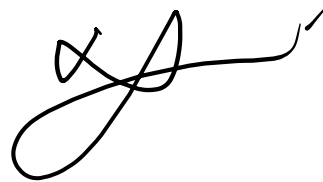
Yours truly,



(Beh Jing Han)

## DECLARATION

I hereby declare that the dissertation is based on my original work except for quotations and citations which have been duly acknowledged. I also declare that it has not been previously or concurrently submitted for any other degree at UTAR or other institutions.



BEH JING HAN  
Name \_\_\_\_\_

Date \_\_\_\_\_ 28.01.2022 \_\_\_\_\_



## TABLE OF CONTENTS

|  | Page        |
|--|-------------|
| <b>ABSTRACT</b>                        | <b>ii</b>   |
| <b>ACKNOWLEDGEMENTS</b>                | <b>iv</b>   |
| <b>APPROVAL SHEET</b>                  | <b>v</b>    |
| <b>SUBMISSION OF DISSERTATION</b>      | <b>vi</b>   |
| <b>DECLARATION</b>                     | <b>vii</b>  |
| <b>TABLE OF CONTENTS</b>               | <b>viii</b> |
| <b>LIST OF TABLES</b>                  | <b>xi</b>   |
| <b>LIST OF FIGURES</b>                 | <b>xii</b>  |
| <b>LIST OF SYMBOLS / ABBREVIATIONS</b> | <b>xiv</b>  |
| <b>LIST OF APPENDICES</b>              | <b>xvii</b> |

## **CHAPTER**

|            |  |           |
|------------|--|-----------|
| <b>1.0</b> | <b>INTRODUCTION</b>  | <b>1</b>  |
| 1.1        | Background of Research   | 1         |
| 1.2        | Problem Statement  | 5         |
| 1.3        | Objectives of Research   | 7         |
| 1.4        | Scope of Research Work   | 8         |
| 1.5        | Significance of Research   | 9         |
| 1.6        | Thesis Overview  | 10        |
| <b>2.0</b> | <b>LITERATURE REVIEW</b>   | <b>12</b> |
| 2.1        | Introduction   | 12        |
| 2.2        | Thermal Degradation, Flammability, and Flame Retardancy                  | 19        |
| 2.3        | Passive Fire-Protective Coatings   | 23        |
| 2.4        | Passive Fire-resistant Intumescent Coating                               | 24        |
| 2.4.1      | Relationships and interactions between acid, charring, and blowing agent | 29        |
| 2.4.2      | Intumescent Flame Retardants   | 30        |
| 2.4.3      | Intumescence Reactions   | 31        |
| 2.4.4      | Chemical Mechanism of Intumescence                                       | 33        |
| 2.4.5      | Physical Mechanism of Intumescence                                       | 36        |
| 2.5        | Intumescent Flame Retardants   | 38        |
| 2.5.1      | Acid Source  | 38        |
| 2.5.2      | Carbon Source  | 42        |
| 2.5.3      | Blowing Agent  | 43        |
| 2.5.4      | Binder   | 44        |
| 2.5.5      | Pigment  | 50        |
| 2.5.6      | Flame-retardant Mineral Fillers  | 51        |

|            |  |            |
|------------|--|------------|
| 2.6        | Intumescent Coatings incorporated with Natural By-Products                     | 57         |
| 2.6.1      | Intumescent Coatings formulated with Vegetable Compounds                       | 57         |
| 2.6.2      | Intumescent Coatings formulated with Rice Husk Ash                             | 60         |
| 2.6.3      | Intumescent Coatings formulated with Clam Shell                                | 62         |
| 2.6.4      | Intumescent Coatings Formulated with Chicken Eggshell                          | 65         |
| 2.6.5      | Intumescent Coatings Formulated with Hybrid Rice Husk Ash and Chicken Eggshell | 68         |
| 2.7        | Wood Ash Wastes and Their Physical and Chemical Properties                     | 74         |
| <b>3.0</b> | <b>RESEARCH METHODOLOGY</b>  | <b>85</b>  |
| 3.1        | Introduction   | 85         |
| 3.2        | Raw Materials and Their Properties   | 86         |
| 3.2.1      | Raw Materials Characterization   | 88         |
| 3.3        | Sample Preparation   | 95         |
| 3.4        | Experiment Test Methods for BioAsh Intumescent Coating                         | 97         |
| 3.4.1      | Brunauer-Emmett-Teller Surface Area Analysis (BET)                             | 99         |
| 3.4.2      | Fire Resistance Test (FRT)   | 99         |
| 3.4.3      | Carbolite Furnace Test (CFT)   | 101        |
| 3.4.4      | Weight Load Test (WLT)   | 102        |
| 3.4.5      | Thermogravimetric Analysis (TGA)   | 102        |
| 3.4.6      | Scanning Electron Microscopy Analysis (SEM)                                    | 103        |
| 3.4.7      | Energy-dispersive X-ray Spectroscopy (EDX)                                     | 104        |
| 3.4.8      | Instron Adhesion Test (IAT)  | 105        |
| 3.4.9      | Fourier-transform Infrared Spectroscopy (FTIR)                                 | 106        |
| 3.4.10     | Freeze-thaw Cycle Test (FTC)   | 107        |
| 3.4.11     | Static Immersion Bath Test   | 108        |
| 3.4.12     | X-ray Diffractometer (XRD)   | 109        |
| <b>4.0</b> | <b>RESULTS AND DISCUSSION</b>  | <b>111</b> |
| 4.1        | Characterisation of BioAsh   | 111        |
| 4.1.1      | BET Analysis   | 111        |
| 4.1.2      | Thermogravimetric Analysis   | 114        |
| 4.1.3      | Surface Electron Microscopy  | 118        |
| 4.1.4      | Fourier-Transform Infrared Spectroscopy  | 119        |
| 4.1.5      | Energy-dispersive X-ray Spectroscopy   | 121        |
| 4.1.6      | X-ray Diffractometer   | 123        |
| 4.2        | Fire Resistance Performance  | 126        |
| 4.3        | Carbonaceous Char Formation  | 130        |
| 4.4        | Char Strength  | 132        |
| 4.5        | Thermal Degradation Analysis   | 133        |
| 4.6        | Char Surface Morphology  | 136        |
| 4.7        | Pozzolanic Reactions and Antioxidation Properties                              | 138        |
| 4.8        | Molecular Functional Group Analysis  | 141        |

|            |                                       |            |
|------------|---------------------------------------|------------|
| 4.9        | Elemental Compound Analysis           | 145        |
| 4.10       | Adhesion Strength                     | 148        |
| 4.11       | Weather Resistance                    | 150        |
| 4.12       | Water Resistance                      | 152        |
| <b>5.0</b> | <b>CONCLUSION AND RECOMMENDATIONS</b> | <b>156</b> |
| 5.1        | Conclusions                           | 156        |
| 5.2        | Recommendations of Future Research    | 157        |
|            | <b>REFERENCES</b>                     | <b>159</b> |
|            | <b>APPENDICES</b>                     | <b>179</b> |

## LIST OF TABLES

| Table |  | Page |
|-------|--|------|
| 2.1   | The fundamental intumescence components and reactions  | 34   |
| 2.2   | Potential fire-retardant mineral fillers and the physical properties   | 54   |
| 2.3   | Fire-retardant mineral fillers and the contributions to heat absorbing effects   | 54   |
| 2.4   | Intumescent coatings using natural by-products, and their formula with the best performance in fire resistant and TGA test | 71   |
| 2.5   | The pH and CCE of different wood ash sources   | 74   |
| 2.6   | Wood ashes element total concentration   | 75   |
| 2.7   | Chemical reactions of wood combustion, hydration, and carbonization of wood ash compound                                   | 78   |
| 2.8   | Possible compounds existed in the wood ash suggested by XRD analysis   | 79   |
| 3.1   | Raw Materials, properties, and sources   | 85   |
| 3.2   | Potential physical and chemical properties of APP II   | 87   |
| 3.3   | Physical and chemical properties of Melamine   | 88   |
| 3.4   | Physical and chemical properties of Pentaerythritol  | 89   |
| 3.5   | Physical and Chemical properties of Titanium dioxide   | 90   |
| 3.6   | Physical and Chemical properties of Vinyl acetate copolymer  | 91   |
| 3.7   | Physical properties of Wood Ash  | 92   |
| 3.8   | BAIC samples formula   | 93   |
| 4.1   | BET analysis of BioAsh   | 108  |
| 4.2   | Primary elemental composition changes of original BioAsh and BioAsh after being wet-dried                                  | 118  |
| 4.3   | Elemental compounds present in BioAsh  | 121  |

|     |  |     |
|-----|--|-----|
| 4.4 | End temperatures of BAIC samples after the FRT   | 123 |
| 4.5 | Total weight of BAIC char layers can withstand in the weight load test   | 128 |
| 4.6 | Potential compound in BAIC samples, decomposition reaction and temperature   | 130 |
| 4.7 | Potential compounds and their reactions occurred during the hydration of BioAsh  | 134 |
| 4.8 | Potential mineral compounds present in the BioAsh and BAIC3-5 (after fire-resistance test) and their diffraction peak. | 143 |
| 4.9 | Results summary of all experiment works  | 150 |

## LIST OF FIGURES

| Figure |  | Page |
|--------|--|------|
| 2.1    | Emman's fire triangle  | 19   |
| 2.2    | Simplified combustion mechanisms   | 20   |
| 2.3    | The order of intumescent mechanism   | 25   |
| 2.4    | Swelling mechanism of intumescent coating  | 26   |
| 2.5    | Temperature of uncoated steel as compared to coated steel                          | 27   |
| 2.6    | The interactions between acid, charring, and blowing agent                         | 29   |
| 2.7    | Schematic diagram of intumescence reactions before and after the coating is heated | 31   |
| 2.8    | Chemical reactions involved in the intumescence                                    | 33   |
| 2.9    | Schematic diagram of physical mechanisms of intumescence                           | 35   |
| 2.10   | The condensation of phosphoric acid produced pyrophosphate structure               | 37   |
| 2.11   | The dehydration of alcohol group resulted in the carbon=carbon double bonds        | 38   |
| 2.12   | Ammonium polyphosphate (APP) structure   | 38   |
| 2.13   | Ammonium polyphosphate I (APP I) structure   | 39   |
| 2.14   | Ammonium polyphosphate II (APP II) structure                                       | 39   |
| 3.1    | Sieve Analysis of BioAsh   | 85   |
| 3.2    | Ammonium polyphosphate II (APP II) structure                                       | 86   |
| 3.3    | SEM surface micrograph of APP II   | 87   |
| 3.4    | The decomposition mechanism of APP to release ammonia and phosphoric acid          | 87   |
| 3.5    | Melamine structure   | 88   |
| 3.6    | SEM surface micrograph of Melamine   | 89   |

|      |   |     |
|------|---|-----|
| 3.7  | Pentaerythritol structure   | 89  |
| 3.8  | SEM surface micrograph of Pentaerythritol   | 90  |
| 3.9  | Titanium dioxide structure  | 90  |
| 3.10 | SEM surface micrograph of Titanium dioxide  | 91  |
| 3.11 | Vinyl acetate copolymer structure   | 91  |
| 3.12 | SEM surface micrograph of vinyl acetate copolymer   | 92  |
| 3.13 | Flowchart of water-based intumescent coating materials, samples preparation, experiment procedures and test methods | 95  |
| 3.14 | Brunauer-Emmett-Teller surface area analysis (BET)  | 96  |
| 3.15 | Fire-resistant Test   | 97  |
| 3.16 | Carbolite Furnace   | 98  |
| 3.17 | Weight Load Test  | 99  |
| 3.18 | Thermogravimetric Analysis  | 100 |
| 3.19 | Scanning Electron Microscope  | 101 |
| 3.20 | Energy-dispersive X-ray Spectroscopy  | 101 |
| 3.21 | Instron Universal Testing Machine   | 102 |
| 3.22 | Fourier Transform Infrared Spectroscopy   | 103 |
| 3.23 | Freezer and Universal Drying Oven   | 104 |
| 3.24 | Static immersion test   | 105 |
| 3.25 | X-ray Diffractometer  | 106 |
| 4.1  | Adsorption Isotherm linear plot of BioAsh   | 109 |
| 4.2  | BET surface area linear plot of BioAsh  | 110 |
| 4.3  | dV/dW Pore volume vs. Pore width  | 110 |
| 4.4  | TGA and DTG curves of original and hydrated BioAsh  | 111 |
| 4.5  | Cumulative weight loss curve vs. temperature of BioAsh (original) and BioAsh (wet-dried)                            | 112 |

|      |   |     |
|------|---|-----|
| 4.6  | TGA curves of APP, PER, MEL, TiO <sub>2</sub> , Binder, and BioAsh (original), BioAsh (wet-dried)                       | 113 |
| 4.7  | SEM of original BioAsh, wet-dried BioAsh  | 114 |
| 4.8  | FTIR peak of original BioAsh  | 115 |
| 4.9  | FTIR peak of wet-dried BioAsh   | 116 |
| 4.10 | Elemental composition changes of (a) original BioAsh and (b) BioAsh after being wet-dried                               | 118 |
| 4.11 | XRD Peak of BioAsh.   | 120 |
| 4.12 | Fire resistance test setup  | 122 |
| 4.13 | Fire-protective char layer of BAIC samples after the FRT  | 123 |
| 4.14 | Temperature profiles and standard deviations of unprotected and protected steels with BAIC samples after a one-hour FRT | 124 |
| 4.15 | After FRT: (a) BAIC 0-0, (b) BAIC 1-0, (c) BAIC 3-5, (d) BAIC 5-0, (e) BAIC 10-0  | 124 |
| 4.16 | Char thickness of BAIC samples after the CFT  | 126 |
| 4.17 | Thermogravimetric analysis (TGA) curves of BAIC samples   | 129 |
| 4.18 | Derivative thermogravimetric analysis (DTG) of BAIC samples   | 130 |
| 4.19 | Char morphology of BioAsh and BAIC samples  | 133 |
| 4.20 | BioAsh (original), BioAsh (wet), BioAsh (wet-dried), holding vertically from left to right                              | 135 |
| 4.21 | Oxygen and carbon composition, and O/C ratio of BAIC samples  | 136 |
| 4.22 | Infrared spectra of BAIC samples  | 137 |
| 4.23 | FTIR peaks of char residue of BAIC 0-0  | 138 |
| 4.24 | FTIR peaks of char residue of BAIC 1-0  | 139 |
| 4.25 | FTIR peaks of char residue of BAIC 3-5  | 139 |
| 4.26 | FTIR peaks of char residue BAIC 5-0   | 139 |



|      |  |     |
|------|--|-----|
| 4.27 | FTIR peaks of char residue of BAIC 10-0  | 140 |
| 4.28 | XRD Peak of BAIC 3-5 char (after fire resistance test)   | 142 |
| 4.29 | Crack charge and adhesion strength of BAIC samples   | 144 |
| 4.30 | After 70 cyclic tests: <b>(a)</b> BAIC 0-0, <b>(b)</b> BAIC 1-0, <b>(c)</b> BAIC 3-5, <b>(d)</b> BAIC 5-0 and <b>(e)</b> BAIC 10-0 | 146 |
| 4.31 | Water absorption rate of BAIC samples  | 148 |

## LIST OF SYMBOLS / ABBREVIATIONS

|   |                                    |
|---|------------------------------------|
| $\text{Al}_2\text{O}_3$                                       | Aluminium oxide                    |
| $\text{AlOH}_3$   | Alumina trihydrate                 |
| $\text{Al}_2\text{O}_3 \cdot 3\text{H}_2\text{O}$ (ATH)       | Alumina trihydrate                 |
| $\text{Al}(\text{OH})_3$                                      | Aluminium hydroxide                |
| $\text{Al}$   | Alumina                            |
| $\text{AlO}(\text{OH})$                                       | Boehmite                           |
| $A = \pi(d^2)/4$  | Surface area ( $\text{mm}^2$ )     |
| $\text{AlPO}_4$   | Aluminium phosphate                |
| $\text{Br}^-$   | Bromide ion                        |
| $\text{CaCO}_3$   | Calcium carbonate/ calcite         |
| $\text{Ca}(\text{OH})_2$                                      | Calcium hydroxide/ portlandite     |
| $\text{CO}$   | Carbon monoxide                    |
| $\text{CO}_2$   | Carbon dioxide                     |
| $\text{C}$  | Carbon                             |
| $\text{C}=\text{C}$   | Carbon-carbon bonding              |
| $\text{Cl}^-$   | Chloride ion                       |
| $-\text{C}=\text{O}$  | Ester carbonyl bond                |
| $-\text{C}-\text{O}$  | Ester bond                         |
| $\text{CaO}$  | Lime                               |
| $\text{Ca}_2\text{SiO}_4$                                     | Calcium silicate                   |
| $\text{C}-\text{S}-\text{H}/ \text{CaH}_2\text{O}_4\text{Si}$ | Calcium silicate hydrate           |
| $\text{C}\equiv\text{N}$                                      | Triple bonds nitriles and carbenes |
| $\text{C}=\text{C}$   | Aromatic ring                      |

|  |   |
|--|---|
| $\text{CO}_3^{2-}$   | Calcium carbonate ion                         |
| $\text{C}_3\text{H}_6\text{N}_6$   | Melamine                                      |
| $\text{C}_5\text{H}_{12}\text{O}_4$  | Pentaerythritol                               |
| $(\text{C}_2\text{H}_4)_n(\text{C}_4\text{H}_6\text{O}_2)_m$                     | Vinyl acetate copolymer                       |
| $\text{C} = \text{O}$  | Carbonyl group                                |
| $\text{—C—O}$  | Ester bond                                    |
| $\text{—C} = \text{O}$   | Ester carbonyl                                |
| $\text{CaAl}_2\text{O}_4$  | Calcium aluminates                            |
| $\text{Ca}_3(\text{PO}_4)_2$   | Calcium phosphate                             |
| $E_{\text{sw}}$  | Water uptake ratio                            |
| $\text{Fe}_2\text{O}_3$  | Ferric oxide                                  |
| $f_b$  | Adhesion strength (MPa)                       |
| $F$  | Maximum fracture load (N)                     |
| $\text{H}_2\text{O}$   | Water vapor                                   |
| $\text{HCl}$   | Hydrogen Chloride                             |
| $(\text{HPO}_3)_n$   | Metaphosphoric acid                           |
| $\text{K}_2\text{Ca}(\text{CO}_3)_2$   | Potassium and calcium carbonate/ fairchildite |
| $\text{LaFeO}_3$   | Lanthanum ferrite nanocrystalline             |
| $\text{Mg}(\text{OH})_2$   | Magnesium hydroxide                           |
| $\text{MoO}_3$   | Molybdenum trioxide                           |
| $\text{MgCO}_3$  | Magnesium carbonate                           |
| $\text{MgCO}_3 \cdot 3\text{H}_2\text{O}$  | Nesquehonite                                  |
| $\text{Mg}_5(\text{CO}_3)_4(\text{OH})_2 \cdot 4\text{H}_2\text{O}$              | Hydromagnesite                                |
| $\text{Mg}_3\text{Ca}(\text{CO}_3)_4$  | Huntite                                       |
| $\text{Mg}_6\text{Al}_{12}\text{CO}_3(\text{OH})_{16} \cdot 4\text{H}_2\text{O}$ | Hydrotalcite                                  |

|   |                           |
|---|---------------------------|
| Mg  | Magnesium                 |
| m <sup>2</sup> /g   | Specific surface area     |
| M <sub>8</sub> Si <sub>8</sub> O <sub>20</sub> (OH) <sub>8</sub>            | M-S-H                     |
| MgSiO <sub>3</sub>  | Magnesium silicate        |
| Mg <sub>3</sub> (PO <sub>4</sub> ) <sub>2</sub>                             | Magnesium phosphate       |
| NH <sub>3</sub>   | Ammonia                   |
| NaOH  | Sodium hydroxide          |
| Na(MnCa) <sub>2</sub> Si <sub>3</sub> O <sub>8</sub> (OH)                   | Serandite                 |
| (NaCa) <sub>2</sub> (FeMn) <sub>3</sub> Fe <sub>2</sub> (SiAl) <sub>8</sub> | Riebeckite                |
| (NH <sub>4</sub> PO <sub>3</sub> ) <sub>n</sub> (OH) <sub>2</sub>           | Ammonium polyphosphate II |
| NO <sub>3</sub> <sup>-</sup>  | Nitrate ion               |
| O–H   | Hydroxyl group            |
| (PO <sub>4</sub> ) <sup>3-</sup>  | Phosphate anions          |
| P <sub>2</sub> O <sub>5</sub>   | Phosphorus pentoxide      |
| P/P <sub>0</sub>  | Relative pressure         |
| P   | Phosphorus                |
| SiO <sub>4</sub> <sup>2-</sup>  | Silicate ion              |
| Si  | Silica                    |
| SiO <sub>2</sub>  | Quartz/ silicon dioxide   |
| TiO <sub>2</sub>  | Titanium dioxide          |
| TiP <sub>2</sub> O <sub>7</sub>   | Titanium pyrophosphates   |
| T <sub>Eq</sub>   | Equilibrium Temperature   |
| W <sub>e</sub>  | Wet weight                |
| W <sub>0</sub>  | Initial dry weight        |
| σ   | Standard deviation        |

| $\lambda$ | Wavelength  |
|-----------|---|
| AA        | Alkaline activator  |
| ABS       | Acrylonitrile-butadiene-styrene   |
| AFP       | Active fire protection  |
| APP       | Ammonium polyphosphate  |
| ASTM      | American Society for Testing Materials  |
| BAIC      | BioAsh Intumescent Coating  |
| BET       | Brunauer-Emmett-Teller  |
| BioAsh    | Rubberwood biomass ash  |
| BSPPO     | Bi(4-methoxy-1-phospho-2, 6, 7-trioxabicyclo [2.2.2]- octane-1-sulfide) phenylphosphate |
| CCE       | Calcium carbonate equivalent  |
| CEC       | Cation exchange capacity  |
| CES       | Chicken eggshell  |
| CFT       | Carbolite Furnace Test  |
| Chk       | Coffee husk   |
| CS        | Clamshell   |
| DTA       | Differential thermal analysis   |
| EDX       | Energy Dispersive X-ray spectroscopy  |
| ES        | Chicken eggshell  |
| EVA/IFR   | Ethylene-vinyl acetate intumescent flame-retardant                                      |
| EVA       | Ethylene-vinyl acetate copolymer  |
| FAO       | Food and Agriculture Organization   |
| FRT       | Fire Resistance Test  |

|            |  |
|------------|--|
| FSR        | Flame Spread Rate                                      |
| FTC        | Freeze-Thaw cycle                                      |
| FTIR       | Fourier- Transform Infrared                            |
| Ggp        | Ginger   |
| HRR        | Heat release rate                                      |
| IAT        | Instron Adhesion Test                                  |
| IC         | Intumescent coating                                    |
| ISO 5660-1 | International Organization for Standardization         |
| JCPDS      | Joint Committee on Powder Diffraction Standards        |
| MEL        | Melamine   |
| MFR        | Melt flow rate   |
| PA6T       | Poly hexamethylene terephthalamide                     |
| PER        | Pentaerythritol  |
| PFP        | Passive fire protection                                |
| RH         | Rice husk  |
| RHA        | Rice husk ash  |
| SDG        | Sustainable Development Goal                           |
| SEM        | Surface Electron Micrograph                            |
| SF         | Silica fume  |
| SIB        | Static Immersion Bath                                  |
| SIRIM      | Standard and Industrial Research Institute of Malaysia |
| SOP        | Standard operating procedures                          |
| SSA        | Silicone acrylate                                      |
| TGA        | Thermogravimetric Analysis                             |
| THEIC      | Tris hydroxyethyl isocyanurate                         |

|      |   |
|------|---|
| THR  | Total heat release                      |
| TPP  | Triphenyl phosphate                     |
| TTI  | Time to ignition                        |
| USDA | United States Department of Agriculture |
| VAC  | Vinyl acetate copolymer                 |
| VOCs | Volatile organic compounds              |
| WLT  | Weight Load Test                        |
| XRD  | X-ray Diffractometer                    |
| ZnP  | Zinc phosphate                          |

## LIST OF APPENDICES

| Appendix |  | Page |
|----------|--|------|
| A        | Table of TGA and DTA Results of BioAsh.                                | 174  |
| B        | Table of TGA Results of BioAsh, VAC, APP, PER, MEL, TiO <sub>2</sub> . | 174  |
| C        | Diagrams of EDX Results of BioAsh.                                     | 175  |
| D        | Table of TGA Results of BAIC samples.                                  | 176  |
| E        | Table of DTG Results of BAIC samples.                                  | 176  |
| F        | Table of Oxygen and Carbon Composition Results of BAIC samples.        | 177  |
| G        | Table of Crack Charge and Adhesion Strength Results of BAIC samples.   | 177  |
| H        | Table of Water Resistance Test Results of BAIC samples.                | 177  |
| I        | List of Publications.  | 178  |



# **CHAPTER 1**

## **INTRODUCTION**

### **1.1 Background of Research**

Fire safety rules and regulations in buildings are important to reduce deaths and injuries (Harada, 2018; Prabir, 2018; Sigmann, 2018; Altarawneh et al., 2019). Fire resistance efficiency of building structural system is very crucial to save human lives. Many precedents reported a huge loss of precious human lives and assets in fire accidents (Prabir, 2018; Sigmann, 2018). From the statistics, 96.47% of these fire accidents were caused by electrical faults, neglections and lacking fire safety knowledge reported by the Fire and Rescue Department Malaysia in 2017. The high risks and threats of fire to human assets have driven the research inventions and innovations of more effective products and reliable approaches for fire protections. Fire resistance, combustibility, flammability, and toxicity of materials are underpinning concerns of the fire safety (Bal, 2018; Kobes et al., 2010). Fire resistance of materials is the key fire safety measure in building design and construction industry.

In a fire event, flame temperature could vary from 600 °C to 1500 °C, depending on the combustion types of material, fuel, and oxygen level of the indoor condition. Steel is a major component used in the building structural system such as wall, column, beam, and roof. Steel structure will become ductile, deform, and collapse eventually when it reaches the critical temperature of 500 °C and above in a fire accident. This is due to the disappearing of strength in steel (Jimenez et al., 2006; Farkas and Jarmai, 2008; Clarke, 2014). Two fire protection systems namely active fire protection (AFP) and passive fire protection (PFP) measures are

engaged in the real-life practises to secure buildings, structures, human lives, and assets from fire damages. AFP systems perform as the first phase of fire defence. Smoke detection alarm, water sprinkles system, fire detection alarm, and fire extinguisher are among the example of AFP. This AFP equipment employs mechanical mechanism and require electricity and motion to actively function. PFP systems perform as the second phase of defence against fire. There are two types of PFP, group as non-reactive and reactive categories. Non-reactive PFP help to hinder the spreading of fire through compartmentalisation. These compartmentalisations are created using building components such as fire panel made of fire-resistant materials such as gypsum, calcium silicate, magnesium hydroxide and cementitious mortar to limit the fire spreading from one space across another to delay fire damage to the entire property. Fire wall and fire door fall under the non-reactive category of PFP system.

Fire resistive intumescent coating applies onto the steel surface fall under the reactive category (Panias et al., 2015; Sutton, 2017). Intumescent coating is developed to apply onto the steel surface as a fire protective barrier to extend the life span of steel structure during a fire event (Xu et al., 2019). The period of emergency evacuation can be lengthened to save more human live when the integrity of steel structures is retained. When the intumescent coating is exposed to extremely high temperature fire, it will swell and form a multi-cellular carbonaceous char barrier to constraint further heat transfer to the steel substrate, hence delay the steel substrate from reaching the melting point (Mustafa et al., 2017). Intumescent refers to the swelling of coating, physical changes that caused by the chemical reactions between flame retardant additives, binder and fillers when exposed to high temperature heat (Camino et al., 1989; Camino et al., 1990). The reaction of fire protective intumescent coating involves three major stages: (1) the decomposition of coating substances; (2) the release of inert gases; (3) the formation and expansion of char layer that subsequently limit the heat transmittance to steel structure (Jimenez et al., 2006; Gu et al., 2007; Toro et al., 2007). Many research have been

conducted to study the effects of different intumescent coating composition, flame retardant additives and fillers characterisation, swelling mechanism, physical and chemical properties (Anna et al., 2001; Ramazani et al., 2008; Han et al., 2010; Li et al., 2012; Fan et al., 2013; Li et al., 2015; Aziz and Ahmad, 2016; Wang and Zhao, 2019). Intumescent coatings have recently garnered more attentions particularly from the building and construction sectors because of its reliable and efficient fire protective performance (Mariappan, 2016; Lucherini and Maluk, 2019).

Intumescent coatings have been applied as passive fireproof protection to steel structures in buildings for more than 20 years. The main function of intumescent coating is to protect the steel structure from fire damage through the generation of char barrier. Severe fire will ultimately lead to the loss of material strength and collapse of the whole steel structure without preventative measures. When expose to high heat fire, intumescence mechanism happens. Intumescent coating will swell and expand to form a carbonaceous char layer with thickness up to 100 times more than the existing original thickness (min. 1 mm to max. 100 mm thick) of the intumescent coating. This thick carbonaceous char barrier performs to block the heat transfer from reaching the steel substrate. In such case, carbonaceous char barrier shields the steel from reaching its critical temperature of 500 °C to maintain the steel structural integrity in a fire event. Hence, the safety of human lives, assets and buildings are assured (Horacek and Pieh, 2000).

An increasing application of intumescent coatings is noticed especially in buildings that demand a higher level of fire protection such as multi-storey buildings, stadiums, skyscrapers, high-rises, and steel work constructions. Intumescent coatings provide good fire ratings and surface finishes become popular as passive fire protection system among these major buildings. Enhanced char quality such as smaller char cell size, stronger char cell structural strength can extend the fire protection timeframe to steel substrates, even in higher floor with intense

velocity of wind. In the past, most of the intumescent coatings used were inorganic formulated using soluble alkali silicates because of the low price. Nonetheless, drawbacks like poor water resistance and durability were observed and remained as serious issues. Thin film intumescent coatings that are organic take over as the favourable option as they offer higher aesthetic and better performances. In common, an organic intumescent coating comprises the main ingredients as follows:

- (a) An acidification agent such as ammonium polyphosphate (APP)
- (b) A carbonizing agent such as pentaerythritol (PER)
- (c) A blowing agent such as Melamine (MEL)
- (d) A binding agent such as epoxy and polyvinyl acetate

Thin film intumescent coatings (organic coatings) swell and expand to form a carbonaceous char layer with certain thickness when they are subjected to fire. Other application of thin film intumescent coatings is such as to apply as topcoat surface finish in outdoor environment. Thin film intumescent coatings are associated with additional benefits for example, they have a higher degree of flexibility and aesthetic, and easy to apply. However, thin film intumescent coatings are found with challenges such as lead to weak and fluffy char layer. These fluffy char layers will easily dislodge under high wind pressure, restrict, and decline the fire protection timeframe to steel substrates.

Conventional intumescent coatings consist of binder, three main flame-retardant additives: APP, MEL, and PER, and flame-retardant mineral fillers. The mechanism of intumescent coating is attributed to the reaction of binder, flame-retardant additives, and mineral fillers upon heating (Anees and Dasari, 2018). Intumescent coatings have been used as passive fire protection design measures in building industries specially to protect steel structures from fire damage (Bourbigot et al., 2004). Flame-retardant intumescent coating can ensure the structural

integrity by providing a protective barrier to building material from reaching its critical temperature when exposed to fire. Intumescent coating can delay the propagation of fire and offer enough time for the safe evacuation of occupants during a fire incident (Zia-ul-Mustafa et al., 2017). The fire-protective mechanism of intumescent coating is working via the formation of uniform multicellular char layer, with the ability to delay the speedy heat transfer to building structure.

## **1.2 Problem statement**

Flame retardant mineral fillers are inert and non-combustible. The incorporation of mineral fillers into the intumescent coating can minimize the flammability, through the reduction of fuel amount, and oxygen diffusion rate in the coating polymer. Mineral fillers can increase the capacity of heat, conductivity, reflectivity, and emissivity of thermal. These reactions involve the catalytic of antagonism and synergism, surface effects, and melt rheology of polymers link to mineral fillers (Hull et al., 2002; Rothon, 2003). Flame-retardant fillers such as aluminium hydroxide ( $\text{Al}_2\text{O}_3$ ), alumina trihydrate ( $\text{Al}(\text{OH})_3$ ), magnesium hydroxide ( $\text{Mg}(\text{OH})_2$ ), calcium carbonate ( $\text{CaCO}_3$ ) are among the inert mineral fillers in the intumescent coating composition. The addition of mineral fillers can reduce the use of polymer (hydrocarbon) in the intumescent coating, and there are no adverse effects associated with smoke toxicity, human health and environment reported (Hull et al., 2005).

Fire protective intumescent coatings are not widely applied in most of the buildings in Malaysia as compared to those active fire protection system such as water sprinklers, smoke detection alarms, and fire extinguishers. In general, people are lacking information, and knowledge about the fire-resistant performance of intumescent coating how it can help to block the fire spread and to protect the building structures. The application of intumescent coating is

expensive and will incur additional costs to the building. The cost of fire-protective intumescent coatings is generally higher due to the industrial materials used to formulate it. Flame-retardant fillers such as aluminium hydroxide ( $\text{Al}_2\text{O}_3$ ), magnesium hydroxide ( $\text{Mg}(\text{OH})_2$ ) and calcium carbonate ( $\text{CaCO}_3$ ) in the intumescent coating composition are industrial manufactured fillers. Numerous studies have been conducted to investigate the use of various by-products such as chicken eggshell (aviculture wastes), rice husk ash (agriculture wastes) and clamshell (aquaculture wastes) as mineral fillers in the intumescent coatings (Yew et al., 2018; Khairunisa et al., 2020; Li et al., 2020). In line with the sustainable movement and Sustainable Development Goals (SDG- 17) of the United Nations, global research is shaping towards the sustainable inventions and innovations in various disciplines. Many on-going studies in building and construction materials, green infrastructures & technologies are constantly innovated with sustainable ideas and approaches. For instance, in the field of fire-protective intumescent coating, the incorporation of reusable and renewable by-product materials in the intumescent coatings are invented (Azadeh et al., 2018; Almiron et al., 2019; Khairunisa et al., 2020; Zhan et al., 2020).

BioAsh is a low-cost agricultural by-product waste derived from the fuel combustion of rubberwood (hardwood) biomass. The rubberwood will be logged down once its latex production life cycle ended. This lodging activity led to the leftover of readily available rubberwood biomass that will be sent to local factories to use as fuel materials. Combustion of rubberwood biomass in factories generate abundance of ash waste which will be dumped into landfill, leach into the soil and water eventually contaminate and hazard the environment. It is essential and urgent to search for alternative re-use of this ash waste to conserve the environment in a more sustainable way. This research serves to explore the potential use of rubberwood biomass ash (BioAsh) waste in intumescent coatings in relation to fire-resistance and mechanical properties. Thermal, physical, and chemical properties of BioAsh were

characterized. Physical and chemical properties of coating samples incorporated with BioAsh were studied. Intumescent coatings developed and investigated in this research contribute to the knowledge gap about the role of BioAsh (rubberwood biomass ash waste) as natural mineral fillers substitute in the intumescent mechanism of water-based fire protective coating contributing to ground toward a more sustainable and resilience environment.

### **1.3 Objectives of Research**

The aim of this research is to develop a water-based intumescent coating incorporated with BioAsh as the natural substitute of mineral fillers. BioAsh is a low-cost agricultural waste derived from the fuel combustion of rubberwood biomass. The incorporation of BioAsh into water-based intumescent coating generates an alternative reuse of this agricultural by-product to lessen the burden of environmental wastes. The BioAsh Intumescent Coating (BAIC) developed in this research presents a green invention that fulfils the requirements of fire protection. The formulations of BAIC samples comprise of vinyl acetate copolymer as water-based binder, flame-retardant additives, white pigment and BioAsh as mineral fillers.

Based on the aim, several specific objectives are outlined as follows:

- a) To formulate the water-based intumescent fire-resistant coating samples incorporating with BioAsh.
- b) To characterise the thermal, physical, and chemical properties of BioAsh
- c) To evaluate the fire protection, thermal, chemical, physical, and mechanical properties of BioAsh intumescent coating samples.

## 1.4 Scope of Research Work

A series of experimental works were carried out to achieve the objectives outlined in this research. Three main flame-retardant additives namely, Ammonium polyphosphate: APP (an acid source), Melamine: MEL (a blowing agent), Pentaerythritol: PER (a carbon source); binder: water-based vinyl acetate copolymer (VAC); white pigment: titanium dioxide ( $\text{TiO}_2$ ) and mineral filler: BioAsh were used to formulate the BioAsh intumescent coating samples (BAIC). The BioAsh and coating samples were characterised through a series of twelve testing methods: fire-resistance, physical, chemical and mechanical tests: Brunauer-Emmett-Teller (BET), Fire Resistance Test (FRT), Carbolite Furnace Test (CFT), Weight Load Test (WLT), Thermogravimetric Analysis (TGA), Surface Electron Micrograph spectroscopy (SEM), Energy Dispersive X-ray spectroscopy (EDX), Instron Adhesion Test (IAT), Fourier-Transform Infrared spectroscopy (FTIR), Freeze-Thaw cycle (FTC) and Static Immersion Bath (SIB), and X-ray Diffractometer (XRD).

The specific surface area of BioAsh particles was determined using BET. The properties of BioAsh were further characterised via TGA, SEM, EDX, FTIR, and XRD. It is crucial to understand the properties of BioAsh and how it will have impacts as mineral filler in BAIC samples. The fire-resistant performance of how effective the BAIC samples can protect the steel from reaching critical temperature when exposed to fire was revealed. Carbonaceous char layers were formed when the BAIC samples were exposed to fire. It was essential to understand the transformation of physical structure of the BAIC samples before and after exposed to fire. Char strength revealed how solid and strong the char layer can sustain for a longer period. Surface morphology of char layers was examined in SEM. Char topography, cavities, inner structures were revealed in surface micrographs. Thermal stability of BAIC sample justified the effectiveness of thermal insulation properties of BAIC samples in limiting



the heat transfer to steel substrate. Appropriate adhesion strength of coating samples to steel was effective to prolong the fire protection.

It is important to understand what are the functional groups and molecular bonding that contribute to the performances of BAIC samples. The physical stability of BAIC samples when exposed to drastic changes in temperature and water over a specified timeframe was revealed. Thermally stable compounds formed in the char of BAIC 3-5 after the FRT were revealed in X-ray Diffractometer (XRD). It is important to understand and identify what type of thermally stable compounds contribute to the most promising fire resistance performance in BAIC 3-5.

## **1.5 Significance of Research**

The significances of this experimental research are as follows:

1. Formulating water-based fire-protective intumescent coating via the alternative reuse of BioAsh as natural substitute of industrial mineral fillers to achieve environmental conservation.
2. Characterisation of the physical and chemical properties of BioAsh for its suitable use in the water-based fire-protective intumescent coatings, which has not been done in any previous and current research.
3. Developing BioAsh Intumescent Coatings (green coatings) that contribute toward the enhancement of fire-resistance and mechanical performances that are compatible with others bio-based water intumescent coatings.
4. Green coating of this research is working in aligned with SDG 17 goals to realise a more sustainable environment and better living quality for the current and future generations.

## 1.6 Thesis Overview

This thesis comprises of five chapters. **Chapter 1** presents the research background, problem statement, research objectives, research scope, and significance of this research. **Chapter 2** describes literature review, the concept of thermal degradation, flammability, and flame-retardancy, passive fire protective systems, fire-resistant intumescent coatings and their chemical and physical intumescence reactions, intumescent flame retardants, intumescent coatings incorporated with natural by-products, wood ash wastes and their physical and chemical properties. **Chapter 3** explains the details of research methodology conducted in this research. The source of materials and their properties, characterisation of BioAsh, samples preparation methods, the type of experimental tests and techniques were described. **Chapter 4** reveals the quantitative and qualitative results. The analysis of intumescent coating samples after a series of experiment investigations were implemented. The performances of fire resistance, char formation, char strength, char surface morphology, thermal degradation, pozzolanic and antioxidation properties, cross-linking molecular functional groups, elemental composition, thermally stable compounds, adhesion strength, weather and water resistance were discussed. This chapter forms the overall discussions of all research data obtained. **Chapter 5** presents the conclusion and recommendations of this research. Research results are summarised and concluded in this chapter. Recommendations are proposed for potential future investigation and enhancement of this research.

## **CHAPTER 2**

### **LITERATURE REVIEW**

#### **2.1 Introduction**

An overview of previous research done in the field of fire protection, fire protection systems, fire-retardant materials, fire-protective intumescent coatings for steel, intumescent ingredients, intumescence mechanisms, intumescent coatings incorporated with natural by-products, properties of wood ash waste were studied. Flame-retardant additives, mineral fillers, pigments, binders found in the literature pool were studied and summarised in tables. Physical and chemical mechanisms of intumescent coating when exposed to heat were reviewed. Intumescent coatings incorporated with by-products and their performances were summarised. This overview of literature review is useful to ground the research of developing fire-protective intumescent coating incorporated with BioAsh in this thesis.

In nature, fire event can be devastative and bring huge risks to human lives and assets. A severe fire can lead to fatal injuries, death, and damaging of possessions. More attentions are focused on the rules and regulations of fire safety in recent years. There are increasing requirements and demands to minimise the risks associated with fires, mainly caused by combustible materials such as textiles, plastics, woods (Saxena and Gupta, 1990), and the loss of material structural strength such as steels (load bearing structure). Novel materials and solutions are continuously being explored in the research to advance the current stage of applications to prevent the flame propagation, and risks of hazardous fire as minimum as possible. Original materials that are intrinsically flame-retardant or modified materials imposed with flame-retardant properties for example, coatings, intumescent coatings, and composites

are among the applications to protect human and assets from fire (Bourbigot and Duquesne, 2007). Countries, governments, agencies around the world have come out with a series rules and regulations, by-laws, and standard operating procedures (SOP) to safeguard human lives and assets in any fire events. Education to the public is essential as one of the precautions measures to prepare them how to prevent and respond to fire if any fire outbreaks happen. Fire preventative solutions are as follows (Puri and Khanna, 2017):

- (a) ***Prevention of fire through awareness***: For example, educations on fire safety, fire drills and emergency evacuation, and responses to fire services.
- (b) ***Active fire protection system***: This method involving active actions and mechanisms to quench the fire, engaging with firefighting systems such as fire extinguishers and water sprinklers, and smoke detection alarms.
- (c) ***Passive fire protection system***: This method indicating the use of fire-resistant materials, fire-resistant coatings, intumescent coatings, structure with modified fire-rating to inhibit and suppress the combustion and spread of fire.

Steel structure is a major component use in the building and construction industries nowadays, especially in industrial buildings and high-rises. Steel is a popular material among construction professionals. This due to its flexibility in design and fabrication that allows the construction of a single to multi-storey high structures to be done in rapid and efficient way. Steel is safe to use and not susceptible to mild flame in common. Nevertheless, when there is a severe fire outbreak, continuous burning of fire reaches temperature of more than 500 °C can weaken the mechanical strength of steel. The melting point of steel is defined as 500 °C and above. In this case, the steel structure will start to lose its ductility and more than 50% of its load bearing capacity under the pressure of high temperature fire. Eventually, the entire bare steel structure will collapse after it loses all the material strength completely. Hence, it is crucial to consider the fire safety of steel structure when designing a building particularly in high-rise

to minimise the associated fire risks. Passive fire protection measure using intumescent coatings is one of the effective solutions to block flame and heat transfer to steel, and hence protect the steel from ductile and collapse due to fierce fire. Fire protective intumescent coatings can inhibit the fire spread, extend the lifespan of steel, and permit a longer duration of emergency evacuation for building residents.

Cementitious materials are the traditional type of passive fire protective ‘coatings’ or ‘fireproof barriers’ used in the buildings. In general, these cementitious materials are categorised into two major groups: dense and lightweight fireproof cementitious coats. Dense concretes are created from the curing of Portland cement, hence associated with higher density in weight. Lightweight concretes are produced by mixture with other materials such as foaming agent, vermiculite, perlite, gypsum, lightweight expanded clay aggregates, and other fillers and binders to reduce the density and to enhance the overall performances. These cementitious coatings are applied through spraying onto the structures up to a few inches thick to form a fireproof coating on the substrate surface. When expose to fire, these cementitious materials provide thermal insulation and the evaporation of moisture inside help to cool down the surrounding.

Cementitious materials are low-cost and easily available. Nonetheless, their challenges in weight, thickness, poor aesthetics, and mechanical strength have been highlighted. It is because of the poor aesthetic of the spraying fireproof cement, architectural professionals disincline to apply it onto building structures such as steels that are visually disclose (Challener, 2007). Meantime, cementitious materials have a higher tendency to crack and dislodge from the substrate when facing violent fire. Their undesirably poor surface finish (low visual aesthetic) permits the penetration of more moisture. Absorption and accumulation of higher level of moisture in the cementitious coatings give rise to the corrosion of steel substrates, therefore, restrict its overall performances (Mike Reed, 2015). Nowadays, synthetic polymers

are widely used in many applications such as electronics, buildings, insulation materials, furniture, and transportation in the household, working and travelling environments exposed human lives and assets to the flammability- fire risk (Shaw et al., 2010; Hull et al., 2011). Various flame retardants have found to be increasing in the numbers of usage to prevent the flammability (Hull et al., 2011). The fire retardants consumption are estimated to raise from \$5.8 bn (2008) to \$6.9 bn (2023) over the next 5 years (BCC Research, 2018).

Vinyl acetate-ethylene copolymer (VAC) emulsion was chosen as the binder due to its more eco-friendly, less flammable and a lower level of VOCs contents as compared to the solvent-based binder. It is also less hazardous and harmful to the environment and can offer good adhesion strength and humidity resistance (Amir et al., 2011). However, direct, and continuous exposure of VAC binder to moisture will affect its chemical bonding and weakens the adhesion strength (Duquesne et al., 2004). The binder used in the intumescent coating is crucial because it assists in the expansion of char and ensures the formation of a uniform char foam layer, which acts as an insulating layer to protect the steel substrate (Duquesne et al., 2015; Yang et al., 2019). Hydrophilic fire-retardant additives such as ammonium polyphosphate (APP) and pentaerythritol (PER) in the intumescent coating are sensitive to corrosive components like water, acid, and alkali. These additives could easily migrate to the coating's surface when exposed to a corrosive environment. These phenomena will significantly suppress the performance of intumescent coating. VAC copolymer binder used in the intumescent coating can limit the migration of flame-retardant additives from migration and in accessing to the corrosive substances (Wang and Yang, 2010; Yew and Sulong, 2012; Yew et al., 2014).

An acidifying agent are such as inorganic acid, acid salt or other acids that elevate the dehydration of carbonizing agent, for example Ammonium polyphosphate (APP). Pentaerythritol (PER) is a carbonizing agent which is a type of carbohydrate that will be

dehydrated by an acid source to become a char. Melamine (MEL) is a blowing agent that will decompose to release gases resulting in the increment of polymer's volume and the formation of a swollen multi-cellular char layer to protect the steel underneath from fire (Laoutid et al., 2009). This will tremendously reduce the structural degradation of buildings during fire events. Industrial pigments and mineral fillers such as titanium dioxide, magnesium hydroxide and aluminium hydroxide are vital flame-retardant ingredients added into intumescent coating to enhance the fire-resistance performance.

There is no adverse effect reported on toxic smoke leading to deaths or injuries in fire using flame-retardant mineral fillers. The decomposition temperature of flame-retardant fillers to polymer is important to optimize the use of mineral fillers. Factors such as the coherency of the residual layer and its tendency to reconduct thermal emission are also needed to be considered (Hull et al., 2011). Solvent-based intumescent coating is less subjected to environmental changes such as humidity and temperature as compared to water-based intumescent coating. Nonetheless, volatile organic compounds (VOCs) associated with the solvent-based coating have raised environmental concerns and motivate more research to further investigate the potential of water-based intumescent coatings as alternatives which are less hazardous.

Flame-retardant mineral fillers such as calcium carbonate ( $\text{CaCO}_3$ ), aluminium hydroxide ( $\text{Al}(\text{OH})_3$ ) and magnesium hydroxide ( $\text{Mg}(\text{OH})_2$ ) possess good filling property vitally contribute to a more compact char that better insulate the steel from reaching its critical temperature. Even though mineral fillers share a lower weight proportion in the composition of intumescent coating, the positive impacts to the fire-resistant and mechanical properties of char layer formed are significant. Many research findings indicate the reinforcement of waste such as rice husk ash and eggshell can enhance the intumescent coating in various aspects such as a lower equilibrium temperature in burning, delay in fire spreading, and better char strength.

Conventional intumescent coatings reported an average equilibrium temperature between 160 °C to 190 °C (epoxy-based) and 220 °C to 290 °C (water-based) when the steel substrate was exposed to 1000 °C of heat in a fire test (Yew et al., 2015a; Khairunisa et al., 2020; Li et al., 2020). Studies have been conducted to explore the potential use of aviculture waste (eggshell), agriculture waste (rice husk ash), aquaculture waste (clam shell) and crop-based biomass (ginger powder and coffee husk) to produce eco-compatible intumescent coating formulations with enhanced fire-resistant performance (Yew et al., 2015b; De Sa et al., 2017; Khairunisa et al., 2020; Li et al., 2020). These studies of using natural-based fillers in the intumescent coatings reported various improvements in the fire-resistant properties. Equilibrium temperature of water-based intumescent coatings using eggshell (160 °C to 260 °C), rice husk ash (180 °C to 220 °C), and clam shell (136 °C) was reported (Yew et al., 2018; Khairunisa et al., 2020; Li et al., 2020).

Epoxy resin intumescent coatings formulated with crop-based carbon source can block the transfer of fire heat to steel and maintain the steel temperature at 130 °C to 150 °C (De Sa et al., 2017).  $\text{CaCO}_3$  in eggshell/clamshell, lignin in the ginger and coffee powder respectively were found to be the main components (Li et al., 2020; Yew et al., 2018; De Sa et al., 2017). These components in eggshell, clamshell, ginger and coffee powder have reported with enhancements in the thermal stability and char strength of intumescent coatings. It is noteworthy to investigate the potentials of BioAsh (rubberwood biomass ash) that is a local source in Malaysia to be renewed as natural mineral fillers in developing an environmentally friendly water-based fire-protective intumescent coating. Currently, limited data can be found in the literature pools concerning the use of BioAsh in water-based intumescent coating formulation.



Malaysia is the fifth largest rubber producer and exporter in the world, with rubber plantations occupied approximately 1.07 million hectares land areas in the country (Natural Rubber Statistic, 2018; Rubber Asia, 2020). BioAsh is a type of by-product derived from the combustion of rubberwood biomass in a fuel factory located in Sitiawan, Perak, Malaysia. Rubber tree, scientifically known as *Hevea brasiliensis*, is a type of hardwood species grow in the tropical climates. The rubber tree is renowned for the mass cultivation of latex production in agriculture commercial market. Rubberwood biomass is a leftover from the rubberwood logging activities after the rubber trees ended the life cycles of latex productions. The rubberwood biomass is readily supply to local factories to use as biofuel. Combustion of rubberwood biomass generated large amount of rubberwood ash as waste.

This ash wastes will be dumped into landfill put on extra burdens to the environment if these wastes are not put into proper usage (Demeyer et al., 2001). Properties of wood ash vary depending on the wood species, part of wood, condition of soil, burning rate and temperature. This far, the knowledge on the utilisation of BioAsh in the water-based intumescent coating is limited. The effects of BioAsh on fire-resistant properties of intumescent coating is not well-known. This research seeks to explore the fire-resistant properties of BioAsh incorporated water-based intumescent coating.

In general, wood-based ash are identified with several minerals, such as carbon (C), calcium (Ca), potassium (K), magnesium (Mg), phosphorus (P), and sodium (Na) (Tarun et al., 2003). Wood ash is identified with compounds such as silicon dioxide ( $\text{SiO}_2$ ), aluminium hydroxide ( $\text{Al}(\text{OH})_3$ ), ferric oxide ( $\text{Fe}_2\text{O}_3$ ), calcium oxide (CaO), magnesium oxide (MgO), titanium dioxide ( $\text{TiO}_2$ ), potassium oxide ( $\text{K}_2\text{O}$ ) and sulfur trioxide ( $\text{SO}_3$ ). Most of the decomposed elements possess high thermal degradation after the pyrolysis. Hemicellulose, cellulose, and lignin were reported in plant-based materials and their thermal degradation are

varied (Waters et al., 2017). Wood ash is rich in pozzolans and has been used as partial cement replacement for building materials in the construction industries. A pozzolan is a material rich in silica ( $\text{SiO}_2$ ) and alumina ( $\text{Al}_2\text{O}_3$ ) that will react with calcium hydroxide  $\text{Ca}(\text{OH})_2$ , forming a cementitious-like compound in the presence of moisture (ASTM C 618-05, 2005).

The physical and chemical properties of wood ash are varying and depending on factors such as wood species, type of wood, combustion method, combustion temperature and soil condition. Combustion of hardwood tree species will obtain more ashes than softwood species. The yield of wood ash will decrease when the burning temperature is raising. Many types of research have been done to examine different mix proportion of binders, flame-retardant additives, and mineral fillers to enhance the fire resistance performance of intumescent coatings (Ramazani et al., 2008; Suardana et al., 2011). In this research, BioAsh was incorporated as natural mineral filler substitute to replace the use of industrial mineral fillers in the intumescent coating. Performances of fire resistance, thermal, physical, chemical, and mechanical properties of intumescent coatings incorporated with BioAsh were evaluated and examined.

## **2.2 Thermal Degradation, Flammability, and Flame retardancy**

When expose to heat, organic and inorganic compounds degrade and decompose thermally. Fire is a process of oxidative and with the emission of light and heat. Flame refers to the light (visual sign) emit from the combustible materials, and it is an indication of heat during the combustion process. Combustions generally happen in gas phase. In gas phase, volatile combustible compounds oxidize exothermically. Glowing or afterglow combustion is a non-gas phase combustion, that the substrates oxidize in the condense phase forming both gaseous and solid products. These normally take place right below the material's ignition temperature, for example the carbon residue of a carbon-rich polymer material oxidizes in the solid phase.

Fire process illustrates in Emman's fire triangle (Wolf and Lal Kaul, 1992) as shown in **Figure 2.1**. Fire required three major elements to sustain (Sutker, 1988), namely (i) the fuel (a carbon rich, volatile, combustible substance), (ii) the heat (generated by the exothermic degradation of fuel), (iii) the oxidizing agent (oxygen in the air).

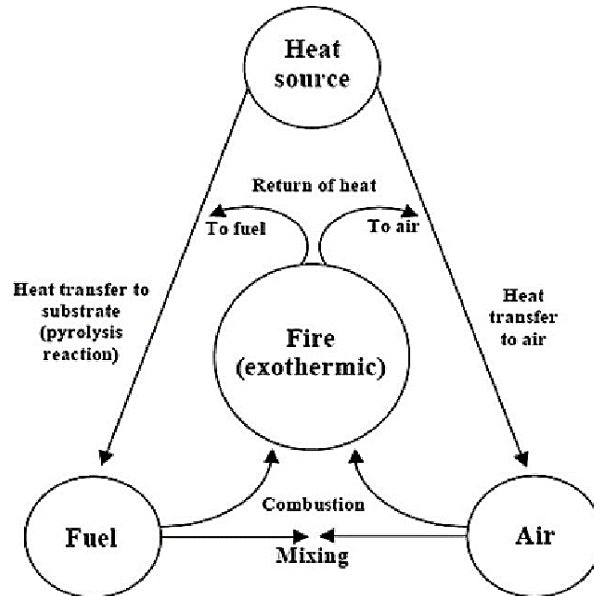


**Figure 2.1:** Emman's fire triangle (Wolf and Lal Kaul, 1992).

Polymeric materials release small number of volatile compounds that act as fuels during thermal decomposition. Meantime, these combustible substances will react with oxygen in the air to create ignitable mixture. The material burned when the exothermic oxidation happens, light and heat (flame) are generated. The fire become self-sustaining if this combustion feedback loop is repeated (**Figure 2.1**). Fire combustion of different substances varied in terms of gases products released. The combustion of polymers produces primarily carbon monoxide (CO), carbon dioxide (CO<sub>2</sub>), water vapor (H<sub>2</sub>O), with carbon (C) and ash (metal oxides) residues (Sutker, 1988; Wolf and Lal Kaul, 1992).

Flame retardant system refers as a compound put onto a certain substrate to resist the combustion of that substrate. The flame-retardant system is considered effective if it can limit one or more elements required for the sustain of fire such as fuel, heat, and oxygen (Sutker,

1998). The fire-retardant system is designed to reduce the combustibility of a material, through lowering the combustion rate and spread of flame in fire. The fire-retardant system can prevent the growth of spark from turning into destructive fire, hence, minimize the fire risks to human and assets (Benbow, 1987; Green 1996). According to Schmidt 1965, an effective flame-retardant system shall be able to interrupt the degradation of host polymer, by interacting at the degradation temperature of that host polymer. Most polymers degrade at temperature between 200 °C to 400 °C (Pearce, 1986). Several mechanisms involve in combustion, flame retardancy, and how fire resistance can be achieved as illustrated in **Figure 2.2** (Focke et al., 1997). Combustion can be interrupted and prevented at the gas phase (oxidation flame zone), or at the condensed and solid phase.

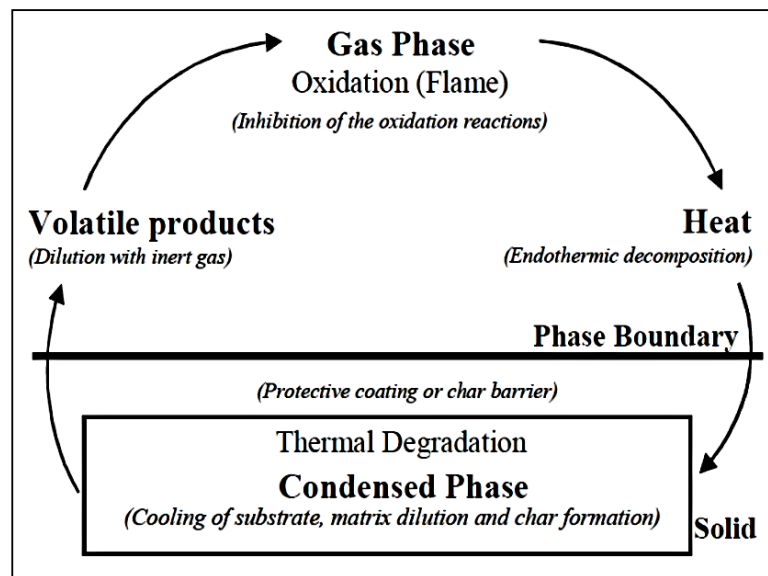


**Figure 2.2:** Simplified combustion mechanisms (Focke et al., 1997).

The flame-retardant compounds are developed to minimize the spreading of flame and prevent propagation of burning, rather than to stop the ignition of a material. Most of the substances will ignite and burn when subject to high level of radiant heat (Sutker, 1988). The flame retardant system enhances the resistance of a polymeric material from ignition.

There are review papers describe and discuss about the flame-retardant systems in relation to their mechanisms (Green, 1996; Green, 1997). These review papers provide an overview on the flame-retardant systems. Flame-retardants varied by their functional mechanisms to interrupt the decomposition path of a polymer. Reactions of vary flame-retardant compositions towards polymers are different. Hence, the design and application of flame-retardant systems need to be specific to certain substrate. Halogen flame-retardants and brominated flame-retardants are applied in 1970 and 1980. When heated, halogen flame-retardants decompose to form acid and halogen radicals. Halogen radicals in the gas phase quench other free radicals such as oxygen and hydrogen require for fuel's oxidation and burning, hence suppress the fire propagation (Lyons, 1970; Pettigrew, 1993; Georlette et al., 2000). Phosphorous and antimony are found to have good synergy with halogen flame-retardants, by promoting more halogen radicals to replace the oxidation radicals (Weil, 1978; Touval, 1993). Halogen flame-retardants reduce in use since 90's due to its environmental risks such as the release of high amount of hydrobromic and hydrochloric acid smoke that was toxic, corrosive and challenging to dispose (Pettigrew, 1993; Green, 1997). Research of halogen free flame-retardants obtain global attentions.

Much research is looking into the development of non-halogenated flame-retardants that can release inert gas (non-combustible) to limit oxygen, minimise surface spread of flame and heat release rate, and able to form a solid surface residue as fire protective barrier. Intumescent system composes of flame-retardant additives that apply on a substrate, that when expose to heat, the intumescent system will swell and form a carbonaceous char layer to shield the substrate underneath from fire (Green, 1996). Flame-retardant system ideally shall (i) minimise flammability, (ii) be more thermally stable at the processing temperature, (iii) compatible with the polymer matrix in long term, (iv) enhance the mechanical strength of the polymer, (v) bring no hazards to environment and health, (vi) be cost-effective (Sutker, 1988; Wolf and Lal Kaul,

1992; Gann, 1993; Green 1996; Miller, 1996; Green 1997). Flame retardant system working through the follows (Pettigrew, 1993):

- (a) ***Release of inert gas*** – The decomposition of flame-retardant additives produces large amount of inert, non-combustible gases that can dilute the concentration of fuel and oxygen to limit fire propagation.
- (b) ***Heat suppression*** – The endothermic decomposition of flame-retardant additives absorbs surrounding heat of the polymer, lower the temperature of polymer, hence reduce the combustion.
- (c) ***Chemical interaction-Physical dilution*** – The decomposition of flame-retardant additives releases inert radicals that interrupt the oxygen and fuel in gas phase. Inorganic mineral fillers in the flame-retardant system can enhance the fire resistivity of the substrate.
- (d) ***Char barrier*** – The decomposition of flame-retardant additives forms a protective char layer on the substrate surface that can insulate the substrate from heat transmission. The char barrier prevents the diffusion of oxygen and fuels to the decomposition zone, hence retard fire.

### **2.3 Passive Fire-protective Coating**

Passive fire protective coating is a type of fire-resistant measure to insulate substrate from fire. An ideal fire protective coating is defined with fire-resistant, non-flammable, low thermal conductivity, good adhesion strength, weather resistant, and water resistant, thin, lightweight, environmentally friendly, and affordable. There are hundred types of passive fire-protective coatings with different properties available in the market. Flame-retardant polymers, thermal

barriers, and intumescent coatings are three major groups of fire protective coatings. Flame-retardant polymer coatings refer to organic resins such as brominated polymers, and inorganic resins such as geopolymers that usually apply less than 5 mm thick on the substrate's surface. These flame-retardant polymers have high thermal stability and low thermal conductivity that can postpone the ignition and combustion of a substrate when exposed to fire. Thermal barrier coatings refer to ceramic materials that have low thermal conductivity and are non-flammable. For instance, ceramic fibrous mats made of silica and rock wool, ceramic plasma sprayed film made of zirconia. When exposed to fire, intumescent coatings will swell and foam to generate an insulating char layer to protect the substrate from fire damage. The swelling mechanism of intumescent coating involves a series of physical and chemical reactions resulting in thermally stable carbonaceous multicellular char (Bourbigot et al., 1995; Sorathia and Beck, 1996; Sorathia et al., 2003).

## **2.4 Passive Fire-resistant Intumescent Coating**

Fire-resistant intumescent coatings fall under the reactive group of passive fire protective measure. When exposed to elevating temperature, the intumescent coating will swell and expand to form thick, multicellular, carbonaceous char layer. The formation of this thermally stable char layer is resulted from the endothermic decomposition of the intumescent coating materials under high temperature. The void air gaps present in the char layer can block the speedy heat transfer and better insulate the substrate underneath it from heat damage (Vandersall, 1971; Kay et al., 1979; Camino et al., 1989; Kandola and Horrocks, 1996). Intumescent coating can be sprayed or painted onto the surface of a substrate with maximum thickness of below 5 mm and air-dried. The intumescent mechanisms involve three important reactions: (i) the endothermic decomposition of intumescent coating materials to cool down the heating

surrounding, (ii) the release of inert gases to suppress the free radicals and fuel combustion, (iii) the formation and expansion of thermally stable char barrier to protect substrate from fire (Kay et al., 1979; Camino et al., 1989; Kandola and Horrocks, 1996).

Organic intumescent coatings are normally composed of ammonium polyphosphate- APP (an acid catalyst), pentaerythritol- PER (a charring agent), and melamine- MER (a blowing agent) formulated either in water-based or solvent-based binder. Organic intumescent coatings are characterised with thin film thickness. This type of intumescent coatings is reported with a better water and weather resistance as compared to alkali silicate intumescent coatings. Architectural professionals more prone to use the organic intumescent coatings for passive fireproof design. This is due to the organic intumescent coatings display a higher visual aesthetic after applied onto the steel structures when compared with the cementitious-based fireproof coatings. Organic intumescent coatings gain increments of use nowadays in various sectors such as skyscrapers, airports, shopping malls, sport centres, hotels and many more. Organic intumescent coatings offer a safe and flexible solution to architects when designing building or structures using steels.

Intumescent coating consists of three major compounds contribute to the intumescent reactions: an acid source, a carbon source, and a blowing agent. These three major compounds need to go through a series of physical and chemical reactions concurrently at a desired sequence for the intumescent mechanisms to happen. The intumescent mechanism will fail if the reaction time taken is delay or prolong, and if the sequence is disorder. The order of physical and chemical intumescent reactions as shown in **Figure 2.3**.



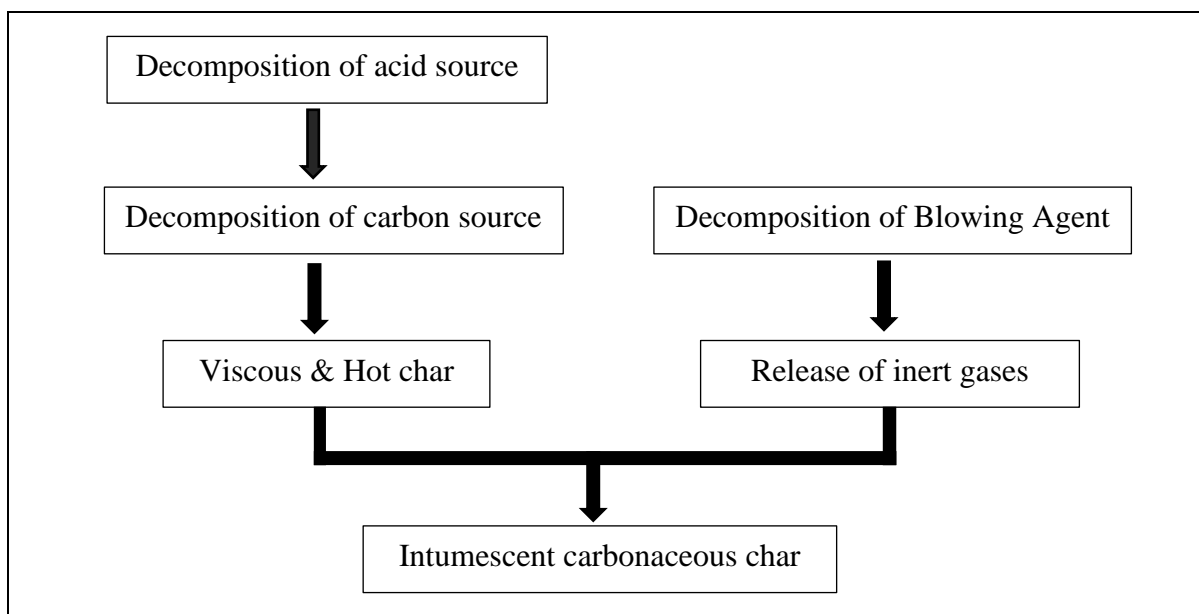


**Figure 2.3:** The order of intumescent mechanism (Vandersall, 1971).

The intumescent mechanism starts with the decomposition of acid source at high temperature. Heat from the sunlight would not be enough for the intumescence mechanism to happen. The temperature must be high enough (the presence of fire) to allow the decomposition of acid source to occur, but lower than the pyrolysis temperature of the coating substrates. The acid source shall decompose prior to the decomposition of other compounds. This step is essential to dehydrate the carbon source. The acid sources including zinc borate, ammonium polyphosphate, amide or amine salt, and organic esters (Bourbigot et al., 1993; Castrovinci et al., 2005). These acid sources decompose at temperature ranging from 100 °C to 250 °C to release acid and water vapour. This range of temperature is below the pyrolysis temperature of most of the compounds used in the coating.

The second stage of intumescent mechanism is the dehydration and decomposition of a carbon source by inorganic salts. The carbon source is then converting into a carbonaceous char. The carbon sources are usually polyhydric compounds rich in carbon, or polycarbonate like polyhydric alcohol, starch, or phenol like phenol-formaldehyde. The third stage is the expansion of the carbonaceous char. The breakdown of blowing agent will trigger the foaming

of hot viscous char. The decomposition temperature of carbon source and blowing agent must be similar and happen concurrently so that the char can swell. The endothermic decomposition of blowing agent release numerous hot inert gases that able to melt and blow the char. The blowing agents are referring to nitrogen compounds like dicyandiamide, urea, guanidine, melamine, and glycine. According to Banerjee and Chattopadhyay (1993), these nitrogen-based blowing agents yield Ammonia ( $\text{NH}_3$ ), water vapour, and carbon dioxide. Chlorinated paraffin is another type of blowing agent that produce Hydrogen Chloride ( $\text{HCl}$ ), water vapour, and carbon dioxide. Inert gaseous products release from the blowing agent will flow into the viscous char creating bubble air gaps in the char, that can expand the char to certain thickness. The swelling thick char will solidify and form multicellular char structures to limit the fire and heat transmission to the substrate underneath (Anderson et al., 1985).

Intumescent coating before and after the intumescent reactions as shown in **Figure 2.4**, indicating the dramatic changed of the intumescent coating after a series of chemical and physical processes. An intumescent coating can swell 50 to 200 times of its original thickness, generate multi-cellular char structures with 20 to 50  $\mu\text{m}$  cell size and 6 to 8  $\mu\text{m}$  wall thickness (Cullins and Hirschler, 1981; Anderson et al., 1985).

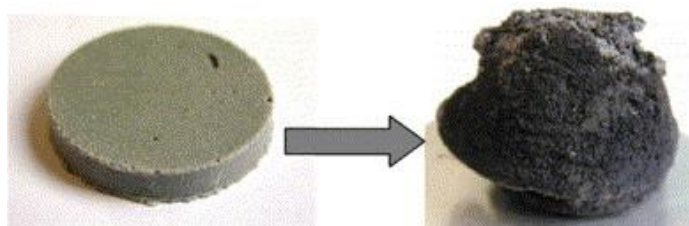


**Figure 2.4:** Swelling phenomena of intumescent coating (Jimenez et al., 2006)

Graphite flakes are found able to enhance the fire-resistant of intumescent coatings by allowing the expansion close to 100 times thicker of fire protective char barrier (Quershi and Krassowski, 1997). Inert fillers like silica and titanium dioxide can reduce the cell size (diameter) of char structure. Other elements such as pigments, thickeners, coalescing agents, antioxidant, and

fibres might be incorporated to the intumescent coatings for appearance and structural enhancement. The fire resistance performance of intumescent coatings is examined on uncoated steel and steel coated with intumescent coating, as shown in **Figure 2.5**.

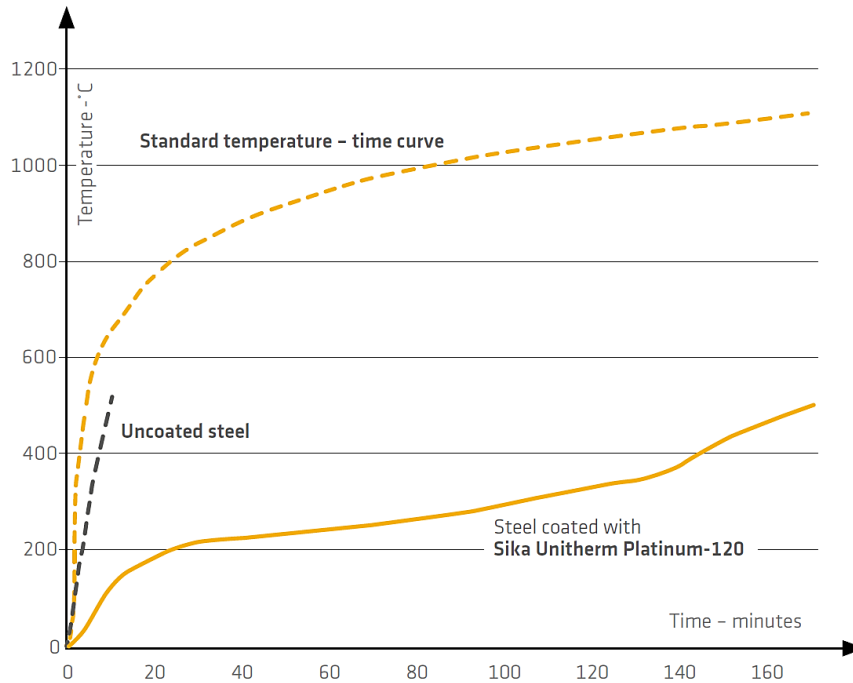


**Figure 2.5:** Temperature of uncoated steel as compared to coated steel after exposed to fire  
(Sika Group, 2021)

Intumescent coatings are declared with the ability to slow down combustion, limit the spread of flame, minimise heat release rate and smoke concentration of a material when exposed to fire (Zhang et al., 2009; Wang et al., 2010). Nonetheless, intumescent coatings are identified with several drawbacks such as weak bonding and easily peel off from the material substrate upon swelling. This scenario is commonly seen when the intumescent coating is applied onto a vertical surface such as wall and overhead structures. Peel-off intumescent coating exposes the structure to direct fire. Mechanical and bonding strength of the intumescent coatings are crucial to achieve a desired fire protection outcome. Other drawbacks including wear durability, and weather resistant (moisture and UV radiation).

Optimisation of intumescent coatings is examined using epoxy-amine-thermoset system, and the performance on steel was characterised (Jimenez et al., 2006). Boric acid and commercial APP are two of the flame-retardant additives incorporated into the formulations, using single dose respectively and in the combination of both. The fire-protective outcome of intumescent coating formulation without any flame-retardant additives was like the bare steel plate. Intumescent coating added with single dose of APP and Boric acid can enhance the fire protection by reducing the heat transfer to the steel (lower back-side temperature). Nonetheless, the char layers formed peel off from the steel after a short period of time, hence failed to provide fire protection to the steel at desired duration. Intumescent coating incorporated with both APP and boric acid showed a better fire protection performance and char adhesion strength to the steel. Phosphates and borophosphates released from APP and boric acid improved the char structural and adhesion strength. Boric acid can increase the viscosity of the intumescent formula, release boron oxide (solid glass) that trapped more inert gases to enhance the char's mechanical strength.

#### **2.4.1 Relationships and interactions between acid, charring and blowing agent**

The process of intumescence is activated at temperature of 250 °C and above via the release of phosphoric acid from an acidifying agent such as ammonium polyphosphate (APP). This follows by the dehydration of the charring agent (carbon source) such as polyol and pentaerythritol (PER) by the acid to create a layer of carbonaceous char. The blowing agent such as Melamine (MEL) decomposes to release gaseous products, blowing the molten mass and expanding the carbonaceous char to a certain thickness. A solidified, thicker carbonaceous char provides a good protection barrier against fire. The interactions between acid, carbon, and blowing agent as shown in **Figure 2.6** (Puri and Khanna, 2017).

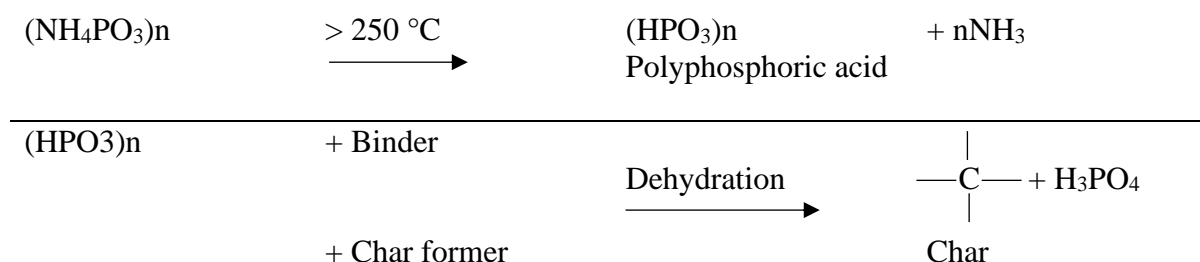


**Figure 2.6:** The interactions between acid, carbon, and blowing agent.

The degradation of APP was assessed in detail by Camino et al. (1985). When heat under an elevating temperature, ammonia and water in the APP are removed. Simultaneously, cross-linking is happened between the structures of P-O-P and P-N-P at high temperature (Camino et al., 1985). The disruption of polyphosphate chain structure take place when the ammonia and water are eliminated, follows by the liberation of polyphosphoric acid. Afterwards, the polyphosphoric acid will react with the charring agent (pentaerythritol) to form cyclic phosphoric acid esters that perform simultaneously as an additional source of charring and blowing in the process (Camino et al., 1984; Camino et al., 1989). In the intumescence reaction process, melamine will combine with polyphosphoric acid to form melamine polyphosphate and dipolyphosphate. Further on, polyphosphoric acid will undergo dehydration to form phosphorus pentoxide. When glycerol is used as a charring agent, it formed an ester that is low in decomposition temperature resulted in a better performance in fire-resistance (Horacek, 2009).

## 2.4.2 Intumescent Flame Retardants

The phenomenon of intumescence is an interesting process. The Latin term ‘tumesce’ meaning ‘to swell up’, similarly the French term ‘tumere’ meaning ‘swell’. It is therefore the term ‘tumescent’ refers as ‘swollen’, and the mechanism of swollen known as ‘intumescent’

(Mount, 1992). Intumescence is the swelling of a material upon heating. Intumescent flame retardant defines as the swelling of a material, derives from a series of physical and chemical reactions when expose to fire, to form a fire-protective multicellular char barrier to protect the structure underneath it from fire damage. The char barrier can limit the release of oxygen and heat from fuel thus to achieve fire extinguish effect. Therefore, the intumescent flame retardants can prevent the collapse of structure when overexpose to serious fire (Duquesne et al., 2004). Intumescent mechanism occurs in condense phase. Analysis of physical and chemical reactions are important to describe the intumescent mechanisms. Intumescent mechanism in relation to fire-resistant, inhibition of flame, melt flow rate, formation of char, char structure and improvement, dehydration of acid source are identified and evaluated. Research in fire-resistant intumescent coatings are broad and different parameters can be adjusted and modified in the intumescent composition. Namely, various intumescent formula can be customised, designed, and developed to protect certain material at a desired fire-protective outcome.

### **2.4.3 Intumescence Reactions**

The reactions of intumescence normally happen in association with the procedures of (i) the breakdown of acid source to release a mineral acid, (ii) the mineral acid then dehydrates, follows by the decomposition of carbon source and carbonization of char occurs, (iii) the decomposition of a blowing source, with the release of gaseous products that trap within the molten matrix to trigger the formation and expansion (swelling) of a multi-cellular char insulation barrier. This char barrier insulates the steel substrate underneath by limiting the heat of damaging fire which will lead to the further degradation of the steel from transferring towards (Camino et al., 1989; Hao and Chow, 2003). The schematic diagram about the

intumescence reactions before and after the coating exposed to heat as shown in **Figure 2.7** (Puri and Khanna, 2017).

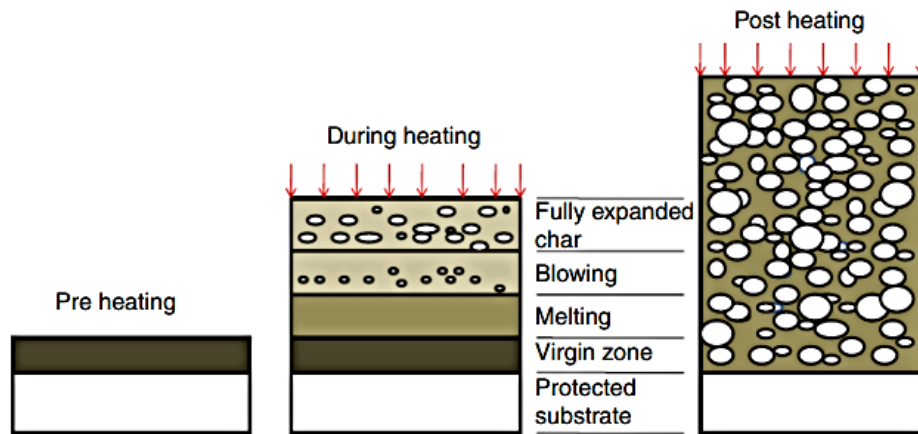
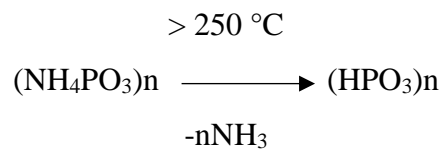


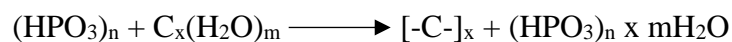
**Figure 2.7:** Schematic diagram of intumescence reactions before and after the coating is heated (Puri and Khanna, 2017).

The intumescence reactions take place with orders and sequences as follow:

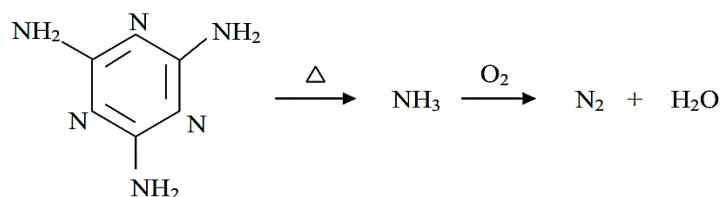
- (a) The polymer binder starts to turn soft and melt when expose to heat.
- (b) The decomposition of an acid source with the release of inorganic mineral acids.



- (c) The decomposition of a carbon source for example pentaerythritol, by inorganic acids, trigger the carbonization process of forming carbonaceous char layer.



- (d) The decomposition of blowing agent such as melamine release the gaseous products.



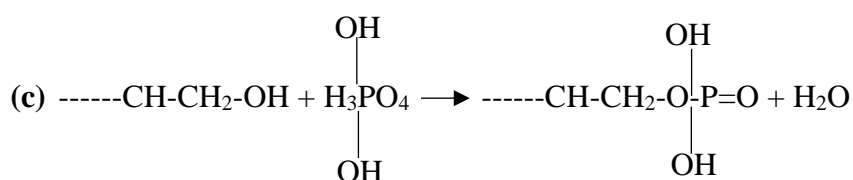
(e) The expansion (swelling) of char layer up to a certain thickness.

(f) Cross-linking of chain and solidification of char layer.

Three primary ingredients that constitute the intumescent coating are an acid source, a carbon source, and a blowing source. The formulation of intumescent coatings is important. The optimization of the intumescence formula is essential to achieve an effective char layer against fire. The quality of char structure has impacts on its fire protection and heat insulation properties. An ideal intumescent coating shall generate a thick char foam, with large volume of connected char cells that are small, narrow, and evenly distribute within the char structure. A solid char foam shall consist of closed-char cell system. Moreover, the intumescent coating shall encompass other abilities to allow its application in various environmental conditions for a longer duration (Camino and Costa, 1986).

#### 2.4.4 Chemical Mechanism of Intumescence

The chemical reactions of intumescent are identified as acid-catalytic and dehydration, as shown in **Figure 2.8**.





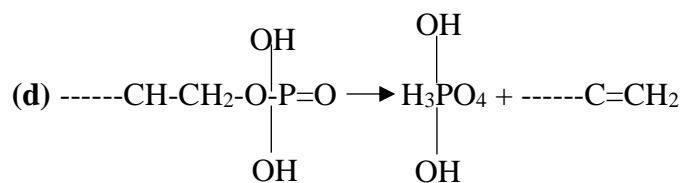


**Figure 2.8:** Chemical reactions involved in the intumescence (Camino and Costa, 1986).

The first phase of chemical reactions (a) and (b) indicated the de-polymerization induced by an acid source. The second phase reactions (c) and (d) involve the dehydration of polymer with the existence of phosphoric acid. These series of chemical reactions produce  $\text{---C=CH}_2$  fragments. The fragments of  $\text{---C=CH}_2$  condensed to generate carbonaceous char residues. According to Weil (1992), phosphorous compounds in the acid source convert the carbon source like PER in the intumescence to polyol phosphates that will further decompose into carbonaceous char. Intumescence forms char barrier as a physical protection to constraint the transfer of heat and mass in condensed and gas phases. The decomposition of intumescent system produces thermally stable char that can minimise the flammability of a material. Intumescent system offers primarily thermal insulation by limiting the heat transfer to substrate below it (physical protection).

Fundamental understanding of the expansion mechanism of intumescence can be revealed through the swelling process. The range of temperature and amount of heat transmit are important to the swelling reactions. The ability of the intumescent system to yield gas bubbles during the swelling process is crucial. The types of ingredients and their composition in the intumescent system are essential to determine the flame retardancy properties. The selection of acid source (acidifying agents), carbon source (carbonific agent), blowing source (foam forming agent), modifiers, and binders will have influences on the efficiency of an intumescent system. For example, the degree of char residues formed and the strength of char

structure. Fundamental intumescence components as shown in **Table 2.1** (Rains, 1994; Puri and Khanna, 2017).

**Table 2.1:** Fundamental intumescence components and reactions.

| <b>Fundamental Components</b>           | <b>Reactions</b>  | <b>Relevant substances</b>   |
|---|---|--|
| Acid sources<br>(Acidification agents)  | Release acid during the thermal decomposition; esterify and dehydrate hydroxyl groups; release of water molecules.                              | Ammonium, aminic salt, esters such as ammonium polyphosphate, phosphate, borates, polyborates, sulfates, halides; Phosphates of amine such as melamine phosphate, urea tributyl phosphate, urea with phosphoric acids; Inorganic acids such as Phosphoric acid, Sulfuric, Boric acid such as borax, ammonium borate; Other phosphates such as tricresyl phosphate, alkyl phosphates, haloalkyl phosphates. |
| Carbonising agents<br>(char formers)    | Produce carbon materials during thermal decomposition that contain large amount of carbon atoms and hydroxyl groups, esterification with acids. | Erythritol and oligomers such as pentaerythritol, pentaerythritol dimer and trimer, arabitol, sorbitol, mannitol, inositol; Polyhydric alcohols; saccharides such as glucose, maltose, arabinose; Polysaccharides such as starch dextrin, cellulose; Polyhydric phenols such as resorcinol.  |
| Blowing agents<br>(foam forming agents) | Release inert gases in large amount, assisting in the foaming of char structure (stimulate char expansion and thickness).                       | Halogens and nitrogen compounds like melamine, phosphoric salts, urea, urea-formaldehyde, dicyandiamide, guanidine, glycine, chlorinated paraffins.  |
| Binding agents                          | -   | Epoxy, acrylic, amino, polyaceticvinyl, polyurethane resins.   |
| Modifying agents                        | -   | Solvents, stabilisers (chemical compounds depend on the types of resin).   |

### 2.4.5 Physical Mechanism of Intumescence

Typically, an efficient intumescent coating consists of a phosphorous acid source like APP, a carbon source like PER, a blowing source like MEL, and a binding agent (Bertelli et al., 1989; Camino et al., 1989; Camino et al., 1990). The formation of physical char layers of intumescent coating is graphically visualized in **Figure 2.9** (Gilman and Kashiwagi, 1997). When exposed to fire, intumescent coating reacts to generate a physical char barrier on top to insulate the substrate layer below it from high temperature. Right below the carbonaceous char is the intumescent front layer where foaming and swelling reactions happen. Followed by an unburn layer where majority of the intumescent components and flame-retardants are located. The last layer at the bottom is the substrate that sits underneath the intumescent coating protected from high temperature fire. The physical char barrier slows down the heat transfer and mass loss hence reduce the combustion (Gilman and Kashiwagi, 1997).

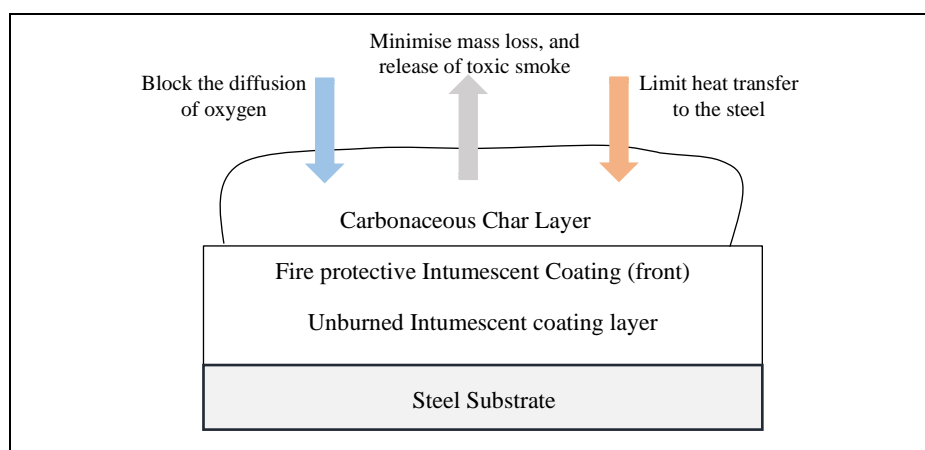


**Figure 2.9:** Schematic diagram of physical mechanisms of intumescence.

It is crucial to determine the intumescent compounds and their respective optimum ratios. Intumescent compounds are replaceable with one or more other compounds in the same group or category. Some studies reveal that incorporation of more than one compound in the molecular matrix can enhance the effectiveness of the intumescent coating (Camino et al., 1990). According to Camino et al (1989), the performance of an intumescent coating depends

on the physical carbonaceous char layer formed. An effective char barrier can minimize the mass loss, diffusion of oxygen, heat transmission, and hence restrict the fuel combustion. Halogenated flame-retardant compounds like chlorinated paraffin are generally used as carbonization agent in most intumescent coatings.

The industries start to look for non-halogenated flame-retardant compounds that are more effective, less expensive, and less hazardous as replacements. Environment concerns and hazards caused by the halogenated compounds started to raise global attentions (Mount, 1992). Nitrogen-based flame-retardant compounds are among the more environmentally friendly alternative. The char formation of non-halogenated intumescent coating releases less smoke, very minimal corrosive, and toxic gases when heating (Horacek and Grabner, 1996).

## **2.5 Intumescent Flame Retardants**

This section described the type of intumescent flame retardant ingredients used in the intumescent coating formulation. These flame retardant ingredients including the acid source, carbon source, blowing source, binder, pigment, and mineral fillers. The properties and usage of these flame retardants are revealed. Generally, three primary flame-retardant additives: Ammonium polyphosphate (APP), Melamine (MEL), Pentaerythritol (PER), white pigment: Titanium dioxide ( $\text{TiO}_2$ ), and flame-retardant mineral fillers such as Aluminium hydroxide ( $\text{Al}_2\text{O}_3$ ), Magnesium hydroxide ( $\text{Mg}(\text{OH})_2$ ), Calcium carbonate ( $\text{CaCO}_3$ ) are used to compose the intumescent coating. These substances in the intumescent coating are adhered by a binder such as VAC. The optimisations of intumescent coating formula to enhance the physical (fire-resistant, char quality, mechanical strength) and chemical properties (thermal stability, antioxidant properties, functional molecular groups) are important to continually enhance the coating's effectiveness (Bourbigot et al., 2010; Wang et al., 2006b). The char layer generated

from APP/MEL/PER coating formula tended to oxidise easily and flaked out (Wang and Shi, 2006). The enhancement of char layer quality is necessary to extend the fire protection time.

### 2.5.1 Acid Source

There are a wide range of phosphorus derived flame-retardant additives can be used as an acid source in the intumescent coating. These acid sources consist of phosphates, red phosphorus, phosphonates, and phosphine oxides. These phosphorous-based flame-retardant additives can be appropriately added into the polymer, and they will remain active in both condensed and vapor phases. According to Aronson (1992) and Weil (2004), the phosphorus flame-retardant additives are found to be more effective in polymers that contain of oxygen and nitrogen, during the condensed phase. Upon heating, these phosphorous-based flame-retardant additives breakdown to release phosphoric acid and water. Condensation of phosphoric acid resulted in the formation of pyrophosphate structure, as shown in **Figure 2.10**.

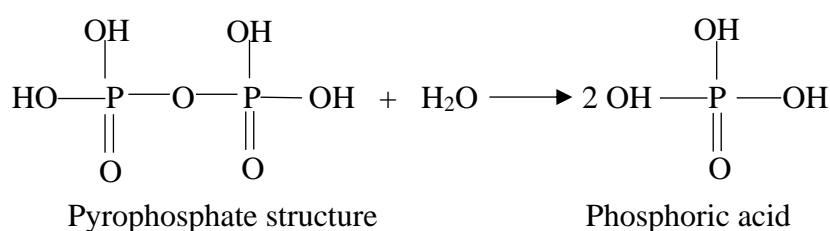


**Figure 2.10:** The condensation of phosphoric acid produced pyrophosphate structure.

The water molecules released during the thermal decomposition of phosphate flame-retardants dilute the oxidation of free radicals in the gas phase. Phosphoric acid and pyrophosphoric acid dehydrate the alcohol group (at the chain end) to form carbocations and carbon=carbon bonding, as demonstrated in **Figure 2.11**.

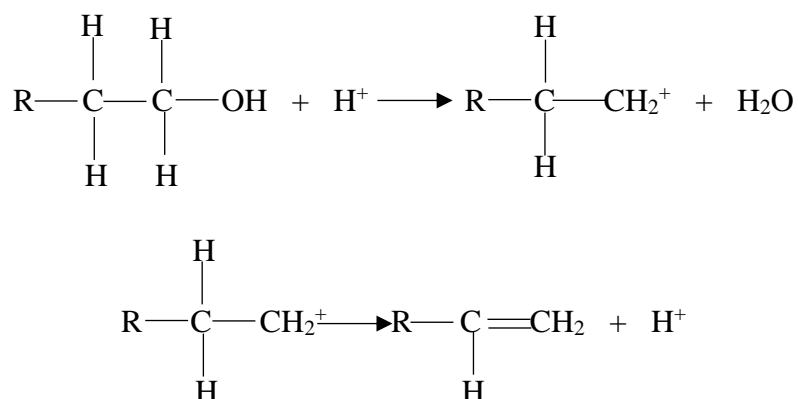


**Figure 2.11:** The dehydration of alcohol group resulted in the carbon=carbon double bonds.

Pyro and ortho-phosphoric acids convert to metaphosphoric acid  $(\text{HPO}_3)_n$ . The phosphate anions  $(\text{PO}_4)^{3-}$  react with carbon atom to form char. The carbonaceous char layer insulates the substrate underneath from high temperature flame (fire) by: (i) constraints the oxidising free radicals and volatile fuel; (ii) blocks the diffusion of oxygen and minimise combustion; (iii) limits the speedy heat transfer to below substrate. Upon heating, phosphorus flame-retardants can volatile into gaseous condition, forming active radicals such as  $\text{PO}_2$ ,  $\text{PO}$  and  $\text{HPO}$  to scavenge  $\text{H}$  and  $\text{OH}$  radicals. Among the combustion inhibitors, volatile phosphates are found to be the most effective. According to Babushok and Tsang (2000), phosphorus radicals are ten times more effectual than chlorine and five times more effectual than bromine radicals.

Ammonium polyphosphate (APP) is an inorganic salt and use as an acid source required for the swelling reaction in the intumescent coating. The structure of APP was exhibited in **Figure 2.12** (Jimenez et al., 2006).

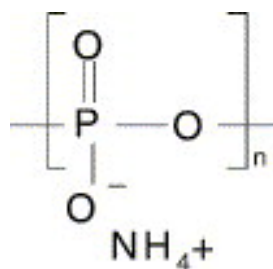


**Figure 2.12:** Ammonium polyphosphate (APP) structure.

APP is a type of phosphate that consists of high molecular weight chain, and possibly branching. The properties of APP vary depending on the monomer number in each molecule, and the extend of its branching. APP with shorter chains ( $n < 100$ ) are more sensitive to water and less stable to heat than longer chains ( $n > 1000$ ). Longer chains are less soluble in water. APP II (**Figure 2.14**) has longer chains with cross-link branching as compared to APP I (**Figure 2.13**), thus APP II has lower water solubility and higher thermal stability.

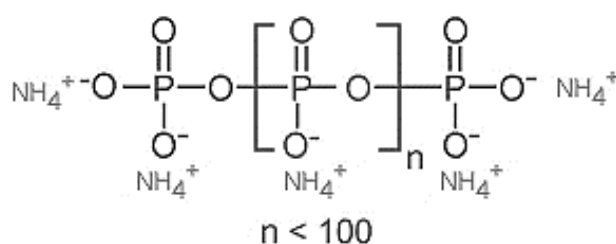


**Figure 2.13:** Ammonium polyphosphate I (APP I) structure.

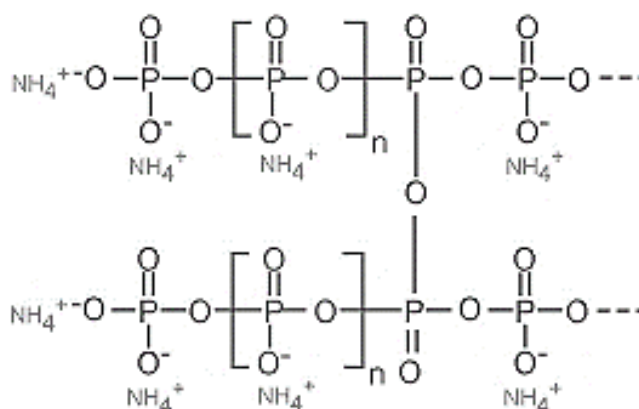


**Figure 2.14:** Ammonium polyphosphate II (APP II) structure.

Short chain and long-chain APPs begin to decompose at 150 °C and 300 °C respectively. APP leads to the yield of char when it is added into polyamides, polyurethane and polymer containing nitrogen or oxygen (Levchik et al., 1996; Duquesne et al., 2001; Shih et al., 2004). The thermal decomposition of APPs produces polyphosphoric acid, ammonia (NH<sub>3</sub>), and hydroxyl groups. The hydroxyl groups dehydrate and condense, produce highly cross-linking ultra-phosphate and polyphosphoric acid structure. The polyphosphoric acid then dehydrates to trigger the yield of char. Different weight percentage of APP has impact on the effectiveness

of the intumescent coating. The use of APP at high weight percentage at between 10 to 30 % in polyamides are found mostly effective (Levchik et al., 1996). Low weight percentage of APP is ineffective in aliphatic polyamides.

### **2.5.2 Carbon source**

Carbon source, or carbonizing agent, or char former, plays a major role to stimulate the char formation through the decomposition of acid source in the intumescent coatings. In general, literature revealed pentaerythritol (PER) was the carbon source that mostly used in the intumescent coating formula with the presence of APP (acid source). PER has a lower melting temperature in the initial stage of intumescence process. A higher water solubility of PER constraint its application in certain weather conditions. Dipentaerythritol and tripentaerythritol are less water soluble, however both are more expensive in price. PER shows an earlier intumescence mechanism in comparison to its dimer and trimer.

On the other hand, di- and tri-pentaerythritol displayed a higher embrittlement temperature, wind, and char cracking resistance on curved surfaces (Andersson et al., 2007). Tris hydroxyethyl isocyanurate (THEIC) was used as PER replacements in the intumescent coatings. This carbonizing agent of THEIC was derived from triazine. Research displayed a synergistic reaction between THEIC and APP, nevertheless, solubility of THEIC remained as a challenge. The used of THEIC mixed with long chain amine in the intumescent coatings was found able to minimize the blooming scenario. Amine blooming also refers as amine ‘sweating’, is an undesirable reaction that will reduce the adhesion strength of the intumescent coating. Sugars, starches, and celluloses that possess groups of pendant hydroxyls were applied as



cheaper options of carbonizing agents, and they were found useful to enhance the performance of intumescent coatings (Reti et al., 2008).

Cyclodextrin nanosponge was used as a carbon source in the intumescent coating, and it was found assisting in the char formation (Alongi et al., 2010). A novel carbonizing agent-poly hexamethylene terephthalamide (PA6T) applied in the intumescent coating brought synergistic reactions with APP stimulating the formation of more compact and uniform char barrier when heating in high temperature (Liu et al., 2012). It was found, the degradation of maleated cyclodextrin and metal salts during the combustion yield metal ions promote a more thermally stable and compact char layer in the poly vinyl alcohol composites (Feng et al., 2013). Another novel carbonizing agent named Bi(4-methoxy-1-phospho-2, 6, 7-trioxabicyclo [2.2.2]-octane-1-sulfide) phenylphosphate (BSPPO) was reported advantageous to the char foaming (Huang et al., 2012). Research evaluated the use of alkali and urea-modified lignin as charring source in the intumescent coatings. Research outcomes revealed, lignin modified with urea synergized with APP offered a better flame-retardant and thermal insulation properties in comparison with unmodified lignin (virgin lignin) (Zhang et al., 2012).

### **2.5.3 Blowing Agent**

Among all, melamine (MEL) reported as the most common and broadly used blowing agent in the formula of intumescent coatings. At high temperature, MEL will undergo thermal decomposition break down to release volatiles and gaseous products, stimulate the swelling of intumescent char layer. Other MEL derivatives such as melamine phosphates and polyphosphates were also used as blowing agents. Melamine decomposes totally at temperature range between 250 °C to 350 °C as disclosed by TGA data. MEL will interact with APP (Taylor

and Sale, 1993). Upon heating, melamine condenses to release ammonia and produce insoluble compounds. When the heating conducted in a closed system, ammonium will vanish, follow by the formation of fused ring structures such as melam, melem and melon (Costa and Camino, 1998; Wirnhier et al., 2013). The decomposed melamine and ammonia function as flame-inhibitors (poor fuels) to suppress the flame propagation in the gaseous phase. The reaction between MEL and APP produce melamine phosphate which could act as an acid source in the intumescent coating.

Numerous melamine phosphorous compounds for example, polyphosphate, pyrophosphate, and phosphate are advantageous flame-retardants, and can perform simultaneously as acid sources and blowing agents in the formula of intumescent coating. Urea weakens the intumescence swelling performance of APP-PER coating system when it was used as a blowing source. This was due to the breakdown of urea released limited gaseous products as compared to MEL (Camino et al., 1984). In the intumescent composition, guanidine and dicyandiamide can be used as blowing sources along with the presence of MEL.

#### **2.5.4 Binder**

Binder is an important element in the intumescent coating contributes to various effects. In the formulation of intumescent coating, binder usually constitutes more than 50 wt% of the total composition (Yew et al., 2018; Khairunisa et al., 2020; Li et al., 2020). Binder together with other flame-retardant additive and fillers, function to generate a more uniform and denser char foam layer when expose to fire (Wang and Yang, 2010b). Appropriate option and combination of binder, flame-retardant additives and fillers are important to ensure a desirable and optimum fire-resistant outcome.

The ingredients nature, types, weight percentage of binder in the composition play important roles in the flammability of the intumescent coating. Wang and Yang (2010) examined the influence of binder in the fire-resistive intumescent coatings. In the research, epoxy-based binder was reinforced with silicone acrylate (SSA) a self-crosslinking film-forming substance, with the presence of flame-retardant additives (APP-MEL-PER),  $\text{TiO}_2$ , expandable graphite (EG), and kaolin. One of the efficiencies of fire-resistive intumescent coating was revealed through the surface morphology of char layer. In the SEM, surface micrograph showed the formation of denser char cell structure, based on an appropriate amount of SSA. When the amount of SSA increasing, thermal insulation performance of the intumescent coating was diminished in the fire test, as well as large char cells were observed under the SEM. Wang and Yang (2010) concluded, appropriate composition of binder and other flame-retardant ingredients were crucial and critical for the fire-resistive intumescent coatings to perform at desirable level.

There are various types of binders used in the fire-protective intumescent coating. Among are vinyl acetate copolymer, polyvinyl acetate emulsion, alkyd resin, epoxy resin, vinyl chloride latex, acrylic resin, and polyurethane resin. The performances in terms of fire-resistivity, flammability, char quality, thermal stability, and mechanical properties varies in these binders, and when combine with other flame-retardant ingredients. It is therefore important to seek for the most appropriate mix proportion of each ingredient in the intumescent coating formulation for optimum fire protection and mechanical performances, to meet the minimum standard of fire protection requirements (Bourbigot et al., 2010). Many other studies have informed about the role of binder in the intumescent coatings. It is important for the binder to have a similar range of degradation temperature with other flame-retardant ingredients for the intumescence and char-forming mechanisms to work.

In addition, the binder shall have an appropriate melt viscosity neither too low nor too high. If the melt viscosity of binder is too low, the molten intumescent coating will slump forcing the char layer to dislodge and fall from the substrate surface. If the melt viscosity of binder is too high, it will prevent the intumescence mechanism from happening (Puri and Khanna, 2017). The binder polymer must melt at desirable viscoelastic level, so that the gaseous products released are able to trap within the molten mass during the expansion of intumescent char. Certain binders assist in the formation process of char. This is attributed to the synergistic activities of binder with APP that allow a more thermally stable char to be formed. Different range of polymer resins are applied as binder in intumescent coatings.

The type and durability of binder chosen in the intumescent coating must match to the environment it service. For example, water-based acrylic resins are good to use in internal areas that are dry and with lesser air moisture content. While solvent-based acrylic resins are good to be applied in outdoor areas that are under shade or indoor. Solvent-based or solvent-less epoxy resins are suitable for use in locations with high humidity and extreme weathers. Thermoplastic binders refer to polymer resins that can be re-processed by re-heating, re-moulding, and re-cooling. Thermoset binders also refer to polymer resins that are irreversible once they have been initially processed, neither can be re-heated nor re-moulded. It was noticed, thermoplastic binders possess a better behaviour of char formation in comparison to thermoset binders. Epoxy resin binders preferable in solvent-based and polyvinyl acetate emulsion in water-based intumescent coating formula. A mixture of binders can lead to an overall better performance. As instance, when chlorinated paraffin combined with chlorinated rubber, a good aging-resistant was observed in the APP/PER/MEL coating formula. On top of the flame-retardancy, halogen substances in the coating formula functioning to rectify the plasticity and flexibility in the dried coating (Puri and Khanna, 2017). Styrene acrylic copolymers consist of phosphorus compounds tend to generate a thicker and denser char foam layer.

The degree of cross-linking present in the binder plays a key role in enhancing the performance of intumescent coating including the thermal stability (Fan et al., 2013). Copolymers contain of styrene and 2-ethylhexyl acrylate p-methyl styrene show positive reactions with APP, enhanced the thermal stability and efficiency of thin film coating. Linear and cross-linking copolymers particularly those generated from monomers reacted positively with APP led to thermal insulation improvement of char (Duquesne et al., 2004; Duquesne et al., 2005). The incorporation of chloroparaffin can enhance the flame retardancy of polyvinyl acetate in the intumescent coatings. The C=C bonds formed into a condensed heterocyclic system, that when mixed with melamine, they reacted with the polyene under a wide range of temperature, transformed into condensed, high thermally stable heteroaromatic structure (Ducrocq et al., 2006). The addition of polymers like Polyamide-6 can function as carbonising agent in ethylene-vinyl acetate copolymer to enhance the fire-resistant performance (Le Bras et al., 1999). Molecular weight of binder will have impacts on the fire-resistant performance of intumescent coatings. Binders with higher molecular weight are found able to enhance the antioxidant properties and thermal stability of coatings. Nonetheless, binders with high molecular weight are also associated with higher melt viscosity that slow down the speed of char expansion, resulting in large char cell structures. Large, uneven, and loose char cell structures might derive from overfull high molecular weight of binder and causing significant drop in the fire protection performance (Wang and Yang, 2012).

Research reported a mixture of thermoplastic and thermoset binders might be a favourable option. Epoxy resin is an example of thermoset binder. Thermoplastic binders such as ketonic resin and hydrogenated castor oil are applied for melt viscosity modifications. Polymer emulsion containing phosphate monomer or phosphonate that are cost-effective and environmentally friendly, together with acrylic and methacrylic monomers are informed beneficial to the intumescent coatings (Puri and Khanna, 2017). Intumescent coating containing

epoxidized polysulphide reported with the formation of thermally stable carbonaceous protective char barrier. Water-based intumescent coatings are notified with the issues of slow drying rate caused by the high thickness of char layer formed, and this is even more obvious when the surrounding humidity level is high. Free radical polymerisation method is found feasible to cure this slow-drying issue of water-based intumescent coatings. Research demonstrated the incorporation of phosphate resin acid and cured cold amino resin in the water-based intumescent coatings. Water-based coatings containing a high dosage of phosphorous exhibited improvements in flame-retardancy, nonetheless, carbonaceous char layer quality exhibits a significant role (Ma et al., 2021). The metal adhesion of intumescent coating mixed with copolymerizable acid monomers (maleic, fumaric, methacrylic) declared an enhancement in the adhesion strength. Silicone and self-cross-linking polyacrylate emulsion mixture in the water-based intumescent coatings claimed an improvement in the fire protection, thermal stability and char residue when exposed to high temperature (Dong et al., 2014). Silicone with self-crosslinking such as silicone acrylate reinforced epoxy emulsion promoted a better fire protection. Meantime, it helped generated a higher degree of cross-linking with binder minimised water permeation and intumescent ingredients migration hence prevented the corrosion from happening (Wang and Yang, 2010).

Research on intumescent coating using silicone-epoxy resin revealed its ability to generate a thin ceramic-like layer that was thermally stable, contributed to a better fire-resistant and thermal insulation behaviour (Otahal et al., 2011). Poly dimethyl siloxane and silica coated bysilane used as modifying agents in the intumescent coatings led to the swelling of char layers with a lower rate of thermal conductivity. The addition of calcium carbonate, expandable graphite, organoclay enhanced the performances of silicone coatings. The calcium carbonate interacted with silicone matrix to form a ceramic-like layer (calcium silicate) and resin that were thermally stable (Gardelle et al., 2013; Gardelle et al., 2014). The char expansion and

antioxidant properties of intumescent coatings will be influenced by the binder concentration (Yew and Ramli Sulong, 2011).

Two types of binder are used in the intumescent fire protective coating: (a) solvent-based and (b) water-based. Binder in the intumescent fire protective intumescent coating contributes to the char expansion and formation of a more uniform char structure (Wang and Yang, 2010). Solvent based binders are for example epoxy resin, acrylic resin, alkyd resin, vinyl chloride latex and polyvinyl acetate emulsion. These binders had relatively good resistant to water and temperature changes of the surroundings. Solvent-based binders are less susceptible to the weather and moisture in the environment. Nonetheless during the curing phase, industrial solvent-based binders will release a higher amount of toxic volatile organic compounds (VOCs). VOCs such as benzene and methylene chloride have high vapour pressure and low water solubility. These VOCs are detrimental to human health and environmentally unfriendly long term.

Water-based binders are for instance vinyl acetate copolymer, polyesters, polyacrylates, epoxy esters, and polyvinyl acetate that rely on water as the major media. Hydrocarbon solvent commonly will be added to control the viscosity and wettability of the water-based binders. The usage of water-based binders complies with the environmental protection regulations as it releases very low or close to zero concentration of VOCs. Water-based binder is a preferable choice to fulfil the environment compliances imposed by the government. This is due to water-based binders has considerably very low VOCs emission, and not harmful to human health as well as more environmentally friendly. One drawback of water-based binder is it can be affected by the humidity and weather condition of the surroundings. High humidity presents in the environment can delay the water from evaporating in the water-based intumescent coating, hence increases the time frame required during the curing phase. Consequently, this will

increase the tendency of steel substrate to corrode once exposed to prolonged period of water molecules in the water-based coating.

In such case, water-based intumescent coatings formula shall design to allow water molecules to dry at the coating film surface before reaching the steel substrate. The common binder used in water-based intumescent coating is vinyl acetate. Recently, the water-based intumescent coating has gained more focus and interest in. The thermal properties of binder will influence the fire-resistant efficiency of intumescent coatings (Anna et al., 2001). It is crucial to understand the thermal properties of vinyl acetate copolymer, to what extent it will degrade in an elevating temperature up to 1000 °C under nitrogen air flow condition in TGA.

### **2.5.5 Pigment**

Intumescent coating formulations are typically incorporated with a variety of pigments ingredients to enhance the coatings' appearance. These pigments are also found beneficial to the fire-resistant performance of the intumescent coatings, resulted in the formation of a more compact cell structures, with narrower and close distribution of cell size. One of the common reported pigments used in the intumescent coating composition is titanium dioxide ( $\text{TiO}_2$ ).  $\text{TiO}_2$  shows interactions with flame-retardant additives, apart from its application to offer white aesthetic to the coating. The interaction between  $\text{TiO}_2$  and APP in the intumescent coatings often exhibited the swelling of white char foam composed mainly of titanium pyrophosphate ( $\text{TiP}_2\text{O}_7$ ).  $\text{TiP}_2\text{O}_7$  is resulted from the reaction between  $\text{TiO}_2$  and phosphorus pentoxide ( $\text{P}_2\text{O}_5$ ) in the intumescent formula (Horacek, 2009). Research found the fire-resistant effects of intumescent coatings persisted longer using rutile-  $\text{TiO}_2$  as compared to anatase-  $\text{TiO}_2$  (Li et al., 2008). This difference in fire-resistant duration could be due to the disparity in crystalline forms



and distribution of particle size between rutile-  $\text{TiO}_2$  and anatase-  $\text{TiO}_2$ . At high temperature above  $900^\circ\text{C}$ , anatase-  $\text{TiO}_2$  can be converted to rutile-  $\text{TiO}_2$  (Li et al., 2015). Chemical reaction conversion from anatase-  $\text{TiO}_2$  to rutile-  $\text{TiO}_2$  as follow:



Research indicated inorganic oxides-added intumescent coating interacted with phosphates created a glassy outer surface layer associated with high reflection rate that was able to resist high temperature and extreme environments for a longer period. Namely, the inorganic oxides able to enhance the mechanical strength of the intumescent coatings. In the APP-PER-MEL intumescent system, it was noticed molybdenum trioxide ( $\text{MoO}_3$ ) and ferric oxide ( $\text{Fe}_2\text{O}_3$ ) enhanced the outer and inner structure of residual char hence offer a better thermal stability (Li et al., 2008). Silica fume (SF) and chicken eggshell (CES) were mixed with binder and flame-retardant filler to formulate water-based intumescent coatings in the research. It was reported with an enhancement in the adhesion strength of coating to steel substrate for a longer protection from fire (Yew and Ramli Sulong, 2012). Sepiolite was used as synergist in the flame-retardant polypropylene intumescent coating system and was reported with a lower rate of heat, smoke, and  $\text{CO}_2$  production (Liu et al., 2011). Research examined the ethylene-vinyl acetate intumescent flame-retardant (EVA/IFR) system incorporated with iron oxide, lanthanide oxide, the mixture of both, and lanthanum ferrite nanocrystalline ( $\text{LaFeO}_3$ ). These ingredients exhibited good flame-retardant and smoke suppression properties.  $\text{LaFeO}_3$  assisted in establishing a more compact and homogenous char cells (Wang et al., 2012).

### **2.5.6 Flame-retardant Mineral Fillers**

In early days, halogenated gaseous flame retardants such as chloride ion ( $\text{Cl}^-$ ) and bromide ion ( $\text{Br}^-$ ) were used to stop flame propagation, by replacing the free radicals in the flame with more

stable  $\text{Cl}^-$  and  $\text{Br}^-$ . Halogenated flame retardants when interfere with the flame reactions, the oxidation of hydrocarbon and CO to  $\text{CO}_2$  conversion are restrained. This phenomenon releases large amount of toxic smoke and fire effluents, with organic compounds generate from incomplete combustion such as benzene, xylene and toluene that are more toxic than carbon monoxide (Huggett and Levin, 1987; Lebek et al., 2005; Hull et al., 2011). The leaching of halogenated fire retardants from polymers into the environment have been identified. The presence of these halogenated fire retardants in the environment are proven disruptive to the endocrine system (de Wit, 2002; Shaw et al., 2010). Many research raise to search for alternative non-halogenated fire-retardant fillers such as metal hydroxides, carbonate fillers, and phosphorous compounds (Rigolo and Woodhams 1992; Rothon and Hornsby 1996; Price et al., 2002; Hull et al., 2003). Research attentions also paid to materials like silica nanoparticles, clay, expandable graphite, carbon nanotubes, and metal chelates as filler for flame retardant intumescent composition (Li and Qu, 2003; Wang et al., 2007; Wang et al., 2008; Hull et al., 2009; Schmaucks et al., 2009; Bourbigot et al., 2010). Generally, the selection of halogen-free flame-retardant fillers require a more specific match and compatible to the thermal decomposition range of the host polymer to achieve a better thermal stability of fire retardancy. Volatile and highly reactive phosphorus compound was one of these halogen-free flame-retardants, that can constrain the combustion activities during gas phase. Other halogen-free fillers stabilise and stimulate the formation of carbonaceous char layer (swelling take place) during the condensed phase to create a protective char insulation barrier. The incorporation of these halogen-free fillers needs to consider the appropriateness of compatible polymers and the availability, suitability of the loading weight, appropriate dispersion rate, processing equipment that able to handle a higher load of fillers with increasing melt viscosities.

Inorganic fillers use in the intumescent coatings are helpful in promoting residual char when expose to high temperature. Fire-resistant and other performances of intumescent

coatings are highly related to the appropriate combination of flame-retardant fillers in the intumescent composition. Magnesium hydroxide ( $\text{Mg}(\text{OH})_2$ ) added as filler into the intumescent system is found able to improve the bonding strength of intumescent coating with the surface of metal substrates. This is attributed to the present of strong interfacial adhesion of  $\text{Mg}(\text{OH})_2$  with the steel surface (Yew et al., 2015a). Inorganic fillers reinforce the char structures, allowing a more efficient and persistent fire protection to happen. Inorganic fillers also react with APP and its by-products resulting in less thermally degraded phosphorous compounds to facilitate a better integration in char structures. The addition of zirconium silicate (inert filler) was reported with enhancement in the char strength, residual char weight, and lesser number of gases produced (Ullah and Ahmad, 2014).

Inorganic compound derivatives such as nitrides, borides, and carbides derive from chemically inert titanium, zirconium, other metals decompose in a much higher temperature range. These inert fillers promote a more stable carbonaceous char in the flame-retardant intumescent system. The addition of glass flake as filler able to modify the intumescence behaviour and lead to a better fire protection and water-resistant performances. The glass flakes prevented the APP and PER from migration when exposed to water, thus, retained a higher intumescent composition ratio and intumescence efficiency (Wang and Yang, 2011). Alumina ( $\text{Al}_2\text{O}_3$ ) and silica ( $\text{SiO}_2$ ) are examples of refractory fibres facilitate to enhance the char residue strength and to prolong the effects of fire-resistant. Intumescent systems added with nepheline syenite, and synthetic glasses reported with an improved fire-resistant performance against fires. Vitreous fillers performed to stabilise char layer and lessen the optical density and toxicity of smoke emission (Olcese and Pagella, 1999). The application of cenospheres (coal combustion by-product contained mostly silica and alumina) as filler in the intumescent system exhibited a creamified layer consisted of silicophosphates and aluminophosphates for char reinforcement and fire protection (Puri and Khanna, 2016). Ceramic fibres and minerals with

high temperature were added into the water-based epoxy intumescent coatings. Research indicated ceramic fibres showed much better integration with the intumescent system, and resulted in improved char toughness (Koo et al., 1997).

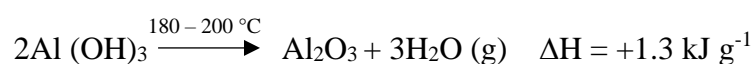
Intumescent coatings formulated with carbon, alumina, glass, and aramid fibres exhibited an enhancement in char strength (Canosa et al., 2011). A variety of ingredients such as kaolin clay, alumina, wollastonite, eggshell was informed with their use as fillers in the intumescent coatings. These fillers interacted with the intumescent system resulted in even carbonaceous char structures with good adhesive ability.  $\text{Al}_2\text{O}_3$  is another feasible option of filler as it is easily available and associated with desirable fire-resistant properties. The used of eggshell as fillers in the intumescent coatings showed evidence of improvement in various aspects such as fire-resistance, thermal stability, water resistance, and mechanical strength (Mohamad et al., 2013; Ullah et al., 2014; Zia-ul-Mustafa et al., 2014; Yew et al., 2014; Yew et al., 2015a). Intumescent coatings are found accompanied with diverse range of intumescent behaviours, char qualities, and thermal degradations when different types of inorganic fillers are applied. Intumescent coatings added with inorganic fillers are detected with a higher melt viscosity. The high melt viscosity coatings limited the relaxation of polymer chains and constrained the intumescence behaviour, led to low ratio of intumescence, char foam thickness, and poor fire resistance as consequences.

Mineral fillers like aluminium hydroxide ( $\text{Al}(\text{OH})_3$ ), magnesium hydroxide ( $\text{Mg}(\text{OH})_2$ ), magnesium carbonate ( $\text{MgCO}_3$ ), and calcium carbonate ( $\text{CaCO}_3$ ) are example of non-combustible mineral fillers. Four fire-retardant characteristics of mineral fillers are identified: (a) the heat capacity of mineral fillers, (b) the endotherm of decomposition, (c) the heat capacity of inert gases and vapours, (d) the heat capacity of residue. These addition of these mineral fillers into a polymer help to lower the fuel amount and diffusion rate of oxygen, hence decrease

the flammability. In addition, these mineral fillers can reinforce the polymer to achieve a better structural integrity. Mineral fillers in the polymer will decompose endothermically when heated and will release vapours and inert gases to quench the flame (Hewitt and Hull, 2017).

The decomposition of mineral fillers shall happen between the narrow gap of above the processing temperature of a polymer, and below the decomposition temperature of a polymer. Flame-retardant mechanisms of mineral fillers can be described in three major phases: (a) the absorption of heat during the endothermic decomposition of fillers help to cool down the polymer; (b) the release of inert gases (CO<sub>2</sub>) and water vapours serve to dilute the concentration of free radicals in the combustion reaction. Fire extinction happens when the free radicals' amount is suppressed; (c) the decomposition of substances creates an inert char layer on the surface. This inert char layer acted as a protective barrier to block the radiant and oxygen from reaching the polymer.

Aluminium hydroxide (Al (OH)<sub>3</sub>), also refers as alumina trihydrate (ATH) with formula Al<sub>2</sub>O<sub>3</sub>.3H<sub>2</sub>O, is one of the flame-retardant minerals used in a polymer. When expose to heat, Al(OH)<sub>3</sub> break down to alumina (Al<sub>2</sub>O<sub>3</sub>), and water during the endothermic reaction. The released of water vapours diluted the free radicals required for flame combustion. The built-up alumina residue formed a protective layer on the surface of a polymer to constraint the heat transmission to the underneath substrate. The decomposition of aluminium hydroxide (Al (OH)<sub>3</sub>) as follows:



The potential fire-retardant metal hydroxide and carbonate mineral fillers, with their formulation, estimated decomposition temperature and decomposition heat released published in the literatures as indicated in **Table 2.2** (Hull et al., 2011). On top of the two most important mineral fillers: Al(OH)<sub>3</sub> and Mg(OH)<sub>2</sub>, other potential mineral fillers such as mixed

magnesium and calcium hydroxides ( $\text{Ca}(\text{OH})_2$ ), and calcium carbonates ( $\text{CaCO}_3$ ) were also studied.

**Table 2.2:** Potential fire-retardant mineral fillers and their physical properties (Hull et al., 2011)

| Mineral Filler      | Formulation   | $T_{\text{decomp}}/^{\circ}\text{C}$ | $\Delta H_{\text{decomp}}/\text{kJ g}^{-1}$ |
|---------------------|---|--------------------------------------|---|
| Aluminium hydroxide | $\text{Al}_2\text{O}_3 \cdot 3\text{H}_2\text{O}$                   | 180 - 200                            | 1300  |
| Magnesium hydroxide | $\text{Mg}(\text{OH})_2$  | 300 - 320                            | 1450  |
| Calcium hydroxide   | $\text{Ca}(\text{OH})_2$  | 430 - 450                            | 1150  |
| Nesquehonite        | $\text{MgCO}_3 \cdot 3\text{H}_2\text{O}$                           | 70 - 100                             | 1750  |
| Hydromagnesite      | $\text{Mg}_5(\text{CO}_3)_4(\text{OH})_2 \cdot 4\text{H}_2\text{O}$ | 220 - 240                            | 1300  |
| Huntite             | $\text{Mg}_3\text{Ca}(\text{CO}_3)_4$                               | 400                                  | 980   |
| Ultracarb           | Hydromagnesite/ Huntite<br>60/40                                    | 220 - 400                            | 1172  |
| Boehmite            | $\text{AlO}(\text{OH})$   | 340 - 350                            | 560   |

The decomposition temperature to the final temperature of an inorganic residue refers as the representative heat capacity. This representative heat capacity is used to determine the heat absorption capacity of an inorganic residue. The heat absorption of mineral filler (%), the decomposition endotherm (%), the released water vapour and carbon dioxide (%), and the residue (%) as shown in **Table 2.3** (Hull et al., 2011).

**Table 2.3:** Fire-retardant mineral fillers and their contributions to heat absorbing effects.

|                     | Contribution of fire-retardant effects |           |             |         |
|---------------------|--|-----------|-------------|---------|
|                     | Filler (%)                             | Endotherm | Residue (%) | Gas (%) |
| Aluminium hydroxide | 9                                      | 55        | 13          | 23      |
| Magnesium hydroxide | 19                                     | 56        | 9           | 15      |
| Calcium hydroxide   | 29                                     | 55        | 5           | 11      |
| Nesquehonite        | 1                                      | 58        | 12          | 29      |
| Hydromagnesite      | 10                                     | 56        | 14          | 21      |
| Huntite             | 20                                     | 58        | 9           | 13      |
| Ultracarb           | 14                                     | 57        | 12          | 18      |
| Boehmite            | 18                                     | 46        | 20          | 15      |

The greatest fire-retardant effects of mineral fillers are contributed by the endothermic reactions in the decomposition process. The heat capacity of the filler, residue and gaseous products are influenced by the decomposition temperature. The decomposition temperature of mineral fillers will increase when it is encompassed by molten polymer. For instance, the common decomposition temperature of aluminium trihydrate (ATH) is 190 °C. When ATH is added into an ethylene-vinyl acetate copolymer (EVA), the water in the copolymer required heating temperature up to 250 °C (McGarry et al., 2000) to be lost. The fire protective barrier formed during the process might be ruptured by the water vapour at this stage (Zilberman et al., 2000).

## **2.6 Intumescent Coatings incorporated with Natural By-Product**

This section describes the intumescent coating formulated using natural by-products. These natural by-products including vegetable compounds such as ginger and coffee powders, rice husk ash, clam shell, chicken eggshell, hybridisation of rice husk ash and chicken eggshell incorporated in the intumescent coating formulation. Results of these approaches are consolidated in this section.

### **2.6.1 Intumescent Coating Formulated with Vegetable Compounds**

The carbonising agent added in an intumescent coating function to stimulate the formation of carbonaceous char in the coating. According to Horrocks et al (2005), current carbon sources used in the intumescent coating like pentaerythritol is non-renewable, and its production process is non-environmentally friendly. It is reported that cellulose and lignin present in the

nature are abundant and can be renewed to use in the intumescent coating as an alternative carbon source of pentaerythritol. Lignin is identified as a naturally present organic aromatic compound that is renewable. Alkaline aromatic lignin is found to be able to enhance the behaviour of flame retardancy of a polymer when it is used as a carbon source (Jiao and Wu, 2013). Cellulose and lignin almost exist in most vegetables; thus, these two compounds are considered renewable and are more affordable than derivatives of petroleum. Vegetable resources can be a potential natural replacement of carbonization agent in the intumescent coating due to the contain of cellulose and lignin. Ginger (*Zingiber officinale*) is the main agricultural crop in India famous for its culinary used as spice in dried and fresh condition. Ginger belongs the botanical family of Zingiberacease (Kumar et al., 2014). Fouda et al (2013) demonstrated the use of ginger as green inhibitor to prevent steel from corrosion.

The chemical structures of ginger consist of aromatic ring such as  $\alpha$ -turmerone,  $\beta$ -turmerone, ar-turmerone, gingerol, curcumene, and curlone. These aromatic compounds contribute to the advantages of the ginger as carbonization agent in the intumescent coating (Fouda et al., 2013). Coffee husks are solid wastes derived from coffee beans. The chemical composition of coffee husks identified with the present of nitrogen, potassium, cellulose, hemicellulose, lignin, pectin, tannins, and caffeine (Pandey et al., 2000; Dzung et al., 2013). Coffee husks have been applied as raw materials for bioprocessing, to produce enzymes, biogas, compost, and mushroom (Neves et al., 2006; Fouda et al., 2013 Shemekite et al., 2014). Coffee husk is another potential source of carbonization agent in the intumescent coating, due to its chemical contain of cellulose, lignin, and aromatic ring.

Non-halogenated phosphorous based flame retardants such as Triphenyl phosphate (TPP) and Zinc phosphate (ZnP) were used due to their environmentally friendliness of zero toxic gases released and ability to retain higher quantity of phosphorus compound in the char layer during the combustion. In contrary to non-halogenates, the combustion of halogenates



(non-phosphorous based flame retardants) emitted toxic gaseous compounds hazardous to human and environment (Butler, 1997; Zhu et al., 2013; Qian et al., 2015). During the combustion, TPP removed the hydrogen radicals to stop the reaction of chains, thus constrained the spreading of flame.

The development of char foam suffocates the flame (Dunn et al., 2012; Ullah et al., 2013). ZnP is toxic less, renowned for its anti-corrosion properties that used to replace chromium flame-retardants (Emira et al., 2012). Stephanie et al (2017) presented the research using ginger (Ggp) and coffee husk (Chk) as carbonization agent in intumescent coatings comprised of Triphenyl phosphate (TPP) and Zinc phosphate (ZnP) as phosphorus flame-retardants. The ginger and coffee husk reinforced intumescent coatings were characterised and the performances were evaluated in terms of fire resistance, morphology of char (SEM), thermal degradation (TGA), molecular functional groups (FTIR), thermally stable compounds (XRD) and volatile gaseous products (Py-Ms-Gc). Result revealed intumescent coatings incorporated with Ggp and Chk as carbon sources reduced the temperature of steel substrate significantly in fire-resistant test and TGA. TPP was found more effective to isolate heat and generate greater char expansion as compared to ZnP. Intumescent coating comprised Ggp/TPP and Chk/TPP in the formulation indicated the most outstanding results among all. Ggp/TPP was recorded with the highest char foam expansion between 1200% to 1670%, cavities with better defined sizes associated with a more cohesive structural layer under SEM, thermally stable oxides that contributed to a better thermal insulation property were identified in XRD, very low toxic level as no CN<sup>-</sup> compounds and phosphine was identified in Py-Ms-Gc.

The good performances of Ggp/TPP and Chk/TPP intumescent coatings were attributed to the present of appropriate amount of lignin, aromatic rings, cellulose, and hemi-cellulose in the composition of Ggp and Chk. According to Stephanie et al (2017), the used of readily available and renewable raw ingredients derived from vegetables and agricultural waste such

as ginger and coffee husk in intumescent coatings were effective, environmentally friendly, and cost-affordable alternatives to existing carbon sources.

### **2.6.2 Intumescent Coating Formulated with Rice Husk Ash**

Mohd et al (2016) examined the fire-retardant performances of geopolymer intumescent coatings incorporated with rice husk ash in the research. Numerous research reported the used of fire-resistant materials consisted of silica to replace halogenates such as chlorinated and brominated retardants. This was due silica-based retardants released of less toxic gases and less harmful to human and environment during the combustion (Zhou and Yang, 2007). Some studies informed the integration of geopolymer coating with metakaolin, and fly ash applied to steel. Thermal behaviour and adhesion properties of geopolymer coating containing metakaolin different ratio of Silica (Si) and Alumina (Al) were evaluated (Temuujin et al., 2009; Fletcher et al., 2005). Fletcher et al (2005) and Temuujin et al (2009) indicated geopolymer coating composition with higher Si-Al and lower water ratio led to a better performance in thermal behaviour.

Geopolymer (alkali-activated aluminosilicate) was synthesized using alkaline activators: sodium silicate ( $\text{H}_2\text{O}$ -30.3%;  $\text{Na}_2\text{O}$ - 11.9;  $\text{SiO}_2$ - 57.8%) and sodium hydroxide ( $\text{NaOH}$ ) and aluminosilicate compounds. Rice husk ash (RH) is a type of biomass waste derived from agricultural processing of rice, and abundant in quantity. RH is biodegradable raw material, affordable in cost, and it has broad potentials to renew and apply in different engineering materials. Omatola and Onojah (2012) reported only a narrow fraction of RH was explored. RH was grounded and burnt 24 hours at 700 °C to generate rice husk ash (RHA). RHA was identified with chemical elemental composition:  $\text{SiO}_2$  (87.4%),  $\text{PdO}$  (6.0%),  $\text{Al}_2\text{O}_3$

(3.0%),  $\text{Fe}_2\text{O}_3$  (1.49%),  $\text{CaO}$  (1.4%),  $\text{K}_2\text{O}$  (0.49%),  $\text{Cr}_2\text{O}_3$  (0.27%),  $\text{MnO}$  (0.19%),  $\text{NiO}$  (0.068%),  $\text{CuO}$  (0.045%), and  $\text{ZnO}$  (0.035%) (Mohd et al., 2016). RHA was used as the aluminosilicate sources to the geopolymer.

Mohd et al (2016) formulated RHA-based geopolymer coatings, with considerations on factors such as alkaline activator (AA) solution ratio, sodium hydroxide (NaOH) solution concentration, RHA-AA ratio, curing temperature and time. Fire-resistant and material properties of RHA-geopolymer coating were assessed (Mohd et al., 2016). Experiment revealed RHA-based geopolymer coating (S7) with Si-Al ratio of 140, and AA-RHA ratio of 1.35: 1.50 indicated the best fire resistance among all samples. S7 was with composition: AA-5.5, RHA-AA-0.3, curing temperature-50 °C, curing time- 7 days, and concentration of NaOH-8M. S7 took the longest time to achieve the lowest equilibrium temperature of 398 °C (at 25 minutes).

After the burning test, the formation of needle-liked structures with various sizes was identified as one of the key criteria contributed to the best fire-resistant outcomes in S7. Zhang et al (2014) informed such scenario with the formation of oligomers, further stimulated the generation of reactive Si- and Al-tetrahedrons. These crystalline tetrahedron structures showed a high polymerisation degree, which could contribute to the best fire-resistant properties in S7. These results proved the effectiveness of RHA as a potential silica alternative in fire-retardant intumescent coatings.

### **2.6.3 Intumescent Coating Formulated with Clam Shell**

Intumescent coatings formulated using APP/PER/MEL were prone to char barrier with increased oxidation and decreased mechanical properties. Hence, the fire protection efficacy of char barrier to the steel substrate was reduced (Yan et al., 2019). Much research are looking to optimise the formula of intumescent coatings in terms of the physical and chemical attributes to enhance the fire-retardant, mechanical, and anti-oxidation strength (Wang et al., 2006a; Wang et al., 2006b). In recent years, bio-fillers (eggshell and clamshell), nano-fillers (graphene and carbon nanotube), boron compounds (zinc borate and boron oxide), metal oxides (iron oxide and titanium dioxide) and inorganic fillers (silicon dioxide and boric oxide) are broadly explored and applied as synergists in flame-retardant intumescent coatings research. Nano-fillers exhibited excellent synergy with intumescent system enhancing the flame-retardancy.

Nonetheless, severe agglomerations were found in the intumescent polymer matrix correlated to the addition of nano-fillers. These agglomerations degraded the integrity of the polymer matrix and char barrier quality for fire protection (Beheshti and Heris, 2016). Yew et al (2018) indicated eco-compatible bio-filler contributed to the superior flame-retardant and mechanical properties of intumescent coatings. Biological shell is a type of raw material consists of natural minerals, it was found with excellent biological affinity ideal to use in composites (Shah et al., 2016; Wen et al., 2020). Abandoned shellfish shell was re-used as bio-filler in polypropylene composites.

It was noticed shellfish shell reinforced polypropylene composites had better mechanical performances as compared to polypropylene composites reinforced with conventional industrial calcium carbonate (Li et al., 2012). Acrylonitrile-butadiene-styrenen composites (ABS) filled with seashell wastes found improvements in flame-retardant, thermal, and mechanical behaviour (Moustafa et al., 2015). Researchers found polyethylene and

synthetic composites reinforced with bio-filler such as fish bones, eggshells, marine shells exhibited lower combustion rate, and better fire-resistance, water-resistance, mechanical strength, and structural integrity (Isaac and Genevive, 2012; Yew and Sulong, 2012; Yew et al., 2014; Nwanonenyi et al., 2018). It was found the char residual weight, antioxidant, thermal insulation, washing resistance, dispersion, interface interaction, and thermal stability in the intumescent coatings, fluorocarbon coatings and SEBS composites were significantly improved (Dong et al., 2009; Beheshti and Heris, 2015; Zhang et al., 2019). Eggshell bio-fillers showed superior synergy with epoxy fire-retardant intumescent coatings displayed lower smoke and heat release rate (Xu et al., 2018). The synergy of clamshell bio-filler with water-based fire-retardant intumescent coatings was not well-known.

Li et al (2021) explored clamshell (CS) as bio-filler synergist to enhance the flame-retardant and ageing resistant properties of waterborne fire-retardant coatings. Clamshells were obtained from a faculty cafeteria of Central South University in Changsha, China. Clam shells were recycled and re-used through washing, grinding, and sieving. The clam shell flame-retardant coatings were characterized via fourier transform infrared spectroscopy analysis (FTIR), x-ray diffraction (XRD), dispersive x-ray analysis (EDX), x-ray fluorescence analysis (XRF), thermogravimetric analysis (TGA). The synergistic effects of clam shells on water-based fire-retardant intumescent coatings in terms of fire protection, char formation, smoke suppression, and anti-ageing were evaluated and analysed.

CS was identified with calcium (30.26%), oxygen (53.89%), carbon (15.48%) and sodium (0.37%). FTIR, XRF, and XRD informed the main component in the CS (bio-filler) is calcium carbonate ( $\text{CaCO}_3$ ). FC-3 added with 3 wt% CS bio-filler achieved the lowest equilibrium temperature at 136.2 °C, weight loss at 3.3 g, Flame Spread Rate value (FSR) at 15.3, char index at 6.8  $\text{cm}^3$ , and the highest intumescent factor at 55 for the best fire protection performance. A noticeable increased in the equilibrium temperature observed when more than

5 wt% CS bio-filler was added to the intumescent coating sample, worsen the fire resistant and thermal insulation. Fire protection tests result revealed FC-3 sample filled with 3 wt% CS bio-filler manifested the optimum synergy of fire-retardancy with the intumescent coating. In the smoke density test, FC-3 exhibited the best effect of smoke suppression at 17.8% as compared to all samples. The smoke density disclosed an increase amount of CS bio-filler (more than 5 wt%) depreciated the ability of intumescent coating to suppress smoke. The suitable quantity of 3 wt% of CS bio-filler generated the best synergy with the intumescent coating hence produced the least smoke. In the FTIR test, it was observed the molecular group peak intensities became more obvious when the ageing cycles increased. This scenario was due to the major flame-retardants: APP, PER, MEL slowly migrated from the polymer binder matrix hence, reduced the effectiveness of flame-retardants in the coatings.

Furthermore, the migration of components induced contraction (release of internal stresses) decreased the aesthetic of coating's surface (blistering) and adhesion strength. The blistering greatly injured the structural integrity of polymer matrix of coatings, cut down the fire-resistant duration and smoke suppression ability. FTIR test indicated the coating structure of FC-3 was the most stable as it had the least molecular peak intensity changes and blistering. The improved molecular structure of FC-3 was able to prevent hydrolysis and migration more effectively. FC-3 added with 3 wt% CS bio-filler hence revealed the best synergy in the intumescent coating in terms of anti-ageing, structural integrity, fire-resistant and smoke suppression durability.

In TGA, the onset decomposition temperature of coating sample FC-3 increased when CS bio-filler was added at 3 wt%, followed by a decreased in FC-5 when 5 wt% of CS bio-filler was added. Addition of CS bio-filler of more than 5 wt% in the coating sample was found declined the coating performance in terms of decomposition temperature and residual weight. The thermal stability was correlated to the residual weight. When the thermal stability of FC-3

(3 wt%) enhanced, the residual weight of FC-3 remained the highest at 34.5 wt%. Namely, then least mass loss was encountered by FC-3. FC-3 was associated with the optimum char expansion. Appropriate amount of 3 wt% CS bio-filler was crucial to assist in enhancing the thermal stability and char formation of the coating sample. The char residue analysis revealed FC-3 incorporated with 3 wt% exerted the thickest, and densest char layer to block the heat and mass transfer (Jiang et al., 2015).

Excessive content of CS bio-filler at 5 wt% restrained the process of intumescent limiting the char foam. The SEM indicated the char structure of FC-3 was the most coherent, and compacted, with only little voids and visible cracks appeared that able to insulate the substrate better as compared to others. The EDS test further revealed FC-3 consisted of more P crosslinking molecular groups remained in the condensed phase. These P crosslinking molecular groups were beneficial to enhance the thermal stability of char layer (Li et al., 2015; Yan et al., 2019). The O/C, N/C, and P/C mass ratio of FC-3 char were the top disclosed the presence of the highest amount of O, N and P crosslinking molecular groups (Yuan et al., 2017). The O, N, and P crosslinking molecular groups present in the char layer were important elements for a more thermally stable char and char compactness to prevent oxygen, combustible gas, and heat transfer (better insulation). 3 wt% was bestowed with the best synergistic effect in the flame-retardant intumescent coating.

#### **2.6.4 Intumescent Coating Formulated with Chicken Eggshell**

Chicken eggshell (ES) is a type of renewable resources derived from aviculture by-product. CES has been used in the coating research due to its huge potentials (Pradhan and Sahoo, 2017). More than 95 % component of ES is calcium carbonate existed in calcite form, remaining 5 %

is other organic components. Calcium carbonate form derived from natural ES waste can replace industrial calcium carbonate due to the compatible quality and performance (Arias and Fernandez, 2003; Ishikawa, 2004; Yi et al., 2004; Tsai, 2006; Yew et al., 2013; Oualha, 2017; Yew et al., 2018). Calcium carbonate ( $\text{CaCO}_3$ ) nano powder is one of the widely and commonly used flame-retardant filler in the coating industry. Organic and inorganic flame-retardant fillers added will modify the properties of intumescent coatings such as ignition resistant and smoke emission (Maurizio et al., 2006). These property enhancements were contributed by the high thermal stability and surface area to volume ratio and non-toxic characteristics of  $\text{CaCO}_3$ .  $\text{CaCO}_3$  can accelerate the time of drying, enhance the thixotropic properties, and generate gloss to the coatings.  $\text{CaCO}_3$  is in favourable use in the coating industry due to its easily availability and low cost (Yoo et al., 2009; Yew et al., 2013). Magnesium hydroxide ( $\text{Mg}(\text{OH})_2$ ) and Aluminium hydroxide ( $\text{Al}(\text{OH})_3$ ) possess better insulation properties and lower flame-retardancy that able to minimise the heat release rate (Mohamad et al., 2013; Yew et al., 2015b; Arogundade et al., 2016).

Suitable composition of flame-retardant ingredients will determine the efficiency of intumescent coatings (Yew et al., 2015a). Yew et al (2018) incorporated ES nano-filler in the water-based flame-retardant intumescent coating formula. Fire-resistant, thermal, and mechanical characteristics of ES incorporated water-based intumescent coating samples were examined and evaluated. In the fire-resistant test, sample D (ES nano biofiller- 3.0 wt%;  $\text{Mg}(\text{OH})_2$ - 3.0 wt%;  $\text{Al}(\text{OH})_3$ - 4.0 wt%;  $\text{TiO}_2$ - 2.0 wt%) showed the lowest equilibrium temperature of 264 °C after 100 mins and generated the thickest, uniform char layer of 31.2 mm to block the fire penetration (Wang and Yang, 2010). This outcome indicated the appropriate amount of 3.0 wt% was able to create the best synergy (positive physical and chemical reactions) with the water-based binder and other flame-retardants. It was found that increased amount of  $\text{Mg}(\text{OH})_2$  at more than 5.0 wt% prevented the char expansion thus leading



to the worst fire resistant properties. The SEM surface micrograph revealed the surface structure of sample D added with 3.0 wt% ES was the most uniform, smooth and with compact surface matrix before the fire-resistant test. Similarly, after the fire-resistant test, sample D showed the most uniform and densest char structure under the high magnification of SEM. This dense, uniform plate-like char cell structure can inhibit penetration of fire effectively. This good quality char structure was correlated to the best fire protection and thermal insulation performance of sample D.

It was reported, 3.0 wt% ES nano bio-filler added into sample D led to the best char layer and interfacial bonding. Sample D encountered the highest mass loss between 320 °C to 420 °C largely attributed to the decomposition of VAC. Followed by another mass loss from 420 °C to 900 °C, which was due to the decomposition of  $\text{TiO}_2$ ,  $\text{Mg}(\text{OH})_2$  and  $\text{Al}(\text{OH})_3$ . In overall, sample D displayed the least mass loss (highest residual weight) in the TGA at 900 °C as compared to other samples, indicated the best thermal stability. Water-based intumescent coating added with 3.0 wt% ES nano filler associated with the best thermal stability, anti-oxidation, and fire protection properties. ES nano bio-filler enhanced the adhesion strength of intumescent coating to steel substrate by filling up the voids in the coating's matrix. Carbonyl groups presented between VAC and surface oxide, or hydroxide of the steel substrate created hydrogen bonding that enhanced the adhesion strength. The cross-linking molecular bonding of ES nano bio-filler with coating had improved the interfacial interaction of coating with steel substrate (Packham, 1996). Mechanical tensile stress induced air spaces in the coating matrix causing the loss of adhesion strength between fillers, coating, and steel substrate (Ramis et al., 2013).

$\text{CaCO}_3$  particles presented in the ES nano bio-filler offered compatible particle sizes that better embedded into the coating interfacial matrix and reinforced bonding to the steel substrate (Yew et al., 2013). Sample D possessed the strongest adhesion strength (2.13 MPa)

and crack charge ( $33.4 \times 10^3$  N). It was noticed the incorporation of 3.0 wt% ES nano bio-filler with the appropriate composition of other flame-retardants in water-based intumescent coating improved the adhesion strength of coating to steel substrate. In the FTIR, intense intramolecular and intermolecular stretching of O-H functional group were found between band peaks ranging from  $3100\text{ cm}^{-1}$  to  $3500\text{ cm}^{-1}$ , which could contribute to the strong interfacial hydrogen bonding between coating and steel substrate (Hong et al., 2010). Ester carbonyl bond ( $\text{-C=O}$ ) and ester bond ( $\text{-C-O}$ ) were found in the intumescent coating ranging from band peaks between  $1726\text{ cm}^{-1}$  to  $1732\text{ cm}^{-1}$  and  $1188\text{ cm}^{-1}$  to  $1282\text{ cm}^{-1}$  indicated the existence of hydrogen bonding. These  $\text{-C=O}$  and  $\text{-C-O}$  groups were sensitive constituted to the hydrogen bond formation in the coating. This experiment manifested 3.0 wt% ES nano bio-filler added into the water-based intumescent coating activated the best positive outcomes in terms of fire protection, thermal stability, and mechanical strength.

#### **2.6.5 Intumescent Coating Formulated with Hybrid Rice Husk Ash and Chicken Eggshell**

The composition of fire-resistant intumescent coating can be formulated to achieve a designated condition of fire protection. Most of the current intumescent coating formula do not contain any environmentally friendly components. Filler is an important ingredient in the intumescent coating that offers good matrix-filling effect and compact char to ensure a better heat insulation performance (Martins et al., 2017). In general, most fillers are minerals (inert or inorganic), commonly used are such as aluminium hydroxide, magnesium hydroxide, and calcium carbonate. Inert fillers are not flame-retardant, nonetheless, when dissolved and after

a series of cross-linking reactions, fillers converted to low heat generators. These cross-linking reactions and conversion of fillers proved the occurrence of synergy in fillers and additives (Zia-ul-Mustafa et al., 2017; Zheng et al., 2019).

Rice husk ash (RHA) has become a popular reactive filler in concrete research due to its pozzolanic behaviour. Pozzolans (cementitious ingredients) in RHA found able to improve the mechanical strength of concrete, producing lightweight high strength concrete that area load, seismic and fire bearable. Challenges were found in the RHA reinforced concrete when applied with steel structure (Celik and Canakci, 2015; Huynh et al., 2018; Khaliq and Mujeeb, 2019). Chicken eggshell (CES) waste was reused as fillers in intumescent coatings indicated positive outcomes in various performances (Yew et al., 2015b; Yew et al., 2018; Xu et al., 2019). For example, CES helped in the swelling of char through the release of inert gases, formed a better char barrier to prevent oxygen diffusion. This char barrier generated over steel surface was able to shield and protect the steel from further fire damage.

Much research proven the effective use of CES waste as bio-filler in the intumescent coatings. This approach of using CES waste to produce eco-friendly intumescent coating assisted in reducing environment burden, conserving a more sustainable environment. Studies are conducted to explore the synergism of single fillers and hybrid fillers in intumescent coatings (Li et al., 2020a; Li et al., 2020b; Xu et al., 2020). Nasir et al (2020) investigated the synergy of bio-fillers and industrial fillers in water-based intumescent coatings in relation to flame-retardant, physical, and mechanical properties. Six water-based intumescent coating samples were formulated with different composition of flame-retardant additives, industrial fillers- titanium dioxide ( $\text{TiO}_2$ ) and aluminium hydroxide ( $\text{Al}(\text{OH})_3$ ), bio-fillers- chicken eggshell (CES) and rice husk ash (RHA). Samples were characterised through Bunsen burner, fire propagation, surface spread of flame, and oxygen index tests.

The synergy of bio-fillers and industrial fillers in the water-based intumescent coating samples were evaluated via water resistant, eco-label, char quality, scanning electron microscopy (SEM), and adhesion tests. The synergistic effects between fillers, flame retardant additives and water-based intumescent coatings derived from an inter-cross-linking network were assessed. It was noticed coating sample- TA incorporated with hybrid industrial fillers (5.0 wt%  $\text{TiO}_2$  and 5.0 wt%  $\text{Al(OH)}_3$ ) experienced the highest water gain among all. Coating sample- TAC (3.4 wt%  $\text{TiO}_2$ , 3.3 wt%  $\text{Al(OH)}_3$ , 3.3 wt% CES) displayed the best water resistance as compared to all, followed by sample- ALL (2.5 wt%  $\text{TiO}_2$ , 2.5 wt%  $\text{Al(OH)}_3$ , 2.5 wt% RHA, 2.5 wt%, 2.5 wt% CES), and sample- TC (5.0 wt%  $\text{TiO}_2$ , 5.0 wt% CES).

Results indicated appropriate amount of CES, RHA bio-filler, hybrid with industrial fillers in water-based intumescent coatings able to slow down water absorption rate, prevent water migration into coating over a period of 15 days. This was largely attributed to a better solubility and particle distribution of bio-fillers, and their ability to form a three-dimensional cross-linking matrix with coating network that bring 'labyrinth' effect to the coating molecular bonding. This 'labyrinth' effect progressively inhibited water permeation into coating (Wang and Wang, 2017; Li et al., 2019). In SEM, sample incorporated with bio-fillers showed a thicker and denser uniform char cell structures due to homogeneous cross-linking formed in the matrix, created effective heat insulation char barrier for fire protection. The eco-label heavy metal test revealed all water-based intumescent coating samples reinforced with hybrid bio-fillers and industrial fillers had very least (less than 0.01 ppm) heavy metal contents fulfilled health safety used. This proved the replacement of synthetic fillers with natural bio-fillers was a safe promising approach to optimise environmentally friendly intumescent coating.

All coating samples show desirable adhesion strength adhered to the steel plate without falling off after one hour of Bunsen burner test. In the fire resistance test, it was found, coating sample-TR reinforced with 5.0 wt% RHA and 5.0 wt%  $\text{TiO}_2$  showed the lowest equilibrium

temperature of 181 °C after exposed to 1000 °C Bunsen burner for 60 mins. Coating sample-TA (5.0 wt% TiO<sub>2</sub> & 5.0 wt% Al(OH)<sub>3</sub>) without addition of any bio-fillers showed the highest equilibrium temperature of 224 °C.

Both bio-fillers- RHA and CES did enhance the fire-resistance performance of intumescent coatings. Reinforcement of intumescent coating using hybrid RHA and TiO<sub>2</sub> brought the best fire resistance outcome. It is suggested RHA induced the best synergy with the water-based intumescent coating and other flame-retardant additives resulted in excellent insulation to heat. Extra amount of Al(OH)<sub>3</sub> more than 2.5 wt% might inhibit the char formation and swelling, expedite the combustion and heat spreading rate. Surface spread of flame test classified all coatings as Class 1. Hybrid bio-fillers and industrial fillers created excellent cross-linking matrix that can suppress the flame spreading and smoke production more effectively (Sun et al., 2019). All coating samples fulfilled the class O classification with low sub-index less than 6 indicated desirably low fire propagation index that fulfilled the fire safety requirement (BS 476: Part 6). Among all, TR (5.0 wt% RHA & 5.0 wt% TiO<sub>2</sub>) expressed the lowest fire propagation. In contrary, TA (5.0 wt% TiO<sub>2</sub> & Al(OH)<sub>3</sub>) exhibited the highest fire propagation index. This demonstrated addition of Al(OH)<sub>3</sub> into intumescent coating without hybrid with bio-filler, leading to poor char quality, thermal insulation, fire resistant and mechanical properties (Zeng et al., 2020).

The used of hybrid bio- and industrial fillers at total ratio of 10.0 wt% activated the char generation and anti-dripping properties of intumescent coating for fire protection of steel substrate underneath. Synergism between flame retardants and fillers can enhanced fire resistance (Zeng et al., 2020). It is recommended, 10 wt% of hybrid bio-fillers exerted good synergistic activities with for flame retardant improvement. All molecules in the intumescent coating were blended and occupied homogenously within the molecular chain structures after the mixing procedure. Cross-linking formed among molecular chain structures in the coating

matrix stimulated bonding interaction, generated cohesion strength between coating and substrate (Wu et al., 2019).

Result demonstrated coating hybrid with CES bio-filler showed better mechanical adhesion strength when compared to coating hybrid with RHA bio-filler. It was certain, coating without hybridized with bio-fillers exhibited the weakest adhesion strength. Char strength was essential to determine the effectiveness of char as fire protective barrier. Char could rupture easily when subjected to mechanical stress and lost its function in a fire event. A high-density molecular compound can enhance the compression and cross-linking attributes of char structure (Zhang et al., 2020). Coating hybrid with CES created thickest char, followed by coating hybrid with RHA. Nonetheless, the thickest char layer was opposed to the char strength. Hybrid CES thick char came with flaky and brittle cell structures, as verified in SEM. When exposed to loads, char derived from hybrid CES encountered great reduction in the char strength and char durability due to its weak char cell structures as described. Coating sample-ALL reinforced with a balance of all bio- and industrial- fillers (2.5 wt% RHA, 2.5 wt% CES, 2.5 wt%TiO<sub>2</sub>, 2.5 wt%Al(OH)<sub>3</sub>) exhibited the best char strength in overall. Intumescent coatings using natural by-products, and their formula with the best performance in fire resistant and TGA test as summarised in **Table 2.4**.

**Table 2.4:** Intumescent coatings using natural by-products, and their formula with the best performance in fire resistant and TGA test.

| Intumescent coating Formula   | Composition (wt. %)                    | Fire Protection Performance  |                           | Reference               |
|---|--|------------------------------|---------------------------|-------------------------|
|   |  | Equilibrium temperature (°C) | Residual mass TGA (wt. %) |                         |
| APP/MEL/PER/SF/CES  | 37.04/18.52/18.52 / 7.40/18.52         | 183.0                        | 40.0                      | Yew and Sulong, 2012    |
| APP/MEL/PER/TiO <sub>2</sub> /Al(OH) <sub>3</sub> /Mg(OH) <sub>2</sub> /CES/AR      | 18.5/9.25/9.25/ 2.5/2.5/ 2.5/2.5/ 53.0 | 259.0                        | 30.0                      | Yew et al., 2015a       |
| AA/RHA-AA   | 5.5/0.3                                | 398.3                        | 27.7                      | Salahuddin et al., 2016 |
| Chk/AR/MEL/BA/ZnP   | 6.19/71.80/6.19/ 6.19/9.63             | 139.0                        | 27.0                      | De Sa et al., 2017      |
| Chk/AR/MEL/BA/TiO <sub>2</sub> /TPP   | 6.19/71.80/6.19/ 6.19/6.20/3.43        | 147.0                        | 26.0                      |                         |
| Ggp/AR/MEL/BA/ TiO <sub>2</sub> /TPP  | 6.19/71.80/6.19/ 6.19/6.20/3.43        | 153.0                        | 26.0                      |                         |
| APP/MEL/PER/VAC/TiO <sub>2</sub> /Al(OH) <sub>3</sub> /Mg(OH) <sub>2</sub> /Nano ES | 22/11/11/ 48/2.0/ 4.0/ 3.0/ 3.0        | 264.0                        | 20.0                      | Yew et al., 2018        |
| IFR/TiO <sub>2</sub> /CS/EP/PR  | 55/1/3/40/4                            | 136.2                        | 34.5                      | Li, et al., 2020        |
| FRA/VAAC/TiO <sub>2</sub> /RHA  | 37/53/5.0/3.0                          | 181                          | -                         | Khairunisa et al., 2020 |

- a. APP= Ammonium Polyphosphate
- b. MEL= Melamine
- c. PER= Pentaerythritol
- d. SF= Silica Fume
- e. CES= Chicken Eggshell
- f. TiO<sub>2</sub>= Titanium dioxide
- g. Al(OH)<sub>3</sub>= Aluminium hydroxide
- h. Mg(OH)<sub>2</sub>= Magnesium hydroxide
- i. AR= Acrylic Resin
- j. AA= Alkaline Activator (Sodium silicate + Sodium Hydroxide)
- k. RHA= Rice Husk Ash
- l. Chk= Coffee husk
- m. BA= Boric Acid
- n. ZnP= Zinc phosphate
- o. TPP= Triphenyl phosphate
- p. Ggp= Ginger powder

- q. VAC= Vinyl Acetate Copolymer
  - r. Nano ES= Nano Eggshell
  - s. IFR= Intumescent flame retardants (APP-MEL-PER)
  - t. CS= Clam Shell
  - u. EP= Epoxy Resin
  - v. PR= Polyamide resin
  - w. FRA= Flame retardant additives
  - x. VAAC= Vinyl acetate acrylic copolymer
- 

## **2.7 Wood Ash Waste and Their Physical and Chemical Properties**

Wood ash and paper mill sludge are among the top waste accumulate and abundant the most in the environment produce by the wood industries (Demeyer et al., 2001). Etiegni et al (1991) and Vance (1996) reported there are about 3 to 5 million Mg of wood ash produced from the wood, paper, and pulp industries every year in the US. In Sweden, there are about 200 thousand Mg of wood ash produced annually (Clarholm, 1994). The combustion of waste wood creates large amount of wood ash that is high in alkali with pH ranging from 9.0 – 13.5. Throughout the years, the environment laws and regulations have been tightened to control the disposal of waste. Most of these wood ash wastes (more than 80% in the US) are disposed to the to the landfills (Vance, 1996). Landfill sites are becoming more expensive, and less landfill sites are available for the disposal of wood ash waste. As a result, it is essential and urgent to seek alternative solutions to mitigate these increasing problems of waste wood ash (Campbell, 1990). The challenges of high cost and in getting new site for landfill, have aroused ideas to encourage the alternative disposals of wood ash wastes. Research have been conducted to re-use the wood ash in the agriculture and forestry industries. These studies revealed the potential utilization of wood ash as lime source to the soil. The wood ash can amend the nutrient deficiencies of the soil caused by the deposition of acid and leaching (Cronan and Grigal, 1995).



Wood ash properties are varying, depending on factors as follow (Etiegni and Campbell, 1991; Ulery et al., 1993; Someshwar, 1996):

- (a) The type of plant.
- (b) The combusted part of plant (eg. leaves, bark, wood).
- (c) The type of waste (eg. wood, paper residue, pulp).
- (d) The combination with other resources of fuel.
- (e) The type of soil and climate condition.
- (f) The type of combustion condition.
- (g) The type of collection and storage condition.

It is due to the above various factors, the available information about the wood ash properties is indeed diverse and variable, and thus a generalization about the collected data is challenging to achieve. The research of Etiegni et al (1991) and Etiegni and Campbell (1991) revealed 80% and above of wood ash particles are less than 1.0 mm, and the rest including unburned wood particles. In the granulometric classes defined by the United States Department of Agriculture (USDA)/Food and Agriculture Organization (FAO), the particle sizes of wood ash consist of wide range distribution from coarse sand to clay. The bulk density of ashes ranging from 0.27 gcm<sup>-3</sup> (ash derived from wood sources) (Huang et al., 1992) to 0.51 gcm<sup>-3</sup> (ash derived from paper and pulp sources) (Muse and Mitchell, 1995). A higher density was noticed in the ash originated from paper and pulp source might be due to the clay and salts that added to the pulp in the paper production process.

The major compound of wood ash is calcite (CaCO<sub>3</sub>) disclosed under XRD and infrared analysis (Etiegni and Campbell, 1991; Erich and Ohno, 1992; Ohno, 1992; Ulery et al., 1993). Other compounds such as lime (CaO), riebeckite ((NaCa)<sub>2</sub>(FeMn)<sub>3</sub>Fe<sub>2</sub>(SiAl)<sub>8</sub>), portlandite (Ca(OH)<sub>2</sub>), calcium silicate (Ca<sub>2</sub>SiO<sub>4</sub>), hydrotalcite (Mg<sub>6</sub>Al<sub>12</sub>CO<sub>3</sub>(OH)<sub>16</sub>.4H<sub>2</sub>O) and serandite

( $\text{Na}(\text{MnCa})_2\text{Si}_3\text{O}_8(\text{OH})$ ) were discovered (Etiegni and Campbell, 1991). In the combustion process of wood, organic compounds undergo mineralisation and basic cations undergo transformation to form their oxides compounds. These organic mineral and oxides compound gradually hydrated and carbonated in the atmosphere. The neutralizing capacity (alkalinity) of wood ash is quite high. Based on the study of 18 samples of wood-fire boiler ash, it was found the calcium carbonate equivalent (CCE) of these ashes range from 13.2% to 92.4%, with a median CCE of 48.1%. These results explained the high variables of alkalinity and OH/CO<sub>3</sub>/HCO<sub>3</sub> ratios of wood ash shown in the disparity of pH-H<sub>2</sub>O (**Table 2.5**) (Demeyer et al., 2001).

**Table 2.5:** The pH and CCE of different wood ash sources.

| Original source | pH-H <sub>2</sub> O | CCE (%)   | Remarks              | Reference                   |
|-----------------|---------------------|-----------|----------------------|-----------------------------|
| Wood & bark     | 12.7                | 54.0      |                      | Kahl et al. (1996)          |
|                 | 8.9                 | 17.0      | 30 days <sup>a</sup> |                             |
|                 | 12.1                | 29.1      |                      | Krejzl and Scanlon (1996)   |
|                 | 12.3                | 48.1      |                      | Vance (1996)                |
|                 | 12.0                | 95.0      | 22 days              |                             |
|                 | 9.3                 | 34.0      | 60 days              |                             |
|                 | 13.1-13.3           | 91.2-92.4 |                      | Etiegni et al. (1991a)      |
|                 | 9-13.5              | 62.8      | 538 °C <sup>b</sup>  | Etiegni and Campbell (1991) |
|                 | -                   | 51.4      | 1093 °C              |                             |
| Paper & pulp    | 9.9                 | 37.5      |                      | Muse and Mitchell (1995)    |
|                 | 12.9                | 35.7      |                      | Huang et al. (1992)         |

<sup>a</sup> Time after incineration

<sup>b</sup> Combustion temperature

These properties were largely attributed by the combustion temperature and storage duration. For example, it was noticed the alkalinity of wood ash diminished with the increment of combustion temperature and storage period. Carbonated and bicarbonate compounds were dominant in the combustion phase with temperature below 500 °C, whereas oxide compounds

were occupied at combustion temperature 1000 °C and above. The hydration of oxides will result in hydroxides. These hydroxides will react with carbon dioxide (CO<sub>2</sub>) and transform into carbonates (CO<sub>3</sub>) (Meiwes, 1995).

The composition of major compounds in wood ash are highly variable. These major compound variants of wood ash as shown in **Table 2.6** (Etiegni et al., 1991; Huang et al., 1992).

**Table 2.6:** Wood ashes element total concentration (macro and micro elements).

| Element        | Ashes of wood and bark (g/kg) |                     |
|----------------|-------------------------------|---------------------|
|                | Etiegni et al. (1991)         | Huang et al. (1992) |
| Macro elements |                               |                     |
| N              | 0.600                         | 0.900               |
| p              | 14.000                        | 6.900               |
| S              | 4.455                         | 6.800               |
| Ca             | 317.400                       | 109.400             |
| Mg             | 22.500                        | 16.200              |
| K              | 41.300                        | 28.600              |
| Na             | 3.400                         | 1.600               |
| Al             | 23.650                        | 13.000              |
| Micro elements |                               |                     |
| Fe             | 19.500                        | 3.300               |
| Mn             | 6.693                         | 3.470               |
| Zn             | 0.700                         | 0.794               |
| Cu             | 1.45                          | 0.78                |
| B              | 0.008                         | 0.127               |
| Mo             | 0.114                         | -                   |
| Pb             | 0.130                         | 0.066               |
| Ni             | 0.047                         | 0.012               |
| Cr             | 0.086                         | 0.014               |
| Co             | -                             | 0.004               |
| Cd             | 0.021                         | 0.003               |

Vance (1996) reported a median of various macro elements in ashes from wood-fired boiler: N (0.06%), P (0.42%), Ca (18.00%), Mg (0.97%), K (2.27%). Someswhar (1996) informed a median of macro elements in bark ashes: P (1.57%), Ca (18.5%), Mg (2.86%), and K (3.52%). Al and silicium might not be negligible, due to sand could be mixed with the wood and bark during the logging activities (Someswhar, 1996). In the mineralogical analysis, it was indicated that alkaline elements were present mostly in oxides, hydroxides, and carbonates compounds.

These compounds contribute to the high sulfate capture capacity of the ash and proven the present of S (sulfur) at 0.3% in the ash (Someswhar, 1996). The C (carbon) and N (nitrogen) elements are normally negligible in quantity, due to these elements go through oxidation and transform into volatile gases during the combustion process. In certain cases, involved with incomplete combustion, the C and N might be present in the ashes (Muse and Mitchell, 1995; Someswhar, 1996). The potassium (K) in the wood ash has high solubility in water, thus it is highly prone to leaching (Ulery et al., 1993). The Ca, Mg, and K elements are found highly soluble in the acid, whereas Si and Al are the least soluble in the acid. It is suggested, Si and Al are the structural elements in the ashes (Ohno, 1992; Ohno and Erich, 1993).

A comparison was done among various wood ashes from direct combustion. Outcome shown wood sources produced higher amount of macro elements as compared to paper and pulp. The wood ashes contain higher amount of Ca and K and lower Al when compared to coal ashes. Fe (iron) presents as the most abundant microelement in the wood ash among all. Similarly, Fe is like Si and Al, it is insoluble in acid. Fe can retain up to as much as 21 g/kg in the ash (Someswhar, 1996), most probably could be one of the structural elements in the ash. The Mn, Zn, and Cd elements are higher while As, Se and Cr are lower in wood ash in comparison to coal ash. Wood ash might come with the content of organic compounds,

polyaromatic hydrocarbons, chlorobenzenes, chlorophenols, and others. However, their small quantity might be negligible (Someshwar, 1996).

As wood ash is identified rich in elements such as potassium, lime and other nutrients required by plants, it has been applied in various agricultural uses (Lerner and Utzinger, 1986; Naylor and Schmidt, 1986; Campbell, 1990; Etiegni, 1990). McWhinnie (1979) used of wood ash as a glazing base in ceramics. Wood ash also has been applied as a binder, a road base, an additive in the production of cement, and as an alkali neutralization agent. When wood ash is applied as liming source (neutralization agent) to amend the soil, it is important to understand the swelling and hydration properties of the wood ash as these will have influences on the soil permeabilities. It is crucial to understand the chemical composition of wood ash especially when it needs to use in the land, in the chemical extraction process, and to dispose in the landfill. Etiegni and Campbell (1991) found the yield of wood ash decreased about 45% when the burning temperature elevating from 538 °C to 1093 °C in pine sawdust. The major elements identified in the wood ash were Ca, K, Mg, Si, and P. Metal elements such as Al, Cr, Fe, L were noticed with increment in the content when temperature raised. In contrary, elements such as K, Na, and Zn decreased in amount in high temperature. This could be attributed to a lower decomposition and boiling temperature of the oxides and carbonate compounds of K, Na, Zn. It was observed the content of carbonates dropped from 63% to 51% at temperature 1093 °C.

The yield of wood ash and its chemical properties will change according to different temperature. The content of hydroxides, carbonates, and bicarbonates will determine the alkalinity of wood ash. At temperature below 500 °C, the wood ash content is predominantly with carbonates and bicarbonates. Oxides are prevalent in the wood ash content when the temperature goes above 1000 °C (Naylor and Schmidt, 1986). The composition of wood ash varies in different storage and environmental conditions. This is because carbon dioxide and moisture in the air will react with the wood ash resulted in the formation of hydroxides,

carbonates, and bicarbonates. The chemical reaction of wood combustion, hydration, and carbonization of wood ash compounds (calcium salts are selected as examples) as shown in **Table 2.7**.

**Table 2.7:** Chemical reactions of wood combustion, hydration, and carbonization of wood ash compound (calcium salts).

|                     |                    |                   |                     |                                    |                     |                   |                    |
|---------------------|--------------------|-------------------|---------------------|------------------------------------|---------------------|-------------------|--------------------|
| Wood                | + O <sub>2</sub>   | →                 | Charcoal            | + CaO                              | + CaCO <sub>3</sub> | + CO <sub>2</sub> | + H <sub>2</sub> O |
| CaO                 | + H <sub>2</sub> O | ↔                 | Ca(OH) <sub>2</sub> |                                    |                     |                   |                    |
| Ca(OH) <sub>2</sub> | + CO <sub>2</sub>  | ↔                 | CaCO <sub>3</sub>   | + H <sub>2</sub> O                 |                     |                   |                    |
| CaCO <sub>3</sub>   | + H <sub>2</sub> O | + CO <sub>2</sub> | ↔                   | Ca(HCO <sub>3</sub> ) <sub>2</sub> |                     |                   |                    |

Wood ash is identified with average particle size of 230  $\mu\text{m}$  through the plotting of wood ash particle size distribution statistical data. Wood ash comprises of large, and porous carbon particles, as well as others inorganic particles that were irregular in shapes. Thin layers are found in some particles. When these particles in the wood ash were wet, they expanded to generate crystalline structures that were rigid, and composed of rosette clusters. These rosette clusters remained the same even after 24 hours of air-dried (Etiegni and Campbell, 1991). The wood expanded differently according to the water immersion duration. Etiegni and Campbell (1991) noticed the wood ash expanded 4.5%, 8.9%, and 12.5% after 1 day, 2 weeks, and 4 weeks immersion in water. Results revealed, these swelling wood ash particles could block the soil pores and inhibit the water permeation and aeration in the soil.

This scenario was reported by Ralston and Hatchell (1971) in forest land with prescribed burning, and Gray and Rock (1987) in the experiments of ash-soil leaching. Possible compounds presented in the expanded wood ash was identified using X-ray diffraction (XRD). Possible compounds existed in the wood ash suggested by the XRD analysis as shown in **Table 2.8** (Etiegni and Campbell, 1991).

**Table 2.8:** Possible compounds existed in the wood ash suggested by XRD analysis.

| Possible Compound        | Chemical formula  |
|--------------------------|---|
| Lime                     | CaO   |
| Calcite                  | CaCO <sub>3</sub>   |
| Riebeckite               | (NaCa) <sub>2</sub> (FeMn) <sub>3</sub> Fe <sub>2</sub> (SiAl) <sub>8</sub>             |
| Portlandite              | Ca(OH) <sub>2</sub>   |
| Calcium chlorite hydrate | Ca(ClO) <sub>2</sub> . 3H <sub>2</sub> O  |
| Calcium silicate         | Ca <sub>2</sub> SiO <sub>4</sub>  |
| Hydrotalcite             | Mg <sub>6</sub> Al <sub>12</sub> CO <sub>3</sub> (OH) <sub>16</sub> . 4H <sub>2</sub> O |
| Serandite                | Na(MnCa) <sub>2</sub> Si <sub>3</sub> O <sub>8</sub> (OH)                               |

A comparison of XRD patterns was made between a dried wood ash sample and a hydrated-air dried wood ash sample. Lime and portlandite were found reduced in the content (lower peak intensity in the XRD), whereas riebeckite, hydrotalcite, and calcium chlorite hydrate compounds were found increased in content (higher peak intensity in the XRD) after wetting. These outcomes obviously indicated the process of hydration used up more than one compounds and created more than one new compound. No clay component was detected in the wood ash, as the 'd' peak was missing in the XRD. Based on the XRD patterns analysis, together with the expected wood ash composition, it was recommended the major compounds in the wood ash was lime (CaO), calcite (CaCO<sub>3</sub>), portlandite (Ca(OH)<sub>2</sub>), and calcium silicate (Ca<sub>2</sub>SiO<sub>4</sub>). In the hydration process, lime could react with the silica to create calcium silicate hydrate (C-S-H or CaH<sub>2</sub>O<sub>4</sub>Si).

C-S-H is a compound with poor crystalline structure, that will swell and expand upon wetting, and go through a series of significant chemical transformations (Kirk-Othmer, 1979). Portlandite is a compound found in the cement, which can also swell when hydrating. It is to take note, the swelling of wood ash involves intricate chemical and physical changes. Oxide compounds present in the wood ash are more likely to get wet when expose to water, then it

will swell, transform, and physically change in structure. This swelling scenario could be caused by the absorption of water via action of capillary, followed by the expansion of porous ash particles. The water absorption at a molecular stage could be caused by the hydrophilic properties of wood ash in nature. Also, could be due to the imbalances of small charge represented by the low cation exchange capacity (CEC) at 2.7 meq/100g which is about the same with inactive clay materials like kaolinite (Grim, 1968).

Wood ash generates from various sources like bark, wood chips, cuttings, and sawdust are one of the largest wastes produced by the industries. This wood ash has been used as a source of energy (Mladenov et al., 2011). Annually, there is close to 10,000 tons of wood ash produced (Serafimova et al., 2011). The amount wood ash generated is expected to grow doubly due to the expansion of industrialisation. The wood ash keeps the overall mineral composition own by the original wood waste, except nitrogen. This is because during the oxidative combustion process, nitrogen compounds degrade, and evaporate into gas vapour in oxide form. These minerals in the wood ash present as fixed substances, are quite stable in the heating. These minerals retain the similar proportions as how much they contain in the wood wastes.

Most of the cases, wood ash derives from the combustion of plant-based wastes are rarely detect with any heavy metals and toxic substances that will cause the secondary contamination upon when it is recycled to use as soil-modifier to the land, soil, and agricultural products (Serafimova et al., 2011). The elution of wood ash in water produces alkali eluate. The alkalinity of wood ash defines its suitability to be produced as soil enhancer, to regulate the pH of acidic soil (Kurshev et al., 1986). The wood ash is rich in unburned carbon particles which could be contributed by the unburned wood and coal particles (Serafimova et al., 2011). In the XRD analysis, Serafimova et al. (2011) identified the existence of numerous major crystalline phases in the wood ash which are calcite ( $\text{CaCO}_3$ ), quartz ( $\text{SiO}_2$ ), and potassium and calcium



carbonate or fairchildite ( $\text{K}_2\text{Ca}(\text{CO}_3)_2$ ). The fine dispersion nature of wood ash particles, with some nano size particles, the wood ash is associated with high absorption capacity.

In line with the sustainable movements and SDG 17 of the United Nations, global research is shaping towards the sustainable inventions and innovations in various disciplines. Many on-going research in building and construction technologies, green infrastructures are constantly sourcing for reusable and renewable materials that are more energy efficient and less hazardous to protect the social environment from fire (Azadeh et al., 2018; Almiron et al., 2019; Khairunisa et al., 2020; Zhan et al., 2020). The research developments in green building materials incorporate with reusable and renewable wastes for environmentally friendly and energy-efficient products ground primarily on the awareness of environmental conservation and to ensure a better human-environment welfare (Yew et al., 2014; Yew et al., 2015a).

Research reports the improvement of fire-resistant performance in epoxy-based intumescent coatings integrated with natural substitutes such as ginger powder and coffee powder (De Sa et al., 2017); aviculture, aquaculture, coal, mining, and alloy wastes such as chicken eggshell, clamshell, fly ash, slag, silica fume and palm oil fuel ash (Yew and Sulong, 2012; Yew et al., 2015b; Syarul, 2017; Wang et al., 2019; Li et al., 2020) over the past 10 years. Numerous studies have been conducted for the enhancement of water-based intumescent coating formulation based on the environmentally friendliness key approach. These research efforts including the exploration of halogen-free flame-retardant additives (Wang, 2008; Levinta et al., 2019) and the continuous search of readily available by-products (Yew et al., 2018; Li et al., 2020). For instance, the research invention of water-based intumescent coatings incorporated with by-products such as rice husk ash, eggshell, and industrial effluent (Salahuddin et al., 2015; Yew et al., 2018; Khairunisa et al., 2020; Liu et al., 2020).

This study explored the potential and appropriate reuse of rubberwood biomass ash (BioAsh) waste in the intumescent coating which the knowledge in this is limited. In this study,

BioAsh was used as natural substitute of mineral fillers in the water-based intumescent for steel. Thermal, physical, and chemical properties of BioAsh were characterized. Fire, thermal, chemical, physical, and mechanical properties of BioAsh formulated water-based intumescent coatings were examined. This study will contribute to on-going sustainable innovations of water-based fire-protective intumescent coating as an environmentally friendly solution to protect the steel, attempting to minimize the reliance on non-renewable exotic resources from the industries. In a wider perspective, this study anticipates playing a role in conserving the environment and creating a better living quality for the current and future generations.

## CHAPTER 3

### RESEARCH METHODOLOGY

#### 3.1 Introduction

This chapter consists of three main sections outlined (i) key materials using to develop intumescent coating samples, (ii) sample preparation methods, and (iii) experiment test methods. The first section depicts the water-based binder: vinyl acetate copolymer (VAC); three main flame-retardant additives: Ammonium polyphosphate (APP), Melamine (MEL), and Pentaerythritol (PER); white pigment: (TiO<sub>2</sub>), and mineral filler substitute: BioAsh (agriculture by-product), used to formulate the intumescent coating samples. Twelve coating formulations were prepared based on a fixed binder: additives ratio of 50:40 with various pigment: BioAsh ratio. A 50:40 ratio of binder: additive flame retardant was selected because this is the optimal ratio for achieving an effective intumescent coating (Kwang yin et al., 2019). Suppliers, locations, and properties of these materials were specified. The second section describes the intumescent coating sample preparation method. The third section describes the sample characterisation through experimental procedures and methods to examine the developed intumescent coating samples in terms of particle size and surface area, fire-resistance, char thickness, char strength, char surface morphology, elemental composition, thermal stability, functional groups and molecular changed structures, antioxidation properties, mechanical properties, weather resistance, water resistance, volatile gaseous products, and thermally stable compounds. A flow chart was used to summarise the sample preparation, experiments' procedures, and methods.

### 3.2 Raw Materials and Their Properties

Vinyl acetate copolymer (VAC) was used as the binding agent for the water based BAIC samples in this research. VAC was a milky white emulsion, with mean particle size of 0.12  $\mu\text{m}$  supplied by Afza Maju Trading, Terrengganu, Malaysia. VAC contributed to 50.0 wt.% of the total weight percentage of the BAIC formulation. Three main halogen-free flame-retardant additives were used in the BAIC formula: Ammonium Polyphosphate II (APP II), Melamine (MEL) and Pentaerythritol (PER) with mean particle size of approximately 18  $\mu\text{m}$ , <40  $\mu\text{m}$  and <40  $\mu\text{m}$  respectively. APP (acid source), MEL (blowing agent), and PER (carbon source) were supplied by Synertec Enterprise Sdn. Bhd., Kuala Lumpur, Malaysia. Titanium dioxide ( $\text{TiO}_2$ ) was an industrial flame-retardant additive (mean particle size <10  $\mu\text{m}$ ; purity >99.0%) supplied by Chemolab Supplies Sdn. Bhd., Selangor, Malaysia.  $\text{TiO}_2$  was used as a white pigment in the BAIC formula. BioAsh was the leftover of natural rubberwood biomass combustion obtained from a fuel factory located in Sitiawan, Perak, Malaysia. BioAsh was renewed as the natural substitute of mineral fillers in the formulation of BAIC samples. This was attributed to a group of high thermally stable elements presence in the BioAsh. Particle sizes of BioAsh were identified through sieve analysis as shown in **Figure 3.1**. Most abundant 300  $\mu\text{m}$  was identified. This particle size was easily available and inexpensive for exploitation. Raw materials details used in this research are summarised in **Table 3.1**.



**Figure 3.1:** Sieve Analysis of BioAsh

**Table 3.1:** Raw materials, properties, and sources.

| Raw materials                        | Properties   | Sources  |
|--------------------------------------|--|--|
| Vinyl acetate copolymer (VAC)        | Milky white emulsion, with mean particle size of 0.12 µm | Afza Maju Trading, Terengganu, Malaysia.               |
| Ammonium Polyphosphate II (APP II)   | Mean particle size of approximately 18 µm                | Synertec Enterprise Sdn. Bhd., Kuala Lumpur, Malaysia. |
| Melamine (MEL)                       | Mean particle size of approximately <40 µm               | Synertec Enterprise Sdn. Bhd., Kuala Lumpur, Malaysia. |
| Pentaerythritol (PER)                | Mean particle size of approximately <40 µm               | Synertec Enterprise Sdn. Bhd., Kuala Lumpur, Malaysia. |
| Titanium dioxide (TiO <sub>2</sub> ) | Mean particle size <10 µm; purity >99.0 %                | Chemolab Supplies Sdn. Bhd., Selangor, Malaysia.       |
| Rubberwood ash (BioAsh)              | mean particle size 300 µm;                               | Sitiawan, Perak, Malaysia.                             |

### 3.2.1 Raw Materials Characterization

The three flame-retardant additives: APP-MEL-PER used in the experiment were halogen-free and had low smoke density. When exposed to fire, the APP-MEL-PER led to an effective intumescent fire protective barrier, and there was no emission of corrosive gases to the environment. APP-MEL-PER was used at a weight ratio of 20-10-10 wt.% in the intumescent coating in this research.

APP II was used in this research due to its lower water solubility and higher decomposition temperature. APP II structure as shown in **Figure 3.2**. Particle size of APP II under SEM shown in **Figure 3.3**. Chemical and physical properties of APP II as shown in **Table 3.2**.

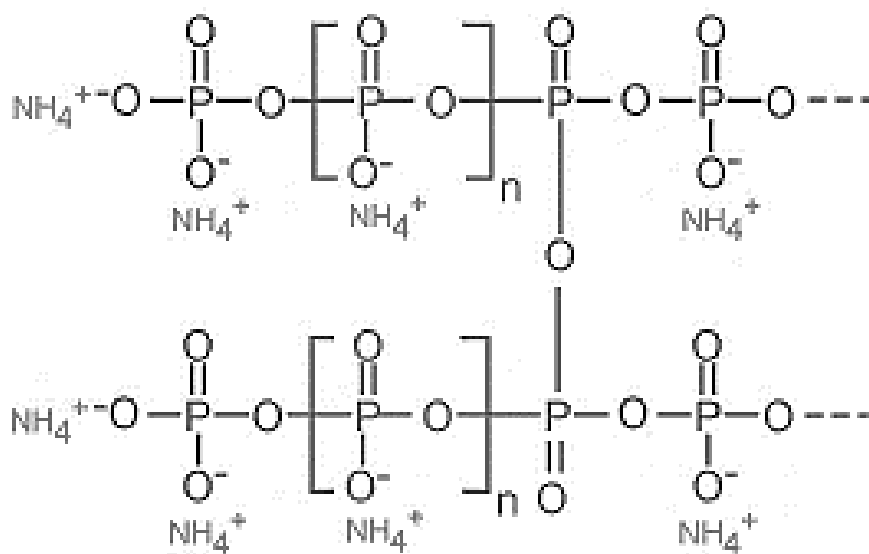


**Figure 3.2:** Ammonium polyphosphate II (APP II) structure.

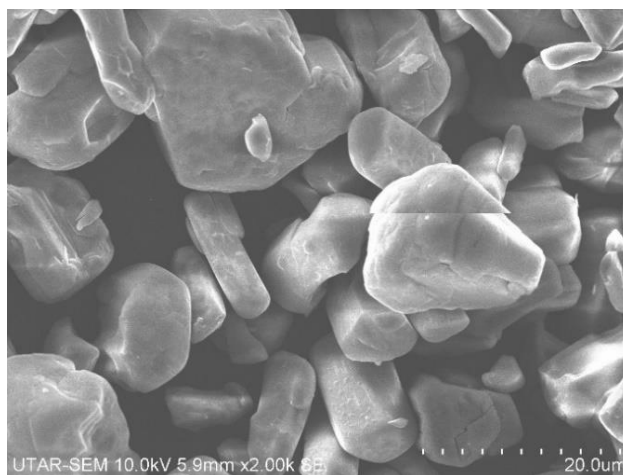


**Figure 3.3:** SEM surface micrograph of APP II.

**Table 3.2:** Potential physical and chemical properties of APP II

|                       |   |
|-----------------------|---|
| Formula               | $(\text{NH}_4\text{PO}_3)_n(\text{OH})_2$ |
| Appearance            | White crystalline powder                  |
| Nitrogen              | 14.0 – 15.0                               |
| Phosphorus            | 31.0 – 32.0                               |
| pH                    | 5.5 – 7.5                                 |
| Molecular weight      | Approximate 97.01 g/mol                   |
| Density               | 1.75 – 1.90 g/cm <sup>3</sup>             |
| Bulk density          | 0.70 g/cm <sup>3</sup>                    |
| Solubility in water   | 0.5 – 40 g/100ml H <sub>2</sub> O         |
| Melting point         | 240 – 275 °C                              |
| Average particle size | 15 μm                                     |

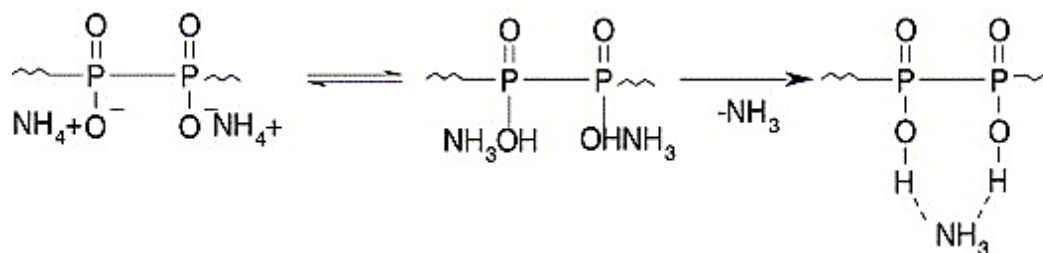


**Figure 3.4:** The decomposition mechanism of APP to release ammonia and phosphoric acid (Jimenez et al., 2006).

APP II is of great potential to act as an acid source and blowing agent in the intumescent mechanism of coating. The condensed phosphoric acid formed during the decomposition of

APP II, reacted with a carbon source to expedite formation of fire protective carbonaceous char layer. Meantime, the ammonia gas released and trapped in the char likely to stimulate the swelling of the char (Lyons 1970; Cullis and Hirschler, 1981; Arthur and Quill, 1992). Phosphoric acid decreased the melt viscosity of coating in liquid phase under high temperature. It also triggered the degradation of polymer, resulted in further decomposition at lower temperature (Jimenez et al., 2006). Melamine (MEL) was used as a blowing agent in the intumescent coating samples in this research. Structure of Melamine as shown in **Figure 3.5**. Physical and chemical properties of MEL as shown in **Table 3.3**. Particle size of MEL illustrated in the SEM as shown in **Figure 3.6**.

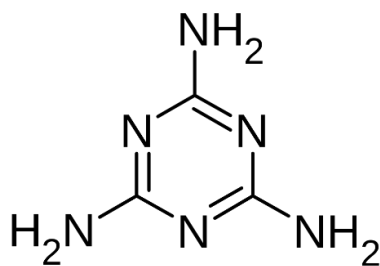


**Figure 3.5:** Melamine structure.

**Table 3.3:** Physical and chemical properties of Melamine.

|                       |  |
|-----------------------|--|
| Formula               | C <sub>3</sub> H <sub>6</sub> N <sub>6</sub> |
| Appearance            | White solid powder                           |
| Odour                 | Odourless                                    |
| pH                    | 7.5 – 9.5                                    |
| Molecular weight      | 126.12 g/mol <sup>-1</sup>                   |
| Density               | 1.573 g/cm <sup>3</sup>                      |
| Vapour density        | 4.34   |
| Solubility in water   | 3240 mg/L                                    |
| Melting point         | 345 °C                                       |
| Average particle size | < 40 μm                                      |



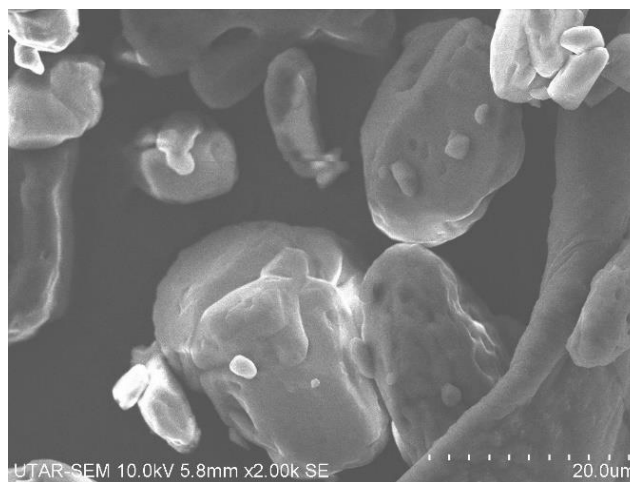


**Figure 3.6:** SEM surface micrograph of Melamine.

In this research, Pentaerythritol (PER) was used as a carbon source in the intumescent coating samples. Structure of PER as shown in **Figure 3.7**. The specification of PER as presented in **Table 3.4**. Particle size of PER as shown illustrated in **Figure 3.8**.



**Figure 3.7:** Pentaerythritol structure

**Table 3.4:** Physical and chemical properties of Pentaerythritol.

|                       |   |
|-----------------------|---|
| Formula               | C <sub>5</sub> H <sub>12</sub> O <sub>4</sub> |
| Appearance            | White solid powder                            |
| Odour                 | Mild odour                                    |
| pH                    | 3.5 – 4.5                                     |
| Molecular weight      | 136.15 g/mol                                  |
| Density               | 1.396 g/cm <sup>3</sup>                       |
| Bulk density          | 750 – 850 kg/m <sup>3</sup>                   |
| Solubility in water   | 5.6 g/100ml                                   |
| Melting point         | 260.5 °C                                      |
| Average particle size | 40 µm   |

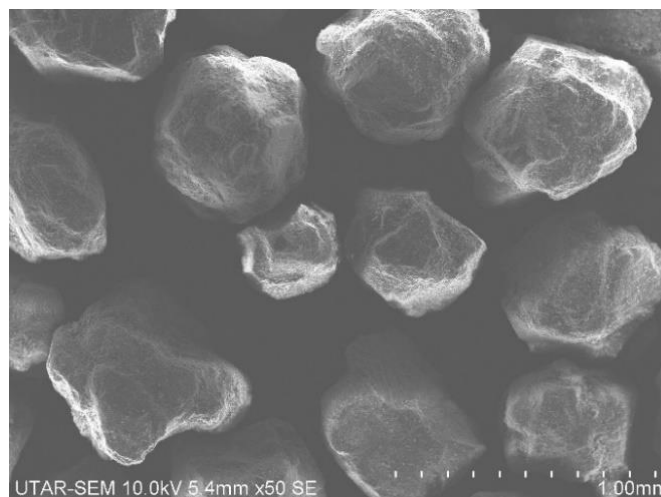


**Figure 3.8:** SEM surface micrograph of Pentaerythritol.

Titanium dioxide ( $\text{TiO}_2$ ) was used as white pigment in the intumescent coating samples. Structure of  $\text{TiO}_2$  as shown in **Figure 3.9**. Physical and chemical properties of  $\text{TiO}_2$  as shown in **Table 3.5**. Particle size of  $\text{TiO}_2$  as illustrated in **Figure 3.10**.



**Figure 3.9:** Titanium dioxide structure

**Table 3.5:** Physical and Chemical properties of Titanium dioxide.

|                       |                               |
|-----------------------|-------------------------------|
| Formula               | $\text{TiO}_2$                |
| Appearance            | White solid powder            |
| Odour                 | Odourless                     |
| pH                    | 2.95                          |
| Molecular weight      | 79.86 g/mol                   |
| Density               | 3.87 – 4.23 g/cm <sup>3</sup> |
| Solubility in water   | Insoluble                     |
| Melting point         | 1843 °C                       |
| Average particle size | 0.2 – 0.3 $\mu\text{m}$       |

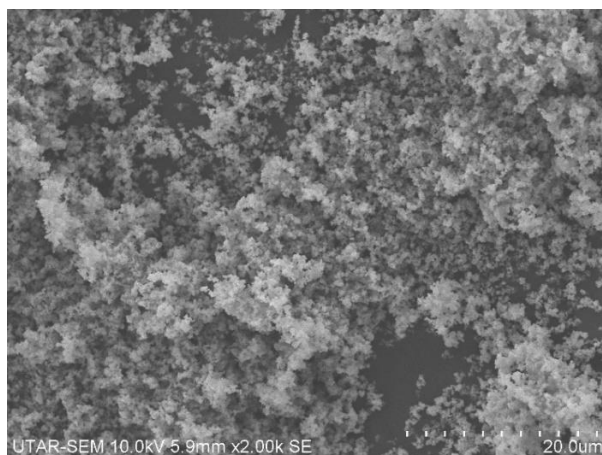


**Figure 3.10:** SEM surface micrograph of Titanium dioxide.

Water-based vinyl acetate copolymer (VAC) was used as the binder for flame-retardant additives and fillers in the intumescent coating samples. The structure of VAC as shown in **Figure 3.11**. Specifications of VAC as shown in **Table 3.6**. VAC was used at a weight ratio of 50.0 wt. % in all intumescent coating samples. The SEM of VAC as shown in **Figure 4.12**.

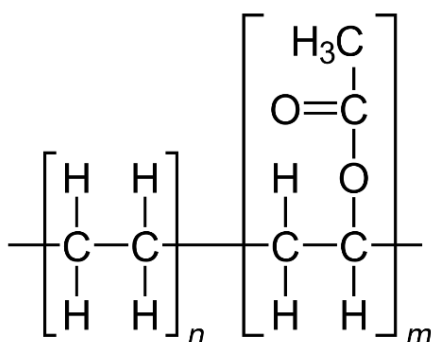


**Figure 3.11:** Vinyl acetate copolymer structure

**Table 3.6:** Physical and Chemical properties of Vinyl acetate copolymer

|                     |  |
|---------------------|--|
| Formula             | $(\text{C}_2\text{H}_4)_n(\text{C}_4\text{H}_6\text{O}_2)_m$ |
| Appearance          | Colourless liquid  |
| Odour               | Sharp odour  |
| pH                  | 3.0 – 4.0  |
| Molecular weight    | 86.09 g/mol  |
| Density             | 930 - 950 kg/m <sup>3</sup>                                  |
| Solubility in water | soluble  |
| Melting point       | 90 – 120 °C  |

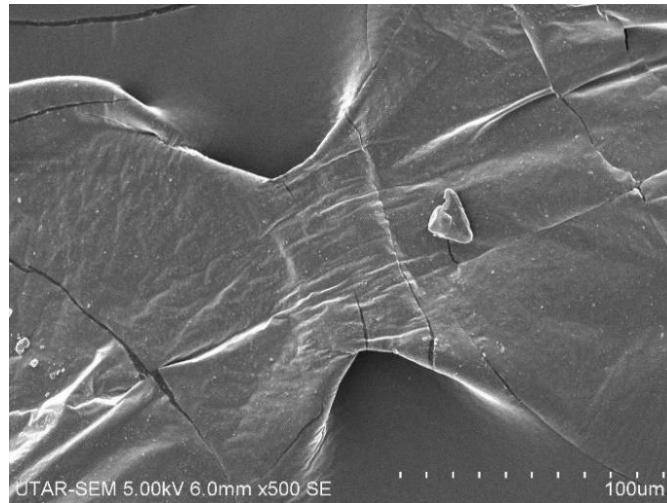


**Figure 3.12:** SEM surface micrograph of vinyl acetate copolymer.

Physical properties of wood ash that potentially possesses the similar characteristic with BioAsh as shown in **Table 3.7**.

**Table 3.7:** Physical properties of Wood Ash (Etiegni and Campbell, 1991; Abdullahi, 2006).

|                       |                          |
|-----------------------|--------------------------|
| Appearance            | Fine greyish ash powder  |
| Odour                 | Odourless                |
| pH                    | 9.0 – 13.5               |
| Average Particle size | 230 µm                   |
| Mean specific gravity | 2.13                     |
| Bulk density          | 760 kg/m <sup>3</sup>    |
| Specific surface      | 3.0975 m <sup>2</sup> /g |
| Melting point         | > 800 °C                 |

### 3.3 Sample Preparation

Sample preparations were divided into two phases. The first phase was the preparation of wet-dried BioAsh sample for characterisation. The raw BioAsh was stored in a closed container to avoid any contaminations. 10 g raw (dry) BioAsh was put onto a round silicone mould. A few droplets of water were added to the 10 g BioAsh for wetting and stirred using a clean wooden

stick to achieve homogenous state. The wet 10 g BioAsh was put air-dried for 7 days. Second phase was the preparation of BAIC formulations. All BAIC samples were formulated in the laboratory. The sample was formulated by homogeneously mixing all raw ingredients based on each specific weight percentage (wt.%) as listed in the **Table 3.8** using a high-speed disperser with rate 1500 rpm for 60 minutes at room temperature. Small volume of water (5 wt.%) was added to the sample to slightly reduce the viscosity of the sample. All formulated BAIC samples were stored in closed containers to avoid contaminations. Binder and flame retardant additive ratio of 50:40 as these was the optimum ratio for achieving an effective coating (Yew and Sulong, 2011; Yew and Sulong, 2012). The weight percentage (wt.%) of VAC/APP-MEL-PER (50.0/20.0-10.0-10.0 wt.%) were fixed parameters in all BAIC samples.

**Table 3.8:** BAIC samples formula

| Sample          | Binder/Flame-retardant additives (wt.%) |                           | Green Mineral Filler |
|-----------------|---|---------------------------|----------------------|
|                 | VAC/APP-MEL-PER                         | Pigment: TiO <sub>2</sub> | BioAsh (wt.%)        |
| <b>BAIC0-0</b>  | 50.0/20.0-10.0-10.0                     | 10.0                      | 0.0                  |
| <b>BAIC0-5</b>  | 50.0/20.0-10.0-10.0                     | 9.5                       | 0.5                  |
| <b>BAIC1-0</b>  | 50.0/20.0-10.0-10.0                     | 9.0                       | 1.0                  |
| <b>BAIC1-5</b>  | 50.0/20.0-10.0-10.0                     | 8.5                       | 1.5                  |
| <b>BAIC2-0</b>  | 50.0/20.0-10.0-10.0                     | 8.0                       | 2.0                  |
| <b>BAIC2-5</b>  | 50.0/20.0-10.0-10.0                     | 7.5                       | 2.5                  |
| <b>BAIC3-0</b>  | 50.0/20.0-10.0-10.0                     | 7.0                       | 3.0                  |
| <b>BAIC3-5</b>  | 50.0/20.0-10.0-10.0                     | 6.5                       | 3.5                  |
| <b>BAIC4-0</b>  | 50.0/20.0-10.0-10.0                     | 6.0                       | 4.0                  |
| <b>BAIC4-5</b>  | 50.0/20.0-10.0-10.0                     | 5.5                       | 4.5                  |
| <b>BAIC5-0</b>  | 50.0/20.0-10.0-10.0                     | 5.0                       | 5.0                  |
| <b>BAIC10-0</b> | 50.0/20.0-10.0-10.0                     | 0.0                       | 10.0                 |

### **3.4 Experiment Test Methods of BioAsh Intumescent Coating**

BioAsh Intumescent Coating was characterised through a series of physical experiments. The fire resistance and mechanical properties of BAIC samples were evaluated using a total of 12 testing methods. These testing methods were Brunauer-Emmett-Teller surface area analysis (BET), Fire Resistance Test (FRT), Carbolite Furnace Test (CFT), Weight Load Test (WLT), Thermogravimetric Analysis (TGA), Surface Electron Micrograph spectroscopy (SEM), Energy Dispersive X-ray spectroscopy (EDX), Instron Adhesion Test (IAT), Fourier-Transform Infrared spectroscopy (FTIR), Freeze-Thaw cycle Test (FTC) and Static Immersion Bath Test (SIB), and X-ray Diffractometer (XRD). The samples preparation, experiment procedures and test methods as shown in **Figure 3.13**.

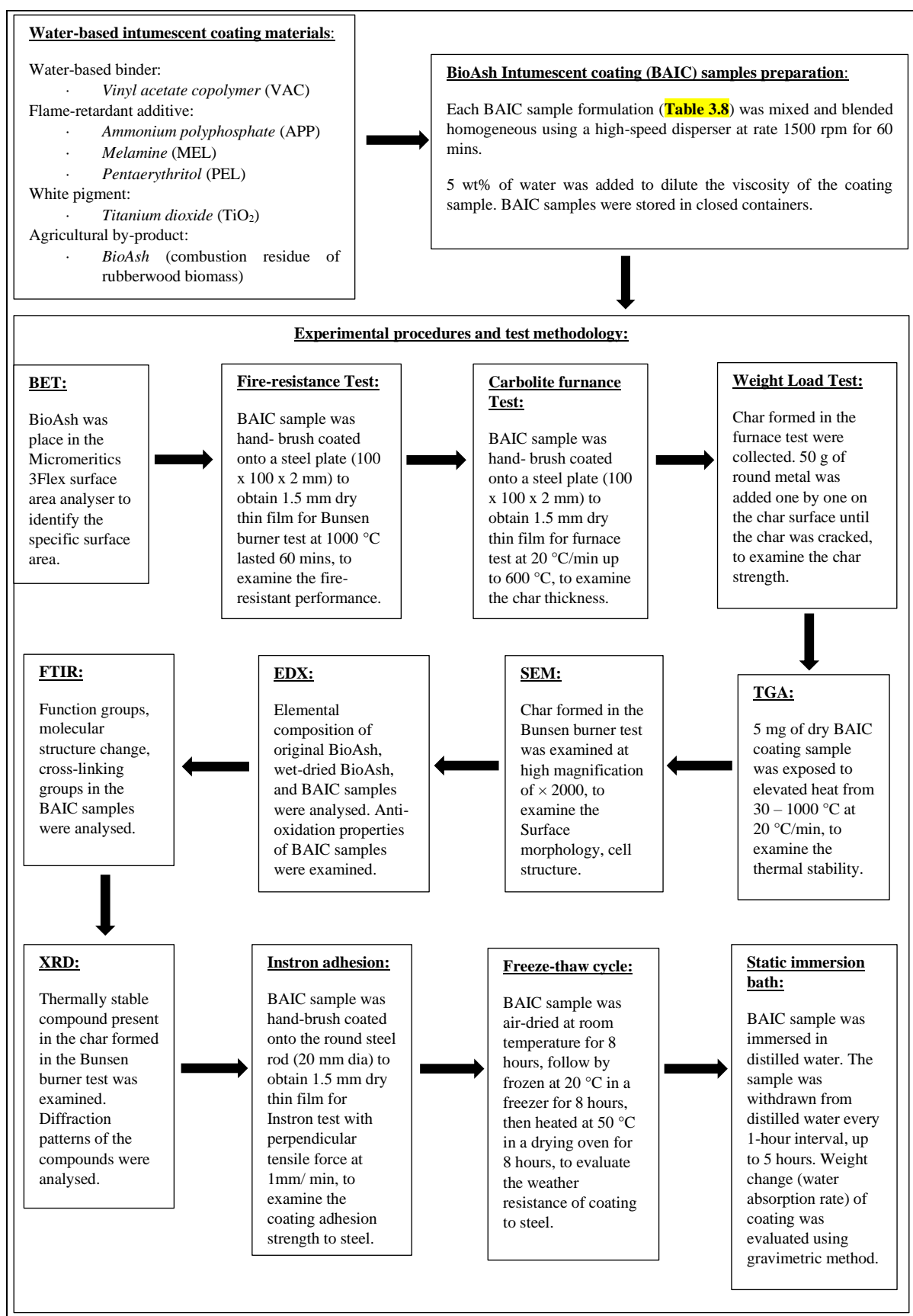


**Figure 3.13:** Flowchart of water-based intumescent coating materials, samples preparation, experiment procedures and test methods.

### 3.4.1 Brunauer-Emmett-Teller Surface Area Analysis (BET)

The specific surface area of BioAsh ( $\text{m}^2/\text{g}$ ) was characterised using a Micromeritics 3Flex surface area analyser manufactured by Micromeritics, Georgia, USA as shown in **Figure 3.26**.



**Figure 3.14:** Brunauer-Emmett-Teller surface area analysis (BET)

One gram of BioAsh sample was measured accordingly using weighing machine. The weighed BioAsh sample was placed in a glass tube and put in a continuously nitrogen gas (inert gas) flow condition for 8 hours. The porous surface structure of the BioAsh absorbed the gas molecules due to weak van der Waals forces and a monolayer was formed. Interaction of gases with the solid surfaces of BioAsh was quantified. The specific surface area (SSA) of BioAsh was identified and analysed through the monomolecular layer and the rate of gas adsorption.

### 3.4.2 Fire Resistance Test (FRT)

The fire resistance efficiency of BAIC coating sample was examined through one hour of Bunsen burner burning test. All twelve BAIC samples were tested in the fire resistance test (FRT). The coating sample was exposed to  $1000\text{ }^{\circ}\text{C}$  of fire directed from a Bunsen burner setup in a confine fume hood as shown in **Figure 3.27**.





**Figure 3.15:** Fire-resistant Test

The coating sample was hand brushed onto the surface of a 100 mm x 100 mm x 2 mm (length x width x thickness) carbon steel plate and air-dried at room temperature for 24 hours. This process was repeated 3-5 times until an end thickness of 1.5 +/- 0.2 mm dry thin film was obtained. The end thickness of dry thin film was measured using a digital Vernier caliper. IDEALGAS Laser 3000- a portable auto ignition blowtorch gun manufactured by Idealgas, Casier, Italy filled with EN417 butane gas cartridge from Providus, Volpiano, Italy was utilised for the burning test. The valve of the blowtorch gun was regulated to 60% of its maximum gas flow to ensure a stable gas pressure throughout one hour burning test. Gas consumption was maintained at 150 g/h. The coated steel plate was hold vertically using a three-fingers clamp attached to a mounting base and distanced 70 mm away from the flame aperture of the Bunsen burner. The coated steel plate was exposed to 1000 °C flame lasted for 60 minutes, and the temperature was measured using a UNI-T UT325 digital thermometer linked to a type-k thermocouple welded to the back of the carbon steel plate. The mean temperature of fire resistance performance was acquired by triplicating the burning test.

### 3.4.3 Carbolite Furnace Test (CFT)

The formation of carbonaceous char layer, and the char thickness of BAIC coating samples tested with the best (BAIC3-5), the average (BAIC1-0, BAIC5-0), the worst (BAIC0-0, BAIC10-0) performances and based on the samples appropriate ingredient formulations were chosen accordingly for further investigation via Carbolite furnace test at 400 °C and 600 °C as shown in **Figure 3.16**.



**Figure 3.16:** Carbolite Furnace

BAIC0-0, BAIC1-0, BAIC3-5, BAIC5-0, and BAIC10-0 samples were chosen to further investigate. The coating sample was hand brushed onto a 50 mm x 50 mm x 2 mm (length x width x thickness) carbon steel plate and air-dried at room temperature for 24 hours. This process was repeated 3-5 times until an end thickness of 1.5 +/- 0.2 mm dry thin film was obtained. The end thickness of dry thin film was validated using a digital Vernier calliper. The coating sample was heated at an elevating temperature rate of 20 °C/ min in a RHF 15/8 Carbolite furnace until it reached the temperature of 600 °C. The thickness of char layer and the fire protection performance of char were evaluated.

#### 3.4.4 Weight Load Test (WLT)

The strength of carbonaceous char layer of BAIC0-0, BAIC1-0, BAIC3-5, BAIC5-0, and BAIC10-0 formed after the CFT were evaluated using the weight load test. The maximum strength of a char layer that can withstand the weight load was tested. The char layer was loaded by putting a 50 g round metal on its surface as shown in **Figure 3.17**.



**Figure 3.17:** Weight Load Test

This process of adding 50 g round metal one by one to the char surface was repeated until the char layer was cracked. The static load of the char layer was indicated by the total number of 50 g round metal added. The char strength was measured by sum up the weight of all 50 g round metals.

#### 3.4.5 Thermogravimetric Analysis (TGA)

Thermal degradation of BAIC0-0, BAIC1-0, BAIC3-5, BAIC5-0, and BAIC10-0 coating samples were analysed using the Perkin Elmer STA 8000 thermogravimetric analyser from Waltham, Massachusetts, USA as shown in **Figure 3.18**.



**Figure 3.18:** Thermogravimetric Analysis

The thermal stability of coatings BAIC0-0, BAIC1-0, BAIC3-5, BAIC5-0, and BAIC10-0 were further examined. 5 mg of a dried coating sample was placed into a crucible and heating in a nitrogen gas flow condition at an elevating temperature of 30 °C to 1000 °C. The heating rate was 20 °C per minute. Mass change and residual weight of the coating sample after exposed to 1000 °C were calculated. The thermal stability of the sample was analysed.

### **3.4.6 Scanning Electron Microscopy Analysis (SEM)**

Characterisation of raw BioAsh and wet-dried BioAsh samples were examined under scanning electron microscope (SEM). Physical changes of BioAsh before and after hydrated were observed under high magnification of x2.0K. A Hitachi EDAX S3400-N scanning electron microscope from Hitachi, Tokyo, Japan as shown in **Figure 3.19**. The carbonaceous char surface morphology of BAIC0-0, BAIC1-0, BAIC3-5, BAIC5-0, and BAIC10-0 samples were further analysed.



**Figure 3.19: Scanning Electron Microscope**

The char sample was sputter coated with an ultra-thin layer gold film (2-20 nm thick) to induce the thermal conductivity and secondary electron emission. The sample surface was projected with a focused low beam energy 1000 V electrons during the analysis to minimise the thermal damage. The char topography, cell size and structure were investigated at magnifications of  $\times 2000$ .

### 3.4.7 Energy-dispersive X-ray Spectroscopy (EDX)

The EDX was conducted simultaneously in the same SEM device as shown in **Figure 3.20**.



**Figure 3.20: Energy-dispersive X-ray Spectroscopy**

The elemental characterisation of raw and wet-dried BioAsh samples were examined through an energy dispersive X-ray spectroscope. Chemical elemental changes in BioAsh before and after hydrated were evaluated. BAIC0-0, BAIC1-0, BAIC3-5, BAIC5-0, and BAIC10-0 sample formulations and their elemental composition were analysed. The qualitative and quantitative of elements presence in the sample was diagnosed.

### 3.4.8 Instron Adhesion Test (IAT)

The adhesion strength of the BAIC0-0, BAIC1-0, BAIC3-5, BAIC5-0, and BAIC10-0 samples were assessed using a model 5586 Instron universal pull-off testing machine manufactured by Illinois Tool Works, Illinois, USA as shown in **Figure 3.21**.

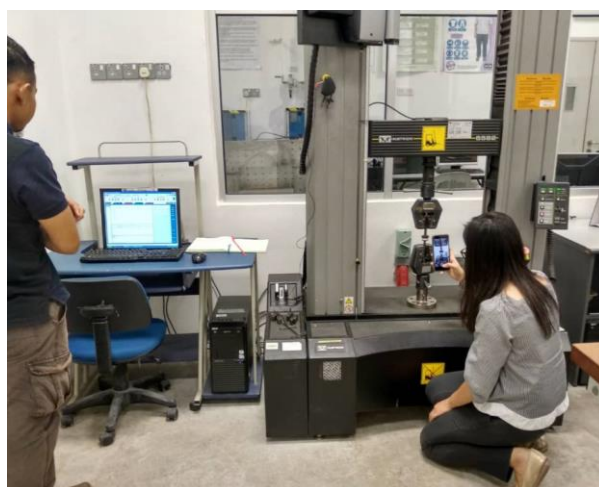


**Figure 3.21:** Instron Universal Testing Machine

The maximum strength required to detach the sample coating from the steel rod is examined. The coating sample was coated onto the surface of a cylinder steel rod (20 mm diameter) and air-dried at room temperature for 24 hours. This process was repeated for 3-5 times until a thin film 1.5 +/- 0.2 mm was formed. The coated steel rod was adhered to the surface of a bare steel rod using epoxy glue and settled for 24 hours in the room temperature (Nishimura et al., 1992).

A perpendicular tensile force with rate 1 mm per minute was applied to detach the coating sample from the steel rod. The adhesion strength of sample was calculated based on Equation (1) (Xu et al., 2015) in accordance with the American Society for Testing and Materials (ASTM) D4541 standard:

$$f_b = F/A \quad (1)$$

in which,

$f_b$  represents the adhesion strength (MPa)

$F$  represents the maximum fracture load (N)

$A = \pi(d^2)/4$  represents the surface area (mm<sup>2</sup>) of the cylinder steel rod

### 3.4.9 Fourier-transform Infrared Spectroscopy (FTIR)

The functional groups, molecular structure changes and cross-linking occurred in the BAIC0-0, BAIC1-0, BAIC3-5, BAIC5-0, and BAIC10-0 coating samples were investigated using a Fourier transform infrared spectroscopy manufactured by Thermo Fisher Scientific, Waltham, Massachusetts, USA as shown in **Figure 3.22**.



**Figure 3.22:** Fourier Transform Infrared Spectroscopy



Coating samples were hand brush coated onto a carbon steel plate 3-5 times until a dry thin film of 1.5 +/- 0.2 mm was formed. The infrared spectrum absorption and emission of the sample at wavelength between 1000 to 4000  $\text{cm}^{-1}$  were evaluated.

#### 3.4.10 Freeze-thaw Cycle Test (FTC)

The weather resistance of the BAIC0-0, BAIC1-0, BAIC3-5, BAIC5-0, and BAIC10-0 coating samples under various extreme physical conditions was assessed through the freezing and thawing cyclic. The coating was applied into a steel plate (50 mm length x 50 mm width x 1 mm thick) and air-dried at room temperature for 24 hours. This process was repeated 3 to 5 times until a thin film 1.5 +/- 0.2 mm was obtained. The coated steel plate was settled at room temperature (27 °C) in an airflow condition for 8 hours. The sample was then frozen at -20 °C in a freezer for 8 hours, followed by heated in a drying oven at 50 °C lasted 8 hours as shown in **Figure 3.23**.



**Figure 3.23:** Freezer and Universal Drying Oven

A complete one freeze-thaw cycle duration was 24 hours (8+8+8 hours). Any fissures, blisters, coagulum, and colour changed of the sample were visually evaluated.



### 3.4.11 Static Immersion Bath Test (SIB)

The water resistance of the thin film of BAIC0-0, BAIC1-0, BAIC3-5, BAIC5-0, and BAIC10-0 samples were investigated using static immersion bath method. The sample was casted into a plastic mould (20mm diameter) at 1.5 +/- 0.2 mm thickness and air-dried in the room temperature for 7 days. The demould dried thin film sample was immersed in a small plastic container filled with distilled water at room temperature as shown in **Figure 3.24**.



**Figure 3.24:** Static immersion bath test

The sample was withdrawn from the distilled water and blotted dried with a paper towel every 1-hour interval. Excess water on the surface of the sample was eliminated and weight changed was measured. The water absorption rate of the sample was assessed up to 5 intervals lasted for a duration of 5 hours. Weight changed of the sample was calculated using gravimetric analysis based on the Equation (2):

$$E_{sw} = [(W_e - W_o) / W_o] \times 100\% \quad (2)$$

In which,

$E_{sw}$  represents the water uptake ratio of the sample

$W_e$  represents the wet weight of the sample at various time

$W_o$  represents the initial dry weight of the sample

#### 3.4.12 X-ray Diffractometer Test (XRD)

Raw and wet-dried BioAsh were characterised through XRD. Changes in the elemental compounds of BioAsh before and after hydrated were examined. The char remnant of the best performance BAIC3-5 coating sample (after the fire resistance test) was further examined by diffracting x-rays to the sample in the X-ray diffractometer. X-ray diffractometer Model XRD-6000 manufactured Shimadzu from Japan shown in **Figure 3.25** was used.



**Figure 3.25:** X-ray Diffractometer

Thermally stable compound formed in the fire resistance test was identified through the intensities and scattering angles of x-rays leaved on the char sample. Diffraction patterns of sample were analysed.

## CHAPTER 4

### RESULT AND DISCUSSIONS

#### 4.1 Characterisation of BioAsh

This chapter starts with the discussion of the characterisation of physical and chemical properties of BioAsh characterised via BET, thermogravimetric analysis (TGA), surface electron microscopy (SEM), Fourier-Transform Infrared Spectroscopy (FTIR), Energy-dispersive X-ray (EDX) Spectroscopy and (XRD). It is followed by the analysis and discussion of BAIC sample results of fire resistance, char formation, char strength, thermal degradation, surface morphology, pozzolanic reaction, antioxidation properties, molecular functional group, adhesion strength, weather resistance, and water resistance.

##### 4.1.1 BET Analysis

When particle size decreases, the surface area to volume ratio increases. According to BET (Brunauer-Emmett-Teller) model, the micropore ( $< 2\text{nm}$ ) is filled up and monolayer is formed along the surface of sample at relative pressure ( $P/P_o$ ) less than 0.3. When the adsorbed gas is dosed continuously, the relative pressure builds up and pore filling is going on by forming multilayer on the external surface, surfaces of mesopore ( $2 - 50\text{ nm}$ ) and macropore ( $> 50\text{ nm}$ ). The average particle size of rubber wood ash as identified by Masae et al (2013) was  $35.4\text{ }\mu\text{m}$ . The particles of rubber wood ash are high in porosity, with a higher surface area of  $42\text{ m}^2/\text{g}$

identified (Masae et al., 2013). The important details of BET analysis conducted in this research as shown in **Table 4.1**.

**Table 4.1:** BET analysis of BioAsh.

| <b>Sample</b>                                    | <b>BioAsh</b>     |
|--|-------------------|
| BET surface area (m <sup>2</sup> /g)             | 3.0975            |
| t-plot micropore area (m <sup>2</sup> /g)        | 0.4336            |
| t-Plot external surface area (m <sup>2</sup> /g) | 2.6639            |
| Total pore volume (cm <sup>3</sup> /g)           | 0.020572          |
| t-Plot micropore volume (cm <sup>3</sup> /g)     | 0.000177          |
| Pore width range (nm)                            | 1.3215 – 300.0000 |
| Adsorption average pore diameter (nm)            | 26.5665           |
| BJH adsorption average pore width (nm)           | 30.8446           |
| Average nanoparticle size (nm)                   | 19370.0427        |

BET surface area indicates the total specific surface area of the BioAsh sample is 3.0975 m<sup>2</sup>/g. While t-plot micropore area shows the area contributed by micropores at 0.4336 m<sup>2</sup>/g in the BioAsh sample. In other words, the external surface areas occupied by other pores (*e.g. mesopore and macropore*) is 2.6639 m<sup>2</sup>/g. The average pore size of Ash 300 is 30.9107 nm. Namely, there is about 14% of the BioAsh particle surface area is occupied by micropores. The rest 86% of BioAsh particle surface area is predominant by the mesopores. **Figure 4.1** shows the adsorption isotherms of the BioAsh sample. According to the IUPAC classification, the BioAsh sample exhibited Type IV adsorption isotherms indicating that the samples contains mesopores (Donohue and Aranovich, 1998).

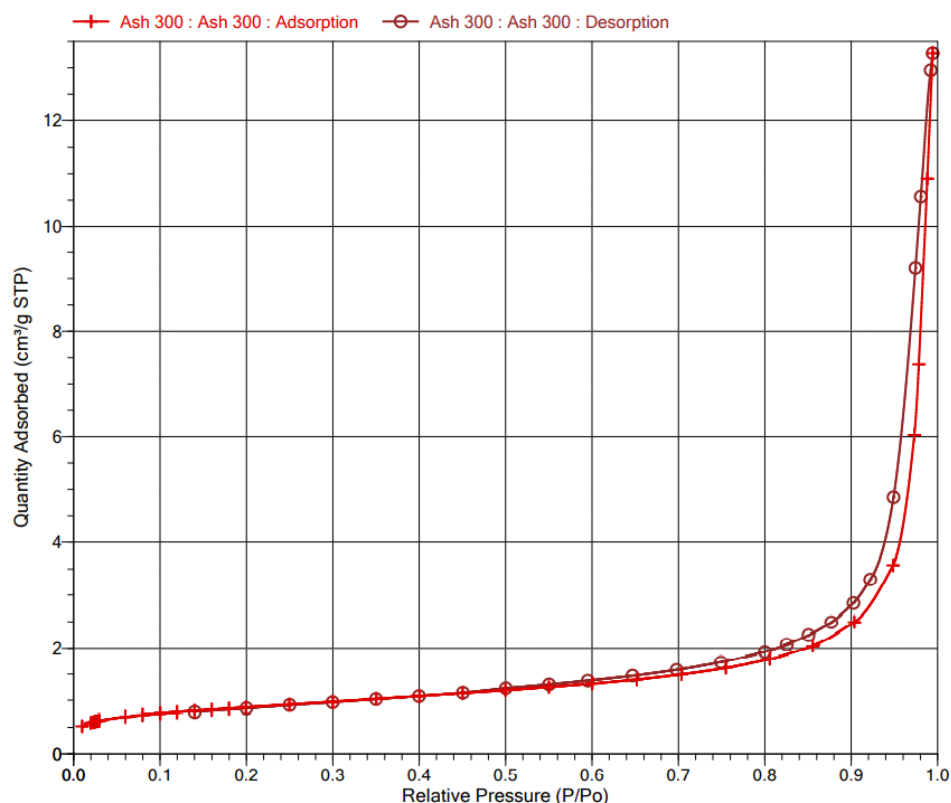


**Figure 4.1:** Adsorption Isotherm linear plot of BioAsh.

**Figure 4.2** shows the BET surface area linear plot of BioAsh. **Figure 4.3** shows the pore size distribution of the analysed BioAsh. The BioAsh sample exhibited almost the same pore size distribution which contain mostly mesopores range from 4 nm to 35 nm and 45 nm to 50 nm. Besides, the sample also contain macropores range from 50 nm to 55 nm and 66 nm to 82 nm.

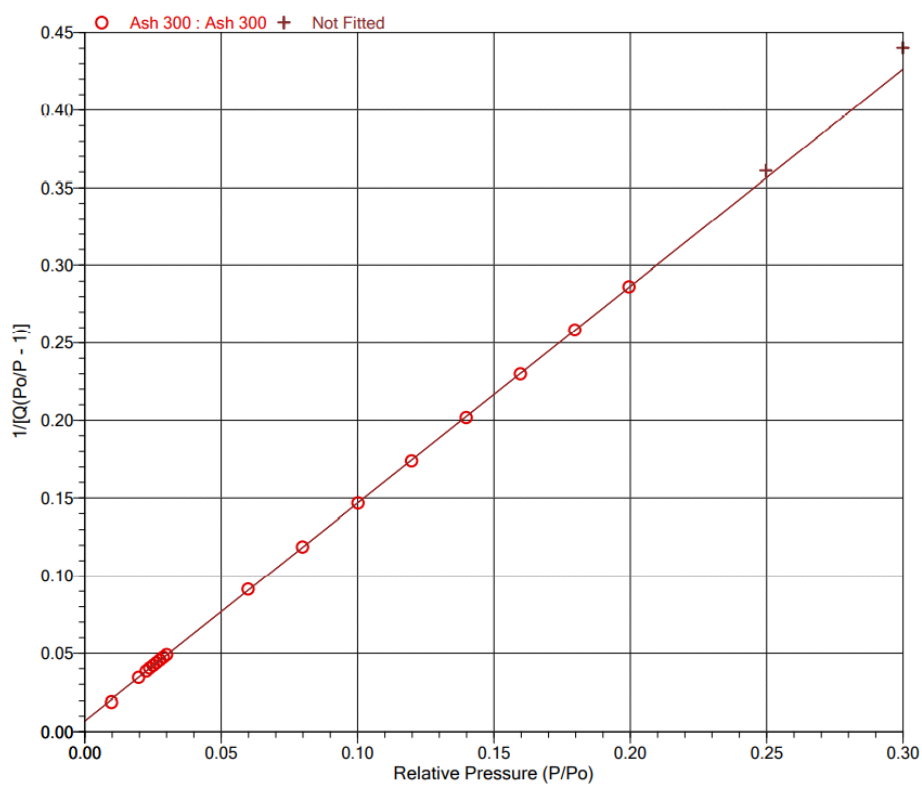


**Figure 4.2:** BET surface area linear plot of BioAsh.

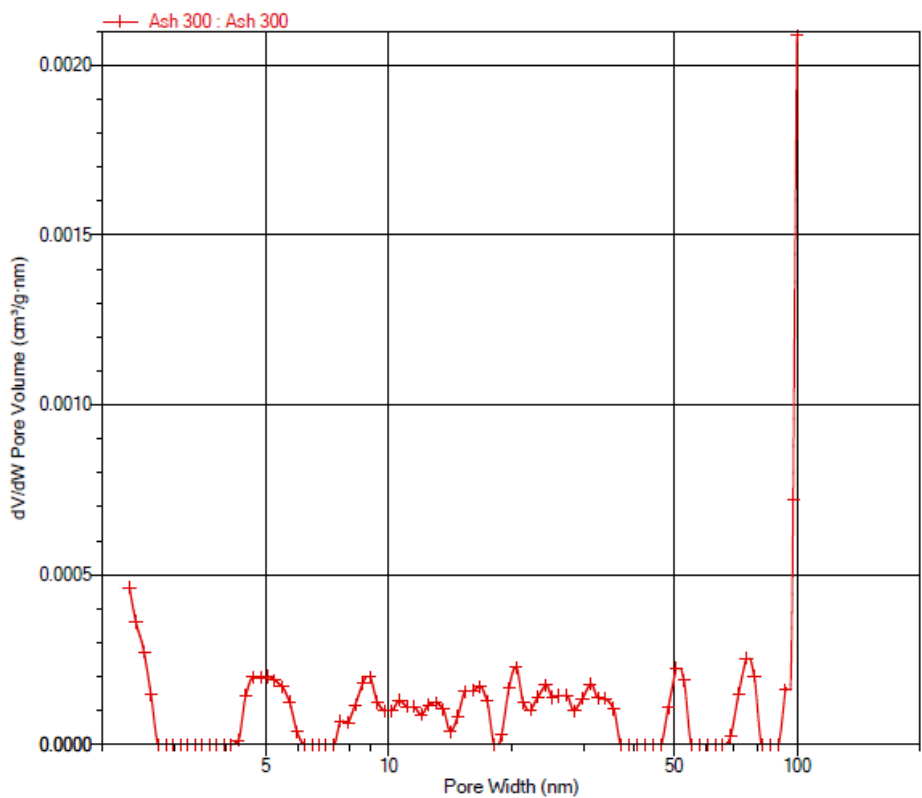


**Figure 4.3:**  $dV/dW$  Pore volume vs. Pore width

### 4.1.2 Thermogravimetric Analysis

The original BioAsh and BioAsh after wet-dried were analysed in thermogravimetric analysis (TGA). The TGA and differential thermal analysis (DTA) curves of BioAsh (original) and BioAsh (wet-dried) as displayed in **Figure 4.4**.

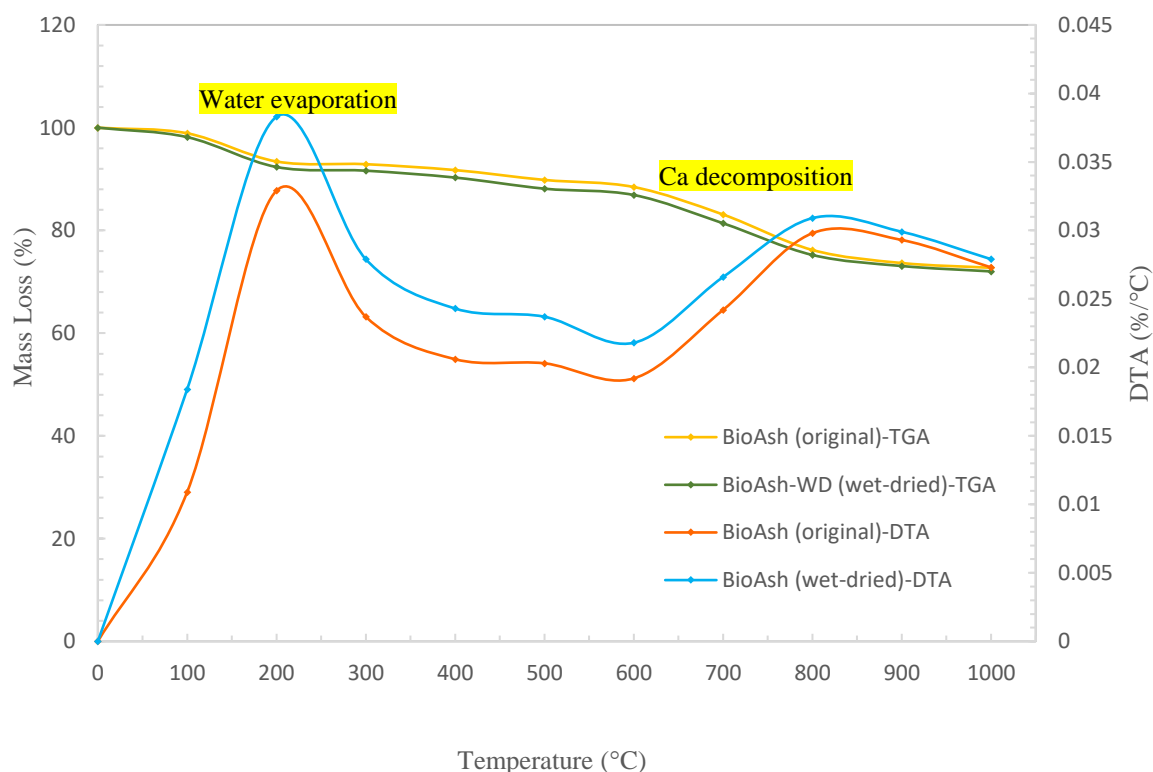


**Figure 4.4:** TGA and DTG curves of original and hydrated BioAsh.

Both BioAsh (original) and BioAsh (wet-dried) slightly degraded at two stages when exposed to elevating temperature up to 1000 °C. The first stage happened at temperature range between 100 to 200 °C, and second stage at 600 to 800 °C in the TGA curves. These two degradation stages observed were mild and did not portray deep drops in the residual weights. Namely, only small mass loss in the BioAsh during these two thermal degradation stages. The mass loss happened between 100 °C to 200 °C was due to the water evaporation (the loss of water molecules). This was proven by the first peak of 200 °C in the DTA showing the highest mass

loss due to eliminate of water. The moisture in the air was absorbed by the BioAsh after some period of storage (Misra et al., 1993). Calcium started to decompose at temperature above 600 °C (Misra et al., 1993). The second stage of thermal degradation happened between 600 °C to 800 °C was due to the decomposition of calcium element in the BioAsh. This was confirmed by the second highest mass loss at 800 °C in the DTA curve. It was noticed, wet-dried BioAsh showed sign of a little higher degradation as compared to original BioAsh in the TGA curves.

The cumulative weight loss (%) curves of BioAsh (original) and BioAsh (wet-dried) were disclosed. The weight loss of original BioAsh and wet-dried BioAsh accumulated at every 100 °C as exhibited in **Figure 4.5**.

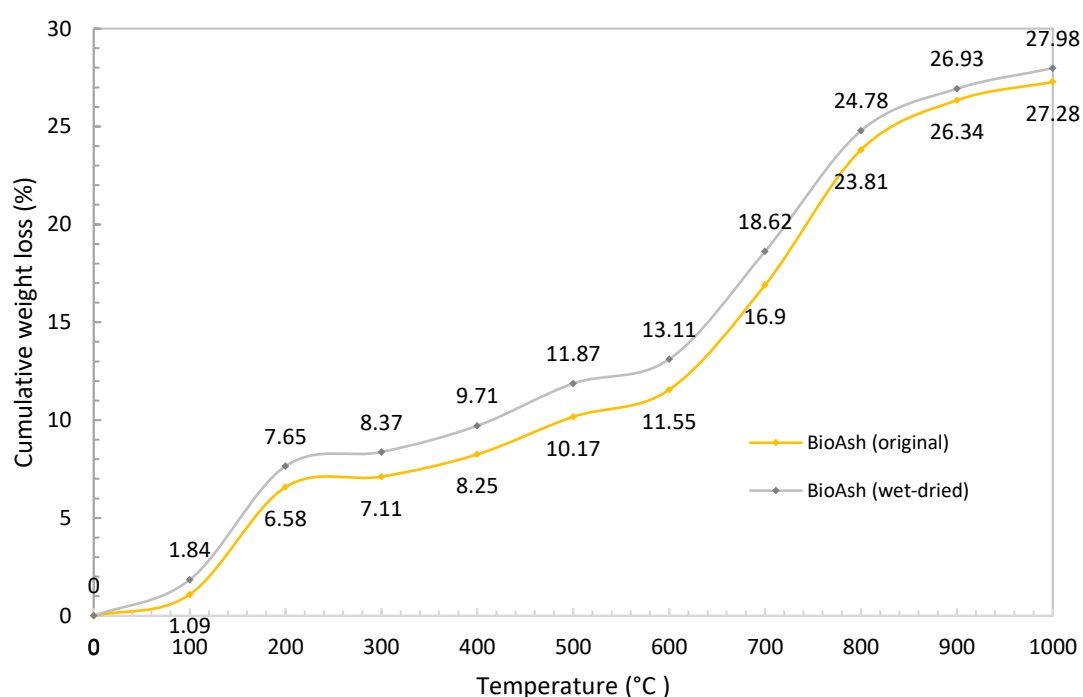


**Figure 4.5:** Cumulative weight loss curve vs. temperature of BioAsh (original) and BioAsh (wet-dried).

It was noticed, original BioAsh associated with remaining residual weight at 72.72% while wet-dried BioAsh at 72.02%. Both condition of BioAsh degraded the most at 200 °C and 800 °C. At temperature 200 °C, the mass loss of BioAsh (original) was 5.49% and BioAsh (wet-



dried) was 5.81%. The difference was 0.32%. At temperature 800 °C, the mass loss of BioAsh (original) was 6.91% and BioAsh (wet-dried) was 6.16%. The difference was 0.75%. The differences of cumulative weight loss at 200 °C and 800 °C for both original BioAsh and wet-dried BioAsh were 1.07% and 0.97%. These data revealed, when the BioAsh was hydrated, the thermal stability slightly drop only at +/- 1.0% as compared to its original status.

The thermal degradation of all ingredients used in the coating formulation: APP, PER, MEL, VAC, TiO<sub>2</sub> and BioAsh were analysed via TGA. The comparison of TGA curves of all materials was combined and as presented in **Figure 4.6**. Refer to **Appendix A**.

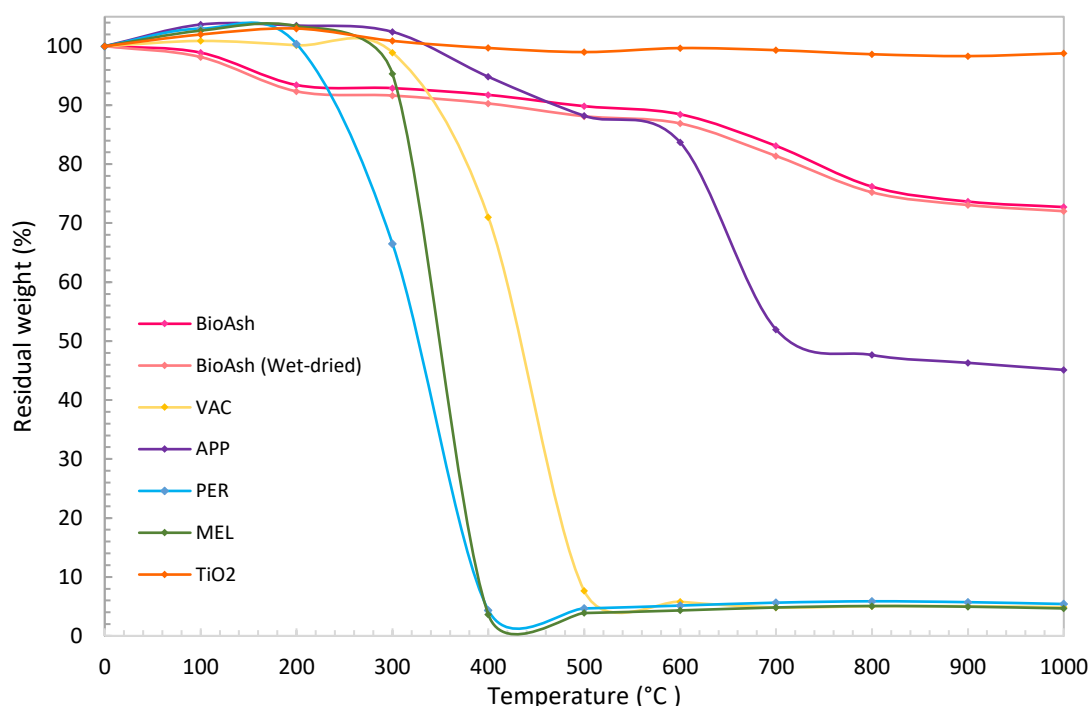


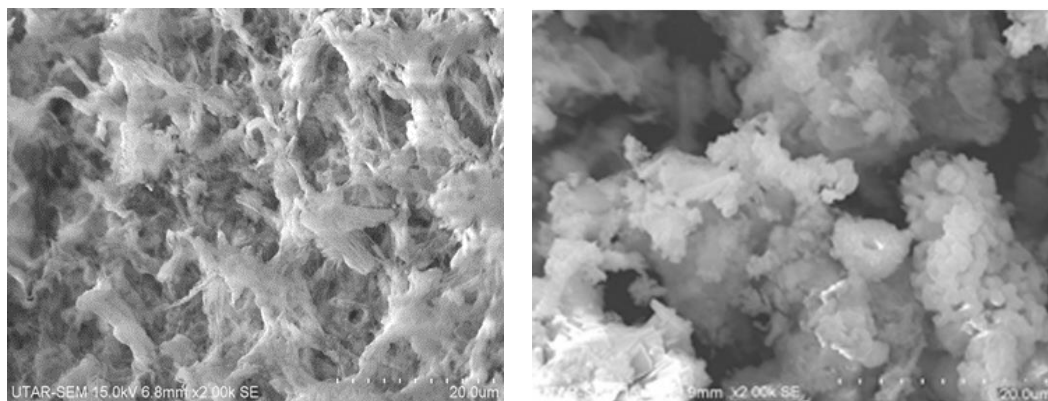
**Figure 4.6:** TGA curves of APP, PER, MEL, TiO<sub>2</sub>, Binder, and BioAsh (original), BioAsh (wet-dried).

It was noticed, MEL exhibited a significant drop at temperature between 300 °C to 400 °C due to the structural decomposition. PER displayed sharp drop in mass loss, degraded at temperature between 200 °C to 400 °C, whereas VAC at 300 °C to 500 °C. APP exhibited two stages of mass loss at 300 °C to 500 °C and 600 °C to 700 °C. TiO<sub>2</sub> showed a slight decomposed

at 300 °C to 400 °C and remained quite stable throughout. Both original and wet-dried BioAsh showed light degradation at two stages at 100 °C to 200 °C (water evaporation) and at 600 °C to 800 °C (calcium decomposition). It was confirmed, the nature of BioAsh possessed elemental composition associated with good thermal stability at high temperature as compared to VAC, APP, PER, MEL as shown in Figure 4.6. Refer to **Appendix B**.

#### 4.1.3 Surface Electron Microscopy

The surface morphology of original BioAsh and after the wet-dried BioAsh were examined via surface electron microscopy (SEM) under the magnification of 2.00 K, as indicated in the **Figure 4.7**.



(a) Original BioAsh

(b) Wet-dried BioAsh

**Figure 4.7:** SEM of (a) original BioAsh, (b) wet-dried BioAsh.

The surface topography of original BioAsh and wet-dried BioAsh differed distinctively. It was noticed the topography of BioAsh displayed a porous, cross-linking fibrous-like network that were dispersive. The physical topography of BioAsh changed entirely after it had been wet-dried. The wet-dried BioAsh showed expanded, harder, rosette-like, crystalline microstructures. The modification of physical structure of BioAsh after wet-dried was a series of complicated

processes involved the changed of physical and chemical elements. Primary compounds identified in the wood ash were calcium oxide (CaO), calcium carbonate (CaCO<sub>3</sub>), calcium hydroxide (Ca(OH)<sub>2</sub>) and calcium silicate (Ca<sub>2</sub>SiO<sub>4</sub>) (Etiegni and Campbell, 1991). When hydrated, these elements will go through major chemical change, swell to form calcium silicate hydrate (C-S-H) (Kirk-Othmer, 1979). As reported by Etiegni and Campbell, 1991 the oxides compound in the wood ash will potentially react with water, induce physical structure transformation, expand to form new compounds. The swelling mechanism of wood ash most probable cause by the action of capillary that expand the pores structure of wood ash. The hydrophilic nature of wood ash may also contribute to the swelling mechanism of wood ash structure.

#### 4.1.4 Fourier-Transform Infrared Spectroscopy

The presence of any functional molecular groups in the BioAsh (original) and BioAsh (wet-dried) were assessed via fourier-transform infrared spectroscopy (FTIR), as shown in **Figure 4.8** and **Figure 4.9**. The FTIR assessment was conducted in the wavelength ranged between 500 cm<sup>-1</sup> to 4000 cm<sup>-1</sup>.

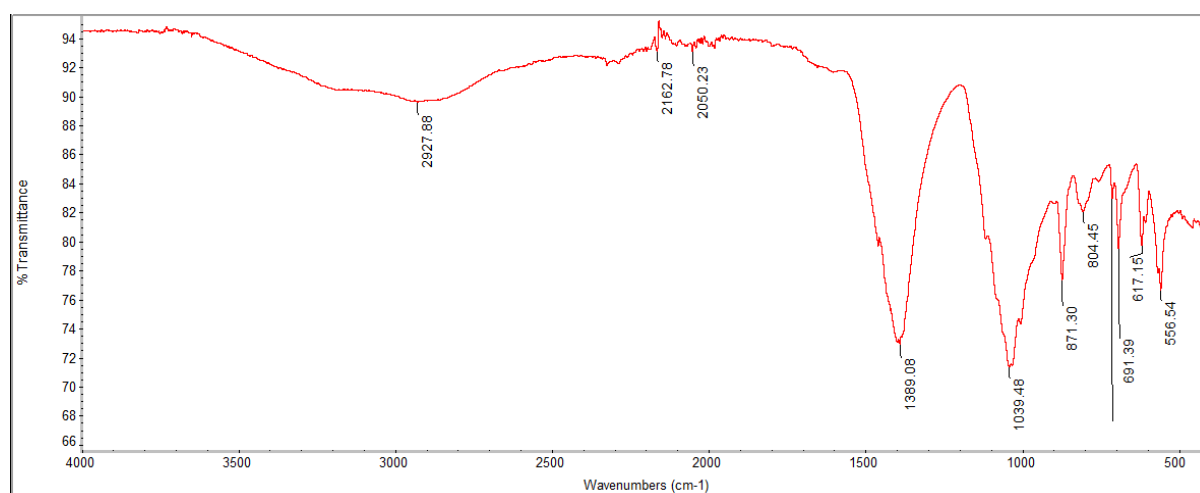


**Figure 4.8:** FTIR peak of original BioAsh.

In the FTIR analysis, the stretching of C-H bond was found in the peak band of  $2927.88\text{ cm}^{-1}$ . The stretching of triple bonds nitriles and carbenes ( $\text{C}\equiv\text{N}$ ) was found in the peak band  $2162.87\text{ cm}^{-1}$  and  $2050.23\text{ cm}^{-1}$ . Double bonds of  $\text{C}=\text{O}$ ,  $\text{C}=\text{N}$ , and  $\text{C}=\text{C}$  were identified at peak band  $1389.08\text{ cm}^{-1}$  and  $1039.48\text{ cm}^{-1}$ . The Other peak bands such as  $871.30\text{ cm}^{-1}$ ,  $804.45\text{ cm}^{-1}$ ,  $691.39\text{ cm}^{-1}$ ,  $617.15\text{ cm}^{-1}$ ,  $556.64\text{ cm}^{-1}$  were noticed.

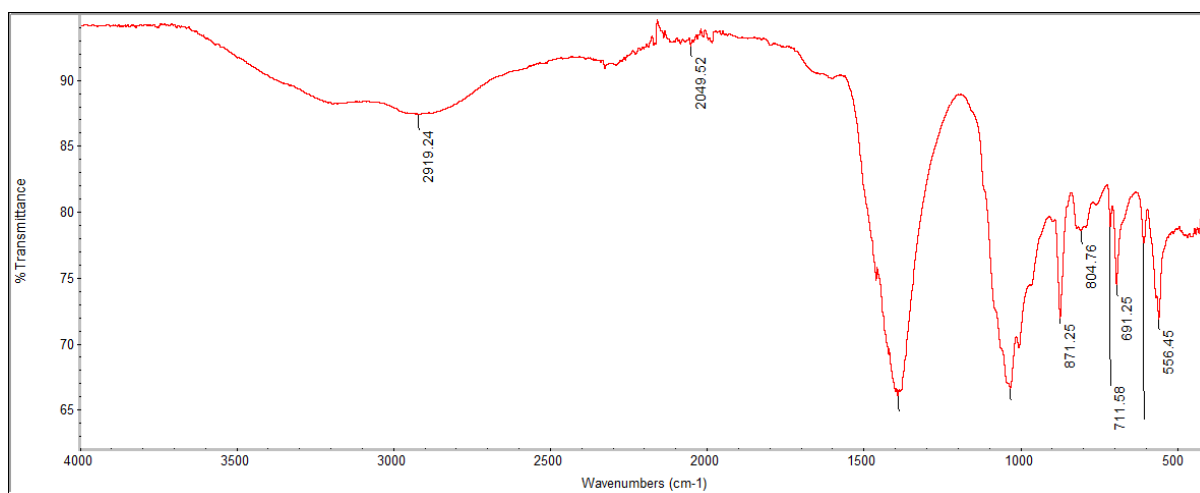


**Figure 4.9:** FTIR peak of wet-dried BioAsh.

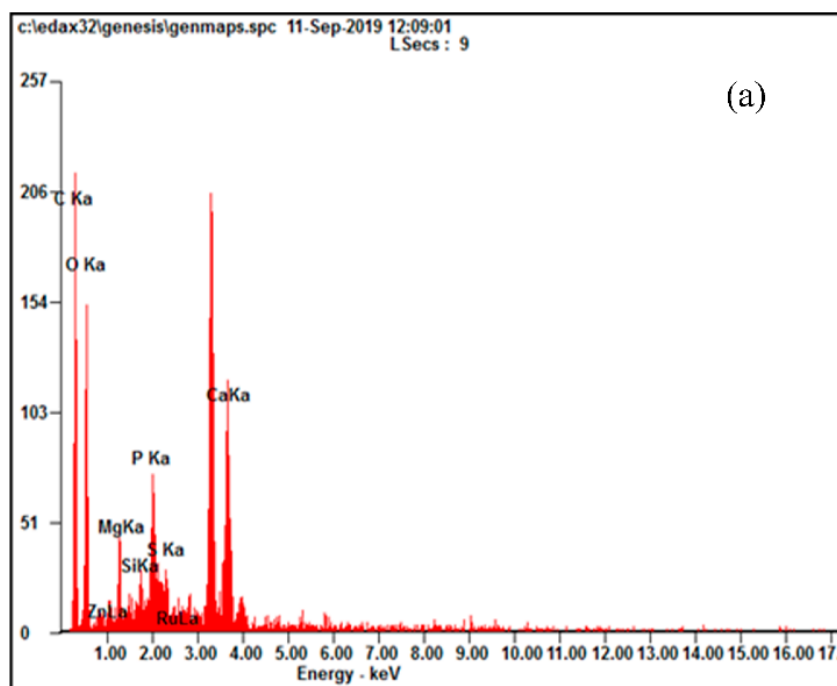
The stretching of C-H bond was found in the peak band  $2919.24\text{ cm}^{-1}$ . The peak band of  $2049.52\text{ cm}^{-1}$  was noticed most probable belong to the bonding of nitriles and carbenes stretch ( $\text{C}\equiv\text{N}$ ). The stretching of  $\text{C}=\text{O}$ ,  $\text{C}=\text{N}$ , and  $\text{C}=\text{C}$  bonds were identified in peak band  $1389.08\text{ cm}^{-1}$  and  $1039.48\text{ cm}^{-1}$ . The rest of peaks noticed in  $871.25\text{ cm}^{-1}$ ,  $804.76\text{ cm}^{-1}$ ,  $711.58\text{ cm}^{-1}$ ,  $691.25\text{ cm}^{-1}$ ,  $556.45\text{ cm}^{-1}$  were identified.

Cayla et al (2019) identified the  $\text{C}=\text{C}$  bond of aromatic ring occurred in the peak band of  $1400\text{ cm}^{-1}$  to  $1700\text{ cm}^{-1}$ . It was noticed,  $\text{C}=\text{C}$  bond (aromatic ring) existed in BioAsh at peak  $1389.08\text{ cm}^{-1}$ . Aromatic rings were also confirmed with their presence in peak between  $691.25\text{ cm}^{-1}$  to  $871.30\text{ cm}^{-1}$ . This is evidence of the presence of lignin in the BioAsh. Fan et al., 2013 informed the presence of aromatic ring and lignin can improve the thermal stability and the formation of good quality char barrier. In addition, this peak band at  $1389.08\text{ cm}^{-1}$  could also attributed to the existence of calcium carbonate ion ( $\text{CO}_3^{2-}$ ) and nitrate ion ( $\text{NO}_3^-$ ). The peak

band at  $1039.48\text{ cm}^{-1}$  could attributed to the presence of silicate ion ( $\text{SiO}_4^{2-}$ ). Aziz and Ahmad reported the stretching of C-H bond in peak  $2915.7$  to  $2916.6\text{ cm}^{-1}$ . The peak band of  $2927.88\text{ cm}^{-1}$  and  $2919.24\text{ cm}^{-1}$  in BioAsh (original) and BioAsh (wet-dried) proven the presence of C-H bond of the alkyl chain derived from the methyl group. The stretching of C-O bond in the oxygen group exhibited peak at  $1039.48\text{ cm}^{-1}$  in the BioAsh. The stretching of Alkynyl group ( $\text{C}\equiv\text{C}$ ) was noticed in peak  $2049.52\text{ cm}^{-1}$  and  $2050.23\text{ cm}^{-1}$  in the BioAsh.

#### 4.1.5 Energy-dispersive X-ray (EDX) Spectroscopy

Condition of original BioAsh and BioAsh after being wet-dried were analyzed using EDX. Changes in mineral contents in the original BioAsh and BioAsh after being wet-dried were identified in **Figure 4.10**. Primary mineral contents and changes in wt.% are as tabulated in **Table 4.2**.



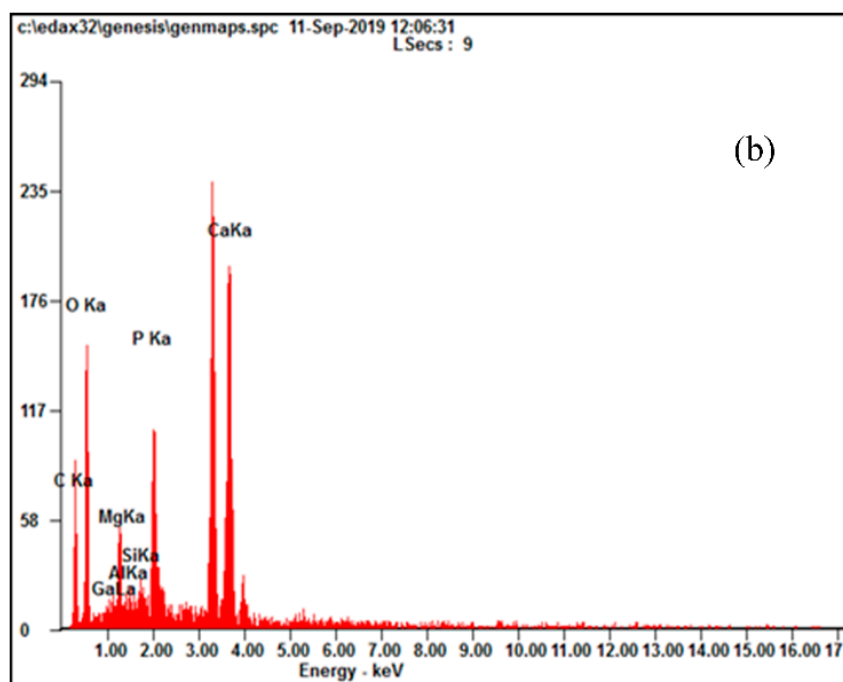


**Figure 4.10:** Elemental composition changes of (a) original BioAsh and (b) BioAsh after being wet-dried.

**Table 4.2:** Primary elemental composition changes of original BioAsh and BioAsh after being wet-dried.

| Sample                    | Element (wt.%) |       |      |      |      |       |      |      |      |       |      |
|---------------------------|----------------|-------|------|------|------|-------|------|------|------|-------|------|
|                           | Si             | Ca    | Mg   | Al   | P    | C     | Zn   | S    | Ru   | O     | Ga   |
| <b>BioAsh (original)</b>  | 1.26           | 11.59 | 3.10 | -    | 5.22 | 41.13 | 1.08 | 1.66 | 0.94 | 34.03 | -    |
| <b>BioAsh (wet-dried)</b> | 1.57           | 22.87 | 5.10 | 0.65 | 8.44 | 21.37 | -    | -    | -    | 38.31 | 1.68 |

Silica (Si) and Calcium (Ca) at 1.26 wt.% and 11.59% were found in the original BioAsh. It was noticed that amount of Si was slightly increased to 1.57 wt.% and the amount of Ca was doubled up to 22.87 wt.% in BioAsh after wet and dried. Minerals such as magnesium (Mg), alumina (Al) and phosphorus (P) in BioAsh were also found increased in amount to 5.10, 0.65 and 8.44 wt.% in a wet-dried condition. Carbon (C) was diminished from 41.13 wt.% to 21.37 wt.% in wet-dried BioAsh (refer to **Appendix C**). Ca was determined as

the primary constituent in rubber tree biomass (Etiegni and Campbell, 1991). Compounds such as  $\text{CaO}$ ,  $\text{CaCO}_3$ ,  $\text{Ca(OH)}_2$ ,  $\text{Ca}_2\text{SiO}_4$  were present in wood ash (Etiegni and Campbell, 1991). Various crop-based plant biomasses were examined and chemical compounds such as  $\text{CaO}$ ,  $\text{SiO}_2$ ,  $\text{MgO}$ ,  $\text{Al}_2\text{O}_3$ ,  $\text{P}_2\text{O}_5$  were found (Hytonen et al., 2019). EDX findings in this research discovered only the chemical elements in BioAsh. This research assumed that major mineral compounds such as  $\text{CaO}$ ,  $\text{CaCO}_3$  and minor mineral compounds such as  $\text{SiO}_2$ ,  $\text{MgO}$ ,  $\text{P}_2\text{O}_5$ ,  $\text{Al}_2\text{O}_3$  were potentially present in the original BioAsh. Primary elemental composition changes, where most elements noticed in EDX were increased in volume (except carbon) in hydrated BioAsh involved a series of complicated chemical and physical reactions. Compounds dissolved, decomposed, and forming new compounds caused variation in chemical and physical changes.

Combination of flame-retardant mineral fillers such as  $\text{Mg(OH)}_2$  and  $\text{Al(OH)}_3$  with an appropriate amount can lower the fire propagation index value, heat release rate and form a more uniform and thicker char layer (Yew et al., 2019). Namely,  $\text{Mg(OH)}_2$  and  $\text{Al(OH)}_3$  that exist in 3.5 wt.% BioAsh might contribute to the best outcomes of BAIC 3-5. This study reveals that potential elemental compounds and their reactions took place in 3.5 wt.% BioAsh produced the most positive effect in APP-PER-MEL/VAC formula in enhancing the fire-resistance properties.

#### **4.1.6 X-Ray Diffractometer**

The analysis of XRD was performed between the range of  $20 - 80^\circ$  ( $2\theta$ ) under the X-ray ( $\lambda$  (wavelength= 1.54) of  $\text{Cu K}\alpha$ , based on the Bragg's Law. The raw and hydrated BioAsh sample displayed peak as shown in **Figure 4.11**.

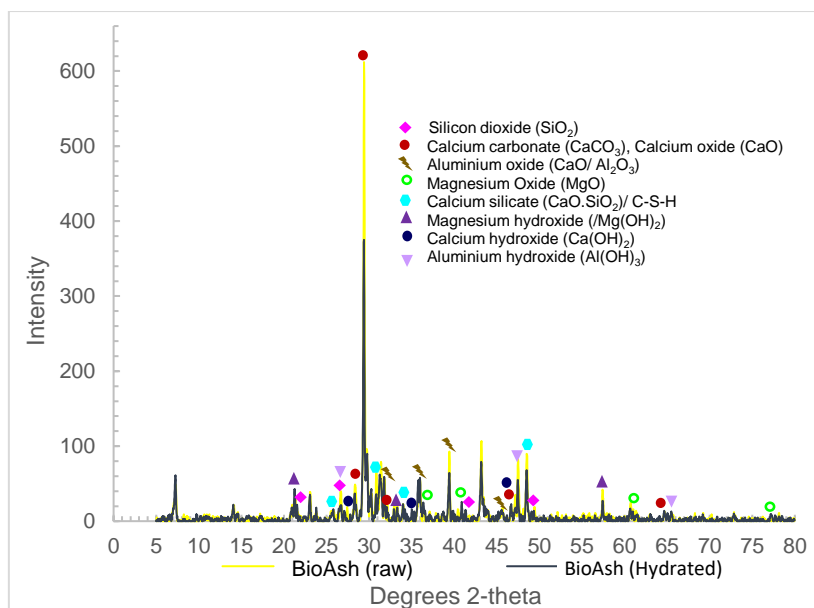


**Figure 4.11:** XRD Peaks of Raw and Hydrated BioAsh.

According to Wang and Dibdiakova (2014), CaO, MgO, CaSO<sub>4</sub>, Ca<sub>5</sub>(PO<sub>4</sub>)<sub>3</sub>, CaSiO<sub>3</sub>, K<sub>2</sub>SO<sub>4</sub>, Ca<sub>5</sub>(PO<sub>4</sub>)<sub>3</sub>OH, CaMgSi<sub>2</sub>O<sub>6</sub>, were identified in wood ash generated from stem wood, stem bark, branch, and twig. Calcium carbonate (CaCO<sub>3</sub>), Silicon dioxide (SiO<sub>2</sub>), Aluminium and aluminium hydroxide (Al, Al(OH)<sub>2</sub>), Calcium aluminate (AlCa<sub>3</sub>FeO<sub>6</sub>), Calcium silicate (2CaO.SiO<sub>2</sub>) were found in raw wood ash identified by the XRD (Saladi, 2019). Calcium carbonate (CaCO<sub>3</sub>) was identified with diffraction peak at  $2\theta \sim 29.3^\circ$ ,  $47.1^\circ$  (Render et al., 2016; Linggawati, 2016). These are corresponding to the XRD diffraction peaks found at  $29.4^\circ$  and  $47.1^\circ$  in the BioAsh confirmed the presence of CaCO<sub>3</sub> compound. Magnesium oxide (MgO) detected in BioAsh was also detected in the diffraction peak of  $2\theta \sim 36.9^\circ$ ,  $\sim 42.9^\circ$ ,  $\sim 62.4^\circ$ , and  $\sim 78.7^\circ$  in Zhang et al (2014) and Zhang et al (2018). Magnesium hydroxide (Mg(OH)<sub>2</sub>) was detected in  $2\theta \sim 21.0^\circ$ ,  $\sim 33.0^\circ$ ,  $\sim 39.0^\circ$ ,  $\sim 57.4^\circ$  (Saoud et al., 2014; Zhang et al., 2018). Calcium oxide (CaO) was detected in the diffraction peak at  $2\theta \sim 32.3^\circ$ ,  $\sim 64.2^\circ$  (Linggawati, 2016; Witoon, 2011). These peaks of Mg(OH)<sub>2</sub> and CaO confirmed their presence in BioAsh.



Silicon dioxide (SiO<sub>2</sub>) was detected in the peak diffraction of 2θ ~ 21.5°, 26.7°, 43.0°, 49.3° (Wonganan et al., 2020). This corresponding to the diffraction peak at 2θ ~ 26.7° and ~ 43.2° in the BioAsh justified the presence of SiO<sub>2</sub>. Al<sub>2</sub>O<sub>3</sub> present in the peak at 2θ~ 32.7°, 36.5°, 39.5°, 47.8° in the BioAsh. Almiron et al (2019) reported the presence of synergistic effects between SiO<sub>2</sub>, Al<sub>2</sub>O<sub>3</sub> and flame-retardant additives, and enhance the fire-resistant performance of the coating. Elemental compounds present in BioAsh as defined in **Table 4.3**.

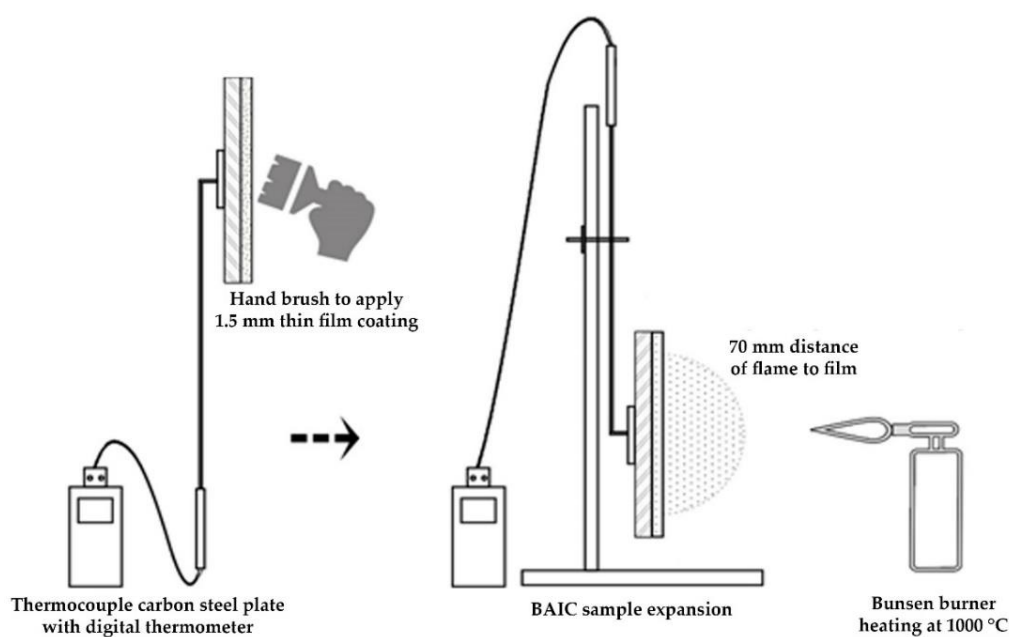
**Table 4.3:** Elemental compounds present in BioAsh

| Mineral Compound            | Mineral Formula                             | 2θ (°)                           | References                                       |
|-----------------------------|---|----------------------------------|--|
| <b>BioAsh</b>               |   |                                  |  |
| Calcium carbonate (Calcite) | CaCO <sub>3</sub>                           | 29.4°<br>47.1°                   | Render et al., 2016;<br>Linggawati, 2016;        |
| Calcium oxide               | CaO   | 32.3°<br>64.2°                   | Linggawati, 2016;<br>Witoon, 2011                |
| Calcium hydroxide           | Ca(OH) <sub>2</sub>                         | 28.6°<br>34.2°<br>47.5°          | Linggawati, 2016;<br>Khan et al., 2018           |
| Calcium silicate            | Ca <sub>2</sub> SiO <sub>4</sub> /<br>C-S-H | 26.0°<br>32.0°<br>34.0°<br>49.0° | Guan et al., 2013;<br>Zhang and Chang, 2010      |
| Silicon dioxide (Quartz)    | SiO <sub>2</sub>                            | 21.5°<br>26.7°<br>43.0°<br>49.3° | Wonganan et al., 2020;<br>Klaithong et al., 2017 |
| Magnesium oxide             | MgO   | 36.9°<br>42.9°<br>62.4°          | Zhang et al., 2014<br>Zhang et al., 2018         |
| Aluminium oxide             | Al <sub>2</sub> O <sub>3</sub>              | 32.7°<br>36.5°<br>39.5°<br>47.8° | Pakrashi et al., 2013                            |
| Magnesium hydroxide         | Mg(OH) <sub>2</sub>                         | 21.0°<br>33.0°<br>57.4°          | Zhang et al., 2018;<br>Saoud et al., 2014        |
| Aluminium hydroxide         | Al(OH) <sub>3</sub>                         | 27.9°<br>48.7°<br>66.0°          | Obada, 2016                                      |

It can be deduced that the raw RWA and hydrated versions, constituted of  $\text{CaCO}_3$ ,  $\text{CaO}$ ,  $\text{Ca(OH)}_2$ ,  $\text{Ca}_2\text{SiO}_4$ ,  $\text{SiO}_2$ ,  $\text{MgO}$ ,  $\text{Al}_2\text{O}_3$ ,  $\text{Mg(OH)}_2$ , and  $\text{Al(OH)}_3$ . The primary compounds in both the raw and hydrated RWA were calcium carbonate ( $\text{CaCO}_3$ ), as indicated by the diffraction peak at  $29.4^\circ$ .

## 4.2 Fire Resistance Performance

The fire resistance performances of all BAIC samples were investigated triplicate via fire resistant test (FRT) using a Bunsen burner device in a confined fume hood as shown in **Figure 4.12**.

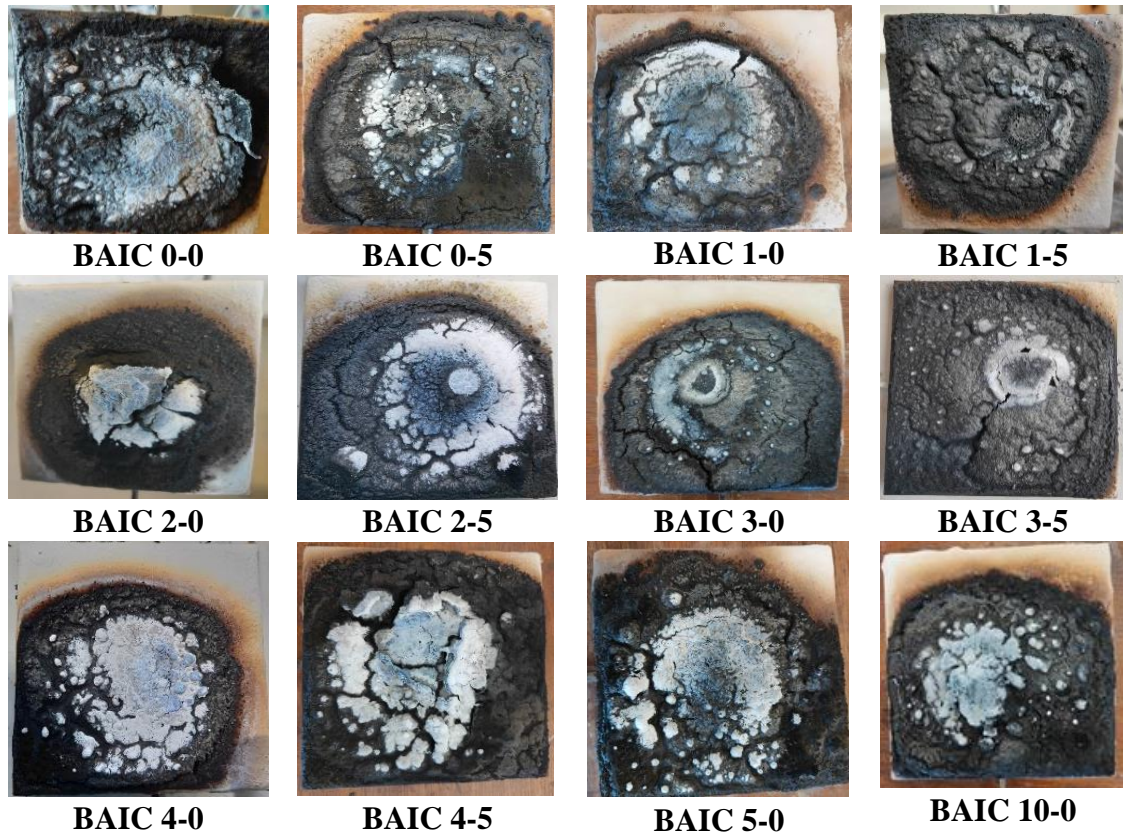


**Figure 4.12:** Fire resistance test setup

The end temperatures of all samples after 60 min of burning were tabulated in **Table 4.4**. Fire-protective char layer of all samples after the FRT as shown in **Figure 4.13**.

**Table 4.4:** End temperatures of BAIC samples after the FRT

| Sample           | FRT1 (°C)       | FRT2 (°C)       | FRT3 (°C)       | Mean (°C)       |
|------------------|-----------------|-----------------|-----------------|-----------------|
|                  | T <sub>Eq</sub> | T <sub>Eq</sub> | T <sub>Eq</sub> | T <sub>Eq</sub> |
| <b>BAIC 0-0</b>  | 173.0           | 174.3           | 179.2           | 175.5           |
| <b>BAIC 0-5</b>  | 144.3           | 149.9           | 150.8           | 148.3           |
| <b>BAIC 1-0</b>  | 135.7           | 136.2           | 137.1           | 136.3           |
| <b>BAIC 1-5</b>  | 132.0           | 134.3           | 135.0           | 133.7           |
| <b>BAIC 2-0</b>  | 129.2           | 131.3           | 132.0           | 130.8           |
| <b>BAIC 2-5</b>  | 128.5           | 123.6           | 127.7           | 126.6           |
| <b>BAIC 3-0</b>  | 117.8           | 124.7           | 126.6           | 123.0           |
| <b>BAIC 3-5</b>  | 114.7           | 109.5           | 113.4           | 112.5           |
| <b>BAIC 4-0</b>  | 128.9           | 133.8           | 129.5           | 130.7           |
| <b>BAIC 4-5</b>  | 142.1           | 151.7           | 150.2           | 148.0           |
| <b>BAIC 5-0</b>  | 156.9           | 158.2           | 162.0           | 159.0           |
| <b>BAIC 10-0</b> | 173.4           | 179.4           | 174.3           | 175.7           |

T<sub>Eq</sub>= Equilibrium Temperature**Figure 4.13:** Fire-protective char layer of BAIC samples after the FRT

BAIC 3-5 had the lowest end temperature and standard deviation ( $\sigma$ ) after exposing to a 60-min FRT as compared to unprotected steel ( $\sigma = 171.19$ ) and other BAIC sample protected

steels. BAIC 3-5 exhibited the best fire-resistant outcome at only 112.5 °C and the lowest  $\sigma$  of 16.42 after one hour of fire resistance testing. However, samples BAIC 10-0, BAIC 5-0 and BAIC 1-0 revealed the  $\sigma$  values of 33.11, 30.70 and 29.98, respectively. The temperature profiles of all samples are presented in **Figure 4.14**.

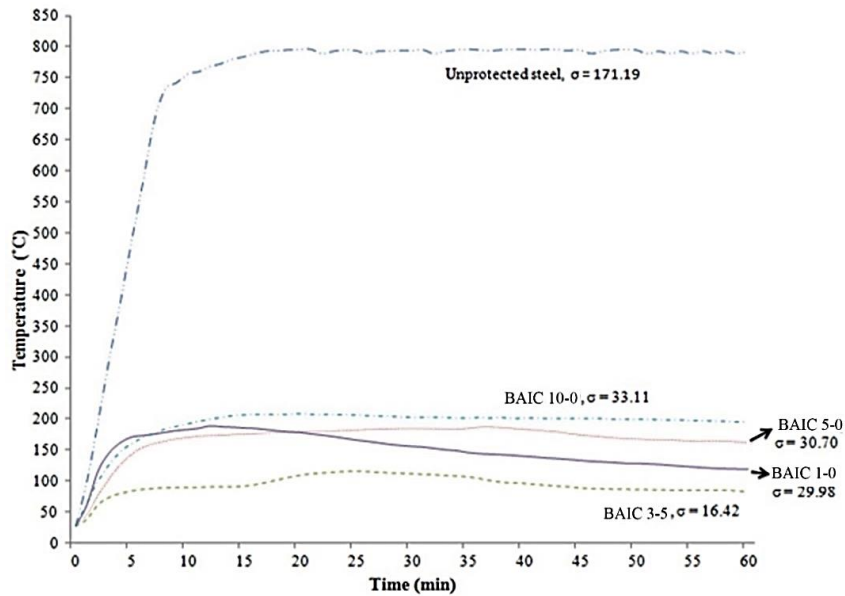


**Figure 4.14:** Temperature profiles and standard deviations of unprotected and protected steels with BAIC samples after a one-hour FRT

The elevations of BAIC samples after one hour of fire resistance testing are shown in **Figure 4.4**.

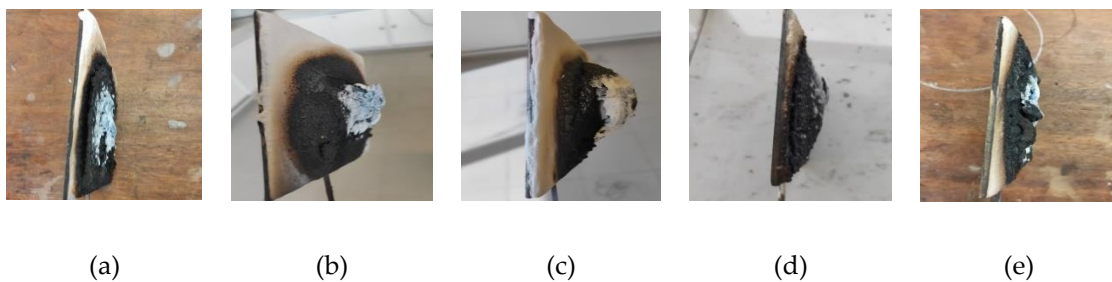


**Figure 4.15:** Intumescent coating samples after fire-resistance test: (a) BAIC 0-0, (b) BAIC 1-0, (c) BAIC 3-5, (d) BAIC 5-0, (e) BAIC 10-0.

This result reveals that 3.5 wt.% of BioAsh added into BAIC3-5 induced an optimum physical and chemical reaction with 6.5 wt.%  $\text{TiO}_2$ , and APP-PER-MER/VAC in the formula, resulting in good-quality char with the best fire-resistance outcome. The secondary rise was

noticed in BAIC 3-5 after 15 min and returned to equilibrium at 45 min. After 15 min,  $\text{TiO}_2$  accumulated at the surface, creating a low emissive material. It changed the boundary condition and thus increased the heat flux received by the material. Fire resistance efficacy was followed by BAIC 1-0 and BAIC 5-0 at 136.3 and 159.0 °C, respectively. BAIC 5-0 started with a lower temperature than BAIC 1-0 in the first 15 min. After 15 min, the temperature of BAIC 5-0 remained equilibrium throughout, whereas BAIC 1-0 was declining in temperature. The decline in burning temperature meaning a more stable char started to take place in BAIC1-0 only after 15 min. This could be due to a slower char formation process in BAIC1-0 as compared to others. 9.0 wt.% of  $\text{TiO}_2$  added could lower the melt flow rate (MFR) of BAIC1-0. Low MFR will inhibit gas released from APP-PER-MEL/VAC decomposition to expand the carbonaceous char (Li et al., 2015).

BAIC 10-0 displayed the worst fire resistance with the highest end temperature at 175.7 °C. This was probably attributable to the elemental composition present in 10.0 wt.% BioAsh that was chemically inert, unable to generate good-quality fire-protective char. This implied single 10.0 wt.% BioAsh in BAIC 10-0 was unideal to activate reaction with APP-PER-MER/VAC formula producing limited poor char to deter heat transmittance. Nonetheless,  $\text{TiO}_2$  shall not be used alone as the only mineral filler in intumescent coating formula as this led to poor adhesion strength of the coating to the steel, exposed the steel to fire resulted in bad fire resistance (Yew et al., 2015a). The combination of mineral fillers (hybrids) in IC formulation was required and crucial to ensuring a promising fire-resistance outcome and adhesion strength to the steel (Yew et al., 2015b). All steel plates coated with BAIC samples displayed a better fire resistance efficiency (below 200 °C) than unprotected steel plate that raised to the maximum temperature of 796 °C when exposed to 60 min of fire (Yew and Sulong, 2012; Yew et al., 2015a). All BAIC samples did not detach from the steel plate, except BAIC0-0. This indicated an acceptable surface adhesion strength of all BAIC samples added with BioAsh to

the steel surface. This result reveals that elemental compositions present in 3.5 wt% BioAsh were able to form the best-quality multicellular char barrier to constrain direct heat transfer to the steel plate. It can be concluded that 3.5 wt% BioAsh is appropriate to use to formulate water-based intumescent coating for a better fire resistance against fire. 3.5 wt% BioAsh contained the most appropriate amount of thermally stable elements such as  $\text{CaCO}_3$ ,  $\text{CaO}$ ,  $\text{Ca(OH)}_2$ ,  $\text{Ca}_2\text{SiO}_4$ ,  $\text{SiO}_2$ ,  $\text{MgO}$ ,  $\text{Al}_2\text{O}_3$ ,  $\text{Mg(OH)}_2$ , and  $\text{Al(OH)}_3$ , and  $\text{C}=\text{C}$  bond (aromatic ring), as verified in the FTIR, EDX, and XRD test of BioAsh characterisation that responsible for the most promising fire protective outcomes in BAIC 3-5.

### 4.3 Carbonaceous Char Formation

Carbolite furnace was used to examine all BAIC samples at a temperature of 600 °C. The char thickness of each sample is shown in **Figure 4.16**.

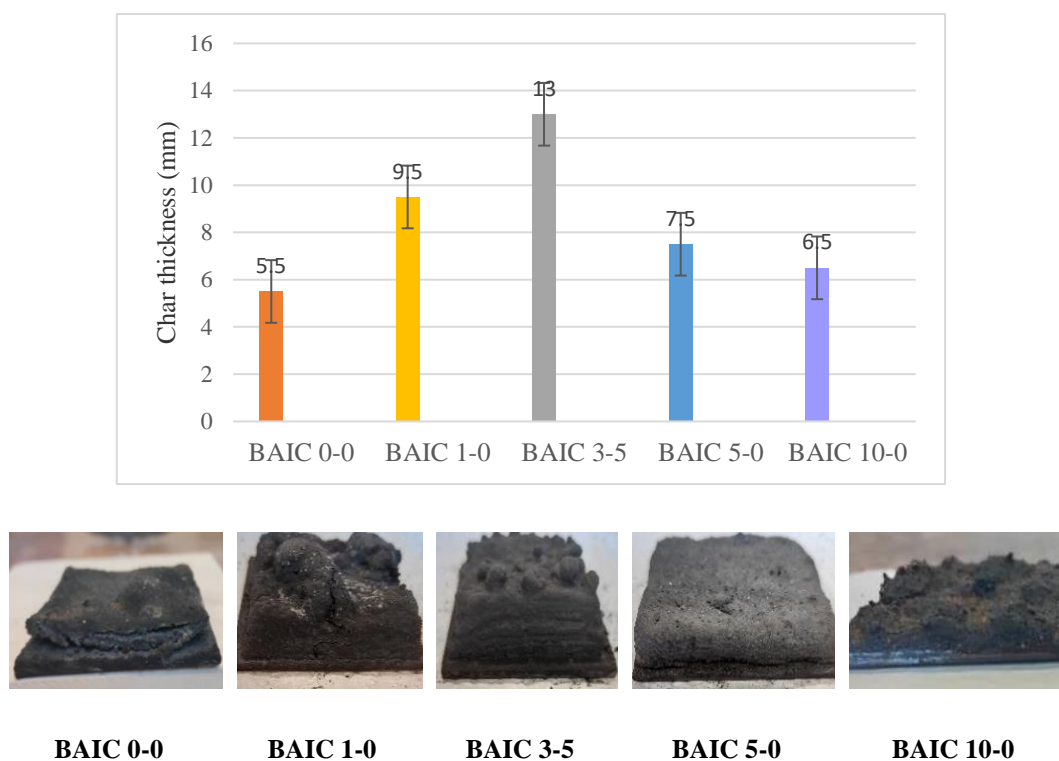


**Figure 4.16:** Char thickness of BAIC samples after the CFT

Various ingredients in IC formulation reacted and swelled when exposed to elevated heat. The property and structure of IC changed differently from low to high temperature. 600 °C is determined as the temperature where most of the reactions taken place in IC were finished and an inert char was formed. At a temperature below 600 °C, ingredients in IC were still reacting and complex chemical reactions were in progress. At a temperature above 600 °C, certain ingredients will start achieving their limiting thermal resistance, decompose and turn into ash instead of inert char that is measurable. BAIC 3-5 with 3.5 wt.% BioAsh formed the thickest char layer of 13.0 mm among the rest. BAIC 0-0, BAIC 1-0, BAIC 5-0 and BAIC 10-0 was 5.5, 9.5, 7.5, and 6.5 mm thick, respectively. This indicated that BAIC 3-5 formulation under the condition of 3.5 wt.% BioAsh had achieved the optimal reaction in APP-PER-MER/VAC formula triggered the densest char layer when exposed to heat. This could be largely contributed by the mineral elements and their appropriate composition present in 3.5 wt.% of BioAsh that promote the greatest char thickness. Full replacement of industrial mineral fillers using 10.0 wt.% of BioAsh in BAIC 10-0 led to the 6.5 mm char thickness. BAIC 0-0 had a char thickness of 5.5 mm which was lower than the char thickness of BAIC 10-0. Higher amount of TiO<sub>2</sub> (more than 10.0 wt%) led ineffective carbonaceous char and poor thermal insulation (Thirumal et al., 2017). Increased of TiO<sub>2</sub> in the coating composition constrained the expansion of char and expedite the thermal transition to the steel (Thirumal et al., 2017; Duquesne et al., 2013).

It was obvious BAIC 0-0 char shrunk and detached from the steel surface. BAIC 0-0 exhibited the poorest adhesion strength to shield the steel substrate from fire for a longer period. Char thickness was not correlated with the increasing amount of BioAsh. The least char expansion in BAIC 10-0 could be attributed to the excessive composition of mineral elements present in 10.0 wt.% BioAsh that suppressed the expansion of desirable char thickness. This

research determined an optimum ratio of 3.5 wt.% BioAsh formulation could ensure the yield of an ideal char thickness to protect the steel from fire.

#### 4.4 Char Strength

The strength of carbonaceous char layer formed after the CFT was examined in the weight load test. A 50 g of round metal was placed on top of the char, one by one until the char layer was eventually cracked. The strength of char was measured by calculating the total weight (numbers) of round metals it can withstand as shown in **Table 4.5**.

**Table 4.5:** Total weight of BAIC char layers can withstand in the weight load test.

| Samples   | Quantity of round metal | Total weight (g) |
|-----------|-------------------------|------------------|
| BAIC 0-0  | 1                       | 50               |
| BAIC 1-0  | 4                       | 200              |
| BAIC 3-5  | 5                       | 250              |
| BAIC 5-0  | 3                       | 150              |
| BAIC 10-0 | 1                       | 50               |

Result revealed BAIC 0-0 and BAIC 10-0 char layers were the weakest and able to withstand a total load of up to only 50 g. The char of BAIC 0-0 and BAIC 10-0 were soft and fragile. The char strength for BAIC 1-0 and BAIC 5-0 were 200 g and 150 g respectively. BAIC 3-5 char was able to withstand up to 250 g of load manifested the strongest char strength among all. It was noticed the enhancement of char strength was not correlated to the increment in TiO<sub>2</sub> and BioAsh amount. The incorporation of 3.5 wt% BioAsh in the VAC/APP-PER-MEL formulation generated the best char strength. The best char strength of BAIC 3-5 was further examined and verified in SEM as shown in **Figure 4.19(e)**. BAIC 3-5 char contained a more solid and compact (minimal void) multicellular rosette-like char cell structure. The char cell



features of BAIC 3-5 confirmed its ability to withstand the highest pressure among the char of all coating samples.

#### 4.5 Thermal Degradation Analysis

Fire protection performance has correlated with the thermal properties of coating (Anna et al., 2001). In this research, thermal degradation of all BAIC samples were examined via TGA. Residual weight vs. temperature of all BAIC samples as plotted in **Figure 4.17** (refer to **Appendix D**). The curves of all samples seem quite similar at the first 100 °C. Obvious thermal decomposition and mass change of all BAIC samples started between 200 and 500 °C indicated by constant drop in curves. The mass loss of BAIC 3-5, BAIC 1-0, BAIC 5-0, BAIC 10-0 and BAIC 0-0 at 500 °C was 60.34%, 61.12%, 63.70%, 66.67%, and 61.05% respectively. Derivative thermogravimetric analysis (DTG) is shown in **Figure 4.18**. The peak thermal degradation of BAIC 3-5, BAIC 1-0, BAIC 0-0, BAIC 5-0 and BAIC 10-0 occurred at a peak temperature of 495, 480, 485, 425 and 400 °C, respectively. Refer to **Appendix E**.

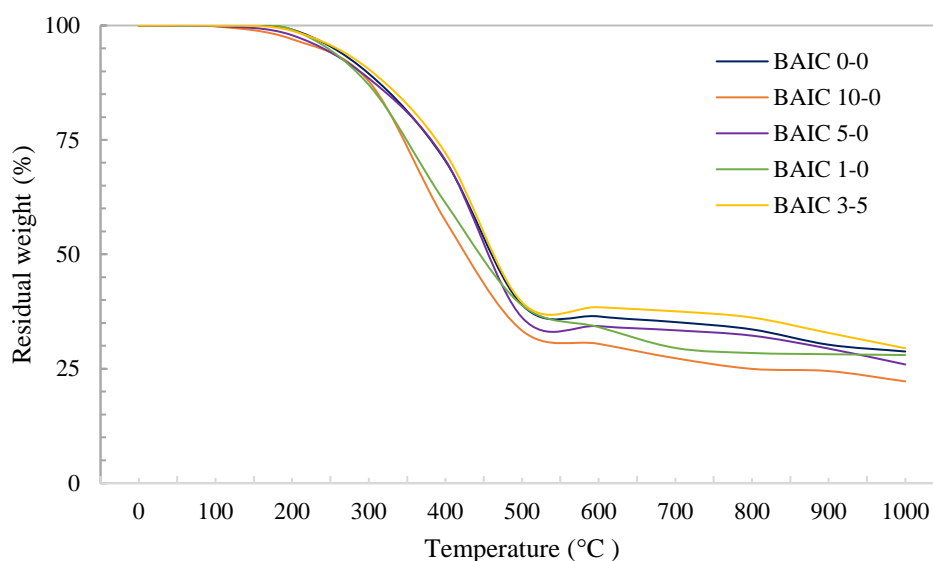


**Figure 4.17:** Thermogravimetric analysis (TGA) curves of BAIC samples

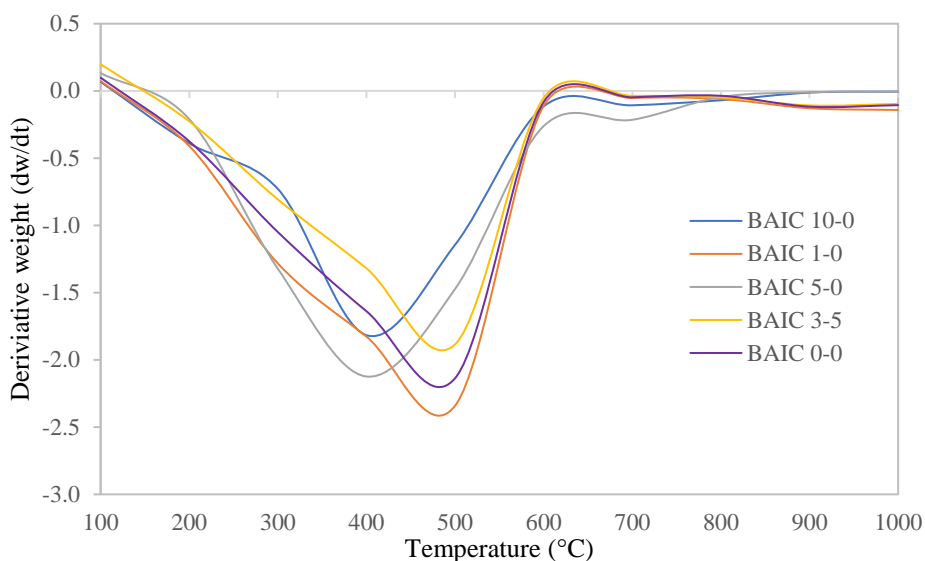


**Figure 4.18:** Derivative thermogravimetric analysis (DTG) of BAIC samples

The potential thermal decompositions of compounds that might take place caused a mass loss of samples, as shown in **Table 4.6** (Anna et al., 2001; Conceicao and Scharnagl, 2015; Wypych, 2016; Karunadasa, et al., 2019; Phosphoric acid, 2020). These mineral compounds were predicted from EDX and FTIR analysis of BioAsh of those most likely to undergo thermal decomposition in coating when heat-treated in TGA.

**Table 4.6:** Potential compound in BAIC samples, decomposition reaction and temperature.

| Compound   | Decomposition Reaction   | Decompose Temperature (°C) |
|--|--|----------------------------|
| CaCO <sub>3</sub>                                | CaCO <sub>3</sub> → CaO + CO <sub>2</sub>  | 700                        |
| Mg(OH) <sub>2</sub>                              | Mg(OH) <sub>2</sub> → MgO + H <sub>2</sub> O   | 360                        |
| Al(OH) <sub>3</sub>                              | Al(OH) <sub>3</sub> → Al <sub>2</sub> O <sub>3</sub> + H <sub>2</sub> O  | 180                        |
| 2H <sub>3</sub> PO <sub>4</sub>                  | 2H <sub>3</sub> PO <sub>4</sub> → H <sub>4</sub> P <sub>2</sub> O <sub>7</sub> + H <sub>2</sub> O                    | 200                        |
| 4AlPO <sub>4</sub>                               | 4AlPO <sub>4</sub> → 2Al <sub>2</sub> O <sub>3</sub> + P <sub>4</sub> O <sub>10</sub>                                | 100                        |
| Mg(H <sub>2</sub> PO <sub>4</sub> ) <sub>2</sub> | Mg(H <sub>2</sub> PO <sub>4</sub> ) <sub>2</sub> → MgH <sub>2</sub> P <sub>2</sub> O <sub>7</sub> + H <sub>2</sub> O | 450                        |
| -C <sub>2</sub> H <sub>5</sub> -                 | -C <sub>2</sub> H <sub>5</sub> - → -C <sub>2</sub> H <sub>4</sub> - + H <sup>+</sup>                                 | 95                         |

The dominant decomposition was mainly contributed to by the reactive phosphates that contained inorganic (PO<sub>4</sub>)<sup>3-</sup> ion potentially found in the compound. The phosphates were very

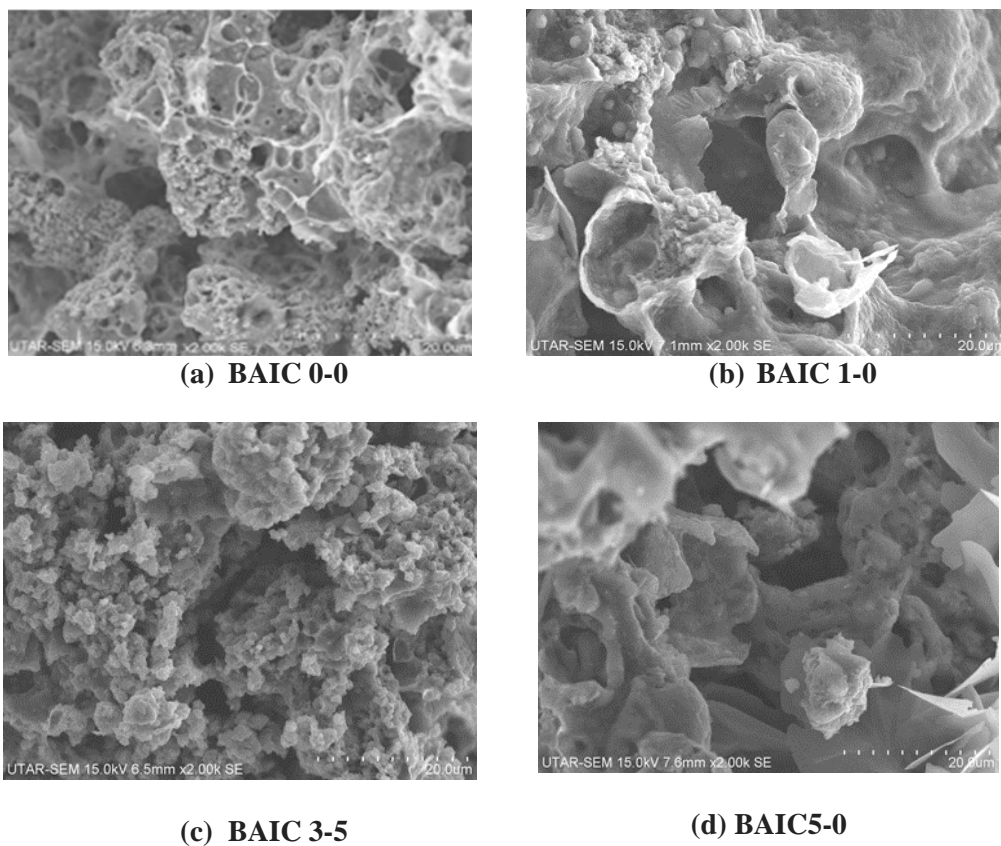
reactive; hence, when hydrated and heated, they can react with other elements, creating new compounds transformed into other phosphate form. BAIC 3-5 had the highest residual weight of 29.48 wt.%, followed by BAIC 0-0 of 28.76 wt.%, BAIC 1-0 of 27.99 wt.% and BAIC 5-0 of 25.93 wt.% at 1000 °C. BAIC 10-0 displayed the lowest residual weight of 24.27 wt.%. BAIC 10-0 supplemented with 10.0 wt.% BioAsh degraded the most. BAIC 1-0 had a higher residual weight than BAIC 5-0 at the end of the test. BAIC 1-0 with filler combination of 1.0 wt.% BioAsh and 9.0 wt.% TiO<sub>2</sub> performed better than BAIC 5-0 with 5.0 wt.% BioAsh and 5.0 wt.% TiO<sub>2</sub>. Pros and cons were reported when TiO<sub>2</sub> load increased in the coating composition. In coating with high TiO<sub>2</sub>, it was noticed the thermal stability and residual mass of coating enhanced in TGA, however the char expansion thickness and thermal insulation performance weaken (Thirumal et al., 2017). Variables in the residual weight of BAIC samples against high heat had been subjected to different BioAsh: TiO<sub>2</sub> ratio given that APP-PER-MEL/VAC was the fixed parameter. The previous study revealed the use of a suitable amount of eggshell (ES) as filler enhanced thermal properties and char thickness by reducing the heat release rate (HRR), time to ignition (TTI) and total heat release (THR) in the IC (Yew et al., 2018). The primary compound found in ES was calcium carbonate (CaCO<sub>3</sub>). A suitable amount of Al(OH)<sub>3</sub>, TiO<sub>2</sub> and ES added to IC formulation assisted in lowering the index value of fire propagation (Anna et al. 2001).

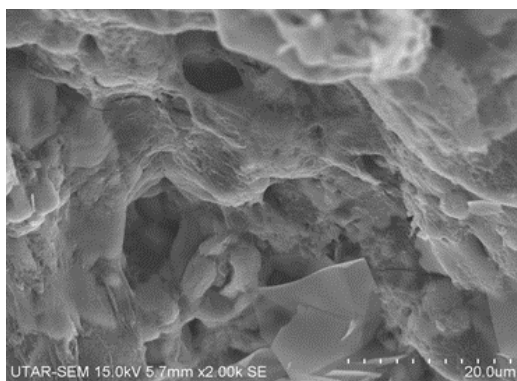
This research predicted the proper combination of CaCO<sub>3</sub> and Al(OH)<sub>3</sub> presence in 3.5 wt.% BioAsh could enhance the thermal stability of BAIC 3-5 as compared to the rest. This research concluded that the reaction of 3.5 wt.% BioAsh in the formulation was able to lower the thermal degradation of BAIC 3-5 at 1000 °C. The incorporation of 3.5 wt% BioAsh induced an optimal thermal char stability with desirable thickness for fire protection. Elemental composition presented in 3.5 wt% BioAsh reacted with water, and other ingredients in the APP-PER-MEL/VAC after heated formed the most appropriate amount of thermally stable

compounds in BAIC 3-5 to resist fire. These thermally stable compounds were  $\text{CaAl}_2\text{O}_4$ ,  $\text{MgSiO}_3$ ,  $\text{Mg}_3(\text{PO}_4)_2$ ,  $\text{AlPO}_4$ , and  $\text{TiP}_2\text{O}_7$ , predominant with  $\text{Ca}_3(\text{PO}_4)_2$  as verified in the XRD test of BAIC 3-5.

#### 4.6 Char Surface Morphology

Surface topography of BioAsh was magnified and assessed under  $\times 2.00\text{ k}$  in SEM. Char surface morphology of all BAIC samples after the fire-resistant test were investigated under high magnification of  $\times 2.00\text{ k}$  in SEM. Surface micrographs of all samples as shown in **Figure 4.19**.





**(e) BAIC 10-0**

**Figure 4.19:** Char morphology of BAIC samples.

Carbonaceous char layer quality of BAIC samples was analyzed. BAIC 3-5 showed a more compact and solid char structure among all samples. Char of BAIC 3-5 displayed a multicellular rosette-like crystalline structure that was rigid with minimal micropores. Complex physical and chemical characteristics of wood ash when hydrated will expand and result in a rosette-like structure. This rosette-like form will remain after being air dried (Etiegni and Campbell, 1991). The multicellular rosette-like crystalline char structure indicated that BAIC 3-5 added with 3.5 wt.% BioAsh was able to form a more solid and uniform carbonaceous matrix resulting in a better fire-protective barrier to resist heat transfer. This rosette-like multicellular matrix was occupied with abundant fine void channels (air gaps) that prevented the speedy spread of heat. The rosette-like structure did not present in other samples. In contrast, BAIC 10-0 showed a soft, fluff and filamentous-like char cell that was fragile and with many obvious irregular macro pores. This soft and spongy fibrous-like char structure could be attributed to the high dosage of plant fibers that existed in 10.0 wt.% BioAsh. Non-multicellular and weak char structure happened in BAIC 10-0 accelerated the heat transfer and declined the fire-retardant efficacy. This resulted in the worst fire resistance in BAIC 10-0. Mineral components that present in 10.0 wt.% BioAsh constrained the chemical reactions with  $\text{TiO}_2$  in APP-PER-MER/VAC formula. The char structure of BAIC 1-0 displayed fewer

macropores and resulted in a better fire-resistant outcome than BAIC 5-0. This research suggests that an appropriate BioAsh at 3.5 wt.% in the APP-PER-MER/VAC formulation could promote uniform, thicker multicellular solid char barrier with better char strength that was excellent in fire resistance.

#### 4.7 Pozzolanic reaction and antioxidation properties

Potential compounds and their series of complex reactions that might happen in the wet-dried BioAsh (Olanders and Steenari, 1995; Bostrom et al., 2011) were tabulated in **Table 4.7**.

**Table 4.7:** Potential compounds and their reactions occurred during the hydration of BioAsh.

| Compound             | Chemical Formula                                   | Reaction (Equation)                           |
|----------------------|--|---|
| Carbon               | C  | $C + O_2 \rightarrow CO_2$                    |
| Calcium oxide        | CaO  | $CaO + H_2O + CO_2 \rightarrow Ca(OH)_2$      |
|                      | CaO  | $3 CaO + SiO_2 \rightarrow Ca_3SiO_5$         |
| Calcium carbonate    | CaCO <sub>3</sub>                                  | $CaCO_3 + H_2O \rightarrow Ca^{2+} + CO_2$    |
| Silicon dioxide      | SiO <sub>2</sub>                                   | $SiO_2 + H_2O \rightarrow Si(OH)_4$           |
| Silicon dioxide      | SiO <sub>2</sub>                                   | $SiO_2 + CaCO_3 \rightarrow Ca_2SiO_4 + CO_2$ |
| Calcium hydroxide    | Ca(OH) <sub>2</sub>                                | $Ca(OH)_2 + Si(OH)_4 \rightarrow C-S-H$       |
|                      | Ca(OH) <sub>2</sub>                                | $Ca(OH)_2 + CO_2 \rightarrow CaCO_3$          |
| Tricalcium silicate  | Ca <sub>3</sub> SiO <sub>5</sub> /C <sub>3</sub> S | $Ca_3SiO_5 + H_2O \rightarrow C-S-H$          |
| Magnesium oxide      | MgO  | $MgO + H_2O \rightarrow Mg(OH)_2$             |
| Phosphorus pentoxide | P <sub>2</sub> O <sub>5</sub>                      | $P_2O_5 + H_2O \rightarrow H_3PO_4$           |
| Aluminum oxide       | Al <sub>2</sub> O <sub>3</sub>                     | $Al_2O_3 + 3 H_2O \rightarrow Al(OH)_3$       |

CaO, CaCO<sub>3</sub>, and SiO<sub>2</sub> were three main potential mineral compounds that contributed to the formation of Calcium silicate hydrate (C–S–H). C–S–H is a gel-like binding agent accountable to cohere admixture for strength in cementitious materials (Devendra and Rangaswamy, 2012). Pozzolan shall consist of SiO<sub>2</sub>, Al<sub>2</sub>O<sub>3</sub> and ferric oxide (Fe<sub>2</sub>O<sub>3</sub>) as

prescribed in American Society for Testing Materials (ASTM C618). Pozzolanic activities might occur in BioAsh when wetting, converting potential pozzolans  $\text{SiO}_2/\text{CaO}/\text{CaCO}_3$  into a very minor quantity of C–H–S with the cementitious property. Original BioAsh, wet BioAsh, and wet-dried BioAsh as shown in **Figure 4.20**.



**Figure 4.20:** BioAsh (original), BioAsh (wet), BioAsh (wet-dried) from left to right.

The raw (before) and wetting dried (after) BioAsh clearly shown the transformation of physical properties of the BioAsh in **Figure 4.20**. This physical change was verified in the SEM test of BioAsh characterisation confirmed that BioAsh transformed from loose fibrous networks to expanded rosette-like crystalline structures. The rosette-like crystalline structures remained unchanged and irreversible after wet-dried. These rosette-like crystalline structures were highly accountable to the presence of minor C-S-H as verified in the wet-dried BioAsh that offered the binding (gel-like) effects and properties to the BioAsh after hydrated. This binding properties was the produce of complex reactions between elemental compounds and their compositions presented in the BioAsh as verified in EDX and XRD tests.

Oxygen and carbon composition of all BAIC samples were examined via EDX. The oxygen to carbon ratio is shown in **Figure 4.21**.

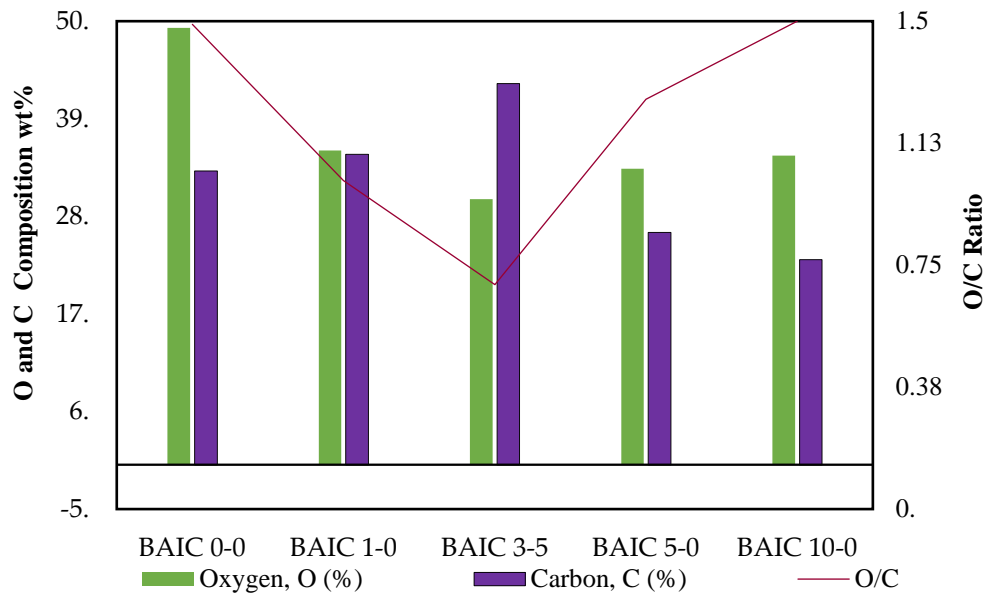


**Figure 4.21:** Oxygen and carbon composition, and O/C ratio of BAIC samples.

Oxygen to carbon (O/C) ratio was crucial in investigating the antioxidation property of the char layer (Kraszkiewicz et al., 2017). The O/C ratio of BAIC 0-0, BAIC 1-0 and BAIC 5-0 were 1.49, 1.01 and 1.26, respectively (**Appendix F**). BAIC 3-5 reinforced with 3.5 wt.% BioAsh had achieved the lowest O/C ratio at only 0.69, which was able to slow down the fire and heat propagation toward the steel underneath it. BAIC 3-5 manifested the best fire-resistant, char thickness and TGA outcomes. In contrast, BAIC 10-0 sample with 10.0 wt.% BioAsh displayed the highest O/C ratio at 1.50 demonstrated the weakest performance to resist fire. Char layer of BAIC 10-0 oxidized tremendously caused the loss of electrons damaged the molecules in char cells.  $\text{SiO}_2$  and  $\text{Al}_2\text{O}_3$  predicted present in the BioAsh were known for their antioxidant properties.  $\text{SiO}_2$  and  $\text{Al}_2\text{O}_3$  in BAIC 3-5 might be assisted in the best reactions with  $\text{TiO}_2$ -APP-PER-MEL/VAC that enhanced the antioxidant quality of the char layer formed. This research suggested, 3.5 wt.% of BioAsh in BAIC 3-5 was appropriate to offer an excellent antioxidant value to enhance the charred quality to better suppress the heat transfer to steel (Li et al., 2020). EDX and XRD tests further verified the presence of  $\text{SiO}_2$ ,  $\text{Al}_2\text{O}_3$  in BioAsh, and their appropriate amount present in 3.5 wt% assisted in the highest antioxidant properties.



## 4.8 Molecular Functional Group Analysis

FTIR was used to characterize the cross linkage of molecular functional groups in all BAIC samples. The relationship of functional groups with adhesion strength can be diagnosed (Aziz and Ahmad, 2016; Yew et al., 2018). Analysis of elemental functional groups with the peak wavenumber and band position of all BAIC samples is shown in **Figure 4.22**.

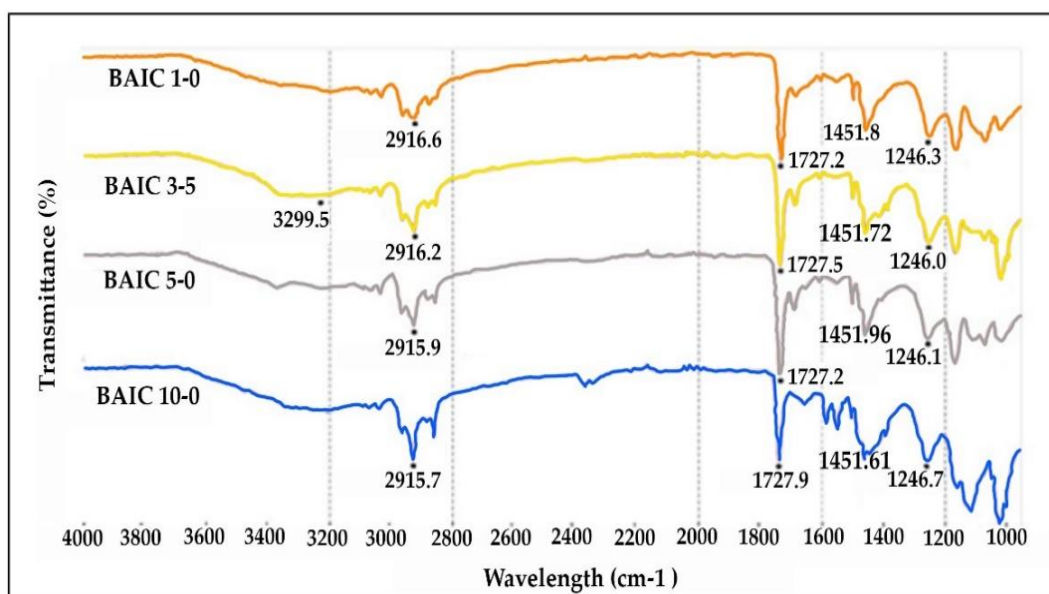


**Figure 4.22:** Infrared spectra of BAIC samples.

Peak ranging from 2915.7 to 2916.6 cm<sup>-1</sup> indicated the symmetrical stretching of C—H of alkyl chain in the methyl group (Aziz and Ahmad, 2016). Stretching of C = O (carbonyl group) in lignin and hemicellulose that originated in BioAsh (rubberwood biomass) displayed at peak 1727.2 to 1727.9 cm<sup>-1</sup>. —C—O (ester bond) and —C = O (ester carbonyl) that were sensitive to form a hydrogen bond can be found in vinyl acetate copolymer. The transmittance of —C—O and —C = O showed peaks ranging from 1246.0 to 1246.7 cm<sup>-1</sup> and 1727.2 to 1727.9 cm<sup>-1</sup>, respectively, in all BAIC samples proving the formation of hydrogen bonds (Wang and Zhao, 2019). The peak from 1246.0 to 1246.7 cm<sup>-1</sup> proved the deformation of the carbonyl group (C—H) present in cellulose, hemicellulose, and lignin (De Sá et al., 2017). Aromatic ring in

lignin was identified at the peak from 1600 to 1585  $\text{cm}^{-1}$  and 1500 to 1400  $\text{cm}^{-1}$  (Cayla et al., 2019). All BAIC samples showed a peak between 1451.61 and 1451.96  $\text{cm}^{-1}$  that manifested the stretching of C = C (aromatic ring) in lignin present in BioAsh. Lignin reported a decomposition temperature of 150–900  $^{\circ}\text{C}$  in the TGA (Yang et al., 2007; Lv et al., 2010; Waters et al., 2017). This wide range of decomposition temperatures of lignin further predicted its present in the BAIC samples. Polymer compounds associated with aromatic rings such as lignin are reported to be advantageous for thermal stability and char barrier formation (Fan et al., 2013). Wide band position from 3100 to 3600  $\text{cm}^{-1}$  was exhibited in all samples. This could be attributed to the stretching of the hydroxyl group (O–H) (Hong et al., 2010) that derived from intense intermolecular and intramolecular of hydrogen bonds. This O–H functional group could contribute to the interfacial hydrogen bonding between BAIC samples and the steel surface (Jessica et al., 2020). FTIR verified the present of cross-linking molecular groups such as C–H, C = O, C–O, C = C, and O–H in all coating samples.

The char residue of sample BAIC 0-0, BAIC 1-0, BAIC 3-5, BAIC 5-5, and BAIC 10-0 remained after the fire resistance test were collected for FTIR analysis. The FTIR of peaks of sample BAIC 0-0, BAIC 1-0, BAIC 3-5, BAIC 5-5, and BAIC 10-0 as presented in **Figure 4.23**, **Figure 4.24**, **Figure 4.25**, **Figure 4.26**, and **Figure 4.27**.

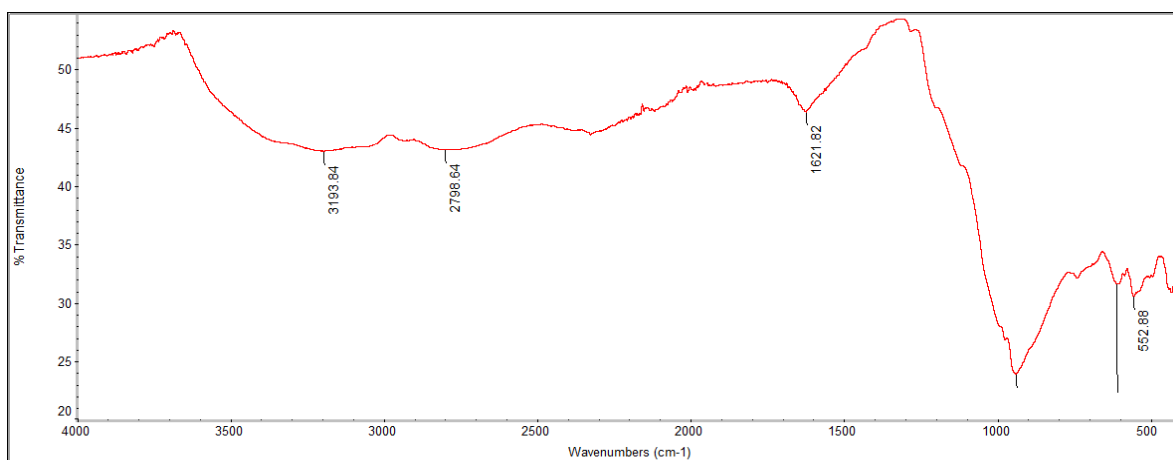


**Figure 4.23:** FTIR peaks of char residue of BAIC 0-0.

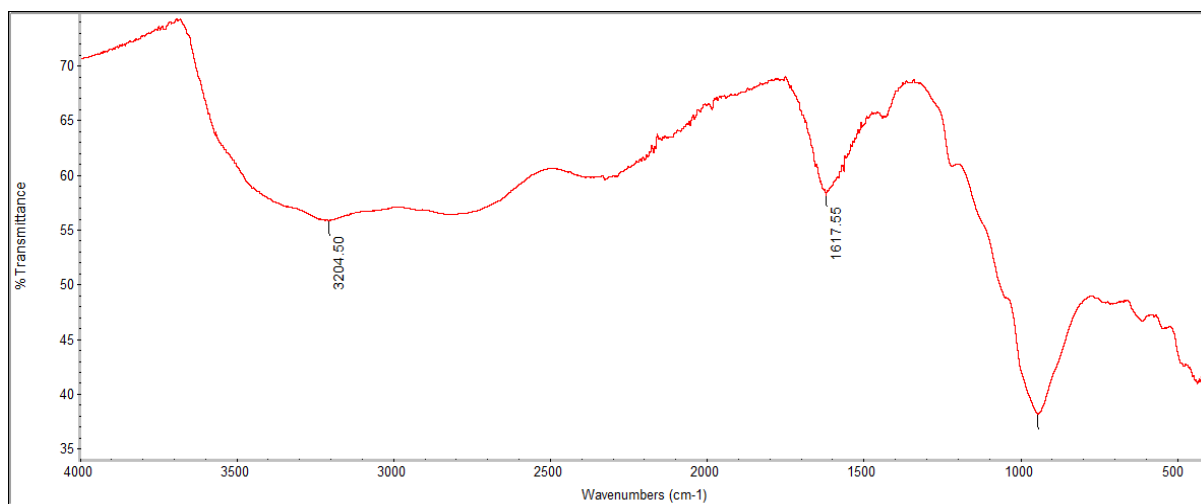


**Figure 4.24:** FTIR peaks of char residue of BAIC 1-0.

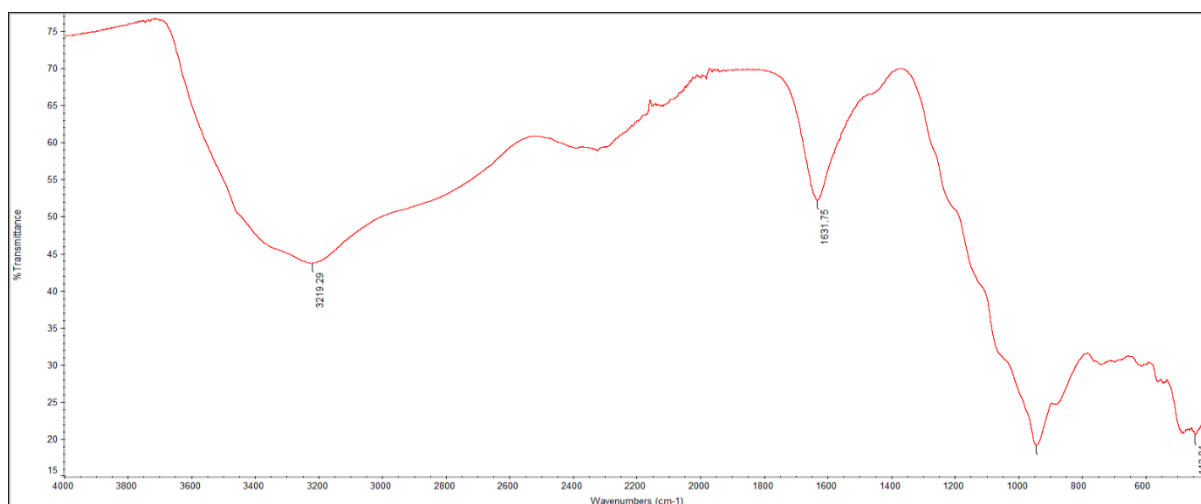


**Figure 4.25:** FTIR peaks of char residue of BAIC 3-5.

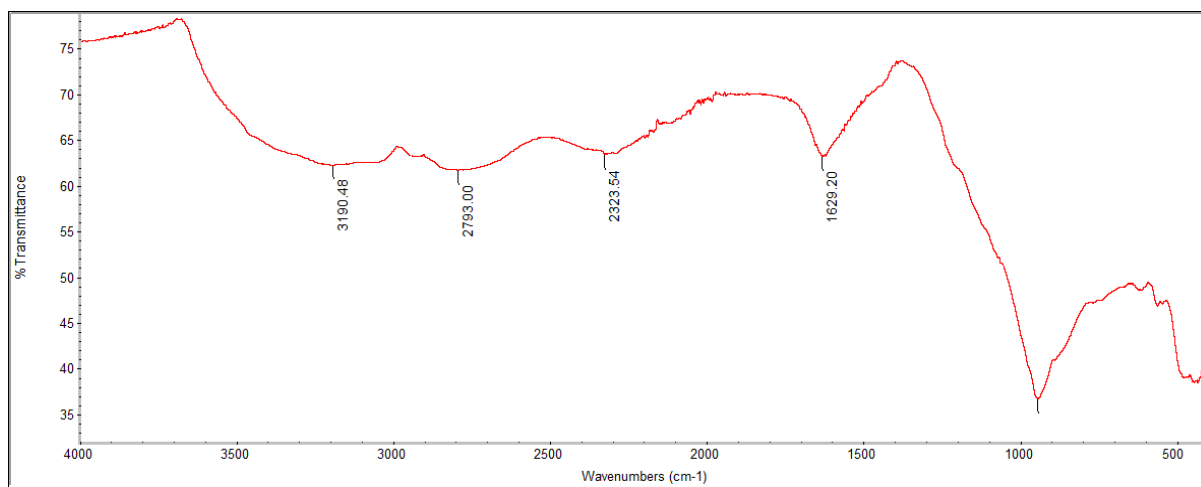


**Figure 4.26:** FTIR peaks of char residue BAIC 5-0.

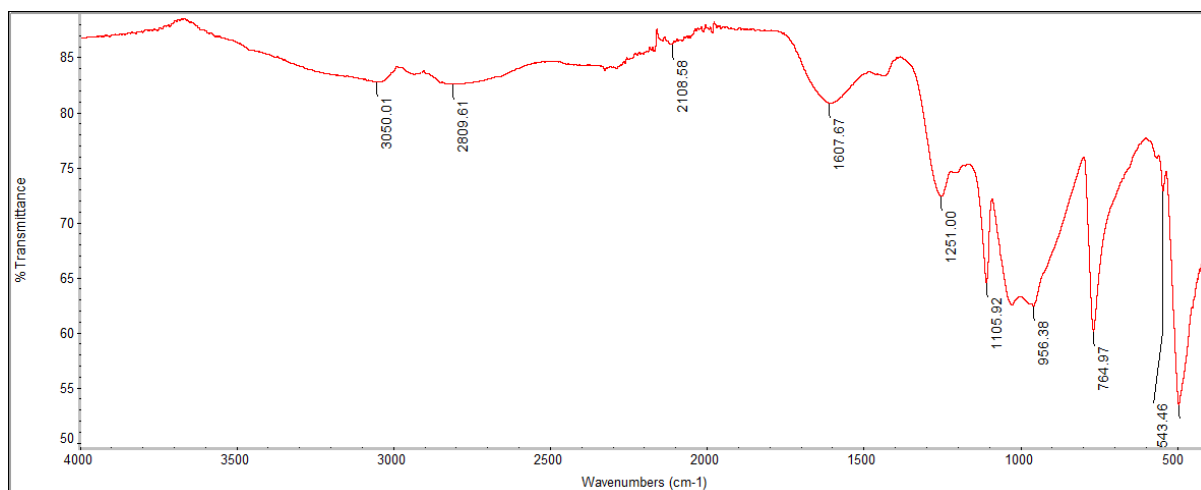


**Figure 4.27:** FTIR peaks of char residue of BAIC 10-0.

The stretching O-H functional groups are represented by  $3300\text{--}2500\text{ cm}^{-1}$ , and  $950\text{--}910\text{ cm}^{-1}$ . It was noticed, the char residue of all samples exhibited broad wavelength at  $3204.50\text{ cm}^{-1}$ ,  $3193.84\text{ cm}^{-1}$ ,  $3219.29\text{ cm}^{-1}$ ,  $3190.48\text{ cm}^{-1}$ ,  $3050.01\text{ cm}^{-1}$ . These wavelengths were related to the stretching of O-H bond in the hydroxyl groups. In addition, all samples exhibited wavelength between  $910\text{ to }950\text{ cm}^{-1}$  confirmed the presence of O-H bonding in the coating. BAIC 3-5 showed the most distinct intensity of peak bands in these two groups of wavelengths among all indicated that it had the strongest O-H bonding in the coating towards the steel substrate after the combustion. BAIC 10-0 and BAIC 0-0 showed the least intensity peak band of O-H bonding revealed its weak adhesion strength to the steel after fire. Another obvious wavelength BAIC 0-0 ( $1617.55\text{ cm}^{-1}$ ), BAIC 1-0 ( $1621.82\text{ cm}^{-1}$ ), BAIC 3-5 ( $1631.75\text{ cm}^{-1}$ ), BAIC 5-0 ( $1629.20\text{ cm}^{-1}$ ), and BAIC 10-0 ( $1607.67\text{ cm}^{-1}$ ) were found. These wavelengths belong to the stretching of C=C bonds in the alkene group derived from the VAC. BAIC 3-5 disclosed the most intense peak in this wavelength confirmed its outstanding adhesion strength among all samples. The wavelength at  $1100\text{--}950\text{ cm}^{-1}$  represented the stretching of  $\text{PO}_4^{3-}$  (phosphate group) and  $\text{SiO}_4^{2-}$  (silicate). This indicated the formation of thermally stable phosphate and silicate compounds in the coating when exposed to fire. The intensity of wavelength at  $950\text{ cm}^{-1}$  appeared as the most obvious in BAIC 3-5 among all. This revealed

that the addition of 3.5 wt% in the formulation of BAIC 3-5 enabled the occurrence of higher amount of thermally stable phosphate and silicate compounds to resist fire. This outcome evidence further verified the outperformed fire-resistance outcome in BAIC 3-5 as compared to other samples. BAIC 3-5 had the most intense O-H bonding demonstrated the best adhesion bonding to the steel at post combustion stage. These verified the outstanding FRT, TGA, SEM, IAT results of BAIC 3-5 as compared to other samples. The addition of 3.5 wt% BioAsh led to the formation of higher thermally stable crosslinking functional groups excellent for fire protection.

#### **4.9 Elemental Compound Analysis of BAIC 3-5**

At elevating temperature, the char layer was slowly oxidised and left only a few inorganic and carbon elements in the char layer (Wang and Yang, 2010). These inorganic remnants in the carbonaceous char became the heat protection shields (thermal barriers) to the steel substrate in the later stage of combustion (Ahmad et al., 2012). These potential thermally stable compounds remained in the char of BAIC 3-5 (after fire resistance test) were examined in XRD. The BAIC 3-5 char residue displayed diffraction peak as shown in **Figure 4.28**. The high peaks indicated the dominance of thermally stable compounds present in the char residue of BAIC 3-5 sample.

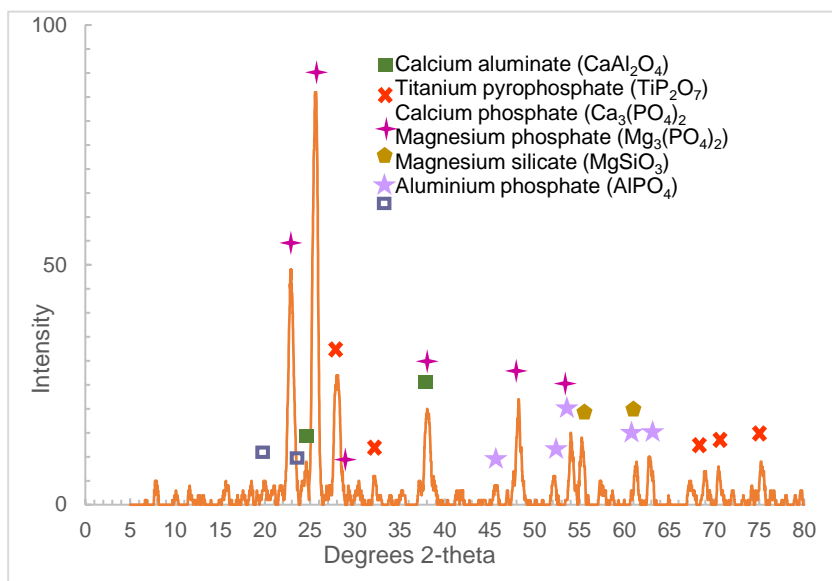
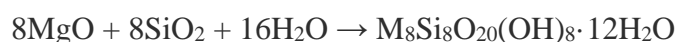


**Figure 4.28:** XRD Peak of BAIC 3-5 char (after fire resistance test).

The heating of calcium oxide (CaO) and aluminium oxide (Al<sub>2</sub>O<sub>3</sub>) at high temperature generated calcium aluminates (CaAl<sub>2</sub>O<sub>4</sub>). Calcium aluminate (CaAl<sub>2</sub>O<sub>4</sub>) was identified in the XRD peak of  $2\theta \sim 25.0^\circ - 38.0^\circ$  (El-Hamid et al., 2019; Ranjbar and Rezaei, 2014), and confirmed its presence in BAIC 3-5 char residue. MgO reacted with SiO<sub>2</sub> to form M-S-H (M<sub>8</sub>Si<sub>8</sub>O<sub>20</sub>(OH)<sub>8</sub>) with the presence of water. The chemical reaction as indicated as follows:



The heating of M-S-H at high temperature of more than 1000 °C resulted in magnesium silicate (MgSiO<sub>3</sub>) (Zhang et al., 2014). The diffraction peak at  $2\theta \sim 45.5^\circ, 52.0^\circ, 54.0^\circ, 61.5^\circ, 63.0^\circ$  proven the presence of MgSiO<sub>3</sub> in the BioAsh. Aluminium oxide (Al<sub>2</sub>O<sub>3</sub>) can react with the APP and resulted in the formation of aluminium phosphate (AlPO<sub>4</sub>). AlPO<sub>4</sub> was identified in the XRD peak between  $2\theta \sim 22.9^\circ$ , and  $21.0^\circ - 24.0^\circ$  (Liu et al., 2017). The peak at  $2\theta \sim 22.9^\circ$  in the char residue of BAIC 3-5 indicated the existence of thermally stable AlPO<sub>4</sub> after the fire test. The interaction between APP and TiO<sub>2</sub> led to the formation of Titanium pyrophosphates (TiP<sub>2</sub>O<sub>7</sub>). (Puri and Khanna, 2017). This compound of TiP<sub>2</sub>O<sub>7</sub> compound was the evidence of

APP and TiO<sub>2</sub> present in coating formulation (Wilkie and Morgan, 2009). The peak at 2θ ~ 28.0°, ~ 33.0°, ~63.0°, ~69.0°, ~70.5°, and ~75.0° verified the formation of thermally stable TiP<sub>2</sub>O<sub>7</sub> in the BAIC 3-5 char residue. The thickness of the carbonaceous char was highly relevant to the occurrence of thermally stable compounds and other oxide compounds in the coating. The thermally stable compounds present BAIC 3-5 char residue as defined in **Table 4.8**.

**Table 4.8:** Thermally stable compounds present in BAIC 3-5 char residue.

| Mineral Compound                         | Mineral Formula  | 2θ (°)   | References   |
|--|--|--|--|
| <b>BAIC 3-5</b>                          |  |  |  |
| Calcium aluminate                        | CaAl <sub>2</sub> O <sub>4</sub>   | 25.0°<br>38.0°   | Torres-Luque et al., 2017; El-hamid et al., 2019                   |
| Magnesium silicate                       | MgSiO <sub>3</sub>   | 45.5°<br>52.0°<br>54.0°<br>61.5°                                     | Klaithong et al., 2017; Zhang et al., 2014                         |
| Calcium phosphate<br>Magnesium phosphate | Ca <sub>3</sub> (PO <sub>4</sub> ) <sub>2</sub><br>Mg <sub>3</sub> (PO <sub>4</sub> ) <sub>2</sub> | 22.5°<br>25.5°<br>29.0°<br>38.0°<br>48.5°<br>54.0°<br>55.0°<br>63.0° | Su et al., 2013; Fang and Zhang, 2020                              |
| Aluminium phosphate                      | AlPO <sub>4</sub>  | 22.9°<br>21-24°  | Nguyen et al., 2019<br>Liu et al., 2017                            |
| Titanium pyrophosphate                   | TiP <sub>2</sub> O <sub>7</sub>  | 28.0°<br>33.0°<br>63.0°<br>69.0°<br>70.5°<br>75.0°                   | Lai et al., 2013; Puri and Khanna, 2017<br>Gerasimova et al., 2020 |

It can be deduced the combination of compounds such as CaCO<sub>3</sub>, CaO, Ca(OH)<sub>2</sub>, C-S-H, SiO<sub>2</sub>, MgO, Al<sub>2</sub>O<sub>3</sub>, Mg(OH)<sub>2</sub>, and Al(OH)<sub>3</sub> that present in the BioAsh underwent chemical and physical changes after reacted with water and heat, and led to the formation of new compounds.

These new compounds such as  $\text{CaAl}_2\text{O}_4$ ,  $\text{MgSiO}_3$ ,  $\text{Ca}_3(\text{PO}_4)_2$ ,  $\text{Mg}_3(\text{PO}_4)_2$ ,  $\text{AlPO}_4$ , and  $\text{TiP}_2\text{O}_7$  remained in the BAIC 3-5 char. The most intense peak was identified at the diffraction peak of  $25.5^\circ$ , which indicated calcium phosphate ( $\text{Ca}_3(\text{PO}_4)_2$ ) was the major thermally stable compounds in the BAIC 3-5 at the post combustion stage. These thermally stable compounds contributed to the promising thermal insulation barrier in BAIC 3-5 to slow down the heat penetration to the steel. The thickness of the carbonaceous char was highly relevant to the occurrence of thermally stable compounds in the coating. It verified the FRT, TGA, SEM, EDX, and FTIR outcomes of BAIC 3-5 achieved the most prominent result. It can be suggested, the addition of 3.5 wt% BioAsh enhanced the char thermal insulation barrier against fire.

#### 4.10 Adhesion Strength

Adhesion strength was referred to the physical and chemical bonding of BAIC samples applied on the steel surface, and the strength required to entirely detach the coating samples from the steel surface. The crack charge value and adhesion strength of all samples are shown in **Figure 4.29**.

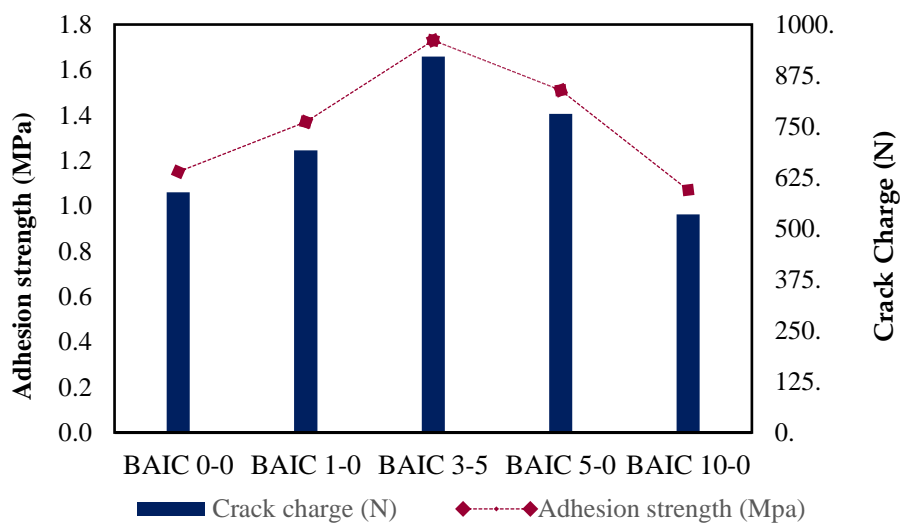


**Figure 4.29:** Crack charge and adhesion strength of BAIC samples.



BAIC 3-5 achieved the highest adhesion strength at 1.73 MPa, followed by BAIC 5-0, BAIC 1-0 and BAIC 0-0 at 1.51, 1.73 and 1.15 MPa. BAIC 10-0 displayed the lowest adhesion strength value at 1.07 MPa (**Appendix G**). BAIC 10-0 with 10.0 wt.% BioAsh exhibited the weakest surface bonding to steel. An increment in BioAsh composition was not correlated to an increment in adhesion strength. BAIC 1-0 with 1.0 wt.% BioAsh showed a better adhesion strength to steel surface as compared to BAIC 10-0. This could be attributed to better interfacial bonding between 1.0 wt.% BioAsh, polymer binder and steel surface. It was observed that the adhesion strength and crack charge decreased when  $\text{TiO}_2$  composition increased. The mechanical properties of matrix reduced in high concentration of  $\text{TiO}_2$ .  $\text{TiO}_2$  was appropriate to use in lower amount to minimize the negative impacts to the mechanical strength of the matrix (Thomas et al., 2004). The adhesion strength of BAIC 3-5 and BAIC 5-0 was better than BAIC 1-0. A higher amount of  $\text{TiO}_2$  at 9.0 wt.% in the formula reduced the adhesion strength of BAIC 1-0 to steel (Yew et al., 2015a). Single use of  $\text{TiO}_2$  as the only mineral filler in the IC formulation was unideal as this will lead to a tremendous loss in adhesion strength of the coating to the steel plate (Yew et al., 2015b). Hybridization of mineral fillers is required.

This study revealed BAIC 3-5 hybrid with 3.5 wt.% BioAsh was able to achieve the best synergic effect of interfacial bonding to the steel surface resulting in the strongest adhesion strength. An appropriate  $\text{Mg}(\text{OH})_2$  and  $\text{CaCO}_3$  help to improve the adhesion strength of the IC (Li et al., 2012). A stronger bonding between the metal surface and Mg/Ca interface allowed for a better stress transfer (Nasir et al., 2020). Magnesium and calcium composition that existed in 3.5 wt.% BioAsh were highly relevant to the best interfacial bonding in BAIC 3-5. The char residue of BAIC 3-5 exhibited a sharp and visible peak at  $3129.29\text{ cm}^{-1}$  and  $1631.75\text{ cm}^{-1}$  revealed the intense stretching of O-H group (hydroxyl group) and C=C bond (alkyl group) as displayed in **Figure 4.25**. The O-H and C=C bonding were accountable to the superior hydrogen bonding of char with steel in BAIC 3-5 even after  $1000\text{ }^\circ\text{C}$ . It can be suggested that

an appropriate O-H and C=C bond, and Mg and Ca elemental composition present in 3.5 wt.% BioAsh were vital to the adhesion strength of the coating to the steel surface. However,  $\text{Al}(\text{OH})_3$  in BioAsh could compromise the adhesion strength of the sample. Factors such as variation in the interface region, the structure of atomic bonding, toughness of fracture, purity, and thickness will also have impacts on the adhesion strength.

#### 4.11 Weather Resistance

Any cracking, color change, blister, and coagulum on all BAIC coating samples were visually assessed. The appearance of BAIC 0-0, 1-0, BAIC 3-5, BAIC 5-0, BAIC 10-0 after 70 freeze–thaw cyclic tests and under SEM x 2000 magnification as shown in **Figure 4.30**.

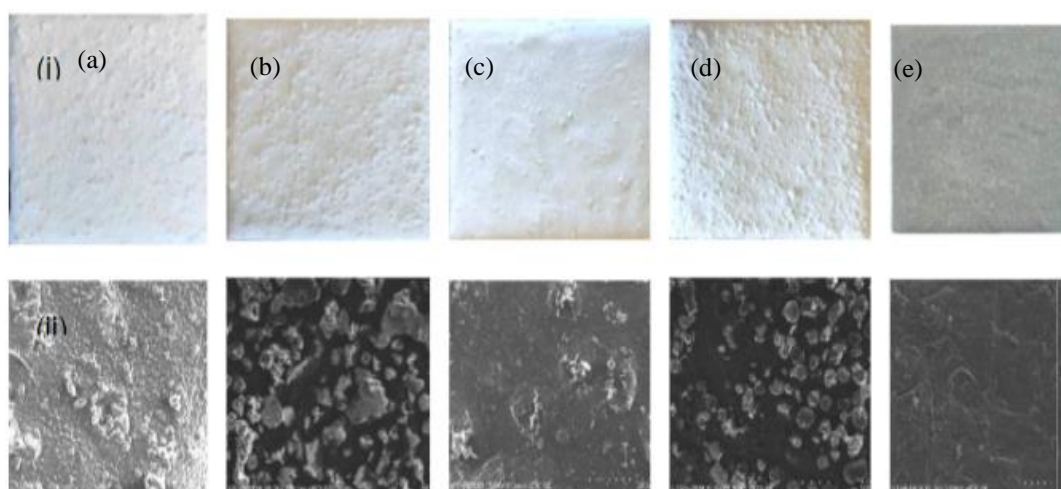


**Figure 4.30:** After 70 cyclic tests (i) and Under SEM x 2000 magnification (ii): (a) BAIC 0-0, (b) BAIC 1-0, (c) BAIC 3-5, (d) BAIC 5-0 and (e) BAIC 10-0.

Obvious coagula were accumulated in BAIC 0-0, BAIC 5-0 and BAIC 1-0. BAIC 3-5 had shown much lesser and finer coagulum in size compared to BAIC 0-0, BAIC 5-0 and BAIC 1-0. These coagula were noticed when the samples were in an air-dried condition before the

freeze–thaw cycle test. After the test, coagula in three samples remained unchanged. No coagulum was found in BAIC 10-0. The coagula condition was due to the difference in mix proportion of BioAsh and  $\text{TiO}_2$ . Coagula was greatly relevant to the combination of lower BioAsh and higher  $\text{TiO}_2$  composition in the formula. Particle to particle interactions in the matrix with high  $\text{TiO}_2$  composition led to agglomerations (Thomas et al., 2004). All coating samples were attached firmly to the steel plate. No crack, blister and color change were found in all BAIC samples after the test. This study revealed 3.5 wt% composition BioAsh in BAIC 3-5 had positive reactions and effects with  $\text{TiO}_2$ -APP-PER-MEL/VAC on weather resistance of BAIC samples. Other factors could be subjected to very minor C-S-H compound potentially formed from the reactions of  $\text{SiO}_2$ , CaO,  $\text{CaCO}_3$  that assisted in enhancing the coating's strength against weathering test as identified in EDX and XRD. Mesoporous particle surface of 3.5 wt% BioAsh as identified in BET was deduced best fitted with particles of other components resulted in the most homogenous surface matrix aesthetic in BAIC 3-5. It can be suggested, 3.5 wt% BioAsh in BAIC 3-5 with the APP-PER-MEL/VAC formulation exerted positive effects in enhancing the coating surface integrity and strength towards extreme weathering conditions, which had been proven under x 2000 high magnification of SEM micrograph (**Figure 4.30**).

#### **4.12 Water Resistance**

Water resistance of all BAIC samples were investigated using static immersion. The weight change of samples during the test was measured every one-hour interval up to 5 h. Water absorption rate of all samples, as shown in **Figure 4.31**.

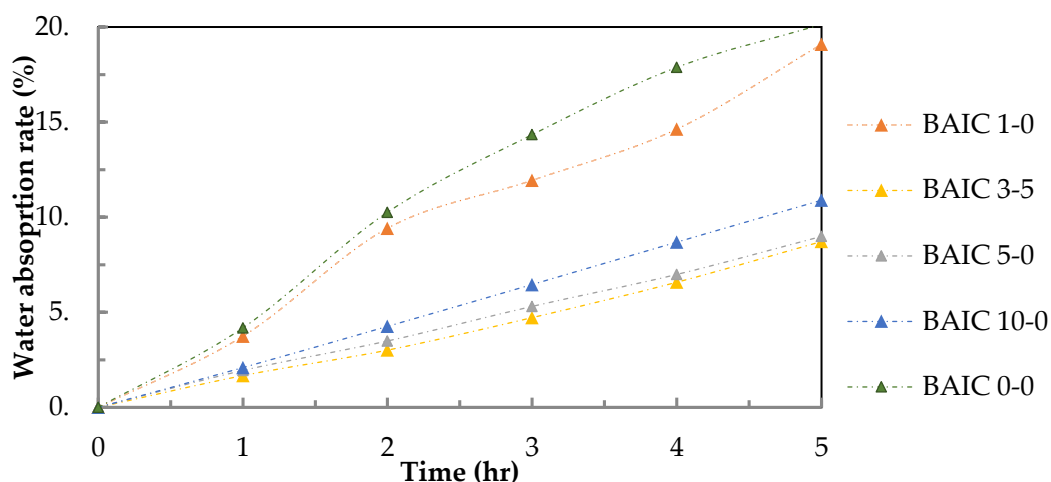


**Figure 4.31:** Water absorption rate of BAIC samples.

BAIC 3-5 with 3.5 wt.% BioAsh had the lowest water absorption rate at 8.72% with the smallest standard deviation of 2.57 as compared to other samples. The standard deviations of samples BAIC 1-0, BAIC 5-0 and BAIC 10-0 were 5.99, 2.74 and 3.44, respectively. In contrast, BAIC 0-0 and BAIC 1-0 exhibited the highest and second highest water absorption rate at 20.13% and 19.09% after 5 hours (**Appendix H**). Water permeation in BAIC 0-0 and BAIC 1-0 added with 10.0 wt.% and 9.0 wt.%  $\text{TiO}_2$  was the highest among all. BAIC 10-0 added with 10.0 wt.% of BioAsh had a lower water absorption rate at 10.89 % compared to BAIC 0-0 and BAIC 1-0. This demonstrated the higher water absorption rate was found to be correlated with the increase in  $\text{TiO}_2$  composition.  $\text{TiO}_2$  with stronger hydrophilic properties than BioAsh reduced the water resistance by allowing more water particles to penetrate the sample.  $\text{Ti}^{4+}$  ions reduced to  $\text{Ti}^{3+}$  reduced when exposed to UV radiation resulting in the vacant of oxygen on the  $\text{TiO}_2$  surfaces. Hydroxyl groups were formed on the  $\text{TiO}_2$  surface when surrounding water vapors were absorbed into the oxygen vacancies. This phenomenon exhibited the transition of  $\text{TiO}_2$  to a more hydrophilic characteristic (Masayuki and Takefumi, 2000).

Inter-surface structure of BAIC samples varied due to different BioAsh: TiO<sub>2</sub> ratio in APP-PER-MEL/VAC formula. BioAsh with a particle size of 300 µm had the largest particles among all ingredients. BAIC 10-0 with the highest portion of 10.0 wt.% BioAsh added forming more pores in the surface structure. Porosity in BAIC 10-0 allowed more water particles (0.275 nm) to penetrate BAIC 10-0, causing decrement in water resistance as compared to BAIC 3-5 and BAIC 5-0. An appropriate ratio of 3.5 wt.% in BAIC 3-5 was able to slow down the water permeation rate due to the formation of a better particles distribution in the inter-surface matrix. Incorporation of the poorly soluble Al(OH)<sub>3</sub> in intumescent coating can help to enhance the water resistance (Cayla et al, 2019). Hence, it is assumed minor Al(OH)<sub>3</sub> that present in 3.5 wt.% may assist in promoting a better water resistance in BAIC 3-5 without compromising the fire-resistance outcomes. However, hydroxyl groups (O-H), as identified in FTIR can readily form hydrogen bonds to increase the water solubility of the compound.

The various number of O-H groups existed in each BAIC sample resulted in the different water-resistance performance. BAIC 3-5 was predicted to have the most appropriate number of O-H groups due to its best water resistance among all others. It can be suggested that the best water resistance of BAIC 3-5 manifested an appropriate amount of 3.5 wt.% BioAsh was more likely to produce a better inter-surface matrix and bonding with APP-PER-MEL/VAC to minimize the water absorption rate. This further verified the best weather resistance and appearance of BAIC 3-5 in freeze-thaw cyclic. A summary of the main findings of BAIC 1-0, BAIC 3-5, BAIC 3-5, BAIC 5-0, BAIC 10-0, BAIC 0-0 samples the experimental works in this thesis as tabulated in **Table 4.9**.

**Table 4.9:** Summary of main findings coating samples in the experimental works.

| Experiment   | Sample   |  |  |  |   |
|--|--|--|--|--|---|
|  | BAIC 1-0   | BAIC 3-5   | BAIC 5-0   | BAIC 10-0  | BAIC 0-0                                      |
| <b>Fire resistant test (°C)</b>                    | 136.3  | 112.5  | 159.0  | 175.7  | 175.5   |
| <b>Carbolite furnace test (mm)</b>                 | 9.5  | 13.0   | 7.5  | 6.5  | 5.5   |
| <b>Weight load test (g)</b>                        | 200  | 250  | 150  | 50   | 50  |
| <b>TGA (residual weight, wt.%)</b>                 | 27.99  | 29.48  | 25.93  | 24.27  | 28.76   |
| <b>Surface morphology</b>                          | Crispy, open, burst cavities, big cell size  | Solid, rigid Compact Multicellular Crystalline cell structure micro cavities, Interconnected airgaps | Soft, puff Char structure Big cavities   | Soft, puff Char structure Big cavities   | Crispy, open, burst cavities, small cell size |
| <b>Anti-oxidation (O/C ratio)</b>                  | 1.01   | 0.69   | 1.26   | 1.50   | 1.49  |
| <b>Adhesion strength (MPa)</b>                     | 1.37   | 1.73   | 1.51   | 1.07   | 1.15  |
| <b>Freeze-thaw cycle</b>                           | Obvious, coarse coagula  | Lesser, finer coagula  | Obvious, coarse coagula  | No coagula   | Obvious, coarse coagula                       |
| <b>Static immersion (water absorption rate, %)</b> | 19.09  | 8.72   | 8.99   | 10.89  | 20.13   |
| <b>FTIR</b>  | C—H<br>C = O<br>Lignin<br>cellulose<br>Hemicellulose<br>—C—O<br>—C = O<br>Aromatic ring<br>O—H | C—H<br>C = O<br>Lignin<br>cellulose<br>Hemicellulose<br>—C—O<br>—C = O<br>Aromatic ring<br>O—H       | C—H<br>C = O<br>Lignin<br>cellulose<br>Hemicellulose<br>—C—O<br>—C = O<br>Aromatic ring<br>O—H | C—H<br>C = O<br>Lignin<br>cellulose<br>Hemicellulose<br>—C—O<br>—C = O<br>Aromatic ring<br>O—H | —C—O<br>—C = O<br>O—H                         |

In summary, the characterisation of BioAsh in EDX, XRD, FTIR confirmed the presence of elemental compounds such as  $\text{CaCO}_3$ ,  $\text{CaO}$ ,  $\text{Ca}(\text{OH})_2$ ,  $\text{Ca}_2\text{SiO}_4$ ,  $\text{SiO}_2$ ,  $\text{MgO}$ ,  $\text{Al}_2\text{O}_3$ ,  $\text{Mg}(\text{OH})_2$ , and  $\text{Al}(\text{OH})_3$ , and C=C bond (aromatic ring). SEM confirmed the physical

transformation of BioAsh after hydrated to form rosette-like crystalline structures. Among all twelve water-based intumescent coatings incorporated with BioAsh (BAIC samples), BAIC 3-5 achieved the best fire-resistance, char thickness, char strength, surface morphology, thermal stability, anti-oxidation, adhesion strength, weather resistance, and water-resistance outcomes. These most prominent results in BAIC 3-5 were highly associated with the appropriate number of elements compounds found in 3.5 wt% BioAsh after hydrated and reacted in the APP-PER-MEL/VAC formulation forming potential new elemental compounds. When exposed to fire, these elemental compounds reacted when heated and transformed into a combination of thermally stable compounds notable for fire-protection. These thermally stable compounds were  $\text{CaAl}_2\text{O}_4$ ,  $\text{MgSiO}_3$ ,  $\text{Mg}_3(\text{PO}_4)_2$ ,  $\text{AlPO}_4$ , and  $\text{TiP}_2\text{O}_7$ , predominant with  $\text{Ca}_3(\text{PO}_4)_2$  in the char residue of BAIC 3-5 verified in XRD. Suitable number of elemental compounds found in 3.5 wt% BioAsh were accountable to the formation of appropriate composition of these thermally stable compounds in BAIC 3-5 for the most excellent fire protection to steel.

## CHAPTER 5

### CONCLUSIONS AND RECOMMENDATIONS

#### 5.1 Conclusions

In this research project, the properties of BioAsh, and all BAIC samples were characterised and examined via Brunauer-Emmett-Teller Test (BET), Fire resistance test (FRT), Carbolite furnace test (CFT), Thermogravimetric analysis (TGA), Fourier-transform infrared spectroscopy (FTIR), Surface electron microscopy (SEM), Energy-dispersive x-ray spectroscopy (EDX), X-ray diffractometer (XRD), Instron adhesion test (IAT), Static immersion bath (SIB) and Freeze-thaw cycle (FTC). BioAsh properties, performances of fire resistance, mechanical, thermal, chemical, and physical properties of all BAIC samples were evaluated. BET revealed the specific surface area (SSA) of BioAsh was  $3.10 \text{ m}^2/\text{g}$  and predominant with mesopores. TGA disclosed the residual weight of BioAsh at 72.0 wt% indicating BioAsh composed of high thermally stable substances. SEM/EDX and XRD confirmed the presence of  $\text{CaCO}_3$ ,  $\text{CaO}$ ,  $\text{Ca(OH)}_2$ , C-S-H,  $\text{SiO}_2$ ,  $\text{MgO}$ ,  $\text{Al}_2\text{O}_3$ ,  $\text{Mg(OH)}_2$ ,  $\text{Al(OH)}_3$  in BioAsh. FTIR verified BioAsh with the existence of C-O, C=C (aromatic structure), lignin,  $\text{CO}_3^{2-}$ ,  $\text{NO}_3^-$ ,  $\text{SiO}_4^{2-}$ .

BAIC 3-5 sample with 3.5 wt.% BioAsh revealed the best results in fire resistance performance, thermal, physical, and mechanical properties. It had the lowest temperature in FRT at  $112.5^\circ\text{C}$ , highest residual weight in TGA at 29.48 wt.%, thickest char layer of 13 mm CFT, more uniform and denser multicellular rosette-like char structure present in SEM, lowest water absorption rate and strongest adhesion strength at 1.73 MPa. The static immersion test showed an appropriate  $\text{Al(OH)}_3$  present in BioAsh (3.5 wt.%) enhanced the water resistance of



BAIC 3-5. BAIC 3-5 incorporated with 3.5 wt.% BioAsh stimulated the carbon composition to 42.96 wt.% and lessened the oxygen composition to 29.93 wt.%, resulting in the lowest O/C ratio against oxidation. The inclusion of BioAsh enabled all BAIC samples to withstand freeze–thaw cycles, which could be attributed to the C–S–H compound formed and as identified in the BioAsh. All BAIC samples displayed a wide band position at 3100 to 3600  $\text{cm}^{-1}$ , indicating the presence of the O-H functional group for interfacial hydrogen bonding to the steel surface. The peak at 1451.61  $\text{cm}^{-1}$  to 1451.96  $\text{cm}^{-1}$  showed in all samples demonstrated the existence of aromatic ring of lignin present in BioAsh accountable for the good thermal stability and the formation of good-quality char. The peak band at 965.43  $\text{cm}^{-1}$  represented the rich  $\text{PO}_4^{3-}$  (phosphate group) and  $\text{SiO}_4^{2-}$  (silicate) formed in BAIC 3-5. EDX and FTIR revealed the highest ratio of O and P cross-linking structures, O-H, C=C,  $\text{PO}_4^{3-}$ , and  $\text{SiO}_4^{2-}$  in the char remnant of BAIC 3-5. Silicate and phosphate compounds (aromatic structures) remained in the char of BAIC 3-5 empowered its superior thermal stability. This verified the outstanding FRT, TGA, and SEM results of BAIC 3-5 among all samples.

The addition of 3.5 wt% BioAsh led to the formation of higher thermally stable crosslinking functional groups excellent for fire protection. XRD further confirmed thermally stable compounds such as  $\text{CaAl}_2\text{O}_4$ ,  $\text{MgSiO}_3$ ,  $\text{Ca}_3(\text{PO}_4)_2$ ,  $\text{Mg}_3(\text{PO}_4)_2$ ,  $\text{AlPO}_4$ ,  $\text{TiP}_2\text{O}_7$  existed in the char residue of BAIC 3-5, with the majority being  $\text{Ca}_3(\text{PO}_4)_2$  after the post-combustion stage. These components were deemed to be accountable to the promising performances of the BAIC3-5 sample's fire resistance properties.

## 5.2 Recommendations of Future Research

Based on the research findings, recommendations are suggested as follows:

- i. Investigation on the heat release rate (HRR), smoke production rate, and mass loss rate of BAIC samples could be examined using cone calorimeter in accordance with International Organization for Standardization (ISO 5660-1) standard in the future.
- ii. Investigation on the water contact angle (wettability) of solid surface of BioAsh,  $\text{TiO}_2$ , and flame-retardant additive particles could be studied using optical tensiometer in the future.
- iii. Investigation on the rheological behaviour of BAIC samples could be conducted using rheometer.
- iv. Investigation on the reaction to fire test: non-combustibility test (BS 476: Part 4), fire propagation test (BS 476: Part 6), surface spread of flame (BS 476: Part 7) of BAIC samples could be assessed in SIRIM (Standard and Industrial Research Institute of Malaysia) QAS International.
- v. Investigation on the impacts of different particle sizes of BioAsh in water-based intumescent coatings on fire resistance and mechanical strength could be studied.
- vi. Investigation on the hybridisation of BioAsh (rubberwood ash), with other ash wastes such as palm oil fuel ash (POFA) and rice husk ash (RHA) in the water-based intumescent coatings and their influences on fire-resistance and mechanical properties could be studied.
- vii. Investigation about the applications and effects of BioAsh incorporated water-based intumescent coatings on different surfaces of building components such as gypsum wall panel, fire timber door, and textiles could be diversified and studied.
- viii. Investigation on how rubberwood ash can be incorporated in higher weight proportion to achieve good grade green coating with superior environmentally friendly trademark.

## REFERENCES

- Aaronson, A.M., 1992. Phosphorous flame retardant for a changing world. *Phosphorus Chemistry, Developments in American Science*, ACS Symposium Series 486, Washington, 218.
- Abdullahi, M., 2006. Characteristics of wood ash/opc concrete. *Leonardo Electronic Journal of Practices and Technologies*, 8, pp. 9-16.
- Ahmad, F., Ullah, S. and Hamizol, M.S., 2012. To study the effect of aluminium trihydrate and fumed silica on intumescent fire retardant coating. *Journal of Applied Sciences*, 12(24), pp. 2631-2635.
- Ahmad, F., Ullah, S., Mohammad, W.F. and Shariff, M.F., 2014. Thermal performance of alumina filler reinforced intumescent fire retardant coating for structural application. *IOP Conference Series: Materials Science and Engineering*, 60, pp. 012023.
- Almiron, J., Roudet, F. and Duquesne, S., 2019. Influence of volcanic ash, rice husk ash, and solid residue of catalytic pyrolysis on the flame-retardant properties of polypropylene composites, *Journal of Fire Sciences*, 37, pp. 434 – 451.
- Alongi, J., Poskovie, M., Frache, A. and Trotta, F., 2010. Novel flame retardants containing cyclodextrin nanosponges and phosphorous compounds to enhance EVA combustion properties. *Polymer and Degradation Stability*, 95(10), pp. 2093 – 2100.
- Altarawneh, M., Saeed, A., Al-Harashsheh, M. and Dlugogorski, B.Z., 2019. Thermal decomposition of brominated flame retardants (BFRs): Products and mechanisms. *Progress in Energy Combustion and Science*, 70, pp. 212 – 259.
- Amir, N., Ahmad, F. and Megat-yusoff, P.S.M., 2011. Study on the fibre reinforced epoxy-based intumescent coating formulations and their char characteristics. *Journal of Applied Sciences*, 11, pp. 1678 – 1687.
- Andersson, A., Lundmark, S. and Maurer, F.H.J., 2007. Evaluation and characterization of ammonium polyphosphate-pentaerythritol-based systems for intumescent coatings. *Journal of Applied Polymer Science*, 104(2), pp. 748 – 753.
- Anderson, C.E., Dziuk, J., Mallow, W.A. and Buckmaster, J., 1985. Intumescent reaction mechanisms. *Journal of Fire Sciences*, 3 (3), pp. 161 – 194.
- Anees, S.M. and Dasari, A., 2018. A review on the environmental durability of intumescent coatings for steels. *Journal of Material Science*, 53, pp. 124 - 145.
- Anna, P., Marosi, G., Csontos, I., Bourbigot, S., Le Bras, M., Delobel, R., 2001. Influence of modified rheology on the efficiency of intumescent flame retardant systems. *Polymer Degradation and Stability*. 74, pp. 423 – 426.
- Anna, P. et al., 2001. Influence of modified rheology on the efficiency of intumescent flame retardant systems. *Polymer Degradation and Stability*, 74, pp. 423 – 426.
- Arias, J.L. and Fernandez, M.S., 2003. Biomimetic processes through the study of mineralized shells. *Materials Characterization*, 50 (2-3), pp. 189 - 195.

- Arogundade, A.I., Ahmad, F., Bhat, A.H., Gillani, Q.F., Megat-Yusoff., 2016. Investigating the synergistic effect of Bauxsol in an epoxy intumescent coating system. *Procedia Engineering*, 148, pp. 223 – 227.
- Arthur, T. and Quill, K., 1992. *Proceedings of Flame Retardant' 92*. London: Elsevier Applied Science, pp. 223.
- ASTM C 618-05., 2005. *Standard Specification for Coal Fly Ash And Raw Or Calcined Natural Pozzolans For Use In Concrete*. West Conshohocken: American Society of Testing and Materials.
- Azadeh, M., Zamani, C., Ataie, A. and Morante, J., 2018. Three-dimensional rice husk originated mesoporous silicon and its electrical properties. *Materials Today Communications*, 14, pp. 141 – 150.
- Aziz, H. and Ahmad, F., 2016. Effects from nano-titanium oxide on the thermal resistance of an intumescent fire retardant coating for structural applications. *Progress in Organic Coatings*, 101, pp. 431 – 439.
- Babushok, V. and Tsang, W., 2000. *Inhibitor rankings for alkane combustion*. *Combustion and Flame*, 123 (4), pp. 488 – 506.
- Bal, N., 2018. Forty years of material flammability: an appraisal of its role, its experimental determination and its modelling. *Fire Safety Journal*, 96, pp. 46 – 58.
- Banerjee, A.N. and Chattopadhyay, S., 1993. Adhesion study of vinylchloride-vinylacetate-maleic acid terpolymer/butylated melamine-formaldehyde resin blends. *International Journal of Adhesion and Adhesives*, 13 (3), pp. 173 – 180.
- BCC Research., 2018. *The global market for flame retardant chemicals*. Stamford CT: BCC Publishing.
- Beheshti, A. and Heris, S.Z., 2015. Experiment investigation and characterization of an efficient nanopowder-based flame retardant coating for atmospheric-metallic substrates. *Powder Technology*, 269, pp. 22 – 29.
- Beheshti, A. and Heris, S.Z., 2016. Is MWCNT a good synergistic candidate in APP-PER-MEL intumescent coating for steel structure. *Progress in Organic Coatings*, 90, pp. 252 – 257.
- Benbow, J., 1987. Minerals in fire protection. *Industrial Minerals*, 240, pp. 61 – 73.
- Bertelli, G., Camino, G., Marchetti, E., Costa, L., Casorati, E. and Locatelli, R., 1989. Parameters affecting fire retardant effectiveness in intumescent systems. *Polymer Degradation and Stability*, 25, pp. 277 – 292.
- Biomedical Applications. *Volume II: Modification and Coating Techniques*. Cambridge: Woodhead Publishing, pp. 3 – 21.
- Bostrom, D. et al., 2011. Ash transformation chemistry during combustion of biomass. *Energy Fuels*, 26, pp. 85 – 93.
- Bourbigot, S., Le Bras, M. and Delobel, R., 1993. Carbonization mechanisms resulting from intumescence association with the ammonium polyphosphate-pentaerythritol fire retardant system, *Carbon*, 31 (8), pp. 1219 – 1230.
- Bourbigot, S., Le Bras, M., Delobel, R., Breant, P. and Tremillon, J., 1995. Carbonization mechanisms resulting from intumescence-part II. Association with an ethylene terpolymer

and the ammonium polyphosphate-pentaerythritol fire retardant system. *Carbon*, 33 (3), pp. 283 – 294.

Bourbigot, S., Le Bras, M., Duquesne, S. and Rochery, M., 2004. Recent advances for intumescent polymers. *Macromolecular Materials and Engineering*, 289, pp. 499 – 511.

Bourbigot, S. and Duquesne, S., 2007. Fire retardant polymers: Recent developments and opportunities. *Journal of Materials Chemistry*, 17(22), pp. 2283-2300.

Bourbigot, S., Samyn, F., Turf, T. and Duquesne, S., 2010. Nanomorphology and reaction to fire of polyurethane and polyamide nanocomposites containing flame retardants. *Polymer Degradation and Stability*, 95 (3), pp. 320 – 326.

Butler, K.M., 1997. Physical modeling of intumescent fire retardant polymers. *Polymer Foams*, 669, pp. 214 – 230.

Camino, G., Costa, L. and Trossarelli, L., 1984. Study of the mechanism of intumescence in fire retardant polymers: Part III- Effect of urea on the ammonium polyphosphate-pentaerythritol system. *Polymer and Degradation Stability*, 7(4), pp. 221 – 229.

Camino, G., Costa, L., Trossarelli, L., Costanzi, F. and Landoni, G., 1984. Study of the mechanism of intumescence in fire retardant polymers: Part IV- Evidence of ester formation in ammonium polyphosphate-pentaerythritol mixtures. *Polymer Degradation and Stability*, 8(1), pp. 13-22.

Camino, G., Costa, L., and Trossarelli, L., 1985. Study of the mechanism of intumescence in fire retardant polymers: Part V- Mechanism of formation of gaseous products in the thermal degradation of ammonium polyphosphate. *Polymer Degradation and Stability*, 12(3), pp. 203-211.

Camino, G. and Costa, L., 1986. Mechanism of intumescence in fire retardant polymers. *Reviews in Organic Chemistry*, 8(1-2), pp. 69-100.

Camino, G., Costa, L. and Martinasso, G., 1989. Intumescent fire-retardant systems. *Polymer Degradation and Stability*, 23(4), pp. 359 - 376.

Camino, G., Martinasso, G. and Costa, L., 1990. Thermal degradation of pentaerythritol diphosphate, model compound for fire retardant intumescent systems: Part I Overall thermal degradation. *Polymer Degradation and Stability*, 27(3), pp. 285 - 296.

Camino, G., le Bras, M., Bourbigot, S. and Delobel, R., 1998. *Fire Retardancy of Polymers- The use of Intumescence*. Cambridge: Royal Society of Chemistry, pp. 48.

Campbell, A.G., 1990. Recycling and disposing of wood ash. *Tappi Journal*, 73(9), pp. 141-146.

Canosa, G., Alfieri, P.V. and Giudice, C.A., 2011. Hybrid intumescent coatings for wood protection against fire action. *Industrial & Engineering Chemical Research*, 50(21), pp. 11897 – 11905.

Castrovinci, A., Camino, G., Drevelle, C., Duquesne, S., Magniez, C. and Vouters, M., 2005. Ammonium polyphosphate-aluminum trihydroxide antagonism in fire retarded butadiene-styrene block copolymer. *European Polymer Journal*, 41 (9), pp. 2-23 – 2033.

Cayla, A. et al., 2019. Influence of Ammonium Polyphosphate/Lignin Ratio on Thermal and Fire Behavior of Biobased Thermoplastic: The Case of Polyamide 11. *Materials*, 12 (7), pp. 1146.

- Celik, F. and Canakci, H., 2015. An investigation of rheological properties of cement-based grout mixed with rice husk ash (RHA). *Construction Building Materials*, 91, pp. 187 – 194.
- Challener, C., 2007. Fire safety with specialty coatings. *Journal of Coatings Technology and Research*, 4(9), pp. 78.
- Clarholm, M., 1994. Granulated wood ash and a N-free fertilizer to a forest soil-effects on P availability. *Forest Ecology and Management*, 66, pp. 127-136.
- Clarke, K.D., 2014. Austenite formation and microstructural control in low-alloy steels. *Comprehensive Materials Processing*, 12, pp. 345 - 361.
- Costa, L and Camino, G., 1988. Thermal behaviour of melamine. *Journal of Thermal Analysis*, 34(2), pp. 423 – 429.
- Cronan, C.S. and Grigal, D.F., 1995. Use of calcium/aluminium ratios as indicators of stress in forest ecosystems. *Journal of Environment Quality*, 24, pp. 209-226.
- Cullis, C.F. and Hirschler, M.M., 1981. *The Combustion of Organic Polymers*. Oxford: Oxford University Press.
- De Wit, C.A., 2002. An overview of brominated flame retardants in the environment. *Chemosphere*, 46 (5), pp. 583 – 624.
- De Sá, S.C. et al., 2017. Environmentally friendly intumescent coatings formulated with vegetable compounds. *Progress in Organic Coatings*, 113, pp. 47 – 59.
- Demeyer, A., Nkana, J. and Verloo, M., 2001. Characteristics of wood ash and influence on soil properties and nutrient uptake: An overview. *Bioresource Technology*, 77, pp. 287 – 295.
- Devendra. K., Rangaswamy, K., 2012. Determination of mechanical properties of Al<sub>2</sub>O<sub>3</sub>, Mg(OH)<sub>2</sub> and Sic filled E-glass/epoxy composites. *International Journal of Engineering Research and Applications*, 2, pp. 2028 – 2033.
- Dong, J.K., Kaushik, P. and Se, J.P., 2009. Effect of eggshell and silk fibroin on styrene-ethylene/butylene-styrene as bio-filler. *Materials & Design*, 31(4), 2216 – 2219.
- Dong, Y., Wang, G. and Yang, J., 2014. Influences of silicone emulsion on fire protection of waterborne intumescent fire-resistive coating. *Journal of Coatings Technology and Research*, 11(2), pp. 231 – 237.
- Donohue, M and Aranovich, G.L., 1998. Classification of Gibbs adsorption isotherms. *Advances in Colloid and interface Science*, 76, pp. 137-152.
- Ducrocq, P., Duquesne, S., Magnet, S., Bourbigot, S. and Delobel, R., 2006. Interactions between chlorinated paraffins and melamine in intumescent paint- Investing a way to suppress chlorinated paraffins from the formulations. *Progress in Organic Coatings*, 57(4), pp. 430 – 438.
- Dunn, R.P., Kafle, J., Krause, F.C., Hwang, C., Ratnakumar, B.V., Smart, M.C. and Lucht., 2012. Electrochemical analysis of Li-ion cells containing triphenyl phosphate. *Journal of Electrochemical Society*, 159, pp. A2100 – A2108.
- Duquesne, S., Le Bras, M., Bourbigot, S., Delobel, R., Camino, G., Eling, B., et al., 2001. Mechanis, of fire retardancy of polyurethanes using ammonium polyphosphate. *Journal of Applied Polymer Science*, 82, pp. 3262 - 3274.

- Duquesne, S., Magnet, S., Jama, C. and Delobel, R., 2004. Intumescent paints: Fire protection coatings for metallic substrates. *Surface and Coatings Technology*, 302, pp. 180 – 181.
- Duquesne, S., Magnet, S., Jama, C. and Delobel, R., 2005. Thermoplastic resins for thin film intumescent coatings-towards a better understanding of their effect on intumescent efficiency. *Polymer Degradation and Stability*, 88, pp. 63 – 69.
- Duquesne, S., Bachelet, P., Bellayer, S., Bourbigot, S. and Mertens, W., 2013. Influence of inorganic fillers on the fire protection of intumescent coatings. *Journal of Fire Sciences*, 31, pp. 258 – 275.
- Dwight, G., 2009. Failure analysis of paints and coatings. A John Wiley & Sons.
- Dzung, N.A., Dzung, T.T. and Khanh, V.T.P., 2013. Evaluation of coffee husk compost for improving soil fertility and sustainable coffee production in Rural Central Highland of Vietnam. *Resources and Environment*, 3, pp. 77 – 82.
- El-Hamid, H.A., Radwan, M.M. and abo-Almaged, H.H., 2019. In vitro bioactivity study of calcium aluminate/calcium phosphate. *International Ceramic Review*, 68, pp. 36-43.
- Emira, H.S., Shakour, A.A., Rehim, S.S.A.E., Saleh, A.I. and El-Hashemy, M.A., 2012. High performance protective coatings for non-ferrous metals. *Anti-Corrosion Methods and Materials*, 59, pp. 139 – 149.
- Erich, M.S. and Ohno, T., 1992. Titrimetric determination of calcium carbonate equivalence of wood ash. *Analyst*, 117, pp. 993-995.
- Etiegni, L., 1990. *Wood ash recycling and land disposal (PhD Dissertation)*. Moscow: University of Idaho.
- Etiegni, L. and Campbell, A.G., 1991. Physical and chemical characteristics of wood ash. *Bioresource Technology*, 37, pp. 173 – 178.
- Etiegni, L., Campbell, A.G. and Mahler, R.L., 1991. Evaluation of wood ash disposal on agriculture land. Potential as a soil additive and liming agent. *Communications in Soil Science and Plant Analysis*, 22, pp. 243-256.
- Fan, F.Q., Xia, Z.B., Li, Q.Y. and Li, Z., 2013. Effects of inorganic fillers on the shear viscosity and fire retardant performance of waterborne intumescent coatings. *Progress in Organic Coatings*, 76, pp. 844–851.
- Fan, F., Xia, Z., Li, Q., Li, Z. and Chen, H., 2013. Thermal stability of phosphorous-containing styrene-acrylic copolymer and its fire retardant performance in waterborne intumescent coatings. *Journal of Thermal Analysis and Calorimetry*, 114 (3), pp. 937 – 946.
- Fang, C.Q. and Zhang, D., 2020. Pore forming with hemp fiber for magnesium phosphate structural supercapacitor. *Materials and Design*, 186, pp. 108322.
- Farkas, J. and Jármai, K., 2008. *Fire resistant design*, Cambridge: Woodhead Publishing.
- Harada, T., 2018. Nuclear flash burns: A review and consideration. *Burns Open*, 2, pp. 1 – 7.
- Feng, J., Zhang, X., Ma, S., Xiong, Z., Zhang, C., Jiang, Y. and Zhu, J., 2013. Syntheses of metallic cyclodextrins and their use as synergists in a poly(vinyl alcohol)/intumescent flame retardant system. *Industrial & Engineering Chemistry Research*, 52(8), pp. 2784 – 2792.

- Focke, W.W., Strydom, C.A. and Bartie, N., 1997. Thermal analysis of commercial inorganic flame retardants. *South African of Chemical Engineering*, 9(2), pp. 41 – 51.
- Fouda, A.E-A.S., Nazeer, A.A., Ibrahim, M. and Fakih, M., 2013. Ginger extract as green corrosion inhibitor for steel in sulfide polluted salt water. *Journal of the Korean Chemistry Society*, 57, pp. 272 – 278.
- Gann, R.G., 1993. *Flame retardants in Kirk Othmer's Encyclopaedia of Chemical Technology*. New York: John Wiley & Sons.
- Gardelle, B., Duquesne, S., Rerat, V. and Bourbigot, S., 2013. Thermal degradation and fire performance of intumescent silicone-based coatings. *Polymers for Advance Technologies*, 24(1), pp. 62 – 69.
- Gardelle, B., Duquesne, S., Vandereecken, P and Bourbigot, S., 2014. Resistance to fire of silicone-based coatings: Fire protection of steel against cellulosic fire. *Journal of Fire Sciences*, 32(4), pp. 374 – 387.
- Georlette, P., Simons, J. and Costa, L., 2000. *Halogen-containing Fire-Retardant Compounds in Fire Retardancy of Polymeric Materials*. New York: Marcel Dekker Inc.
- Gerasimova, L.G., Nikolaev, A.I., Shchukina, E.S., Maslova, M.V. and Kiselev, Yu.G., 2020. Hybrid composites based on silica and titanium (IV) phosphate for sorbents. *Inorganic Materials*, 56, pp. 1167-1173.
- Gilman, J.W. and Kashiwagi, T., 1997. *Intumescent flame retardant*. Gaithersburg: Fire science.
- Gray N.M. and Rock, C.A., 1987. *Boiler ash addition to agricultural soil*. Orono: University of Maine.
- Green, J., 1996. Mechanism of flame retardancy and smoke suppression- A review. *Journal of Fire Science*, 14, pp. 426 – 442.
- Green, J., 1997. 25 Years of flame retarding plastics. *Journal of Fire Science*, 15, pp. 52 – 67.
- Grim, R.E., 1968. *Clay Mineralogy*. New York: McGraw-Hill, pp. 189.
- Gu, J.W., Zhang, G.C., Dong, S.I., Zhang, Q.Y. and Kong, J., 2007. Study on preparation and fire-retardant mechanism analysis of intumescent flame retardant coatings. *Surface and Coatings Technology*, 201(18), pp. 7835 - 7841.
- Guan, W., Ji, F.Y., Cheng, Y., Fang, Z.Y., Fang, D.X., Yan, P. and Chen, Q.K., 2013. A novel synthesis method of porous calcium silicate hydrate based on the calcium oxide/polyethylene glycol composites. *Journal of nanomaterials*, 2013, pp. 542109.
- Han, Z.D., Fina, A., Malucelli, G. and Camino, G., 2010. Testing fire protective properties of intumescent coating by in-line temperature measurements on a cone calorimeter. *Progress in Organic Coating*, 69, pp. 475 – 480.
- Hao, J. and Choe, W.K., 2003. A brief review of intumescent fire retardant coatings. *Architectural Science Review*, 46(10), pp. 89-95.
- Horacek, H. and Grabner, R., 1996. Advantages of flame retardants based on nitrogen compounds. *Polymer degradation and stability*, 54, pp. 205 – 215.
- Horacek, H. and Pieh, S., 2000. The importance of intumescent systems for fire protection of plastic materials. *Polymer International*, 49 (10), pp. 1106-1114.



- Horacek, H., 2009. Reactions of stoichiometric intumescent paints. *Journal of Applied Polymer Science*, 113(3), pp. 1745 – 1756.
- Hewitt, F. and Hull, T.R., 2017. Mineral filler fire retardants. Switzerland: Springer, Cham.
- Hong, S.M., Soleimani, M., Liu, Y.Q. and Winnik, M.A., 2010. Influence of a hydrogen-bonding co-monomer on polymer diffusion in poly(butyl acrylate-co-methyl methacrylate) latex films. *Polymer*, 51 (14), pp. 3006–3013.
- Horrocks, A.R., Kandola, B.K., Davies, P.J., Davies, P.J. and Zhang, S., 2005. Developments in flame retardant textiles- a review. *Polymer Degradation and Stability*, 88, pp. 3 – 12.
- Huang, H., Campbell, A.G., Folk, R. and Mahler, R.L., 1992. Wood ash as a soil additive and liming agent for wheat. Field studies. *Soil Science and Plant Analysis*, 23, pp. 25-33.
- Huang, J., Zhang, Y., Yang, Q., Liao, X. and Li, G., 2012. Synthesis and characterization of a novel charring agent and its application in intumescent flame retardant polypropylene system. *Journal of Applied Polymer Science*, 123(3), pp. 1636 – 1644.
- Huggett, C. and Levin, B.C., 1987. Toxicity of the pyrolysis and combustion products of poly(vinyl chlorides): a literature assessment. *Fire and Materials*, 11, pp. 131 – 142.
- Hull, T.R., Quinn, R.E., Areri, I.G., Purser, D.A., 2002. Combustion toxicity of fire retarded EVA. *Polymer Degradation and Stability*, 77(2), pp. 235 – 242.
- Hull, T.R., Price, D., Liu, Y., Wills, C.L. and Brady, J., 2003. An investigation into the decomposition and burning behaviour of Ethylene-vinyl acetate copolymer nanocomposite materials. *Polymer Degradation and Stability*, 82(2), pp. 365 – 371.
- Hull, T.R., Wills, C.L., Artingstall, T., Price, D., Milnes, G.J., 2005. *Mechanisms of smoke and CO suppression from EVA composites*. London: Royal Society of Chemistry, pp. 372 – 385.
- Hull, T.R., Stec, A.A. and Nazare, S., 2009. Fire retardant effects of polymer nanocomposites. *Journal of Nanoscience and Nanotechnology*, 9(7), pp. 4478 – 4486.
- Hull, T.R., Witkowski, A. and Hollingbery, L., 2011. Fire retardant action of mineral fillers. *Polymer Degradation and Stability*, 96 (8), pp. 1462 – 1469.
- Husin, H., Asnawi, T.M., Firdaus, A., Husaini, H., Ibrahim, I and Hasfita, F., 2018. Solid catalyst nanoparticles derived from oil-palm empty fruit bunches (OP-EFB) as a renewable catalyst for biodiesel production. *IOP Conference Series: Materials Science and Engineering*, 358, pp. 012008.
- Huynh, T.P., Hwang, C.L., Lin, K.L. and Ngo, S.H., 2018. Effect of residual rice husk ash on mechanical-microstructural properties and thermal conductivity of sodium-hydroxide-activated bricks. *Environmental Progress & Sustainable Energy*, 37, pp. 1647 – 1656.
- Hytonen, J., Nurmi, J., Kaakkurivaara, N. and Kaakkurivaara, T., 2019. Rubber tree (*hevea brasiliensis*) Biomass, nutrient content, and heating values in southern Thailand. *Forests*, 10, 638.
- Isaac, O.I. and Genevive, C.O., 2012. Studies on properties of eggshell and fish bone powder filled polypropylene. *American Journal of Polymer Science*, 2(4), pp. 56 – 61.

- Ishikawa, S., Sekine, S., Miura, N., Suyama, K., Arihara, K., Itoh, M., 2004. Removal of selenium and arsenic by animal biopolymers. *Biological Trace Element Research*, 102 (1-3), pp. 113 – 127.
- Jessica, J.K.Y., Yew, M.C. and Yew, M.K., 2020. Development of advanced intumescent flame-retardant binder for fire rated timber door. *MATEC Web of Conferences*, 306, pp. 02006.
- Jiang, J.X., Li, J.Z. and Gao, Q., 2015. Effect of flame retardant treatment on dimensional stability and thermal degradation of wood. *Construction and Building Materials*, 75, pp. 74 – 81.
- Jiao, L. and Wu, Z., 2013. Alkali lignin as a carbonization agent on the thermal degradation and flame retardancy of intumescent flame retardant coating. *Advance Materials Research*, 750-752, pp. 1385 – 1388.
- Jimenez, M., Duquesne, S. and Bourbigor, S., 2006. Intumescent fire protective coating: Toward a better understanding of their mechanism of action. *Thermochimica Acta*, 449, pp. 16 - 26.
- Kandola, B.K and Horrocks, A.R., 1996. Complex char formation in flame-retarded fibre-intumescent combination- II. Thermal analytical studies. *Polymer Degradation and Stability*, 54, pp. 289 – 303.
- Karunadasa, K.S.P., Manoratne, C.H., Pitawala, H.M.T.G.A. and Rajapakse, R.M.G., 2019. Thermal decomposition of calcite, carbonate (calcite polymorph) as examined by in-situ high-temperature X-ray powder diffraction. *Journal of Physics and Chemistry of Solids*, 134, pp. 21 – 28.
- Kay, M., Price, F.A. and Lavery, I., 1979. A review of intumescent materials, with emphasis on melamine formulations. *Journal of Fire Retardant Chemistry*, 6, pp. 69 – 91.
- Khairunisa, M.N., Sulong, N.H.R., Mohd, R.J. and Amalina, M.A., 2020. Synergistic effect of industrial- and bio-fillers waterborne intumescent hybrid coatings on flame retardancy, physical and mechanical properties. *Progress in Organic Coatings*, 149, pp. 105905.
- Khaliq, W. and Mujeeb, A., 2019. Effect of processed pozzolans on residual mechanical properties and macrostructure of high-strength concrete at elevated temperatures. *Structural Concrete*, 20, pp. 307 – 317.
- Khan, S.R., Jamil, S. and Ashraf Janjua, M.R.S., 2018. Radiation assisted synthesis of dumb bell-shaped calcium hydroxide nanostructures from egg shells and study of its thermal and catalytic applications. *Chemical Physics Letters*, 710(16), pp. 45-53.
- Kirk-Othmer., 1979. *Encyclopaedia of Chemical Technology*. New York: John Wiley & Sons, pp. 169 – 172.
- Klaithong, S., Opdenbosch, D.V., Zollfrank, C. and Johann, P., 2017. Preparation of magnesium oxide and magnesium silicate replicas retaining the hierarchical structure of pine wood. *Zeitschrift für Naturforschung B*, 72(5), pp. 341-349.
- Kobes, M., Helsloot, I., De Vries, B. and Post, J.G., 2010. Building safety and human behaviour in fire: a literature review. *Fire Safety Journal*, 45, pp. 1 – 11.
- Koo, J.H., Ng, P.S. and Cheung, F.B., 1997. Effect of high temperature additives in fire resistant materials. *Journal of Fire Sciences*, 15(6), pp. 488 – 504.

- Kraszkievicz, A., Kachel-Jakubowska, M. and Niedziolka, I., 2017. The chemical composition of ash from the plant biomass in terms of indicators to assess slagging and pollution of surface heating equipment. *Fresenius Environmental Bulletin*, 26, pp. 6383 – 6389.
- Kumar, N.V., Murthy, P.S., Manjunatha, J.R. and Bettadaiah, B.K., 2014. Synthesis and quorum sensing inhibitory activity of key phenolic compounds of ginger and their derivatives. *Food Chemistry*, 159, pp. 451 – 457.
- Kurshev, I., Bozadjiev, P., Gruncharov, I., Naidenov, N., Bogdanov, K. and Tudjarova, F., 1986. *Guide of mineral fertilizers*, Sofia (Bulgaria): Technika.
- Kwang ying, JJ., Yew, M.C., Yew, M.K., Saw, L.H., 2019. Preparation of intumescent fire protective coating for fire rated timber door. *Coatings*, 9(11), pp. 738.
- Lai, C., Wang, W.G., Gao, J.J., Wang, Y.L., Ye, S.H., Li, L. and Wang, C., 2013. Titanium pyrophosphate hexagonal nanoplates for electrochemical lithium storage. *RSC Advances*, 32, pp. 13137-13139.
- Le Bras, M., Bourbigot, S. and Revel, B., 1999. Comprehensive study of the degradation of an intumescent EVA-based material during combustion. *Journal of Materials Science*, 34(23), pp. 5777 – 5782.
- Lebek, K., Hull, T.R. and Price, D., 2005. *Products of burning rigid PVC burning under different fire conditions*. Oxford: Oxford University Press, pp. 334 – 347.
- Lerner, R.B. and Utzinger, J.D., 1986. Wood ash as soil liming material. *HortScience*, 21(1), pp. 76-78.
- Levchik, S.V., Camino, G., Costa, L. and Luda, M.P., 1996. Mechanistic study of thermal behaviour and combustion performance of carbon fibre-epoxy resin composites fire retarded with a phosphorus-based curing system. *Polymer Degradation and Stability*, 54 (2-3), pp. 317 – 322.
- Levinta, N., Vuluga, Z., Teodorescu, M. and Corobea, M.C., 2019. Halogen-free flame retardants for application in thermoplastics based on condensation polymers. *Springer Nature Applied Science*, 1, pp. 422.
- Li, Z.Z. and Qu, B.J., 2003. Flammability characterization and synergistic effects of expandable graphite with magnesium hydroxide in halogen-free flame-retardant EVA blends. *Polymer Degradation and Stability*, 81(3), pp. 401 – 408.
- Li, G., Yang, J., He, T., Wu, Y. and Liang, G., 2008. An investigation of the thermal degradation of the intumescent coating containing  $\text{MoO}_3$  and  $\text{Fe}_2\text{O}_3$ . *Surface Coatings and Technology*, 202(13), pp. 3121 – 3128.
- Li, Y., Li, B., Dai, J., Jia, H. and Gao, S., 2008. Synergistic effects of lanthanum oxide on a novel intumescent flame retardant polypropylene system. *Polymer Degradation and Stability*, 93(1), pp. 9 – 16.
- Li, H.Y., Tan, Y.Q., Zhang, L., Zhang, Y.X., Song, Y.H. and Ye, Y., et al., 2012. Bio-filler from waste shellfish shell: preparation, characterisation, and its effect on the mechanical properties on polypropylene composites. *Journal of Hazardous Materials*, 217-218, pp. 256 – 262.
- Li, G.Q., Zhang, C., Lou, G.B., Wang, Y.C. and Wang, L.L., 2012. Assess the fire resistance of intumescent coatings by equivalent constant thermal resistance. *Fire Technology*, 48, pp. 529 – 546.

- Li, H.F., Hu, Z.W., Zhang, S., Gu, X.Y., Wang H.J. and Jiang, P., 2015. Effects of titanium dioxide on the flammability and char formation of water-based coatings containing intumescent flame retardants. *Progress in Organic Coatings*, 78, pp. 318 – 324.
- Li, J., Li, X., Wei, Q., Yang, J., Qiu, B., Xu, J. and Wang, X., 2019. Synergistic effect of organophosphate functionalized montmorillonite on properties and water resistance of intumescent flame-retarded SEBS. *Fire and Materials*. 43, pp. 74 – 83.
- Li, L., Liu, X., Shao, X., Jiang, L., Huang, K. and Zhao, S., 2020a. Synergistic effects of a highly effective intumescent flame retardant based on tannic acid functionalised graphene on the flame retardancy and smoke suppression properties of natural rubber. *Composites Part A: Applied Science and Manufacturing*, 129, pp. 105715.
- Li, Y.Z. et al., 2020b. Synergistic effect of clam shell bio-filler on the fire-resistance and char formation of intumescent fire-retardant coatings. *Progress in Organic Coatings*, 9 (6), pp. 14718 – 14728.
- Linggawati, A., 2016. Preparation and characterization of calcium oxide heterogeneous catalyst derived from anadara granosa shell for biodiesel synthesis. *Conference on Science and Engineering for Instrumentation*, 1(1).
- Liu, Y., Zhao, J., Deng, C.L., Chen, L., Wang, D.Y. and Wang, Y.Z., 2011. Flame-retardant effect of sepiolite on an intumescent flame-retardant polypropylene system. *Industrial & Engineering Chemistry Research*, 50(4), pp. 2047 – 2054.
- Liu, Y., Yi, J. and Cai, J., 2012. The investigation of intumescent flame-retarded polypropylene using poly(hexamethylene terephthalamide) as carbonization agent. *Journal of Thermal Analysis and Calorimetry*, 107(3), pp. 1191 – 1197.
- Liu, B.L., Jiang, P, P., Zhang, P.B., Zhao, H. and Huang, J., 2017. Aluminium phosphate-based solid acid catalysts: Facile synthesis, characterization and their application in the esterification of propanoic acid with n-butanol. *Comptes Rendus Chimie*, 20(5), pp. 540-548.
- Liu, S. et al., 2020. Intumescent fire retardant coating with recycled powder from industrial effluent optimized using response surface methodology. *Progress in Organic Coatings*, 140, pp. 105494.
- Lucherini, A. and Maluk, C., 2019. Intumescent coatings used for the fire-safe design of steel structures: a review. *Journal of Construction Steel Research*, 162, pp. 105712.
- Lv, D. et al., 2010. Effect of cellulose, lignin, alkali and alkaline earth metallic species on biomass pyrolysis and gasification. *Fuel Process Technology*, 91, pp. 903 – 909.
- Lyons, W., 1970. *The Chemistry and Uses of Fire Retardants*. New York: John Wiley and Sons.
- Ma, Z., Wang, J., Chen, S., Li, X., Ma, H., 2012. Synthesis and characterization of water borne intumescent fire-retardant varnish based on phosphate resin acid cold cured amino resin. *Progress in Organic Coatings*, 74(3), pp. 608-614.
- Mariappan, T., 2016. Recent developments of intumescent fire protection coatings for structural steel: a review. *Journal of Fire Sciences*, 34, pp. 120 – 163.
- Martins, M.S., Scharrel, B., Magalhaes, F.D. and Pereira, C., 2017. The effect of traditional flame retardants, nanoclays and carbon nanotubes in the fire performance of epoxy resin composites. *Fire and Materials*, 41, pp. 111 – 130.

- Masayuki, K. and Takefumi, M., 2000. Hydrophobic drawings on hydrophilic surfaces of single crystalline titanium dioxide: surface wettability control by mechanochemical treatment. *Surface science*, 463, pp. 609 – 612.
- Maurizio, A., Cosimo, C., Pierfrancesco, C., Maria, D.E., Gennaro, G., 2006. Ipp based nanocomposites filled with calcium carbonate nanoparticles: Structure/properties relationships. *Trends and Perspectives in Polymer Science and Technology*, 234, pp. 163 – 169.
- McGarry, K., Zilberman, J., Hull, T.R. and Woolley, W.D., 2000. Decomposition and combustion of EVA and LDPE alone and when fire retarded with ATH. *Polymer International*, 49, pp. 1193 – 1198.
- McWhinnie, H.J., 1979. Formulas for Chinese ash glazes. *Keram Z*, 31(7), pp. 410-411.
- Meiwes, K.J., 1995. Application of lime and wood ash to decrease acidification of forest soils. *Water, Air, Soil & Pollution*, 85, pp. 143-152.
- Mike Reed, G.M., 2015. *US Coatings, Intumescent coatings vs. cementitious coating. Coatings World* [Online]. Available at: Intumescent Coating Vs. Cementitious Coating - Coatings World [Accessed on 04 April 2021].
- Miller, B., 1996 Intumescent, FR efficiency pace flame retardant gains. *Plastic World*, pp. 44 – 59.
- Misra, M.K., Ragland, K.W. and Baker, A.J., 1993. Wood ash composition as a function of furnace temperature. *Biomass and Bioenergy*, 4(2), pp. 102-116.
- Mladenov, M., Serafimova, Ek., Pelovski, Y., 2011. Examinations on granulations of soil-improvers base on biomass ashes. *Journal of Environmental Protection and Ecology*. 12, pp.3
- Mohamad, W.F., Ahmad, F. and Ullah, S., 2013. Effect of inorganic fillers on thermal performance and char morphology of intumescent fire retardant coating. *Asian Network for Scientific Information*, 6(2), pp. 263 – 271.
- Mohd, S.M.B., Faizal, M., Norkhairunnisa, M. and Mohamad R.I., 2016. Fire retardant performance of rice husk ash-based geopolymer coated mild steel- A factorial design and microstructure analysis. *Materials Science Forum*, 841, pp. 48 – 54.
- Mount, R.A., 1992. The Three Sisters of Intumescence. *Proceedings of the FRCA Conference*, Orlando, Florida.
- Moustafa, H., Youssef, A.M. and Duquesne, S., 2015. Characterization of bio-filler derived from seashell wastes and its effect on the mechanical, thermal, and flame retardant properties of ABS composites. *Polymer Composites*, 38, pp. 2788 – 2797.
- Muse, J.K. and Mitchell, C.C., 1995. Paper mill boiler-ash and lime by-products as soil liming materials. *Agronomy Journal*, 87, pp. 432-438.
- Natural Rubber Statistic., 2018, *Malaysia Rubber Board* [Online]. Available at: [http://www.lgm.gov.my/nrstat/Statistics%20Website%202018%20\(Jan-Dec\).pdf](http://www.lgm.gov.my/nrstat/Statistics%20Website%202018%20(Jan-Dec).pdf) [Accessed on 29 June 2020].
- Naylor, R.B. and Schmidt, E.J., 1986. Agricultural use of wood ash as a fertilizer and liming material. *Tappi Journal*, 69(10), pp. 114-119.
- Neves, L., Oliveira, R. and Alves, M.M., 2006. Anaerobic co-digestion of coffee waste and sewage sludge. *Waste Management*, 26, pp. 176 – 181.

- Nguyen, V.T., Thu, Q.L., Nguyen, T.A., Ly, Q.C., Thi, L.P., Thi, H.P. and Thi Mai, T.D., 2019. Arc thermal spray NiCr20 alloy coating: Fabrication, sealant, heat treatment, wear, and corrosion resistances. *International Journal of Electrochemistry*, 2019, pp. 8796958.
- Nishimura, A., Hirose, I., Tanaka, N. and ASME, J., 2016. A New Method for Measuring Adhesion Strength of IC Molding Compounds. *Journal of Electronic Packaging*, 114(December 1992), pp.407 – 412.
- Nwanonenyi, S.C., Obidiegwu, M.U., Onuchukwu, T.S. and Egbuna, I.C., 2018. Studies on the properties of linear low density polyethylene filled oyster shell powder. *International Journal of Engineering Science*, 2(7), pp. 42 – 48.
- Obada, D.O., 2016. Effect of mechanical activation on mullite formation in an alumina-silica ceramics system at lower temperature. *World of Journal Engineering*, 13(4), pp. 288-293.
- Ohno, T., 1992. Neutralization of soil acidity and release of phosphorus and K by wood ash. *Journal of Environment Quality*, 21, pp. 433-438.
- Ohno, T. and Erich, M.S., 1993. Incubation-derived calcium carbonate equivalence of papermill boiler-ashes derived from sludge and wood sources. *Environmental Pollution*, 79, pp. 175-180.
- Olanders, B and Steenari, B.M., 1995. Characterization of ashes from wood and straw. *Biomass and Bioenergy*, 8(2), pp. 105 – 115.
- Olcese, T and Pagella, C., 1999. Vitreous fillers in intumescent coatings. *Progress in Organic Coatings*, 36(4), pp. 231 – 241.
- Omatola, K.M. and Onojah, A.D., 2012. Rice husk as a potential source of high technology raw materials: A review. *Journal of Physical Sciences and Innovation*, 4, pp. 1 – 6.
- Otahal, R., Vesely, D., Nasadova, J., Zima, V., Nemec, P. and Kalenda, P., 2011. Intumescent coatings based on organic-inorganic hybrid resin and the effect of mineral fibres on fire-resistant properties of intumescent coatings. *Pigment and Resin Technology*, 40(4), pp. 247 – 253.
- Oualha, M.A., Amdouni, N., Laoutid, F., 2017. Synergistic flame-retardant effect between calcium hydroxide and zinc borate in ethylene-vinyl acetate copolymer (EVA). *Polymer Degradation and Stability*, 144, pp. 315 – 324.
- Packham, D.E., 1996. Work of adhesion: contact angles and contact mechanics. *International Journal of Adhesion and Adhesives*, 16(2), pp. 121 – 128.
- Pakrashi, S., Dalai, S., Humayun, A., Chakravarty, S., Chandrasekaran, N. and Mukherjee., 2013. Ceriodaphnia as a potential bio-indicator for assessing acute aluminium oxide nanoparticle toxicity in fresh water environment. *PLoS ONE*, 8(9), pp. 74003.
- Pandey, A., Soccol, C.R., Nigam, P., Brand, D., Mohan, R. and Roussos, S., 2000. Biotechnical potential of coffee pulp and coffee husk for bioprocess. *Biochemical Engineering Journal*, 6, pp. 153 – 162.
- Panias, D., Balomenos, E. and Sakkas, K., 2015. *The fire resistance of alkali-activated cement-based concrete binders*. Cambridge: Woodhead Publishing.
- Pearce, E.M., 1986. Flame retardants for polymer systems. *Pure and Applied Chemistry*, 58, pp. 925 – 930.

- Pettifrew, A., 1993. *Halogenated flame retardants in Kirk Othmer's Encyclopedia of Chemical Technology*. New York: John Wiley & Sons.
- Prabir, B. 2018. *Biomass Gasification, Pyrolysis and Torrefaction: Practical Design and Theory*, 3rd ed. Cambridge: Academic Press.
- Pradhan, A.K. and Sahoo, P.K., 2017. Synthesis and study of thermal, mechanical and biodegradation properties of chitosan-g-PMMA with chicken egg shell (nano-CaO) as a novel bio-filler. *Materials Science and Engineering*, 80, pp. 149 – 155.
- Price et al., 2002. Flame retardance of poly(methyl methacrylate) modified with phosphorus-containing compounds. *Polymer degradation and stability*, 77(2), pp. 227 – 233.
- Puri, R.G. and Khanna, A.S., 2016. Effect of cenospheres on the char formation and fire protective performance of water-based intumescent coatings on structural steel. *Progress in Organic Coatings*, 92, pp. 8 – 15.
- Puri, R.G. and Khanna, A.S., 2017. Influence of heat-stable filler on the thermal shielding performance of water-based intumescent fire-resistive coating for structural steel applications. *Journal of Coatings Technology and Research*, 14, pp. 323-331.
- Puri, R.G. and Khanna, A.S., 2017. Intumescent coatings: A review on recent progress. *Journal of Coatings Technology and Research*, 14(1), pp. 1-20.
- Qian, W., Li, X.Z., Wu, Z.P., Liu, Y.X., Fang, C.C. and Meng, W., 2015. Formulation of intumescent flame retardant coatings containing natural-based tea saponin. *Journal of Agricultural and Food Chemistry*, 63, pp. 2782 – 2788.
- Quershi, S.P. and Krassowski, D.K., 1997. Intumescent resin system for improving fire resistance of composites. In: *Proceedings of the 29<sup>th</sup> International SAMPE Technical Conference*, pp. 625 – 629.
- Ralston, C.W. and Hatchell, G.E., 1971. Effects of prescribed burning on physical properties of soil. In *Prog: Prescribed Burning Symposium*, pp. 68-81.
- Ramazani, S.A.A., Rahimi, A., Frounchi, M. and Radman, S., 2008. Investigation of flame retardancy and physical-mechanical properties of zinc borate and aluminum hydroxide propylene composites. *Materials & Design*, 20, pp. 1051 – 1056.
- Ramis Rau, S., Vengadaesvaran, B., Naziron, N.N. and Arof, A.K., 2013. Strength and adhesion properties of acrylic polyol-epoxy polyol resin protective coating on mild steel substrate. *Pigment & Resin Technology*, 42(2), pp. 111 – 116.
- Ranjbar, A. and Mehran, R., 2014. Low temperature synthesis of nanocrystalline calcium aluminate compounds with surfactant-assisted precipitation method. *Advanced Powder Technology*, 25(1), pp. 467-471.
- Render, D., Samuel, T., King, H., Vig, M., Jeelani, S., Babu, R.J. and Rangari, V., 2016. Biomaterial-derived calcium carbonate nanoparticles for enteric drug delivery. *Journal of Nanomaterials*, 2016, pp. 3170248.
- Reti, C., Casetta, M., Duquesne, S., Bourbigot, S. and Delobel, R., 2008. Flammability properties of intumescent PLA including starch and lignin. *Polymers for Advanced Technologies*, 19(6), pp. 628 – 635.
- Rigolo, M. and Woodhams, R.T., 1992. Basic magnesium carbonate flame retardants for polypropylene. *Polymer Engineering and Science*, 32(5), pp. 327 – 334.

- Rothon, R.N. and Hornsby, P.R., 1996. Flame retardant effects of magnesium hydroxide. *Polymer Degradation and Stability*, 54(2-3), pp. 383 – 385.
- Rothon, R.N., 2003. Effects of particulate fillers on flame retardant properties of composites. Shrewsbury: Smithers Rapra Technology, pp. 263 – 302.
- Rubber Asia., 2017, *Malaysia for Model Sustainable Rubber Industry* [Online]. Available at: <https://rubberasia.com/2017/11/28/malaysia-model-sustainable-rubber-industry-dr-zairossani-bin-mohd-director-general-mrb> [Accessed on 29 June 2020].
- Saladi, N. 2019. Potential value-added utilization of wood ash in construction materials [Online]. Available at Potential Value-added Utilization of Wood Ash in Construction Materials (umaine.edu) [Accessed on 28 April 2021].
- Saoud, K.M., Saeed, S., Al-Soubaihi, R.M. and Bertino, M., 2014. Microwave assisted preparation of magnesium hydroxide nano-sheets. *American Journal of Nanomaterials*, 2, pp. 21-25.
- Saxena, N.K. and Gupta, D.R., 1990. Development and evaluation of fire retardant coatings. *Fire Technology*, 26(4), pp. 329-341.
- Schmaucks, G., Friede, B., Schreiner, H. and Roszinski, J.O., 2009. *Amorphous silicon dioxide as additive to improve the fire retardancy of polyimides*. Cambridge: Royal Society of Chemistry, pp. 35 – 48.
- Schmidt, W.G., 1965. Flame retardant additives in plastics and recent patents. *Transactions and Journal*, 33 (108), 247 – 255.
- Serafimova, Ek., Mladenov, M., Mihailova, I. and Pelovski, Y., 2011. Study on the characteristics of waste wood ash. *Journal of the University of Chemical Technology and Metallurgy*, 46(1), pp. 31-34.
- Shah, A.U.R., Prabhakar, M.N., Wang, H.F. and Song, J., 2016. The influence of particle size and surface treatment of filler on the properties of oyster shell powder filled polypropylene composites. *Polymer Composites*, 39, pp. 2420 – 2430.
- Shaw, S.D., 2010. Halogenated flame retardants: Do the fire safety benefits justify the risks?. *Review on Environmental Health*, 25 (4), pp. 261 – 305.
- Shemekite, F., Gomez-Brandon, M., Franke-Whittle, I.H., Praehauser, B., Insam, H. and Assefa, F., 2014. Coffee husk composting: an investigation of the process using molecular and non-molecular tools. *Waste Management*, 34, pp. 642 – 652.
- Shih, Y.F., Wang, Y.T., Jeng, R. J. and Wei, K. M., 2004. Expandable graphite systems for phosphorous-containing unsaturated polyesters. Enhanced thermal properties and flame retardancy. *Polymer Degradation and Stability*, 86, pp. 339.
- Sigmann, S.B., 2018. Playing with fire: Chemical safety expertise required. *Journal of Chemical Education*, 95 (10), pp. 1736 – 1746.
- Sika Group, 2021. *Fire Protective Coatings for Load-Bearing Structures*. URL: Fire Protective Coatings for Load-Bearing Structures (sika.com). Accessed in August 2020.
- Someshwar, A.V., 1996. Wood ash and combination wood-fired boiler ash characterization. *Journal of Environment Quality*, 25, pp. 962-972.
- Sorathia, U. and Beck, C., 1996. Fire protection of glass/vinyl ester composites for structural applications. In: *Proceedings of the 41<sup>st</sup> International SAMPE Symposium*, March 1996, pp. 687 – 697.



- Sorathis, U., Gracik, T., Ness, J., Durkin, A., Williams, F., Hunstad, M., et al., 2003. Evaluation of intumescent coatings for shipboard fire protection. *Journal of fire Sciences*, 21, pp. 423 – 450.
- Stephanie, C.de.Sa., Milena, M.de.Souza., Rafael, S.P., Ariane, V.Z., Renata, M.B., Dulce, M.de.A.M. and Carlos, A.F., 2017. Environmentally friendly intumescent coatings formulated with vegetable compounds. *Progress in Organic Coatings*, 113, pp. 47 – 59.
- Su, Y.C., Niu, L.Y., Lu, Y.B., Lian, J.S. and Li, G.Y., 2013. Preparation and corrosion behaviour of calcium phosphate and hydroxyapatite conversion coatings on AM60 magnesium alloy. *Journal of The Electrochemical Society*, 160(11), pp. 536-541.
- Suardana, N.P.G., Ku, M.S. and Lim, J.K., 2011. Effects of diammonium phosphate on the flammability and mechanical properties of biocomposites. *Materials & Design*, 32, pp. 1990 – 1999.
- Sun, Y., Liu, C., Hong, Y., Liu, R., Zhou, X., 2019. Synthesis and application of self-crosslinking and flame retardant waterborne polyurethane as fabric coating agent. *Progress in organic coatings*, 137, pp. 105323.
- Sutker, B.J., 1988. *Flame retardants in Ullman's Encyclopedia of Industrial Chemistry*. Weinheim: Wiley-VCH Verslag, pp. 123 – 140.
- Sutton, I., 2017. *Plant Design and Operation*, 2<sup>nd</sup> ed. Texas: Gulf Professional Publishing.
- Syarul, H.M., 2017. *Optimizations and recycling industrial waste (palm oil fly ash) as a pigment in coating technology*, MSc. Thesis, UHTM: Batu Pahat, Johor, Malaysia.
- Tarun, R.N., Rudolph, N.K. and Rafat, S., 2003. *Use of Wood Ash in Cement-Based Materials*. Milwaukee: University of Wisconsin-Milwaukee.
- Taylor, A.P. and Sale, F.R., 1993. Thermoanalytical studies of intumescent systems. *Makromol Chem-Macromol Symp*, 74(1), pp. 85 – 93.
- Thiago, F.da.C. and Nico, S., 2015. Fluoride conversion coatings for magnesium and its alloys for the biological environment. In: *Surface Modification of Magnesium and its Alloys for Biomedical Applications. Volume II: Modification and Coating techniques*. Cambridge: Woodhead Publishing, pp. 3 – 21.
- Thirumal, M., Aishvaree, A. and Sushma, R., 2017. Influence of titanium dioxide on the thermal insulation of waterborne intumescent fire protective paints to structural steel. *Progress in Organic Coatings*, 111, pp. 67 – 74.
- Thosmas, P.S., Joseph, K. and Thomas, S., 2004. Mechanical properties of titanium dioxide filled polystyrene microcomposites. *Materials Letters*, 58, pp. 281 – 289.
- Toro, P., Quijada, R., Yazdani-Pedram, M., and Arias, J. L., 2007. Eggshell, a new biofiller for polypropylene composites. *Materials Letters*, 61(22), pp. 4347 - 4350.
- Torres-Luque, M., Osmá, J.F., Sanchez-Silva, M., Bastidas-Arteaga, E. and Schoefs, F., 2017. Chloridetec: Commercial calcium aluminate based conductimetric sensor for chloride presence detection. *Sensors*, 17, pp. 2099.
- Touval, I., 1993. *Antimony and other inorganic flame retardants in Kirk Othmer's Encyclopedia of Chemical Technology*. New York: John Wiley & Sons.
- Tsai, W.T., Yang, J.M., Lai, C.W., Cheng, Y.H., Lin, C.C., Yeh, C.W., 2006. Characterization and adsorption properties of eggshells and eggshell membrane. *Bioresource Technology*, 97 (3), pp. 488 – 493.

- Ulery, A.L., Graham, R.C. and Amrhein, C., 1993. Wood-ash composition and soil pH following intense burning. *Soil Science*, 156, pp. 358-364.
- Ullah, S., Ahmad, F. and Yusoff, P.S.M.M., 2013. Effect of boric acid and melamine on the intumescent fire-retardant coating composition for the fire protection of structural steel substrates. *Journal of Applied Polymer Science*, 128, pp. 2983 – 2993.
- Ullah, S. and Ahmad, F., 2014. Effects of zirconium silicate reinforcement on expandable graphite based intumescent fire retardant coating. *Polymer Degradation and Stability*, 103, pp. 49 – 62.
- Ullah, S., Ahmad, F., Shariff, A.M. and Bustam, M.A., 2014. Synergistic effects of kaolin clay on intumescent fire retardant coating composition for fire protection of structural steel substrate. *Polymer Degradation and Stability*, 110, pp. 91 – 103.
- Vance, E.D., 1996. Land application of wood-fired and combination boiler ashes: an overview. *Journal of Environment Quality*, 25, pp. 937-944.
- Vandersall, H.L., 1971. Intumescent coating systems, their development and chemistry. *Journal of Fire and Flammability*, 2, pp. 97 – 11.
- Wang, Q. and Shi, W., 2006. Kinetics study of thermal decomposition of epoxy resins containing flame retardant components. *Polymer Degradation and Stability*, 91 (8), pp. 1747 – 1754.
- Wang, Z.Y., Han, E.H. and Ke, W., 2006a. An investigation into fire protection and water resistance of intumescent nano-coatings. *Surface and Coatings Technology*, 201 (3-4), pp. 1528 – 1535.
- Wang, Z.Y., Han, E.H. and Ke, W., 2006b. Effects of nanoparticles on the improvement in fire-resistant and anti-ageing properties of flame-retardant coating. *Surface and Coatings Technology*, 200 (20-21), pp. 5706 – 5716.
- Wang, D.Y., Liu, Y., Wang, Y.Z., Artiles, C.P., Hull, T.R. and Price, D., 2007. Fire retardancy of a reactively extruded intumescent flame retardant polyethylene system enhanced by metal chelates. *Polymer Degradation and Stability*, 92(8), pp. 1592 – 1598.
- Wang et al., 2008. Effect of metal chelates on the ignition and early flaming behaviour of intumescent fire-retarded polyethylene system. *Polymer Degradation and Stability*, 93(5), pp. 1024 – 1030.
- Wang, Y.Z., 2008. *Halogen-free flame retardants*. Cambridge: Woodhead Publishing Series in Textiles.
- Wang, G. and Yang, J., 2010. Influences of binder on fire protection and anticorrosion properties of intumescent fire resistive coating for steel structure. *Surface and Coatings Technology*, 204, pp. 1186 – 1192.
- Wang, G. and Yang, J., 2010. Influences of expandable graphite modified by polyethylene glycol on fire protection of waterborne intumescent fire resistive coating. *Surface and Coatings Technology*, 204, pp. 3599-3605.
- Wang et al., 2010. Flame retardancy and thermal degradation mechanism of epoxy resin composites based on a DOPO substituted organophosphorus oligomer. *Polymer*, 51 (11), pp. 2435 – 2445.

- Wang, G. and Yang, J., 2011. Influences of glass flakes on fire protection and water resistance of waterborne intumescent fire resistive coating for steel structure. *Progress in Organic Coatings*, 70(2-3), pp. 150 – 156.
- Wang, G. and Yang, J., 2012. Influences of molecular weight of epoxy binder on fire protection of waterborne intumescent fire resistive coating. *Surface and Coatings Technology*, 206(8-9), pp. 2146 – 2151.
- Wang, L., Yang, W., Wang, B., Wu, Y., Hu, Y., Song, L. and Yuen, R.K.K., 2012. The impact of metal oxides on the combustion behaviour of ethylene-vinyl acetate copolymers containing an intumescent flame retardant. *Industrial & Engineering Chemistry Research*, 51(23), pp. 7884 – 7890.
- Wang, L. and Dibdiakova, J., 2014. Characterization of ashes from different wood parts of Norway spruce tree. *Chemical Engineering Transactions*, 37, pp. 37-42.
- Wang, X. and Wang, D.Y., 2017. Fire-retardant polylactic acid-based materials: preparation, properties, and mechanism. *Novel Fire Retardant Polymers and Composite Materials*, 2017, pp. 93 – 116.
- Wang, Y.C., and Zhao, J.P., 2019. Facile preparation of slag or fly ash geopolymer composite coatings with flame resistance. *Construction and Building Materials*, 203, pp. 655 – 661.
- Waters, C.L., Janupala, R.R., Mallinson, R.G. and Lobban, L.L., 2017. Staged thermal fractionation for segregation of lignin and cellulose pyrolysis products: An experimental study of residence time and temperature effects. *Journal of Analytical and Applied Pyrolysis*, 126, pp. 380 – 389.
- Weil, E.D., 1978. *Phosphorous-Based Flame Retardants*. Boston: Springer.
- Weil, E.D., 2004. *Flame Retardancy*. *Encyclopedia of Polymer Science and Technology*, 11, New York: Wiley Interscience.
- Wen, Y.H., Tsou, C.H., Gao, G., Chen, J.C., Tang, Z.J. and Chen, Z.J., et al., 2020. Evaluating distillers grains as bio-fillers for high-density polyethylene. *Journal of Polymer Resources*, 27, pp. 167.
- Wiley Online Library., 2006. *Phosphoric acid* [Online]. Available at: <https://onlinelibrary.wiley.com/doi/abs/10.1002/0471743984.vse5529> [Accessed on 17 June 2020].
- Wilkie, C.A. and Morgan, A.B., 2009. Fire retardancy of polymeric materials. *CRC Press*, Boca Raton.
- Witoon, T., 2011. Characterization of calcium oxide derived from waste eggshell and its application as CO<sub>2</sub> sorbent. *Ceramics International*, 37(8), pp. 3291-3298.
- Wirnhier, E., Mesch, M.B., Senker, J. and Schnick, W., 2013. Formation and characterization of melam, melam hydrate, and a melam-melem adduct. *Chemistry*, 19(6), pp. 2041 – 2049.
- Wolf, R. and Lal Kaul, B., 1992. *Plastics, Additives in Ullman's Encyclopedia of Industrial Chemistry*. Weinheim: Wiley-VCH Verlag, pp. 459 – 507.
- Wonganan, N., Athisakul, C., Mahasuwanhai, P., Tanchirapat, W., Sahamitmongkol, R. and Leelataviwat, S., 2020. Ancient materials and substitution materials used in Thai historical masonry structure preservation. *Journal of Renewable Materials*, 9(2), pp. 179-204.

- Wu, Y., Zhou, X., Xing, Z. and Ma, J., 2019. Metal compounds as catalysts in the intumescent flame retardant system for polyethylene terephthalate fabrics. *Textile Research Journal*, 89, pp. 2983 – 2997.
- Wypych, G., 2016. *Fillers—Origin, Chemical Composition, Properties and Morphology: Handbook of Fillers*, 4th ed. Toronto: ChemTec Publishing.
- Xu, Q.F. et al., 2015. Combustion and charring properties of five common constructional wood species from cone calorimeter tests. *Construction and Building Materials*, 96, pp. 416 - 427.
- Xu, Z.S., Chu, Z.Y., Yan, L., Chen, H.G., Jia, H.Y. and Tang, W.F., 2018. Effect of chicken eggshell on the flame-retardant and smoke suppression properties of an epoxy-based traditional APP-PER-MEL system. *Polymer Composites*, 40(7), pp. 2712 – 2723.
- Xu, Z., Liu, D., Yan, L. and Xie, X., 2020. Synergistic effect of sepiolite and polyphosphate ester on the fire protection and smoke suppression properties of an amino transparent fire-retardant coating. *Progress in Organic Coatings*, 141, pp. 105572.
- Yan, L., Xu, Z.S. and Deng, N., 2019. Effects of polyethylene glycol borate on the flame retardancy and smoke suppression properties of transparent fire-retardant-coatings applied on wood substrates. *Progress in Organic Coatings*, 135, pp. 123 – 134.
- Yang, H., Yan, R., Chen, H., Lee, D.H. and Zheng, C., 2007. Characteristics of hemicellulose, cellulose and lignin pyrolysis. *Fuel*, 86, pp. 1781 – 1788.
- Yang, H., Yu, B., Song, P., Maluk, C. and Wang, H., 2019. Surface-coating engineering for flame retardant flexible polyurethane foams: A critical review. *Composites Part B: Engineering*, 176, pp. 107 – 185.
- Yarahmadi, N., Vega, A. and Jakubowicz, I., 2017. Accelerated ageing and degradation characteristics of rigid polyurethane foam. *Polymer Degradation and Stability*, 138, pp. 192 – 200.
- Yew, M.C. and Ramli Sulong, N.H., 2011. Effect of epoxy binder on fire protection and bonding strength of intumescent fire protective coatings for steel. *Advanced Materials Research*, 168-170, pp. 1228 – 1232.
- Yew, M.C. and Ramli Sulong, N.H., 2012. Fire-resistive performance of intumescent flame-retardant coatings for steel. *Material & Design*, 34, pp. 719 – 724.
- Yew, M.C., Ramli Sulong, N.H., Chong, W.T., Poh, S.C., Ang, B.C., Tan, K.H., 2013. Integration of thermal insulation coating and moving-air-cavity in a cool roof system for attic temperature reduction. *Energy Conservation and Management*, 75, pp. 241 – 248.
- Yew, M.K., Mahmud, H.B., Ang, B.C. and Yew, M.C., 2014. Effects of heat treatment on oil palm shell coarse aggregates for high strength lightweight concrete. *Materials & Design*, 54, pp. 702 - 707.
- Yew, M.C., Sulong, N.H.R., Yew, M.K., Amalina, M.A. and Johan, M.R., 2014. Fire propagation performance of intumescent fire protective coatings using eggshells as a novel biofiller. *The Scientific World Journal*, 805094, pp. 1 – 9.
- Yew, M.C., Sulong, N.H.R., Yew, M.K., Amalina, M.A. and Johan, M.R., 2015a. Influences of flame-retardant fillers on fire protection and mechanical properties of intumescent coatings. *Progress in Organic Coatings*, 78, pp. 59 – 66.

- Yew, M.C., Sulong, N.H.R., Yew, M.K., Amalina, M.A. and Johan, M.R., 2015b. Eggshells: A novel bio-filler for intumescent flame-retardant coatings. *Progress in Organic Coatings*, 81, pp. 116 - 124.
- Yew, M.C., Yew, M.K., Saw, L.H., Ng, T.C., Durairaj, R. and Beh, J.H., 2018. Influences of nano bio-filler on the fire-resistive and mechanical properties of water-based intumescent coatings. *Progress in Organic Coating*, 124, pp. 33 – 40.
- Yew, M.C., Yew, M.K., Saw, L.H., Ng, T.C., Chen, K.P., Durairaj, R., Beh, J.H., 2018. Experimental analysis on the active and passive cool roof systems for industrial buildings in Malaysia. *Journal of Building Engineering*, 19, pp. 134 – 141.
- Yew, M.C.; Beh, J.H., Yew, M.K.; Saw, L.H., 2019. Fire protection performance and thermal behavior of thin film intumescent coatings. *Coatings*, 9, 483.
- Yi, F., Guo, Z.X., Zhang, L.X., Yu, J., Li, Q., 2004. Soluble eggshell membrane protein: preparation, characterization and biocompatibility. *Biomaterials*, 25(19), pp. 4591 – 4599.
- Yoo, S., Hsieh, J.S., Zou, P., Kokoszka, J., 2009. Utilization of calcium carbonate particles from eggshell waste as coating pigment for ink-jet printing paper. *Bioresource and Technology*, 100 (24), pp. 6416 – 6421.
- Yuan, B., Fan, A., Yang, M., Chen, X.F., Hu, Y., Bao, C.L., et al., 2017. The effects of graphene on the flammability and fire behavior of intumescent flame retardant polypropylene composites at different flame scenarios. *Polymer Degradation and Stability*, 143, pp. 42 – 56.
- Zeng, Y., Weinell, C.E., Dam-Johansen, K., Ring, L. and Kiil, S., 2020. Effects of coating ingredients on the thermal properties and morphological structures of hydrocarbon intumescent coating chars. *Progress in Organic Coatings*, 143, pp. 105626.
- Zhan, W., Chen, L., Cui, F., Gu, Z. and Jiang, J., 2020. Effects of carbon materials on fire protection and smoke suppression of waterborne intumescent coating, *Progress in Organic Coatings*, 140, pp. 105491.
- Zhang, P., Song, L., Lu, H., Hu, Y., Xing, W., Ni, J., et al., 2009. Synergistic effect of nanoflaky manganese phosphate on thermal degradation and flame retardant properties of intumescent flame retardant polypropylene system. *Polymer Degradation and Stability*, 94, pp. 201 – 207.
- Zhang, M. and Chang, J., 2010. Surfactant-assisted sonochemical synthesis of hollow calcium silicate hydrate (CSH) microspheres for drug delivery. *Ultrasonics Sonochemistry*, 17(5), pp. 789-792.
- Zhang, R., Xiao, X., Tai, Q., Huang, H and Hu, Y., 2012. Modification of lignin and its application as char agent in intumescent flame-retardant poly(lactic acid). *Polymer Engineering & Science*, 52(12), pp. 2620 – 2626.
- Zhang, T.T., Vandeperre, L.J. and Cheeseman, C.R., 2014. Formation of magnesium silicate hydrate (M-S-H) cement pastes using sodium hexametaphosphate. *Cement and Concrete Research*, 65, pp. 8-14.
- Zhang, M., El-Korchi, T., Zhang, G., Ling, J. and Tao, M., 2014. Synthesis factors affecting mechanical properties, microstructure, and chemical composition of red mud-fly ash based geopolymers. *Fuel*, 134, pp. 315 – 325.

- Zhang, T.T., Zou, J., Wang, B., Wu, Z., Jia, Y. and Cheeseman, C., 2018. Characterization of magnesium silicate hydrate (MSH) gel formed by reacting MgO and Silica Fume. *Materials*, 11(6), pp. 909.
- Zhang, P., Tang, J., Tang, Q., Zhang, M.Z., Shen, L.W. and Tian, W.B., et al., 2019. Shell powder as a novel bio-filler for thermal insulation. *Chinese Journal of Chemical Engineering*, 27(2), pp. 452 – 458.
- Zhang, S., Zhang, Q., Sun, J., Gu, X., Li, H., Liu, X., Fei, B., 2020. Simultaneously improving the fire performance and toughness of polylactic acid by reactive blending with castor oil-based polyurethane and ammonium polyphosphate. *Journal of Fire Science*, 38(3), pp. 253 – 269.
- Zheng, Z., Liu, Y., Dai, B., Meng, C. and Guo, Z., 2019. Fabrication of cellulose-based halogen-free flame retardant and its synergistic effect with expandable graphite in polypropylene. *Carbohydrate Polymers*, 213, pp. 257 – 265.
- Zhou, W. and Yang, H., 2007. Flame retarding mechanism of polycarbonate containing methylphenyl-silicone. *Thermochimica Acta*, 452, pp. 43 – 48.
- Zhu, B., Lam, J.C.W., Yang, S. and Lam, P.K.S., 2013. Conventional and emerging halogenated flame retardants (HFRs) in sediment of Yangtze River Delta (YRD) region, East China. *Chemosphere*, 93, pp. 555 – 560.
- Zia-ul-Mustafa, M., Ahmad, F., Megat-Yusoff, P.S.M. and Aziz, H., 2014. The effect of wollastonite filler on thermal performance of intumescent fire retardant coating. *Advanced Materials Research*, 970, pp. 328 – 331.
- Zia-ul-Mustafa, M., Faiz, A., Sami, U., Norlaili, A. and Qandeel, F.G., 2017. Thermal and pyrolysis analysis of minerals reinforced intumescent fire retardant coating. *Progress in Organic Coatings*, 102, pp. 201 – 216.
- Zilberman, J., Hull, T.R., Price, D., Milnes, G.J. and Keen, F., 2000. Flame retardancy of some ethylene-vinyl acetate copolymer-based formulations. *Fire and Materials*, 24, pp. 159 – 164.

## APPENDICES

**APPENDIX A:** Table of TGA and DTA Results of BioAsh.

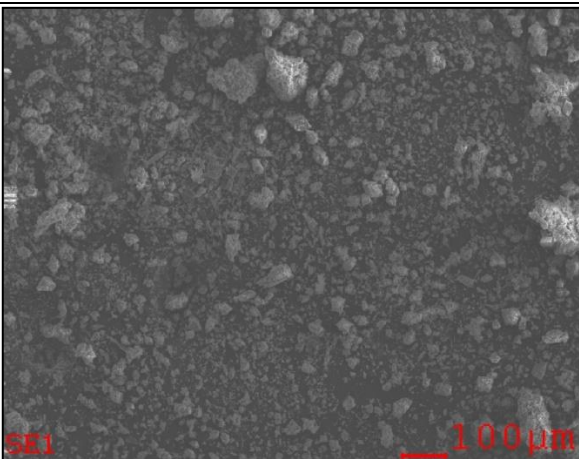
| BioAsh (original)-<br>TGA | BioAsh-WD (wet-<br>dried)-TGA | BioAsh (original)-<br>DTA | BioAsh (wet-dried)-<br>DTA |
|---------------------------|-------------------------------|---------------------------|----------------------------|
| 0                         | 100                           | 100                       | 0                          |
| 100                       | 98.90922                      | 98.16344                  | 0.0109                     |
| 200                       | 93.42392                      | 92.34803                  | 0.0329                     |
| 300                       | 92.89214                      | 91.63394                  | 0.0237                     |
| 400                       | 91.74692                      | 90.28832                  | 0.0206                     |
| 500                       | 89.83125                      | 88.12818                  | 0.0203                     |
| 600                       | 88.44946                      | 86.8986                   | 0.0192                     |
| 700                       | 83.09396                      | 81.38445                  | 0.0242                     |
| 800                       | 76.19127                      | 75.22315                  | 0.0298                     |
| 900                       | 73.65589                      | 73.07418                  | 0.0293                     |
| 1000                      | 72.72423                      | 72.02089                  | 0.0273                     |

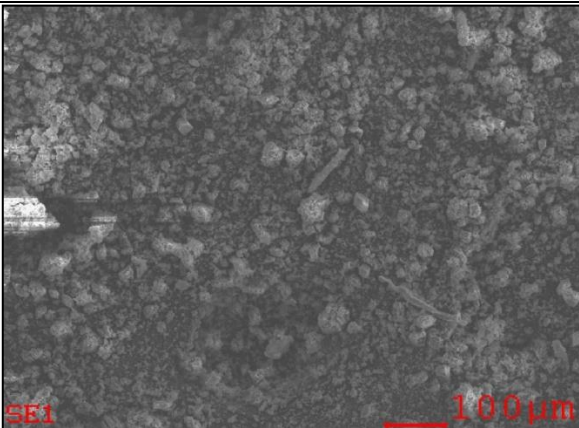
**APPENDIX B:** Table of TGA Results of BioAsh, VAC, APP, PER, MEL, TiO<sub>2</sub>.

|     | BioAsh   | BioAsh<br>(Wet-<br>dried) | VAC      | APP      | PER      | MEL      | TiO <sub>2</sub> |
|-----|----------|---------------------------|----------|----------|----------|----------|------------------|
| 0   | 100      | 100                       | 100      | 100      | 100      | 100      | 100              |
| 100 | 98.90922 | 98.16344                  | 100.8946 | 103.6744 | 102.9711 | 102.6437 | 101.9842         |
| 200 | 93.42392 | 92.34803                  | 100.1655 | 103.5038 | 100.3903 | 103.3877 | 102.9985         |
| 300 | 92.89214 | 91.63394                  | 98.93275 | 102.4342 | 66.52413 | 95.30104 | 100.9051         |
| 400 | 91.74692 | 90.28832                  | 70.99962 | 94.81684 | 4.367746 | 3.633054 | 99.696           |
| 500 | 89.83125 | 88.12818                  | 7.631427 | 88.19622 | 4.656522 | 3.881062 | 99.0074          |
| 600 | 88.44946 | 86.8986                   | 5.796719 | 83.68864 | 5.147998 | 4.321672 | 99.6836          |
| 700 | 83.09396 | 81.38445                  | 4.839793 | 51.96292 | 5.639474 | 4.825603 | 99.3331          |

|      |          |          |          |          |          |          |         |
|------|----------|----------|----------|----------|----------|----------|---------|
| 800  | 76.19127 | 75.22315 | 5.053243 | 47.63924 | 5.875493 | 5.070973 | 98.6401 |
| 900  | 73.65589 | 73.07418 | 5.038853 | 46.31061 | 5.725551 | 4.954884 | 98.3242 |
| 1000 | 72.72423 | 72.02089 | 4.870971 | 45.11335 | 5.414561 | 4.664661 | 98.7948 |

**APPENDIX C:** Diagrams of EDX Results of Raw and wet-dried BioAsh.

| Element | Wt%        | At%   |  |
|---------|------------|-------|---|
| CK      | 41.13      | 54.71 |   |
| OK      | 34.03      | 33.98 |   |
| ZnL     | 01.08      | 00.26 |   |
| MgK     | 03.10      | 02.03 |   |
| SiK     | 01.26      | 00.72 |   |
| PK      | 05.22      | 02.69 |   |
| SK      | 01.66      | 00.83 |   |
| RuL     | 00.94      | 00.15 |   |
| CaK     | 11.59      | 04.62 |   |
| Matrix  | Correction | ZAF   |   |

| Element | Wt%        | At%   |  |
|---------|------------|-------|--|
| CK      | 21.37      | 33.37 |  |
| OK      | 38.31      | 44.92 |  |
| GaL     | 01.68      | 00.45 |  |
| MgK     | 05.10      | 03.94 |  |
| AlK     | 00.65      | 00.45 |  |
| SiK     | 01.57      | 01.05 |  |
| PK      | 08.44      | 05.11 |  |
| CaK     | 22.87      | 10.71 |  |
| Matrix  | Correction | ZAF   |  |



**APPENDIX D:** Table of TGA Results of BAIC samples.

|      | BAIC 0-0 | BAIC 10-0 | BAIC 5-0 | BAIC 1-0 | BAIC 3-5 |
|------|----------|-----------|----------|----------|----------|
| 0    | 100      | 100       | 100      | 100      | 100      |
| 100  | 99.9672  | 99.8038   | 99.8716  | 99.9561  | 99.9812  |
| 200  | 99.1024  | 97.0022   | 97.8666  | 99.0863  | 98.8196  |
| 300  | 89.4827  | 87.8216   | 88.4458  | 87.0335  | 90.4304  |
| 400  | 70.3892  | 57.3256   | 70.5607  | 61.2243  | 72.1388  |
| 500  | 38.9423  | 33.3271   | 36.1877  | 38.859   | 39.495   |
| 600  | 36.4285  | 30.438    | 34.3075  | 34.0987  | 38.4324  |
| 700  | 35.1947  | 27.2949   | 33.4004  | 29.5384  | 37.5471  |
| 800  | 33.5891  | 24.9648   | 32.2282  | 28.4349  | 36.182   |
| 900  | 30.2456  | 24.4923   | 29.3977  | 28.171   | 32.8197  |
| 1000 | 28.7633  | 22.2349   | 25.9331  | 27.9922  | 29.478   |

**APPENDIX E:** Table of DTG Results of BAIC samples.

|      | BAIC 10-0 | BAIC 1-0 | BAIC 5-0 | BAIC 3-5 | BAIC 0-0 |
|------|-----------|----------|----------|----------|----------|
| 100  | 0.0674    | 0.0733   | 0.13275  | 0.19753  | 0.09825  |
| 200  | -0.38955  | -0.4096  | -0.2095  | -0.22599 | -0.3746  |
| 300  | -0.729    | -1.2831  | -1.3224  | -0.80712 | -1.0496  |
| 400  | -1.8166   | -1.8269  | -2.12379 | -1.31985 | -1.6385  |
| 500  | -1.1437   | -2.3408  | -1.4723  | -1.88437 | -2.1365  |
| 600  | -0.1147   | -0.1097  | -0.2611  | -0.0511  | -0.08147 |
| 700  | -0.1069   | -0.05294 | -0.2144  | -0.0365  | -0.04725 |
| 800  | -0.0694   | -0.05988 | -0.0454  | -0.04925 | -0.03619 |
| 900  | -0.0125   | -0.1285  | -0.00965 | -0.10782 | -0.11684 |
| 1000 | -0.00537  | -0.14157 | -0.00588 | -0.09645 | -0.10583 |

**APPENDIX F:** Table of Oxygen and Carbon Composition Results of BAIC samples.

|           | Oxygen, O (%) | Carbon, C (%) | O/C  |
|-----------|---------------|---------------|------|
| BAIC 0-0  | 49.23         | 33.12         | 1.49 |
| BAIC 1-0  | 35.42         | 35            | 1.01 |
| BAIC 3-5  | 29.93         | 42.96         | 0.69 |
| BAIC 5-0  | 33.36         | 26.18         | 1.26 |
| BAIC 10-0 | 34.83         | 23.13         | 1.5  |

**APPENDIX G:** Table of Crack Charge and Adhesion Strength Results of BAIC samples.

|           | Crack charge (N) | Adhesion strength (Mpa) |
|-----------|------------------|-------------------------|
| BAIC 0-0  | 588.9            | 1.15                    |
| BAIC 1-0  | 691.26           | 1.37                    |
| BAIC 3-5  | 921.59           | 1.73                    |
| BAIC 5-0  | 781.25           | 1.51                    |
| BAIC 10-0 | 534.47           | 1.07                    |

**APPENDIX H:** Table of Water Resistance Test Results of BAIC samples.

| BAIC 1-0 | BAIC 3-5 | BAIC 5-0 | BAIC 10-0 | BAIC 0-0 |
|----------|----------|----------|-----------|----------|
| 0        | 0        | 0        | 0         | 0        |
| 3.74     | 1.67     | 1.94     | 2.09      | 4.18     |
| 9.42     | 3.01     | 3.49     | 4.26      | 10.26    |
| 11.94    | 4.72     | 5.31     | 6.46      | 14.34    |
| 14.63    | 6.58     | 6.99     | 8.69      | 17.88    |
| 19.09    | 8.72     | 8.99     | 10.89     | 20.13    |

#### APPENDIX D: List of Publications

- 1) Beh, J.H., Yew, M.C. and Saw, L.H. **2019**. Development of lightweight fire resistant sandwich panel. *IOP Conference Series: Earth and Environmental Science*, 476 (1), pp. 012031. (*Published*).
- 2) Beh, J.H., Yew, M.C., Saw, L.H. and Yew, M.K. **2020**. Fire Resistance and Mechanical Properties of Intumescent Coating Using Novel BioAsh for Steel. *Coatings*, 10 (11), pp. 1117. (*Published*). IF: 2.881
- 3) Beh, J.H., Yew, M.C., Saw, L.H. and Yew, M.K. **2020**. Fire-resistant properties of green intumescent coating incorporated with BioAsh for steel protection. *Lecture Notes in Mechanical Engineering Springer*, pp. 257-264. (*Published*).
- 4) Beh, J.H., Yew, M.K., Yew, M.C. and Saw, L.H., **2021**. Characterisation and fire protection properties of rubberwood biomass ash formulated intumescent coatings for steel. *Journal of Materials Research and Technology*. (*Published*). IF: 5.039